Gamma-ray Bursts in the local Universe

Robert Chapman

A report submitted in partial fulfilment of the requirements of the
University of Hertfordshire for the degree of
Doctor of Philosophy

This programme of research was carried out in the
Centre for Astrophysics Research,
Department of Physics, Astronomy and Mathematics,
Faculty of Engineering and Information Sciences,
University of Hertfordshire

September 2008

Abstract

Robert Chapman

Gamma-ray Bursts in the local Universe

University of Hertfordshire, 2008

With energy outputs $\gtrsim 10^{51}$ erg in 0.1 - 1000 seconds, Gamma-ray Bursts (GRBs) are the most powerful events yet observed in the Universe. As such they are potential probes of the very early Universe, back to the era of re-ionisation and the first stars, but at the same time they have been observed to span a wide range in luminosity and redshift from the relatively local Universe ($z \sim 0.0085$) out to $z \sim 6.29$. GRBs divide into two classes based primarily on their duration as measured by T_{90} (the time taken to observe 90% of the total burst fluence). Long bursts (L-GRBs) have $T_{90} \gtrsim 2$ seconds, and shorts (S-GRBs) $T_{90} \lesssim 2$ seconds.

Though much has been learned regarding long duration GRBs since the first afterglow discovery in 1997 (including their likely association with massive core collapse supernovae), much remains unknown regarding short duration GRBs. In this work, after a brief historical introduction and review, we present analyses of the angular cross-correlation on the sky of short GRBs from the BATSE catalogue with galaxies in the local Universe sampled from the PSCz Redshift Survey and the Third Reference Catalogue of Bright Galaxies (RC3). In particular we show that $20\% \pm 8\%$ (1σ) of all BATSE short duration bursts (localised to 10° or better) show correlation with galaxy samples (morphological T-type ≤ 4) within ~ 112 Mpc.

Our statistics thus provide evidence that a substantial fraction of BATSE short GRBs show a tendency to be associated with large scale structure on the sky traced by a variety of galaxy types. Short GRBs are believed to be produced in the final merger of compact object (neutron star–neutron star or neutron star–black hole) binaries, though other possible progenitors are known to exist. The short initial spike of a giant flare from a Soft Gamma Repeater (SGR) such as the December 27th 2004 event from SGR1806-20 would have been detectable by BATSE as a short GRB if it occurred in a galaxy within $\sim 30 - 50$ Mpc (assuming a distance to SGR 1806-20 of 15 kpc). Using the observed luminosities and rates of Galactic SGR giant flares, as well as theoretical predictions for the rate of binary mergers, we investigate the ability of plausible Luminosity Functions (LF), singly and in combination, to reproduce our observed correlations and a cosmological S-GRB

population. We find the correlations are best explained by a separate population of lower luminosity S-GRBs, with properties consistent with them being due to giant flares from extra-galactic SGRs. Overall predicted number counts are a good fit to the observed BATSE number counts, and furthermore, the wider redshift distribution is consistent with the early *Swift* S-GRB redshift distribution.

The three closest GRBs which have been observed to date were all long duration bursts, and we have therefore also searched for cross-correlation signals between the BATSE long GRBs and local galaxies. The three nearby bursts shared several similar properties such as being under-luminous, spectrally soft and of low variability. We have therefore also investigated a subset of L-GRBs with light curve properties similar to these known nearby bursts. The whole sample is found to exhibit a correlation level consistent with zero (1σ upper limit = 10%, equivalent to 144 bursts) out to a radius of ~ 155 Mpc, but a spectrally soft, low observed fluence and low variability subset shows a correlation level of $28\% \pm 16\%$ ($\equiv 50 \pm 28$ bursts) within 155 Mpc. These results are consistent with low-luminosity, low-variability bursts being a separate sub-class of L-GRBs which may be much more prevalent in the local Universe than their high-luminosity, cosmologically distant counterparts. To investigate this further, we once again examined plausible luminosity functions for single and dual high and low luminosity populations, based on observed intrinsic rates from the literature. The local population was once again found only to be produced to a sufficient level (while maintaining consistency with the observed overall number counts) by a separate low luminosity population with intrinsic rates several hundred times greater than their cosmological counterparts. Constraining the models via the *Swift* overall redshift distribution instead of threshold-adjusted BATSE number counts showed that the dual LF models were able to produce excellent fits to the entire redshift distribution while adequately reproducing a local population.

Finally, suggestions are made as to the direction future work may follow in order to build on these initial investigations, as well as to how observations with future missions and detectors such as *Fermi* (formerly *GLAST*), Advanced LIGO and LOFAR may shed further light on nearby GRBs.

Acknowledgements

First and foremost I would like to thank Prof. Nial Tanvir for providing the unexpected inspiration for me to return to physics, and, in taking me on as a student, providing the opportunity to fulfil a dream. I also thank him for all the time, patience, expertise and encouragement he has provided throughout this research.

I am also grateful to Prof. Jim Hough for having the faith to offer me a place in the department, and for organising a University of Hertfordshire bursary to support my research, for which I am indebted.

My colleagues in CAR (and E117/1E125 in particular), have been a continual source of support and friendship. I'd like to thank Robert Priddey (my second supervisor) for always knowing more than surely is humanly possible about everything but never making me feel small, and along with Mark having provided such an easy and welcoming start to my work; Avon and Kim for providing light in the dark of the office; and Avril for being a good friend and joining in so willingly with the University Challenge adventure. Thanks to Andrew and Palli for being invaluable sources of knowledge, expertise and insight, and always making me realise how much I need to learn! To everybody else, thanks for being there.

Finally of course, none of this would have been possible without the support of my family. Firstly thanks to my mother for the struggles and sacrifices she made for my education. Unfortunately she did not live to see me start this project - she would have been proud, as would my father. Most importantly of course, my love and thanks go to my partner, Amanda, who (despite doubts!) has continually encouraged, supported and enabled me to pursue this project.

This work is dedicated to my children, Luke and Marc, whom I hope will find encouragement in it to follow their dreams.

Contents

List of Figures

List of Tables

Chapter 1

Introduction

1.1 Observational History

Klebesadel, Strong & Olson (1973) announced the detection of 16 bursts of gamma-ray emission detected by the military Vela satellites between 1969 and 1972, and the science of Gamma-ray Burst (GRB) astronomy was born. They had been searching the Vela data for gamma-ray emission coincident with supernovae as predicted by Colgate (1968), but instead found a selection of events with a variety of temporal and energetic properties not coincident with any known celestial or solar activity.

For the next 20 years at least, GRBs remained an enigma even to the extent as to whether they were 'local' events occurring within our Galaxy (or even possibly the Solar System), or whether they were of truly cosmological origin. A flavour of this uncertainty and debate can be drawn for example from Rees (1998). The unravelling of this enigma began in earnest in the 1990s with data from BATSE, the Burst and Transient Source Experiment onboard the *Compton Gamma Ray Observatory* launched in 1991. Results from BATSE showed that the distribution of GRBs on the sky was highly isotropic (see Figure 1.1) and therefore GRBs were not of Galactic origin (Briggs et al. 1996), though their cosmological nature remained controversial until the discovery of the first afterglows and redshifts in 1997 (van Paradijs et al. 1997; Frail et al. 1997; Metzger et al. 1997; Kulkarni et al. 1998a).

Confirmation of their location did not however solve the problem of what GRBs are (indeed, even today there is still debate regarding the number of different classes of GRB and types of progenitor). BATSE further provided spectral and temporal data for many bursts which enabled several empirical properties of GRBs to be

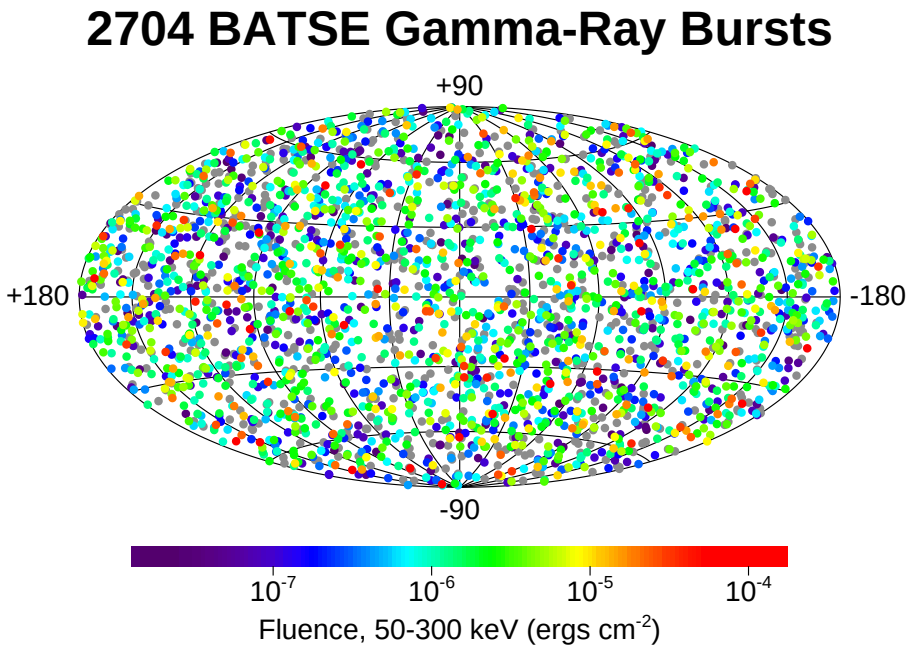

Figure 1.1: 2704 BATSE GRBs in Galactic coordinates. This figure illustrates the highly isotropic nature of GRBs as detected by BATSE. From BATSE website, http://cossc.gsfc.nasa.gov/docs/cgro/batse/, (Paciesas et al. 1999).

classified. In particular, it was found that GRBs were divided into two observational classes (see Figure 1.2) based primarily on their duration: long bursts (L-GRBs) where T_{90} (the time for 90% of the observed counts to arrive) $\gtrsim$ 2 seconds, and short bursts (S-GRBs) where $T_{90} \lesssim 2$ seconds (Kouveliotou et al. 1993; Norris et al. 1984). These two classes also differ in their spectral hardness, with short bursts in general being spectrally 'harder' than longs (Kouveliotou et al. 1993) as shown in Figure 1.3. For several years, these two classes have been the definitive classification scheme regarding GRBs and the over-arching paradigm for progenitor models. It is important to recall however, that this is an observationally defined categorisation, and as such will not only reflect any intrinsic distinction (and associated statistical dispersion), but may very well be instrument dependent as well. Indeed recently, this simple split between long and short GRBs has been called into question, particularly following the observations of GRBs 060505 and 060614, as we will discuss below (see section 1.2.3).

The next major breakthrough in GRB research came in 1997 with the detection of an X-ray afterglow by the Italian/Dutch satellite *Beppo-SAX* (Costa et al. 1997), providing a precise enough location to enable optical (van Paradijs et al. 1997)

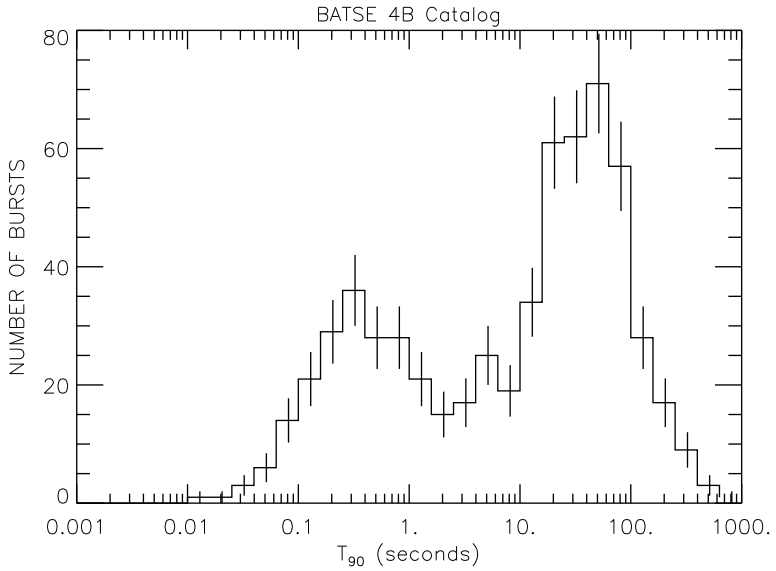

Figure 1.2: Bimodal distribution of BATSE GRBs. This figure illustrates the bimodal nature of GRBs as detected by BATSE. (From Ghisellini (2001), after (Paciesas et al. 1999)).

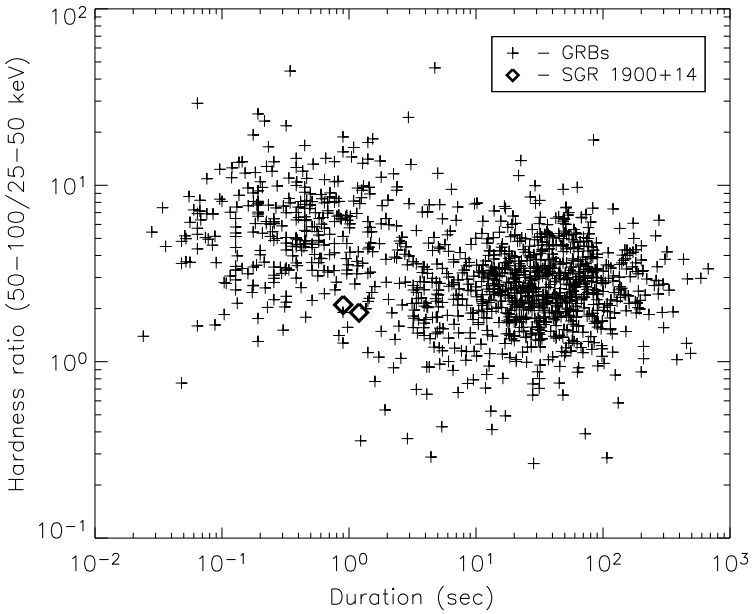

Figure 1.3: Spectral hardness v duration of BATSE GRBs. This figure plots the spectral hardness ratio (defined as the ratio of 50–100 keV fluence to 25–50 keV fluence) against T_{90} duration for all BATSE GRBs from the 4B catalogue (Paciesas et al. 1999). The figure also shows for later comparison two spectrally hard bursts from the Soft Gamma Repeater SGR 1900+14. Figure from Woods & Thompson (2004).

and radio observations (Frail et al. 1997). GRB astronomy had come of age, and within months, redshifts for GRB 970508 ($z = 0.695$) (Metzger et al. 1997) and GRB 971214 ($z = 3.42$) (Kulkarni et al. 1998a) had been measured, providing direct proof of their cosmological origin. Afterglow detection and analysis has now almost become routine in GRB astronomy, particularly with the rapid and precise location provided by the *Swift* mission, and redshift determination is common, at least for long duration bursts.

Localisation alone of course does not answer the fundamental question of what GRBs are, though it does provide important clues regarding progenitor populations, and constraining evidence for source models. Many theoretical possibilities were suggested (see Rees (1998) and Ruderman (1975) for a flavour of the debate), but with the strong BATSE confirmation of cosmological origin and therefore associated isotropic-equivalent energy releases of $10^{50} - 10^{54}$ erg, then the only known astrophysical phenomenon capable of this level of energy production is the release of gravitational binding energy via accretion on to a compact object (Neutron Star (NS) or Black Hole (BH)). Two major progenitor models therefore came to the fore: the merging of binary neutron stars (or a neutron star and a black hole), or the collapse of a single massive star in a process similar (if not identical) to a core collapse supernova, though there is a further viable progenitor possibility for S-GRBs as we shall see below (Section 1.2.2). Additionally, the timescale of this energy release (a few to a few 100s of seconds) demands that the energy is carried by relativistic ejecta with Lorentz factor $\Gamma \sim 100$ in order to explain the clearly non-thermal spectrum from what would otherwise be expected to be a highly optically dense source (the "compactness" problem - see section 1.8).

1.2 The Inner Engines: viable models

1.2.1 Compact Object Mergers

The merger of compact object binaries was suggested early on (Paczynski 1986; Eichler et al. 1989; Narayan, Paczynski & Piran 1992) as a viable source of the requisite energy to produce a GRB via the release of the gravitational binding energy of one of the pair objects on coalescence. Energetically, $> 10^{53}$ erg are available in this type of event (Narayan, Paczynski & Piran 1992), ample to produce a GRB at cosmological distances. Even if both original objects are neutron stars, the final

product of merger is most likely a black hole, and for this energy to be released (rather than simply swallowed by the resultant BH), an accretion disk must be formed at or beyond the last stable orbit. Indeed, given that the infalling material is bound to have some angular momentum, a disk must form. In order to be able to produce the ultra-relativistic outflow necessary to power a GRB, the outflow must be relatively baryon-free in order to be able to be accelerated to the requisite high Lorentz factors, and an accretion disk provides a natural (if not entirely understood in detail) mechanism for the production of collimated outflow through the less dense polar regions of the disk. This "beaming" of a GRB is also an important feature of (at least long) GRBs for their overall energy budget. With the limited amount of mass available from a NS progenitor, and the short dynamical and accretion timescales ($\sim$ milliseconds to a few seconds) of such a low mass disk, it would seem that compact object merger events are only likely to be able to produce short GRBs: in order to produce long GRBs, the disk must therefore be fed from a surrounding supply of material on a timescale similar to the duration of a long GRB. An accretion disk formed around the collapsed core of a massive star and fed by a surrounding torus of the remaining stellar mantle is the main feature of the Collapsar model for production of long GRBs which will be discussed in Section 1.2.3.

Given the plausible energetics and timescales of binary NS mergers as S-GRB engines, a significant observational fact in favour of this model is that it relies on a known population of objects. There are currently 9 known Galactic NS binary systems (Stairs 2008) (observationally detected as binary pulsars) with merger times (due to gravitational radiation) spanning 0.087 – 9600 Gyr (Champion et al. 2004), about half of which will merge within a Hubble time. The properties of this Galactic binary population can then be used to constrain population synthesis models in order to predict general NS-NS binary formation and merger rates. These studies predict general rates between 10^{-4} and 10^{-6} per year per Milky Way equivalent galaxy (Kalogera et al. 2007).

The significant delay time from formation to merger in this model obviously has implications for the type of stellar population, and therefore host galaxy, expected to be associated with GRBs produced in this manner. We would expect to see the resultant burst associated primarily with old stellar populations, and therefore earlier type galaxies. In addition, there is strong evidence that neutron stars receive substantial "kicks" of the order of several 10s to several 100s km s^{-1} at birth from asymmetrical supernovae explosions (see for example Podsiadlowski, Pfahl & Rappaport (2005); Wang, Lai & Han (2006) and references therein), leading

to the displacement of binary systems by several 10s kpc from their formation site. GRBs formed in this mechanism would therefore show no preference for high Star Formation Rate (SFR) galaxies, and certainly not association with young stellar populations within their hosts. No L-GRB has so far been found associated with an early type galaxy, and they appear to show a preference for small, irregular star forming galaxies, and moreover regions within those hosts likely to be sites of a young, massive stellar population (Fruchter et al. 2006). Conversely, the few host associations of S-GRBs found so far consist of a variety of galaxy types, including some with little or no star formation (Prochaska et al. 2006; Soderberg et al. 2006a; Nakar 2007; Berger 2008). There is also some preliminary evidence for different populations of S-GRBs with different host galaxy offset distributions, possibly explained by differing nascent kick velocities between NS-NS and NS-BH mergers, though the analysis is dependent on many only putative host associations (Troja et al. 2008). It would thus seem that binary compact object mergers are not a viable model to explain the observed properties of L-GRBs, but do remain a favoured model for the production of S-GRBs.

1.2.2 Magnetars: the Soft Gamma Repeaters

Compact Object mergers are not the only viable model for short GRBs. There are currently 4 known Soft Gamma Repeaters (SGR), 3 in the Galactic Plane and one in the Large Magellanic Cloud (LMC), and one further candidate as yet unconfirmed [1,2]. First detected in 1979, their characteristic behaviour is the emission of bursts of short duration, soft spectrum gamma-rays, and they were originally classified as a subtype of GRB (Mazets & Golenetskii 1981). With further observations however, these sources were later found to repeat (unlike "classical" GRBs) and to have similarities sufficient that they were designated as a separate astrophysical class of their own. Shortly after the very first SGR detection, on March 5th 1979, an extraordinarily bright flare was detected with with an initial spike of peak luminosity $\sim 10^{45}$ erg s^{-1}, followed by an exponentially decaying tail of 8 s period pulsations (Mazets et al. 1979; Golenetskii, Ilinskii & Mazets 1984). This "Giant Flare" was to remain the most energetic flare observed from an SGR until 2004.

Several models were proposed for the SGRs, including that of them being

[1] http://www.physics.mcgill.ca/∼pulsar/magnetar/main.html

[2] During writing a new SGR (SGR 0501+4516) was detected by *Swift* (Barthelmy et al. 2008), with measurements of the period (Göğüş et al. 2008), period derivative and estimated magnetic field (Woods et al. 2008), and a potential nIR counterpart (Tanvir & Varricatt 2008).

"Magnetars" - rotating neutron stars with an extremely high magnetic field $\geq 10^{14}$ G (Duncan & Thompson 1992; Paczynski 1992; Thompson & Duncan 1995, 1996). A major success of this model was that it could provide explanations for both the ordinary and giant flares, as well as being able to explain the persistent X-ray emission of the SGRs and the (soon recognised to be related) Anomalous X-ray Pulsars (AXP). This model received spectacular confirmation in 1998 with the measurement of a spindown rate of 2.8×10^{-11} s s^{-1} and 7.5 s pulsations of the X-ray counterpart to SGR 1806-20 (Kouveliotou et al. 1998). If we assume the moment of inertia, I, of a neutron star to be $\sim 10^{45}$ erg cm^2, then the rate of loss of rotational kinetic energy E at the current angular spin frequency ω (or period P) available to power the persistent emission is given by Equation 1.1

$$\frac{dE}{dt} = \frac{d}{dt}\left(\frac{1}{2}I\omega^2\right) = I\omega\dot{\omega} = -\frac{4\pi^2 I\dot{P}}{P^3} \tag{1.1}$$

and is only $\sim 3\times10^{33}$ erg s^{-1} (for $P = 7.5$ s and $\dot{P} = 2.8 \times 10^{-11}$ s s^{-1}). Given that the observed persistent luminosity is $\sim 2\times10^{35}$ erg s^{-1}, the available rotational energy is clearly insufficient to be responsible for the observed persistent luminosity, let alone any much more luminous flares. Assuming the SGR to be spinning down due to the emission of magnetic dipole radiation, then the implied (Manchester 1977) surface magnetic field strength, $B = 3.2 \times 10^{19}\ (P\dot{P})^{1/2} = 8 \times 10^{14}$ G. The total energy contained within this (assumed) dipole field at the surface of a NS of typical radius $R = 10^6$ cm is then $\sim B^2R^3 \approx 10^{48}$ erg, which is sufficient to power the persistent emission and several flares. The position of the magnetars (both SGRs and AXPs) in relation to the rest of the pulsar population in a $P\dot{P}$ diagram is shown in Figure 1.4.

The SGR common bursts have typical durations of ~ 0.1 s and luminosities $\leq 10^{41}$ erg s^{-1}. Their isotropic equivalent energies have been found to follow a power law distribution, $dN \propto E^{-\gamma}dE$ where $\gamma \sim 1.4 - 1.8$ (Cheng et al. 1996; Göğüş et al. 2000) similar to that found in earthquakes and solar flares. There is evidence for (Cheng et al. 1996) and against (Göğüş et al. 2000) a high energy cutoff in this distribution. However, SGRs also occasionally produce flares of much greater magnitude than the common bursts. Since observations began in the late 1970s, there have been 3 of these giant flares observed from the 4 known SGRs (there have also been several "intermediate" flares recorded following the giant flares which seem to be some form of aftershock following a giant flare episode). The giant flares have initial short, hard spikes of duration ~ 0.2 s with much higher luminosities

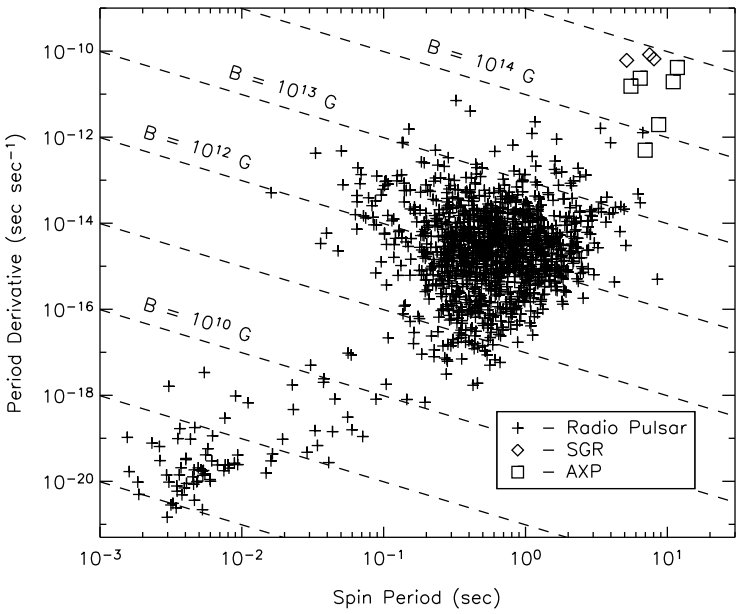

Figure 1.4: Period vs. period derivative diagram for ordinary radio pulsars (plus signs) and the magnetars: AXPs (squares), and SGRs (diamonds). The diagonal dashed lines are contours of constant inferred magnetic field strength. After Figure 14.11 of Woods & Thompson (2004).

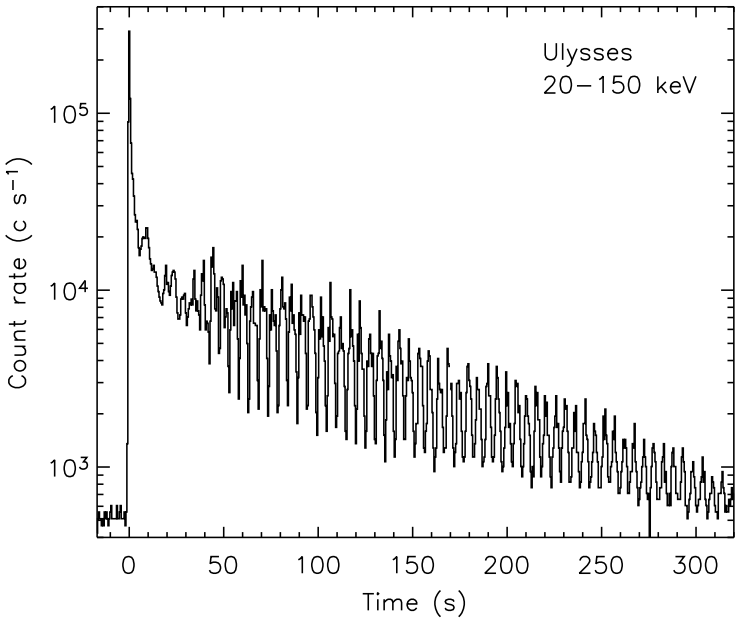

Figure 1.5: The Ulysses light curve of the SGR 1900+14 giant flare. From Woods & Thompson (2004), after Hurley et al. (1999a).

SGR	Peak Luminosity (initial spike) (erg s^{-1})	Total Energy (initial spike) (erg)	Total Energy (pulsating tail) (erg)
SGR 0526-66	$3.6 \times 10^{44} d_{55}^2$	$1.6 \times 10^{44} d_{55}^2$	$3.6 \times 10^{44} d_{55}^2$
SGR 1900+14	$(2.3^{+2.7}_{-0.8}) \times 10^{46} d_{15}^2$	$(4.3^{+5.3}_{-1.5}) \times 10^{44} d_{15}^2$	$1.2 \times 10^{44} d_{15}^2$
SGR 1806-20	$(5.1^{+2.3}_{-1.2}) \times 10^{47} d_{15}^2$	$(5.4^{+2.4}_{-1.3}) \times 10^{46} d_{15}^2$	$1.2 \times 10^{44} d_{15}^2$

Table 1.1: The properties of the three known SGR giant flares, where d_x is the distance to each SGR in units of x kpc. Data from Tanaka et al. (2007).

($\sim 10^{44} - 10^{47}$ erg s^{-1}), followed by an exponentially decaying tail of emission seen to pulsate at the rotational frequency of the underlying NS (see Figure 1.5).

On December 27th 2004, SGR 1806-20 emitted the most powerful giant flare seen so far. The initial peak saturated all spaceborne gamma-ray detectors (including the BAT onboard *Swift* (Palmer et al. 2005) even though it was only observed through the shielding of the instrument) and was the most intense cosmic or solar transient yet observed in terms of photon energy flux at the Earth (Hurley et al. 2005). Its luminosity was initially estimated by particle detectors on board RHESSI and Konus-Wind (Hurley et al. 2005) and its Compton reflection from the moon (Frederiks et al. 2007a). The most recent current estimates of the luminosities and energies of all 3 observed giant flares are shown in Table 1.1. They are of course, all dependent on the measured distances to the relevant SGRs, and recently, the distance to SGR 1806-20 has been revised down by a factor $d_{15} \approx 0.6$ from the previously accepted 15 kpc to $8.7^{+1.8}_{-1.5}$ kpc (Bibby et al. 2008), thus reducing the luminosity of the giant flare initial peak by about a third. With the best recent estimates of the luminosity of the 2004 event from the GEOTAIL spacecraft (Tanaka et al. 2007), this still remains $\sim 10^{47}$ erg s^{-1}.

This estimated peak luminosity of the initial spike of $\sim 10^{46} - 10^{47}$ erg s^{-1} reignited the suggestion that flares such as this may have been seen by BATSE as S-GRBs out to about $30 d_{15}$–$50 d_{15}$ Mpc (Hurley et al. 2005; Palmer et al. 2005; Taylor & Granot 2006; Nakar 2007), and maybe $80 d_{15}$ Mpc or so by *Swift* (Hurley et al. 2005): thus some fraction of BATSE short GRBs may have been due to extragalactic giant flares. Estimates of the possible upper limits of percentages of BATSE S-GRBs to be such flares were made on the basis of the lack of viable host

candidates for well-localised S-GRBs (Nakar et al. 2006), the lack of an excess of GRBs from the direction of the Virgo cluster (Popov & Stern 2006; Palmer et al. 2005), and spectral constraints (Lazzati, Ghirlanda & Ghisellini 2005). This quickly became, and remains, a hot topic in S-GRB research and will be discussed further in the following Chapters of this work where we present results based on the angular cross-correlations between positions on the sky of BATSE S-GRBs and galaxies within ~ 150 Mpc.

1.2.2.1 Formation and burst mechanism

Magnetars are believed to be relatively slowly rotating neutron stars compared to their faster rotating cousins, the ordinary radio pulsars (see Figure 1.4). However, their period derivatives, inferred magnetic field strength and characteristic ages imply that they were formed spinning much more rapidly, with periods near breakup velocity of ~ 1 ms. NS are generally formed as remnants in core collapse supernovae, or may also form via the Accretion Induced Collapse (AIC) of a White Dwarf (WD) (e.g. Nomoto & Kondo 1991; Usov 1992; King, Pringle & Wickramasinghe 2001). In either case, the newly formed NS is expected to be rotating rapidly due to angular momentum conservation on collapse. In addition, if the progenitor prior to NS formation has any magnetic field, then flux conservation implies that this will be amplified significantly ($\propto (R_{initial}/R_{final})^2$) on collapse. In the case of the AIC of a significantly magnetised WD, this "fossil field hypothesis" could produce a magnetar (King, Pringle & Wickramasinghe 2001). The necessary field strength for the parent WD is several hundred MG: these fields are rare, but do exist in the WD population (e.g. Wickramasinghe & Ferrario 2000; Schmidt et al. 2003; Norton, Wynn & Somerscales 2004; Vanlandingham et al. 2005). It is likely however, that any fossil field so formed is actually a lower limit on the magnetic field strength of the NS. This is because a newborn NS is likely to undergo dynamo activity, since it is both highly convective (Burrows 1987; Burrows & Lattimer 1988) and rapidly rotating. To support an efficient α–Ω dynamo, a differentially rotating turbulent fluid requires a Rossby number $Ro \lesssim 1$ (where Ro is the ratio of the rotation period to the convective overturn time). A newborn NS is expected to have $Ro \sim 1(P/1 \text{ ms})$ (Duncan & Thompson 1992) and is therefore likely to support an efficient dynamo. Extremely large fields, potentially as strong as $3 \times 10^{17}\ (P/1 \text{ ms})^{-1}$ G, may be generated even from small seed fields in NS with significant (as is likely) differential rotation (Thompson & Duncan 1993).

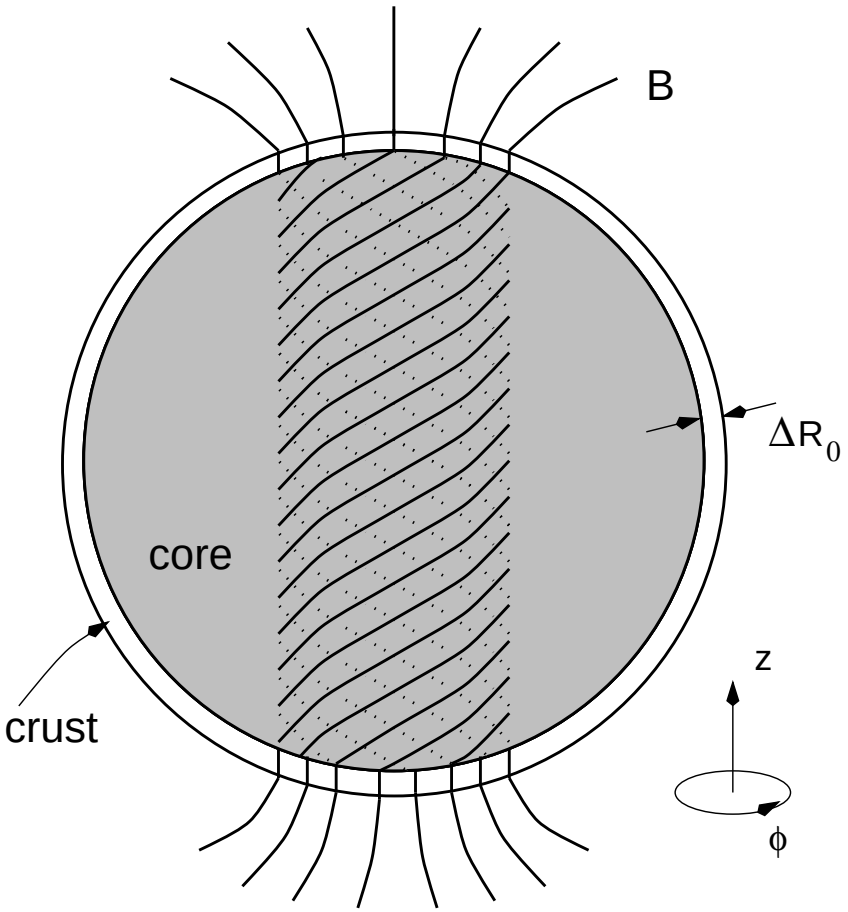

Figure 1.6: The toy model of a magnetar due to Thompson & Duncan (2001), from their Figure 1. A poloidal magnetic field B threads the crust and core of the magnetar. Anchored in the solid crust and also frozen in to the differentially rotating fluid core, the field is twisted and gains a toroidal component which stresses the crust from below.

Thompson & Duncan (2001) defined a model of a cylindrically symmetric magnetar as visualised in Figure 1.6. A poloidal field threading the NS will be anchored in the solid core (owing to flux freezing), and also frozen in to the differentially rotating fluid core. Thus the internal field becomes globally twisted and gains a toroidal component which stresses the crust from below. The crust will probably be able to respond elastically to this stress at first, but once a critical point is reached where the stress exceeds the elastic limit of the crust at some location, then the crust will fracture. The potential energy stored in the twisted field is thus catastrophically released and propagated to the external field. The crust therefore acts as a "gate" to the release of magnetic energy from the internal field, and the relatively small scale fracturing of the crust in this manner is a plausible mechanism for the production of the common SGR bursts.

Larger scale, possibly global, fracturing where an entire cap of crust may be rotated would bring regions of crust and external field of differing strength and orientation into contact creating huge field gradients. Enormous amounts of magnetic energy would then likely be released by magnetic reconnection, and it can be shown that the available magnetic energy is easily enough to power a giant flare similar to that from SGR 1900+14 (Thompson & Duncan 2001). Indeed it is possible that much larger giant flares could be produced (Eichler 2002) if entire hemispheres of the star were to rotate with respect to each other via the Flowers-Ruderman instability (Flowers & Ruderman 1977), resulting in the complete destruction of the external field of the magnetar in a single cataclysmic reconnection event.

Following the initial release of this magnetic energy and its conversion into the relativistic fireball (see section 1.8) responsible for the initial spike in the flare, the magnetar model predicts that some fraction of this fireball will remain trapped in a region close to the NS by its external field. It is the cooling of this trapped fireball, rotating with the NS, which is responsible for the pulsating tail of emission seen in the giant flares. Hence, knowing the energy $E_{\rm tail}$ of this trapped fireball from the observed emission, we can obtain a lower limit on the strength of the magnetic field, $B_{\rm dipole}$, required to confine this amount of energy within $\Delta R = 10$ km of the magnetar via Equation 1.2 (Thompson & Duncan 2001):

$$B_{\rm dipole} > 2 \times 10^{14} \left(\frac{E_{\rm tail}}{10^{44}{\rm erg}} \right)^{1/2} \times \left(\frac{\Delta R}{10 \text{ km}} \right)^{-3/2} \left[\frac{1 + \Delta R / R_{\rm magnetar}}{2} \right]^{3} \text{ G} \quad (1.2)$$

which for an energy of $1.2 \times 10^{44} d_{15}^2$ erg in the 2004 SGR 1806-20 flare (Hurley et al. 2005), gives $B_{\rm dipole} > 2 \times 10^{14} d_{15}$ erg, consistent with the measurement from the spindown period and further confirmation of the magnetar model.

1.2.2.2 Location

It is often argued that due to their formation in a fraction of core collapse supernovae, and relatively short lifetimes $\sim 10^4$ years (e.g. Kouveliotou 1999), that magnetars should trace regions of massive star formation. That is, they should be found only in regions of high star formation in relatively young galaxies. The association of the Galactic magnetars with supernova remnants and their location in the Galactic plane would seem to support this view in the Milky Way. Therefore they would not be expected to be candidates for any S-GRBs associated with older, elliptical galaxies with little or no star formation.

However, given that magnetars may form due to the AIC of a WD, possibly in a relatively long-lived double degenerate binary, then the association of SGRs only with regions of high star formation may not be the whole story. For example, using the observed numbers of magnetic WDs referred to in the section above and predicted merger rates from population synthesis models (Nelemans et al. 2001), we were able to show that the rate of production of magnetars via WD-WD mergers ($3 \times 10^{-4} {\rm yr}^{-1}$) may be comparable to that via core collapse supernovae (4×10^{-4} yr^{-1}) in a galaxy such as the Milky Way (Levan et al. 2006b). Thus in an early-type galaxy with SFR only ~ 0.1 M$_\odot$ yr^{-1} the rate of magnetar formation due to core collapse would be expected to be only 1×10^{-5} yr^{-1} whereas the rate due to WD-WD merger would be unchanged at 3×10^{-4} yr^{-1}. It is therefore possible that SGRs and SGR giant flares may also be associated with older hosts as well.

Before moving on to discuss collapsars, we should note that magnetars have also been suggested as possible inner engines for long GRBs as well (Usov 1992). As mentioned above, it is likely that magnetars are born rotating rapidly with periods ~ 1 ms or less and hence their available rotational energy is $\gtrsim 10^{51}$ erg. The nascent magnetar will then spin down rapidly, releasing this energy over the timescale of a L-GRB via magnetic braking. If formed via AIC of a WD, or the collapse of a WD-WD binary, then a supernova is not expected. It has therefore been suggested that bursts such as GRB 060614 with short duration initial emission, followed by a long extended emission period may well be powered by proto-magnetars (Ramirez-Ruiz 2004; Metzger, Quataert & Thompson 2008; Bucciantini et al. 2008). The initial

prompt emission results from a short accretion phase on to the new born NS, and the extended emission is powered by the spindown of the magnetar (Metzger, Quataert & Thompson 2008). Magnetars may also power lower luminosity L-GRBs (e.g. Soderberg et al. 2006b), and be candidates for explaining the late time activity of some GRB light curves (Fan & Xu 2006; Troja et al. 2007).

1.2.3 Collapsars: the Supernova Connection

The first hard evidence for the association of long GRBs with supernovae (SNe) came with the close temporal and spatial coincidence of the long burst GRB 980425 with supernova SN1998bw (Galama et al. 1998; Kulkarni et al. 1998b). Unfortunately, both these objects were somewhat unusual - GRB 980425 if truly associated with SN1998bw was 3 orders of magnitude under-energetic compared to most long duration bursts, and conversely, SN1998bw was extremely bright compared to most supernovae. Nevertheless, the association of L-GRBs with supernovae appeared promising, and in 2003 GRB 030329 was unambiguously identified with SN2003dh (Hjorth et al. 2003; Stanek et al. 2003). The evolution of the spectrum of GRB 030329, clearly showing the development of the SN spectrum is shown in Figure 1.7. 2003 was to prove a bumper year for GRB-SNe association with the observation of GRB 031203, spectroscopically associated with SN 2003lw (Thomsen et al. 2004; Cobb et al. 2004; Soderberg et al. 2004). Several other GRB light curves have late time bumps which would appear to implicate an underlying rising SN (e.g. Bloom et al. 1999; Castro-Tirado & Gorosabel 1999; Lazzati et al. 2001; Gorosabel et al. 2005). For a comprehensive review of the GRB–SN connection and further references for these and other associations see Woosley & Bloom (2006). Further clear spectroscopic evidence for GRB–SN association was not to come until 2006 with GRB 060218, the second closest GRB observed so far after 980425, and its association with SN 2006aj (Cusumano et al. 2006; Mirabal & Halpern 2006; Pian et al. 2006). The properties of the three GRBs spectroscopically associated with SNe are comprehensively reviewed in Kaneko et al. (2007).

Further indirect evidence for the possible association of L-GRBs with SNe comes from the properties of their host galaxies, and their locations within these hosts. In particular, as mentioned above, the location of L-GRBs directly on host galaxies, and often on regions of high SFR within those galaxies, is evidence against a compact object binary merger progenitor since these are likely to be significantly displaced from their birthplace following the long delays before coalescence. No L-

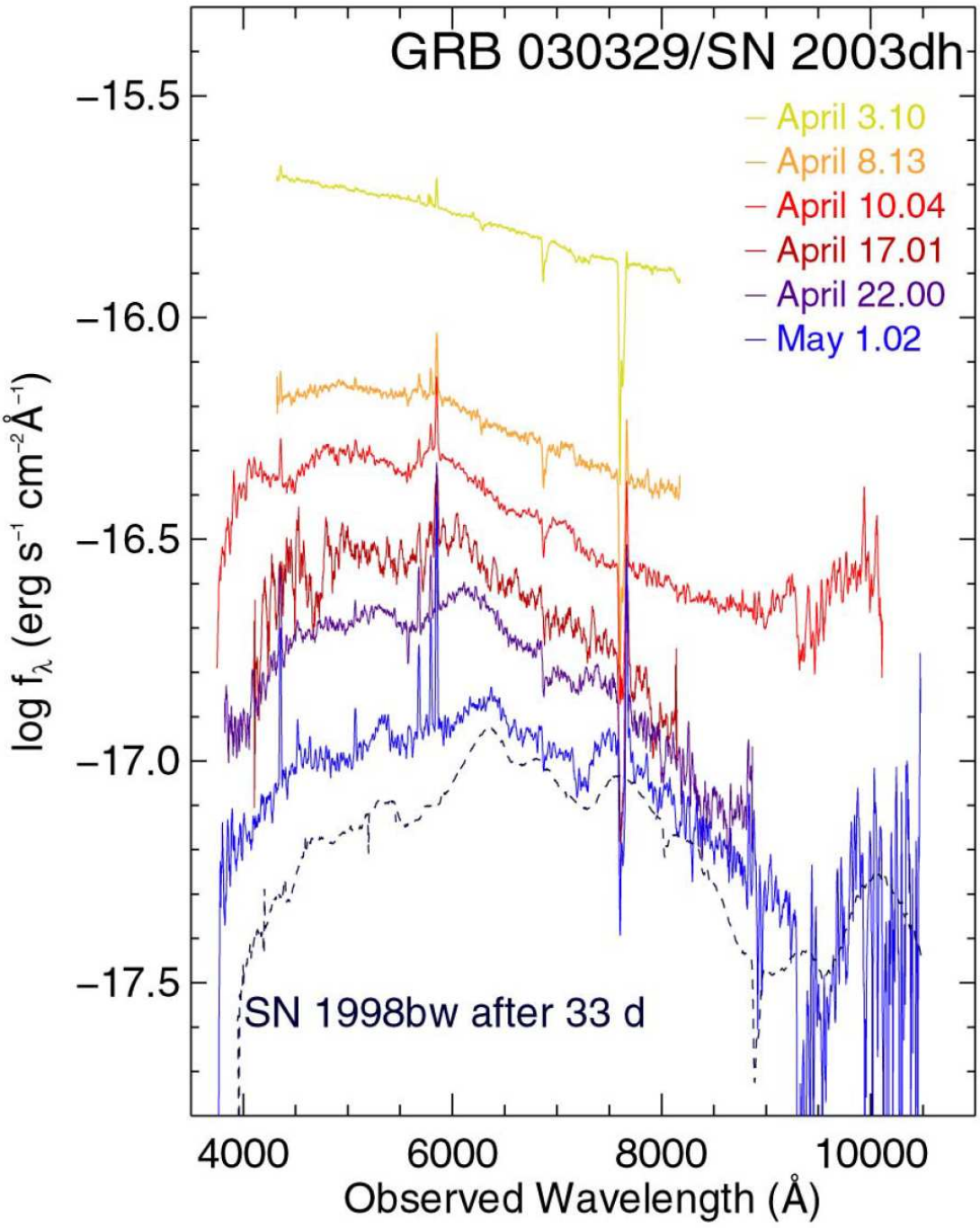

Figure 1.7: The evolution of the spectrum of GRB 030329, and its comparison to the spectrum of SN 1998bw after 33 days. From Figure 1 of Hjorth et al. (2003).

GRB has been associated with an early type galaxy, and their hosts in general are small, irregular, and highly star-forming (e.g. Fruchter et al. 1999; Sokolov et al. 2001; Le Floc'h et al. 2003; Christensen, Hjorth & Gorosabel 2004). Core collapse supernovae (cc-SNe) are the endpoints of the lives of massive ($> 8 - 10$ $M_\odot$) stars, and with these stars having short lifetimes ($\sim$ few Myr), cc-SNe are expected to be associated with regions of star formation. One may therefore expect L-GRBs to follow a similar distribution pattern. Fruchter et al. (2006) compared the distributions of cc-SNe and L-GRBs with respect to their type of host galaxy, and position within those hosts. They concluded that cc-SNe do indeed trace the blue light of their hosts, but L-GRBs tend to occur much more on the very brightest overall regions. Also, the hosts of the two populations show significant differences: while the hosts of cc-SNe are roughly equally split between spiral and irregular galaxies, the majority of L-GRB hosts are small and irregular (irrespective of redshift). Since galaxy mass and metallicity are known to be correlated (e.g. Kobulnicky & Kewley 2004), these results imply that L-GRBs are likely to be produced mostly by the most massive stars in regions of relatively low metallicity.

1.2.3.1 The Collapsar Model

For evolved stars with cores more massive than $\sim$ 8 $M_\odot$ (main sequence mass $\geq$ 25 $M_\odot$) formation of a black hole on collapse is probably inevitable (e.g. MacFadyen & Woosley 1999; Heger et al. 2003). Thus we have a situation similar to that described on the merger of two neutron stars in section 1.2.1, except that we now have a black hole formed inside a massive stellar envelope – this is the basis of the collapsar model for L-GRBs (Woosley 1993; MacFadyen & Woosley 1999). Once again, sufficient angular momentum must be present in the surrounding stellar material for an accretion disk to form if this model is to power a GRB. Therefore, it is presumed that the progenitor star must be fairly rapidly rotating, and the rotation rate (as well as the overall mass) of the collapsing star are strongly influenced by the mass loss rate during the star's evolution. All SNe associated with GRBs so far have been of type Ic, i.e. they show evidence for neither hydrogen nor helium in their optical spectra. Since the jets of the GRB are now produced from an accreting system within a massive star, they must somehow survive intact to blast their way through the surrounding stellar material, and thus it is expected that any potential GRB producing star must have previously lost its hydrogen envelope. It is therefore generally accepted that the progenitors of L-GRBs via the collapsar model are

massive Wolf Rayet (WR) stars.

However, special circumstances must still be required to make a GRB, since not all type Ic SNe are associated with GRBs. Even after correction for beaming is taken into account, the observed rate of L-GRBs is only a small fraction ($< 1\%$) of the Ic supernova rate (Woosley & Bloom 2006). The crucial ingredient responsible for GRB formation is thought to be rotation - the collapsing stellar material must have sufficient angular momentum to form an accretion disk surrounding the newly formed black hole (at least the angular momentum associated with the last stable orbit). Too much angular momentum however, and the disk may form too far out to dissipate its energy effectively and efficiently as neutrinos in order to power the burst (MacFadyen & Woosley 1999; Narayan, Piran & Kumar 2001; Lee & Ramirez-Ruiz 2006). As angular momentum is lost from the progenitor star via mass loss, the mass loss rate (particularly during the WR phase) is crucial to its ability to produce a GRB. Mass loss in WR stars is critically dependent on metallicity since the wind is absorption line driven, and therefore since the model requires low mass loss, L-GRBs formed by collapsars should favour low metallicity regions, as observed. The balance of sufficient but not too much angular momentum may be difficult to achieve in single star progenitors, and several authors suggest that mass loss due to a massive companion during helium burning may be the only way to keep the progenitor core rotating sufficiently (Narayan, Piran & Kumar 2001; Lee & Ramirez-Ruiz 2006). Examination of pre-explosion observations of the type Ic SN 2002ap failed to detect any progenitor object coincident with the position of the explosion, thus ruling out single massive star progenitors including the most luminous WR stars (Smartt et al. 2002). These observations are thus consistent with a binary origin for SN 2002ap, though the authors point out that the observations would have been sensitive to only the most luminous 30% of WR stars, and therefore a single WR progenitor could not be excluded. Interestingly, the binary scenario, as suggested by Paczynski (1998) was the first to coin the term "hypernova", which has now mostly been absorbed into the collapsar terminology. Ironically, the term hypernova obviously suggests an extremely energetic supernova, whereas the collapsar model was originally presented in terms of a "failed" supernova. The crucial ingredient in the production of a GRB is the conversion of sufficient energy to form an ultra-relativistic (and hence by implication relatively baryon free) jet as opposed to the kinetic energy dominated explosion of the star. It is now recognised that a broad spectrum of phenomena may be produced in this balance, from highly energetic supernovae with weak associated GRB through asymmetric jet driven SNe, to potentially failed explosions.

Broadly speaking, there are two possible classes of collapsar: *Type I* where the black hole forms promptly on collapse of the core, and *Type II* where a nascent neutron star forms a black hole following fallback of material after a supernova shock has been launched. Since the variability of the burst depends upon accretion dynamical timescales, whereas its overall length will depend on the feeding timescales of the disk, it is likely that *Type II* collapsars will produce much longer GRBs than *Type I*.

Until recently, it had become generally accepted that most, if not all long duration GRBs were associated with some kind of core collapse event of a massive star, coinciding with the production of a type Ic supernova under the collapsar paradigm. However the recent observations of GRB 060505 and GRB 060614, both classically long GRBs but with no accompanying supernova detected to very deep limits (Fynbo et al. 2006; Gal-Yam et al. 2006; Della Valle et al. 2006) raised several questions regarding both this association and the simple classification of GRBs into two categories based solely on duration. With regards to the SN association, any underlying supernova would have had to be dimmer not only than all previous GRB associated SNe, but dimmer than any SN Ic observed so far (Fynbo et al. 2006). With regards to GRB classifications, both bursts raised several interesting issues. GRB 060505 had a duration (T_{90}) of ~ 4 s, classically long but nevertheless close to the traditional long/short boundary (Figure 1.2 clearly shows that there must be significant overlap between short and long bursts, indeed Donaghy et al. (2006) suggest that the T_{90} at which a burst has equal probability of being long or short is ~ 5 s). Even though GRB 060614 had a nominal $T_{90} \sim 100$s, its spectral lag and peak luminosity (see section 1.4.3) place it clearly in the short burst region of a lag-luminosity plot (Gehrels et al. 2006). Both bursts were nearby compared to the majority of L-GRBs, and both had atypical host galaxies. It was suggested (particularly for 060614) that the host galaxy association may have been coincidence (Cobb et al. 2006a; Schaefer & Xiao 2006) and the burst therefore may have occurred at higher redshift (Schaefer & Xiao 2006), though other observational evidence such as the lack of absorption features in the afterglow spectrum (Fugazza et al. 2006) speak against this (Jakobsson & Fynbo 2007). All these conundra combined led to suggestions that a novel explosive process (Gal-Yam et al. 2006), or a new GRB classification scheme (Gehrels et al. 2006; Zhang et al. 2007) was needed including spectral lag, and possibly many more features, such as pulse width, light curve bumps, isotropic equivalent energy, host type and more (Donaghy et al. 2006). Though there might be some physical merit to these burst distinctions which we may eventually elucidate,

some (such as host type) being observational classifications, lead to chicken–and–egg type ambiguities and are not really very useful as they are not intrinsic observational properties of the burst. Perhaps as Jakobsson & Fynbo (2007) suggest, though these bursts call current paradigms into question, it is best to keep an open mind at the moment. Nevertheless, spectral lag is certainly being utilised more and more in the distinction between bursts, particularly at the earliest stages of observation.

1.3 The Burst Itself

1.3.1 The Fireball Model

Though the progenitors of GRBs (particularly those of short duration and to some extent the longs as well) may remain subject to debate, the actual mechanism for production of the burst itself (and associated afterglow) is generally accepted (for detailed reviews on GRB models, see Piran (2005); Zhang & Mészáros (2004); Piran (1999a,b); Mészáros (2002)). The basic fireball model was first proposed in 1978 (Cavallo & Rees 1978), and later developed to include internal and external shocks (Rees & Meszaros 1992, 1994).

The essential ingredients of this fireball internal/external shock model are summarised in Figure 1.8 and proceed as follows. A very large amount of energy ($\geq 10^{51}$ erg for L-GRBs) is deposited by the central engine in a relatively small ($\sim$ stellar) volume. This energy may come from the release of the gravitational binding energy of around a stellar mass of material in an accretion disk at the last stable orbit of a stellar black hole, probably via neutrino-neutrino annihilation; the extraction of rotational energy from the rotation of a central black hole via the Blandford-Znajek process (Blandford & Znajek 1977); or by cataclysmic magnetic reconnection on the surface of a magnetar. The release of this level of energy leads to the formation of an ultra-relativistic (Lorentz factor $\Gamma \sim 100$ or more) expanding gamma-ray and electron-positron pair plasma. In order for us to observe the spectrally non-thermal and yet highly variable (on ms timescales) radiation from this fireball, it must be highly relativistic to solve the "compactness problem". A naive calculation of the size of the emitting region as $c\delta t$ (where c is the speed of light and δt the variability timescale) otherwise leads to the conclusion that the fireball would be enormously optically thick to pair-production, leading to a thermal spectrum with obvious pair-annihilation features. Large Γ however changes this picture

in two ways: firstly the photon energy in the comoving frame is substantially reduced (we observe this radiation highly blue shifted) and the likely collision angles between photons substantially decreased owing to relativistic beaming; and secondly the physical size of the emitting region is increased by a factor Γ^2. In order that the optical depth of the plasma be reduced to ~ 1, $\Gamma \sim 100$ or greater is needed.

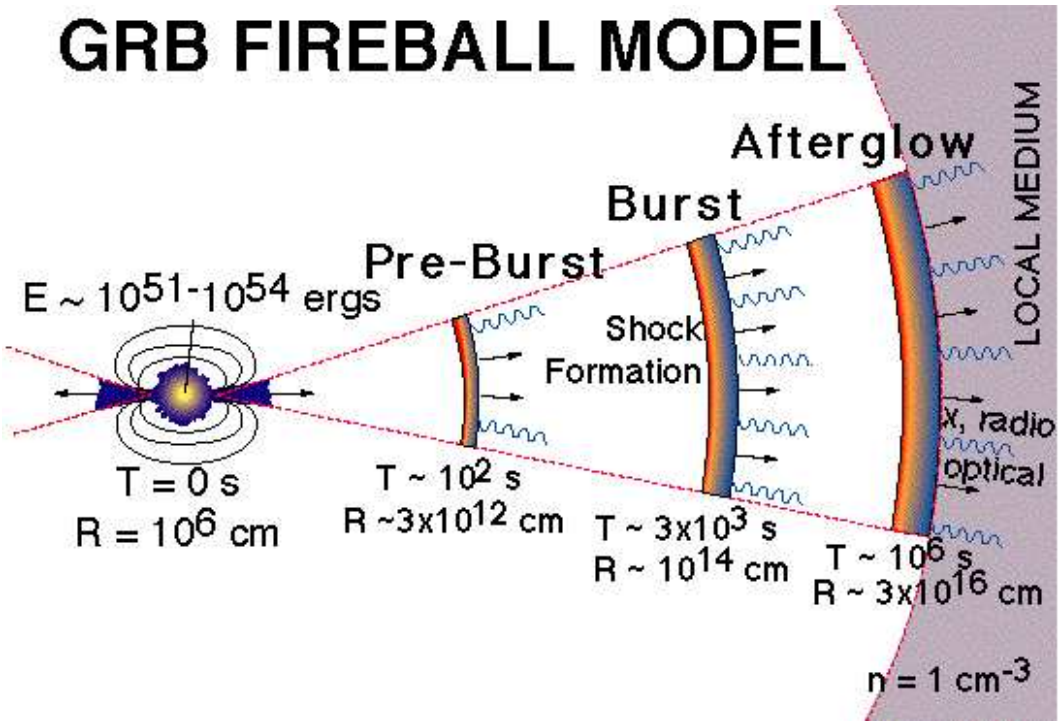

Figure 1.8: Cartoon of the GRB fireball model, from Ghisellini (2001).

To maintain this level of relativistic motion, the fireball must be very baryon-light. Thus, particularly in the collapsar and merger models, it is implied that the fireball must be launched as a jet through the evacuated polar regions of an accretion disk. This leads naturally to the idea that GRBs are substantially geometrically collimated into anti-parallel jets, which in turn reduces their overall energy requirement by the beaming factor (though obviously there must then be proportionally more GRBs in the Universe than we actually observe, owing to their beaming axes pointing away from us). In addition to geometrical beaming, the radiation we observe is relativistically beamed into an angle $1/\Gamma$, and these two collimation effects have observable consequences as discussed in section 1.3.2.

The release of this energy continues in a time-dependent manner according to the dynamical timescales of the accretion process, thus launching successive shells of plasma, with varying Lorentz factor which will necessarily collide with each other.

The internal relativistic shocks involved in these collisions are then believed to be the site of substantial particle acceleration leading to the emission of synchrotron radiation as the relativistic particles spiral around magnetic fields carried within the fireball – this is the source of the non-thermal prompt radiation associated with the burst itself, and various features of this spectrum are well explained by a self-absorbed synchrotron model (e.g. Sari, Piran & Narayan 1998), but we will not discuss these further here. The overall timescale of the burst is then controlled by how long the central engine remains active, which is presumably controlled (in the merger and collapsar models) by the amount of matter available to be accreted and thus provide an on-going energy source. This naturally suggests that merger models are only likely to be able to power S-GRBs, and in L-GRBs the length of the burst is controlled by the fallback timescale of the matter feeding the accretion disk.

Eventually, the fireball will run into the surrounding medium around the burst, and it is the external shocks produced as it ploughs into this medium that produce the optical afterglow. The fireball sweeps up surrounding matter and is therefore decelerated, and it thus serves as a probe of the surrounding medium and whether (for example) it is of constant density, clumpy, or wind-like (see for example Piran (2005) and references therein). In addition, as it is decelerated and its Lorentz factor falls, the angle into which the radiation is beamed increases and becomes comparable to the geometrical collimation angle leading to so-called 'jet breaks' which we discuss briefly below.

1.3.2 Jets and jet-breaks

The realisation that the outflow was probably collimated into some form of jet (Rhoads 1997, 1999) was key to both constraining the total energy budget of GRBs, and in helping to unify their nature. Once beaming is taken into account, the overall spread of total energy between bursts is greatly reduced (Bloom, Frail & Kulkarni 2003) and it becomes clear that (at least long) GRBs have a fairly standard energy reservoir of $\approx 10^{51}$ ergs, broadly equivalent to the energy release of a type II/Ibc supernova. In the supernova case, this energy appears mainly in the form of kinetic energy of the ejecta, whereas in a GRB it appears as the prompt emission of the burst. Observational evidence for beaming comes from achromatic 'jet breaks' in GRB light curves, where the decay of the light curve is seen to steepen at the same time across a broad range of frequencies. This is interpreted as happening when the emitting surface slows enough for the relativistic beaming angle to become compa-

rable to and then larger than the geometric beaming angle, and thus the observer sees an increase in the decay rate of the light curve. The jet opening angle can be calculated from the jet break time, measured isotropic equivalent energy and reasonable assumptions regarding the circumburst density and the efficiency of the fireball in producing gamma-rays (Sari, Piran & Halpern 1999). The measurement of jet breaks, jet angles, and beaming corrected energy output is vital to the investigation of GRBs as 'standard candles', and their use as cosmological probes, both in terms of distance indicators in a Hubble diagram (Amati et al. 2002; Ghirlanda, Ghisellini & Lazzati 2004), and as probes of the surrounding burst environment (Panaitescu & Kumar 2001).

It was hoped that many more jet breaks would be measured in the *Swift* era, however for the few bursts which have been able to be monitored simultaneously in the X-ray and optical bands, the optical light curves have not shown any steepening at the epoch of the X-ray break (Panaitescu et al. 2006). Thus the breaks measured appear to be chromatic, and not the achromatic signal expected from the simple jet model (Liang et al. 2008a). Chromatic breaks require evolving microphysical parameters (e.g. electron energy and magnetic field details) for explanation, and therefore it has been suggested that either the optical and X-ray emissions are produced in different regions of the GRB outflow, or that the afterglow emission is produced via interaction of the outflow with a freely expanding stellar wind, as opposed to a relatively homogeneous circumburst medium, which is inconsistent with previously measured optical breaks (Panaitescu et al. 2006). Later work on larger samples of *Swift* bursts indicate that the paucity of well established achromatic jet breaks may be due to insufficient data, both in depth and time spent monitoring the X-ray and optical afterglows (Racusin et al. 2008; Dai et al. 2007). It remains to be seen if further *Swift* bursts will exhibit the expected achromatic breaks.

1.4 Empirical relations from observed GRB properties

Several empirical relations or correlations between observed properties of the prompt gamma-ray emission of GRBs have been proposed and investigated. The most commonly involved properties in these relations are:

- E_p: The peak energy of a burst, defined as the peak of the νF_ν spectrum.
- E_{iso}: The isotropic equivalent energy of the burst – the total energy emitted if the burst is assumed to be spherically symmetric at known luminosity distance.
- E_γ: The collimation corrected energy of a burst with isotropic equivalent energy E_{iso} and jet opening angle, θ, determined from measurement of a jet break in the burst light curve. $E_\gamma = (1 - \cos\theta)E_{iso}$.
- L_p: Luminosity (peak) of the burst. Sometimes defined separately for different portions of the burst light curve.
- t_{lag}: Spectral lag, defined as the time of arrival difference between light curve features as observed in different spectral bands.
- The 'variability' of the burst: several definitions exist.

We briefly introduce and discuss some of the most well known relations which will feature later in this work (see Chapter 4 particularly) below.

1.4.1 $E_p - E_{iso}$: The Amati Relation

A correlation between E_p and E_{iso} was first suggested for 12 *Beppo-Sax* L-GRBs with known redshifts by Amati et al. (2002). This has since been updated to include HETE-2 bursts (Amati 2003; Lamb, Donaghy & Graziani 2004; Sakamoto et al. 2005) and *Swift* bursts (Amati 2006b,a). The correlation is a power law of slope m and normalisation K such that $E_p = K \times E_{iso}^m$ for long duration GRBs. S-GRBs (though very much a limited sample in terms of definite redshifts at the moment) do not follow the relationship. An up to date (as at time of writing) sample is shown in Figure 1.9.

The correlation extends over $\sim$ four orders of magnitude in E_{iso}, but there are significant outliers, particularly GRB 980425 and GRB 031203. Interestingly these are two of the closest 3 GRBs to date, both with well established supernova associations. The second closest burst, GRB 060218 is apparently consistent with the relation (Ghirlanda & Ghisellini 2007).

Neither this relationship, nor the Ghirlanda relationship below (section 1.4.2), is without controversy. Based on trajectories of bursts with varying redshift in the $E_p - E_{iso}$ plane, Nakar & Piran (2005) propose that a significant fraction ($\sim 25\%$)

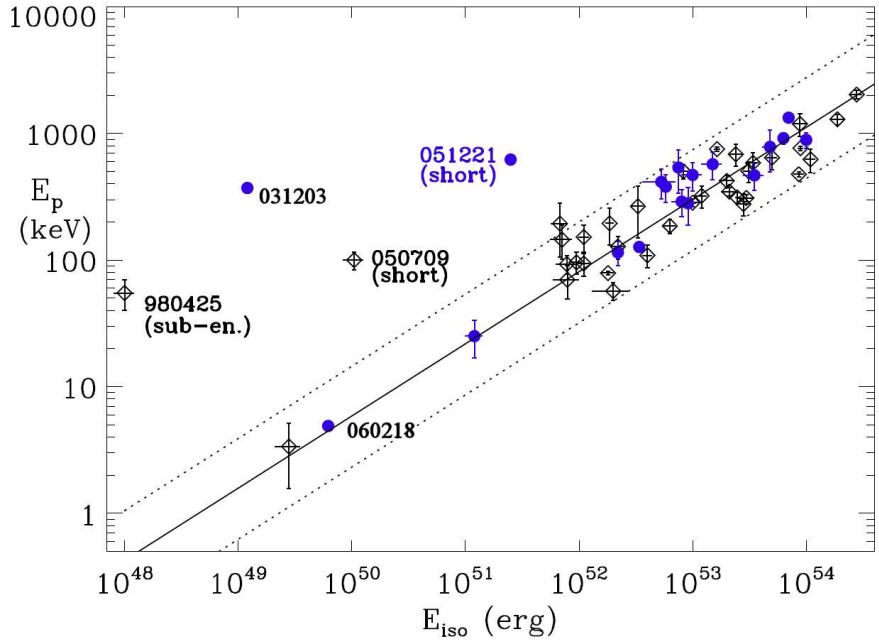

Figure 1.9: The Amati relation for 51 L-GRBs, two S-GRBs and the outlying GRBs 980425 and 031203. *Swift* GRBs are shown as filled circles, and the dashed lines represent 2σ confidence limits for the best fit power law as shown. After Figure 3 of Amati (2006a).

of all BATSE bursts (regardless of redshift knowledge), cannot satisfy the Amati relationship no matter what their redshift. They suggest that the fact there appear fewer outliers than this amongst the current samples with observed redshift is the result of an observational selection effect. Butler, Kocevski & Bloom (2008) also argue that selection effects are dominant in the $E_p - E_{iso}$ relation. Building on the work of Butler et al. (2007) (who found the $E_p - E_{iso}$ relation in 77 *Swift* bursts to be inconsistent with the pre-*Swift* relation), they find both the pre– and post–*Swift* relations to be strongly influenced, if not caused by, instrumental threshold effects in the observer frame.

1.4.2 $E_p - E_\gamma$: The Ghirlanda Relation

In 2004, Ghirlanda, Ghisellini & Lazzati (2004) demonstrated a correlation between the collimation corrected burst energy, E_γ and E_p. This correlation has the attraction of being, in theory, more physical than the Amati relation since by incorporating the beaming factor, it is utilising the true energy of the burst (under the assumption of a uniform jet and a constant density circumburst medium). Unfortunately, it is

therefore dependent not only on redshift observations being available for the burst sample, but also jet break measurements which necessarily require extensive monitoring campaigns across multiple wavebands. A comparison between the Ghirlanda and Amati relations is shown in Figure 1.10.

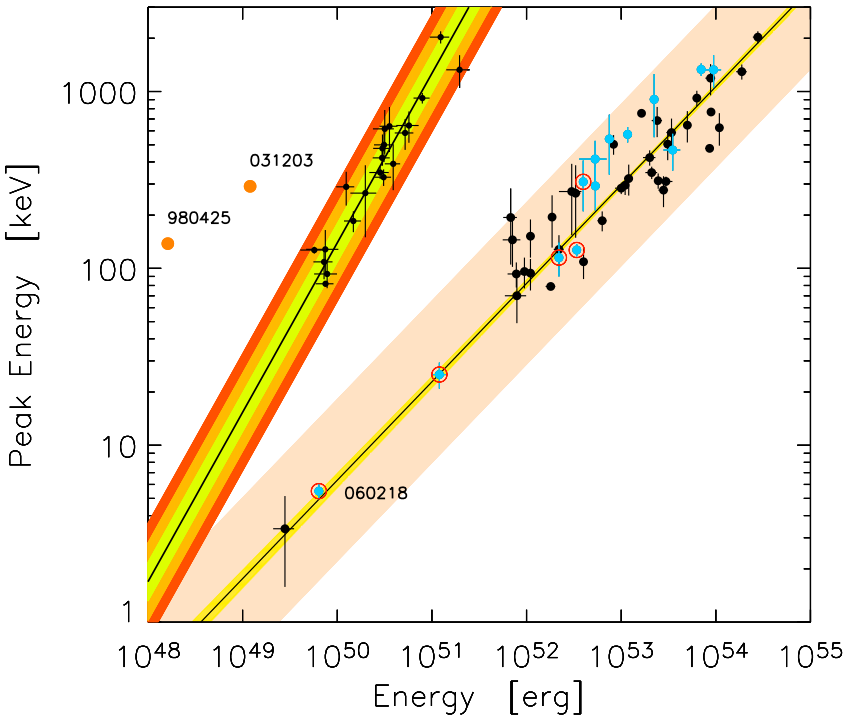

Figure 1.10: The Ghirlanda and Amati relations. The Ghirlanda relation is the steeper relation on the left (c.f. Figure 1.9). From Figure 1 of Ghirlanda & Ghisellini (2007).

Since its discovery, attempts have been made to use this (and other) relations for cosmography (e.g. Amati et al. 2008; Liang et al. 2008b; Avila-Reese et al. 2008; Ghirlanda et al. 2005, 2004) in order to extend the Hubble diagram beyond the $z \sim 1$ limit of Type Ia supernovae and place constraints upon cosmological models and parameters. Though promising, there are many problems with these approaches, most significantly those of circularity (in general a cosmological model must be assumed in order to arrive at the redshift of the bursts), the lack of an underlying physical explanation of the relationships, and the paucity of low redshift bursts to calibrate the relationships (e.g. Friedman & Bloom 2005a,b). It should be noted that these problems are in addition to the selection effect type criticisms discussed above.

1.4.3 $t_{lag} - L_p$: Lag–luminosity Relations

Norris, Marani & Bonnell (2000) first reported a spectral lag–luminosity relation in BATSE long GRBs in 2000. They found an anti-correlation between luminosity and the cross-correlation function peak lags between temporal pulses in different BATSE energy channels, and also noted a similar anti-correlation between spectral hardness and luminosity amongst the 174 brightest bursts in their sample. That is to say, spectrally softer bursts tended to have longer lags. Furthermore, GRBs with long spectral lags also tended to have smoother light curves with broader features, and lower peak fluxes (Norris, Scargle & Bonnell 2001). In addition, the proportion of long lag bursts increased from negligible amongst bright BATSE bursts to around 50% near threshold (Norris 2002), and the bursts with longest lags showed a concentration of distribution on the sky towards the supergalactic plane (Norris 2002), indicative of the fact that they may be associated with relatively nearby extragalactic structure.

Recently Gehrels et al. (2006) included short bursts in an updated lag–luminosity plot including many *Swift* GRBs as shown in Figure 1.11. Two features of major interest stand out in this plot. Firstly, short GRBs are seen to cluster in a region of near zero spectral lag, well away from the L-GRB correlation line. Secondly, 3 of the 4 bursts with associated SNe (all under-luminous GRBs) fall well below the L-GRB correlation line, but are also separated from the S-GRBs. In addition, GRB 060614 (one of the two recent problematic GRBs as discussed in section 1.2.3) despite having a classically long duration, displays a spectral lag which places it in the short region of the plot leading to the possibility that it may have been a short burst with extended emission.

The clear separation of the two classic GRB categories in a lag–luminosity plot has led to spectral lag being increasingly used as an additional criterion to T_{90} for the classification of bursts, particularly early after detection, and is now being calculated and publicised as part of the *Swift* alerts.

1.4.4 Variability and Luminosity

As noted qualitatively by several of the lag–luminosity studies above, light curve variability also seems to correlate with luminosity in the sense that brighter bursts tend to have more obvious variability. A complex quantitative measure of light curve variability was found to correlate with burst luminosity, originally for a relatively

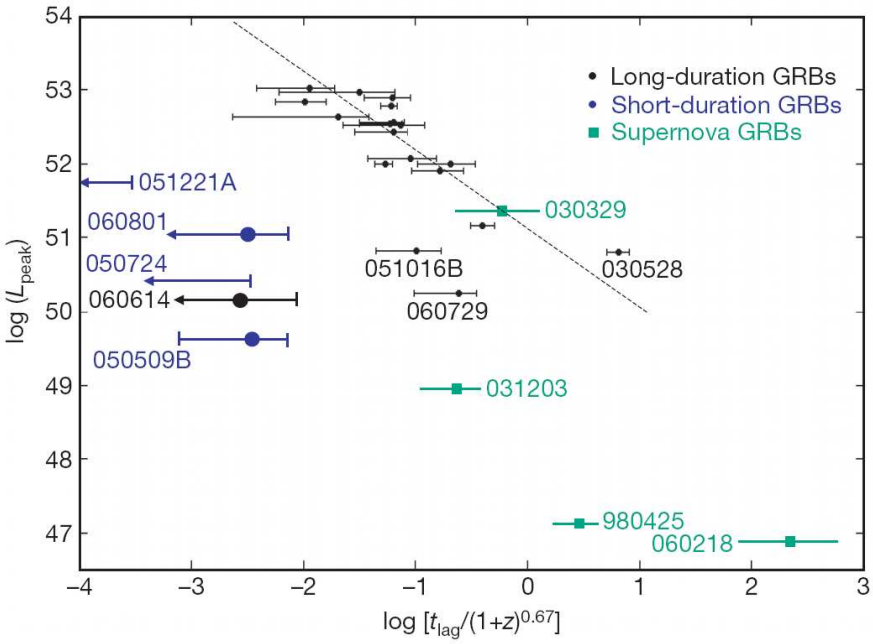

Figure 1.11: Lag-luminosity plot for long and short GRBs, from Figure 2 of Gehrels et al. (2006).

small number of bursts (Reichart et al. 2001; Fenimore & Ramirez-Ruiz 2000) and then confirmed (Guidorzi et al. 2005) for a larger sample, though with a larger scatter in the data. Li & Paczyński (2006) used a different measure of light curve variability and claimed to find a tighter correlation with luminosity than Guidorzi et al. (2005) in an overlapping but not identical sample of bursts. Though the exact form and tightness of the correlation is therefore somewhat a matter of debate (Reichart & Nysewander 2005; Guidorzi et al. 2006; Li & Paczyński 2006), there appears little doubt that the luminosity of long GRBs correlates with variability, certainly in a qualitative sense. In particular, low luminosity bursts such as the three closest GRBs to date (GRBs 980425, 060218 and 031203) tend to be single-peaked, low variability events (see Figure 4.1 in Chapter 4).

1.5 Implications for nearby GRB populations: the structure of this thesis

The fact that short GRBs are a separate population in all the empirical relations is at least supportive evidence that this classical division of GRBs into short and long duration categories is likely to be intrinsically real in some sense, and not merely an

observational artefact of instrumental threshold or selection effects of some kind.

With regards to the short GRBs, there exist two viable progenitor models with significantly different luminosities: compact object mergers and the giant flares from Soft Gamma Repeaters. This implies that, observationally, we may be able to distinguish these populations in terms of their redshift distributions - the lower luminosity SGR giant flares will not be observable as far away as the merger produced S-GRBs. Given that only very few S-GRBs so far have reliable redshift measurements, how can we investigate this? In Chapter 2 we compare the distribution on the sky of BATSE short GRBs with local galaxy populations at varying distances from us in order to estimate what fraction of these bursts may originate in the local Universe. Given that some fraction of nearby events exists, we then move on in Chapter 3 to investigate plausible Luminosity Functions for the two viable S-GRB progenitors in order to compare the predictions of single or dual populations in explaining the observed distribution.

As early as 1998, shortly following the observation of GRB 980425 and its proposed association with SN 1998bw, Bloom et al. (1998) suggested that all SN associated GRBs may have certain similarities, including a simple single-peaked light curve structure. The three closest GRBs observed to date are all associated with SNe, and all have smooth, single-peaked light curves. In addition, these bursts were under-luminous and spectrally soft (even if inconsistent with relations such as the Amati relation in the sense of being spectrally harder than expected, GRBs 980425 and 031203 were still softer than the vast majority of BATSE bursts). Therefore in Chapter 4 we use these common features of light curve shape, spectral softness and low-luminosity to select subsets of BATSE L-GRBs to investigate their possible associations with nearby galaxies.

The situation is not as clear cut for L-GRBs as for S-GRBs in terms of different possible progenitor models, and therefore we do not have distinct theoretical expectations for the intrinsic rates of separate plausible progenitor populations. However, we do have observational limits based on the abundance and properties of at least 3 known local bursts, and we can use these limits, as well as limits from previous analyses in the literature, to attempt the same sort of 'bottom up' luminosity function modelling as for the shorts. In Chapter 5 we investigate whether a nearby population of L-GRBs at the level implied by the correlation results of Chapter 4 can be produced by the low luminosity tail of a single luminosity function, or whether a separate, low luminosity L-GRB population is required.

Finally in Chapter 6 we indicate the likely consequences of the results found in this work, and speculate on the possible findings of future missions with regards to local GRBs.

Chapter 2

Nearby Short GRBs

2.1 Short Burst Progenitors

The vast majority of our information regarding GRBs comes from the long duration bursts and analyses of their afterglows, associated supernovae (if detected), and hosts. Until recently, no afterglow or host had ever been detected for a short duration burst, primarily due to imprecise localisation of bursts by missions such as BATSE. One of the great hopes for the *Swift* mission was that it would change this situation completely, and indeed in the last 3 years, afterglows and putative hosts have now been identified for about a dozen short duration bursts detected by both *Swift* and *HETE-II* (see for example Berger (2007) and references therein). The redshift distribution of the *Swift* detected S-GRB sample including the two most recently localised short bursts, GRB 070714B (Graham et al. 2007) and GRB 071227 (D'Avanzo et al. 2007), will be discussed further in Chapter 3.

The main candidate progenitor model for short duration GRBs is that of compact object (neutron stars or black holes) mergers (Paczynski 1986; Eichler et al. 1989; Rosswog 2005). It is also possible that giant or 'hypergiant' flares from Soft Gamma Repeaters (SGRs) such as SGR1806-20 (Hurley et al. 2005) could be observed extragalactically as S-GRBs. SGRs are thought to be magnetars (Woods & Thompson 2004; Eichler 2002), neutron stars with extreme magnetic fields $\sim 10^{15}$ Gauss, which can produce giant flares through the reconfiguration of this field (Eichler 2002; Woods & Thompson 2004). Magnetars have relatively short lifetimes ($\sim 10^4$ years) (Kouveliotou 1999; Woods & Thompson 2004), and hence are expected to exist primarily in galactic regions of relatively high Star Formation Rate (SFR), though it has been suggested (Usov 1992; King, Pringle & Wickramasinghe

2001; Levan et al. 2006b) that white dwarf mergers can produce magnetars, and thus given the relatively long merger timescale of white dwarf (WD) binary systems ($\sim 10^6$–10^8 years depending on their separation distance) could possibly still exist in regions of low SFR. Indeed in Levan et al. (2006b) we demonstrated that this Accretion Induced Collapse (AIC) formation channel for S-GRBs produced from WD binaries could facilitate a magnetar formation rate comparable to that inferred from core collapse. Compact object binaries have even longer lifetimes (governed by the loss of energy by gravitational radiation) of ≈ 1 Gyr (Taylor & Weisberg 1982), and hence could easily exist in regions with little or no star formation remaining. They may also receive substantial kicks at birth, via anisotropies in mass loss, magnetic winds, neutrino emission or non-axisymmetric gravitational radiation instabilities (Duncan & Thompson 1992), leading to their likely displacement outside the main bulk of the host galaxy.

It is estimated that the initial spike of the giant flare from SGR 1806-20 on December 27th 2004 would have been visible to BATSE as a short GRB out to $30d_{15}$–$50d_{15}$ Mpc (Hurley et al. 2005; Palmer et al. 2005; Taylor & Granot 2006; Nakar 2007) where d_{15} is the distance to SGR 1806-20 in units of 15 kpc. Having seen one such Galactic flare in only ~ 30 years of observation, estimates of the fraction of BATSE S-GRBs that may have been due to similar extragalactic giant flares (Hurley et al. 2005; Palmer et al. 2005; Dar 2005) ranged as high as $\sim 50\%$ or more. However, searches for candidate hosts of short GRBs by examining the individual error boxes of the best localised bursts placed upper limits on the possible fraction of BATSE S-GRBs from a few % (Popov & Stern 2006) to $\lesssim 40\%$ (Nakar et al. 2006, 95% confidence limits). Specifically, Popov & Stern (2006) calculate that the rate of SGR flares similar or greater in energy output to the SGR 1806-20 event should be less than 10^{-3} yr^{-1} per galaxy of SFR similar to the Milky Way based on only 2-5 BATSE S-GRB being consistent with arising from the Virgo cluster. Therefore, given estimates of the SFR within 50 Mpc, BATSE should have observed only about 30 extragalactic flares in its lifetime ($\sim 4\%$ of the total BATSE S-GRB sample). This null detection limit depends on estimates of SFR both locally and within Virgo, and could easily be a factor of two larger. Lazzati, Ghirlanda & Ghisellini (2005) also claimed an upper limit of 4% (2σ confidence) based on extracting a subsample of BATSE short bursts with spectra compatible with giant flares from SGRs. However, their sample was limited to very bright bursts whose spectra could be well modelled, and the limit based on not detecting sufficient potential candidates within that sample compared to the predicted rate. This limit

is sensitive to the estimate of the total number of SGR flares visible to BATSE which depends on the cube of the estimated distance to SGR 1806-20. It now seems likely that this distance is almost half the original estimate of 15 kpc (Bibby et al. 2008), and this limit could therefore be much higher. Nakar et al. (2006) searched the error boxes of six well localised S-GRBs for likely nearby host galaxies, and by assuming S-GRBs to be associated with regions of high SFR, the observed luminosities (and derived SFRs) of putative hosts enabled them to place lower limits on the distances to, and therefore isotropic equivalent energy releases of, the bursts. Finding all six bursts to be at least 2 orders of magnitude more energetic than the SGR 1806-20 event, they suggest that less than 15% of BATSE S-GRBs were extragalactic SGR flares ($< 40\%$ at 95% confidence). They suggest four possible conclusions:

1. The S-GRB population is composed of two unrelated observable phenomena, one local and one cosmological
2. Some SGR giant flares are (perhaps substantially) more energetic than the 2004 SGR 1806-20 event
3. The SGR 1806-20 giant flare was an unlikely event, and the true rate per SGR of such events is lower than 1 per 30 years
4. The distance to SGR 1806-20 was overestimated at 15 kpc and is more likely to be around 6 kpc

With regards to the last point, as we have seen there is now evidence that the distance to SGR 1806-20 may have been overestimated (Bibby et al. 2008). With regards to the other options, instead of concentrating on small samples of bursts or potential hosts, is it possible that there is a statistical signature in the entire collection of known short bursts in the BATSE catalogue that may shed light on these alternatives and the rate of any nearby S-GRBs? By attempting to answer this question in this Chapter and the next, we present evidence for option 1 where the local population is naturally explained as being due to extragalactic SGR giant flares. Furthermore, by considering plausible Luminosity Functions for this local population, the luminosity of the SGR 1806-20 event is seen as part of a continuous distribution of giant flare luminosities consistent with options 2 and 3 as well.

2.2 Statistical approaches

The question of the isotropic (or not) distribution of GRBs on the sky was a major factor in the debate during the 1990s as to whether GRBs had galactic (e.g. Lamb 1995) or cosmological (e.g. Paczynski 1995) origins. Consequently, early studies of burst distributions on the sky were concerned with the search for large scale anisotropy as measured, for example, by dipole and quadrupole moments in the celestial distributions (e.g. Quashnock & Lamb 1993a; Briggs et al. 1996). Though these statistics are sensitive to concentrations of bursts towards some particular direction (e.g. galactic poles or centre) or plane (e.g. the galactic or super-galactic plane), they are not particularly sensitive to anisotropy on a smaller scale, such as produced by correlations with other large scale distributions on the sky. Early claims for anisotropy in GRB distribution (Quashnock & Lamb 1993a) were also based (necessarily) on the limited number of observed bursts, and classification schemes such as a burst's variability on different timescales (Lamb, Graziani & Smith 1993) which have not stood the test of time. Large scale anisotropy for GRBs as a whole was first questioned (Rutledge & Lewin 1993), and then ruled out (for both the whole burst population, and a multitude of subsets) as the number of BATSE results grew (Briggs et al. 1996).

Searches were also carried out for smaller scale anisotropies, but mostly via auto-correlation methods to look for burst repetition. Some claims were made for the possible repetition of GRBs (Quashnock & Lamb 1993b; Wang & Lingenfelter 1995; Lamb & Quashnock 1995; Gorosabel et al. 1998), but once again these were refuted with larger data samples (Meegan et al. 1996; Tegmark et al. 1996). Correlations of GRBs with clusters of galaxies (Cohen, Kolatt & Piran 1994; Kolatt & Piran 1996; Struble & Rood 1997) and radio-quiet quasars (Schartel, Andernach & Greiner 1997) were also reported. Once again, these correlations were either questioned (Marani et al. 1997) or challenged by different samples (Gorosabel & Castro-Tirado 1997), and then later refuted by improved localisations of the burst samples (Hurley et al. 1999b).

With the benefit of hindsight, there is one obvious shortcoming of these previous correlation analyses - the majority did not attempt to split the burst sample by duration into short and long bursts, despite the discovery in 1993 of this relatively clear classification in the BATSE data (Kouveliotou et al. 1993). It is of (at least) historical interest to note that in what appears to be an early version preprint of their later work, Cohen, Kolatt & Piran (1994) find evidence for increased corre-

lation with Abell clusters among short duration bursts, but this conclusion is only obliquely referred to in the final published version (Kolatt & Piran 1996). Without splitting by duration, then any burst sample will be dominated by L-GRBs (which form $75-80\%$ of the BATSE sample for example), and as we shall see below and in more detail in Chapter 4, these as a whole exhibit virtually no correlation with nearby structure.

In the first (to our knowledge) study of the correlation properties of the S-GRB class alone, Magliocchetti, Ghirlanda & Celotti (2003) found evidence for autocorrelation between S-GRBs at the $2^\circ-4^\circ$ scale, which they interpreted as either burst repetition or a correlation with underlying large scale structure, but could not distinguish between these two possibilities[1]. If the latter, then they concluded that this was possible evidence that S-GRBs were hosted by relatively nearby ($z \lesssim 0.5$) galaxies. Below we present the results of our work based on the correlation with galaxies within even smaller redshifts, and will demonstrate that a significant fraction of S-GRBs appear to originate within the very local Universe ($\lesssim 155$ Mpc).

2.2.1 The Cross-correlation Function

In order to investigate whether any correlation could be detected between short bursts and galaxies within the local universe, we chose to compare the collection of all 400 short bursts in the 4B(R) BATSE catalogue (Paciesas et al. (1999) together with web supplement cited therein) localised to within a 10° (statistical) error circle with galaxies in the PSCz galaxy redshift survey (Saunders et al. 2000). This catalogue is based on the *IRAS* Point Source catalogue, and is less affected by dust extinction in the galactic plane (with sky coverage of 84%) than other redshift surveys, making it an appropriate comparison dataset for the all-sky BATSE dataset.

Subsets of galaxies within four concentric spheres of heliocentric recession velocity (2000, 5000, 8000 and 11000 km s^{-1}) were extracted from the PSCz. Distributions of these galaxies on the sky are shown in Galactic coordinates in Figures 2.1 to 2.4, together with overlays showing the distribution of our BATSE S-GRB sample, including their individual 68% confidence statistical error circles. For illustrative purposes, a set of pseudo-bursts generated with 10% having arisen from galaxies within the closest of our considered spheres is also shown in Figure 2.5.

[1]There is also evidence that the very shortest GRBs (duration $\lesssim 100$ ms) exhibit large scale anisotropy, which has been interpreted as possible evidence of a Galactic origin for these extremely short bursts (Cline, Matthey & Otwinowski 2000, 2001, 2003; Cline et al. 2005).

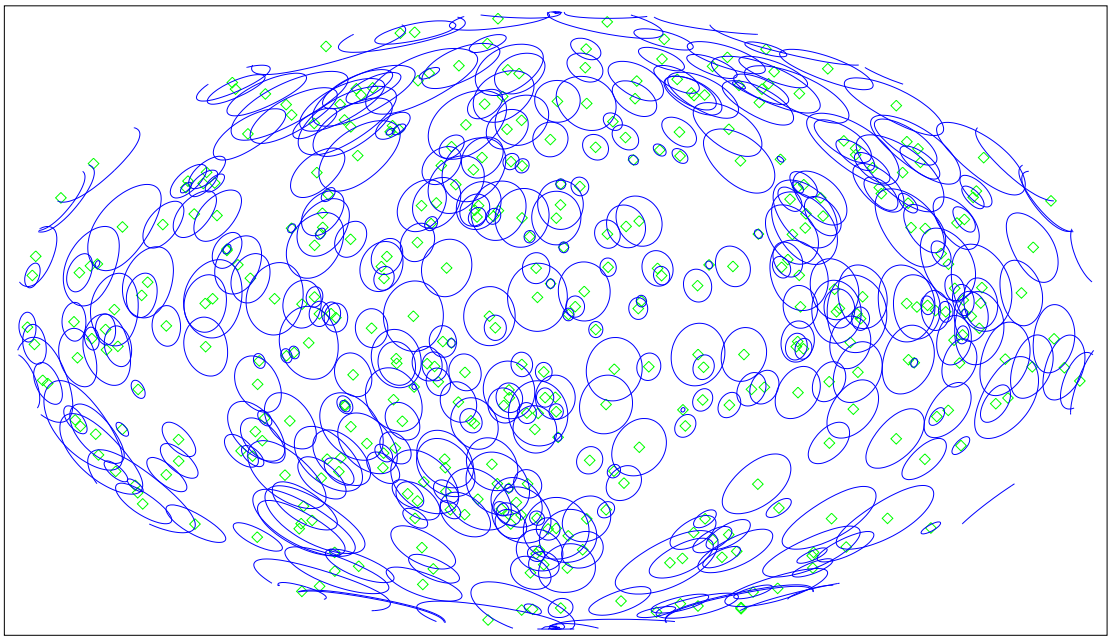

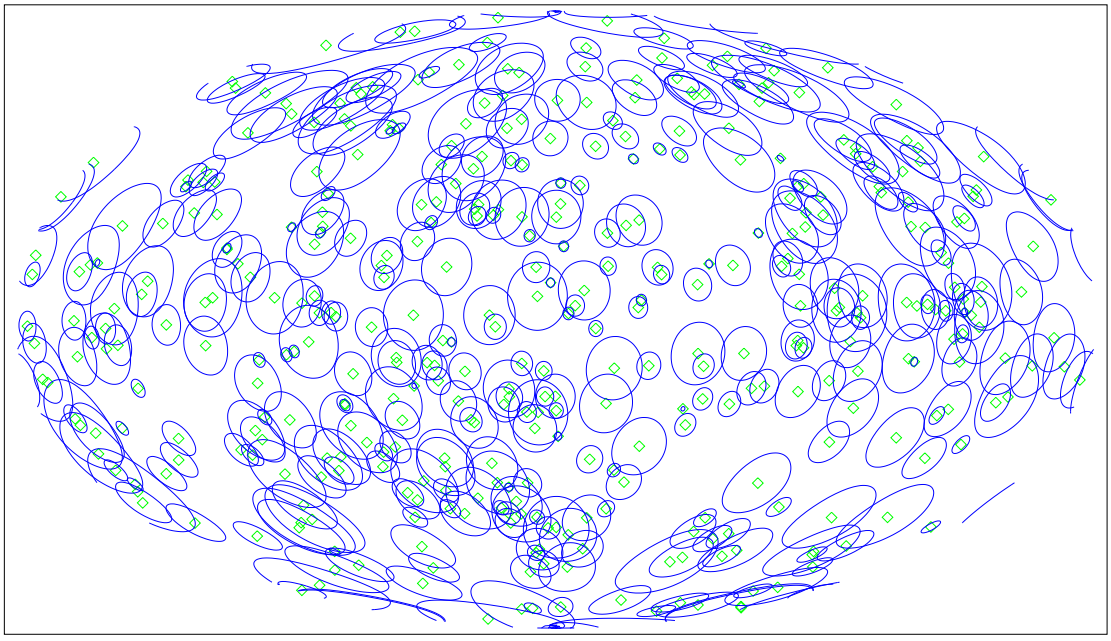

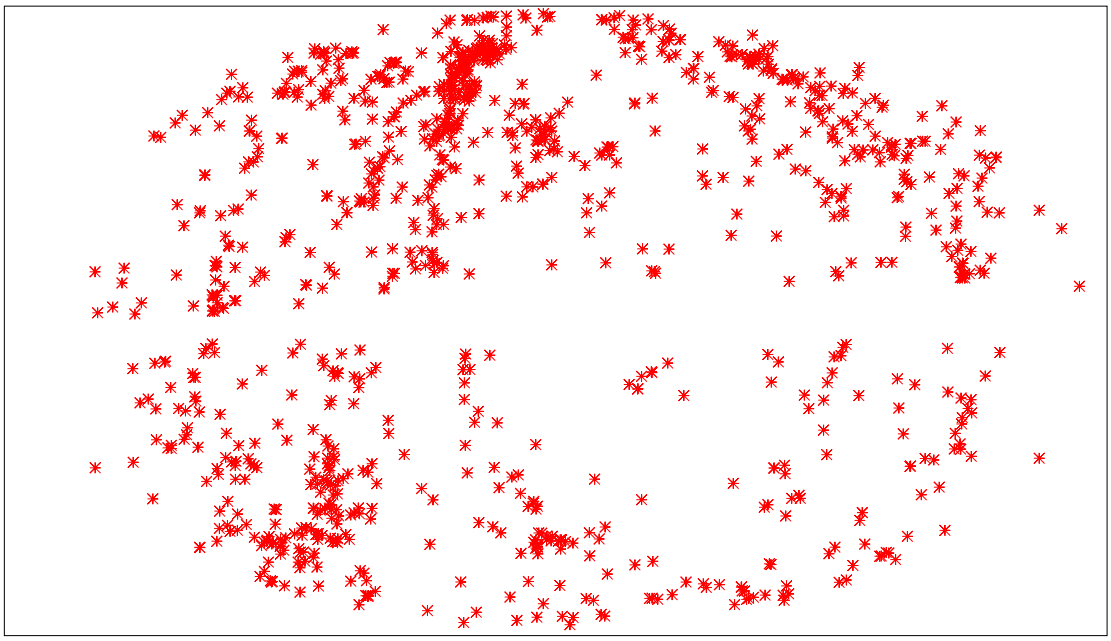

Figure 2.1: All sky Aitoff plot in Galactic coordinates (centred on (l,b)=(0,0)) of PSCz galaxies within $v \leq 2000$ km s^{-1}. Overlay shows BATSE S-GRBs as green diamonds with blue circles showing 1σ statistical errors.

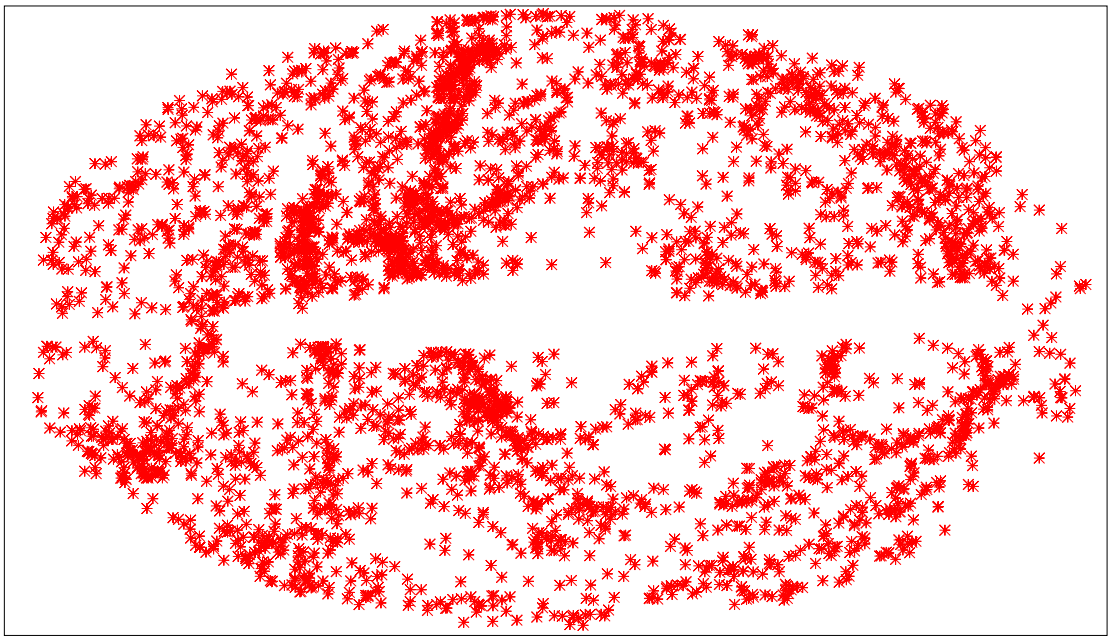

Figure 2.2: All sky Aitoff plot in Galactic coordinates (centred on (l,b)=(0,0)) of PSCz galaxies within $v \leq 5000$ km s^{-1}. Overlay shows BATSE S-GRBs as green diamonds with blue circles showing 1σ statistical errors.

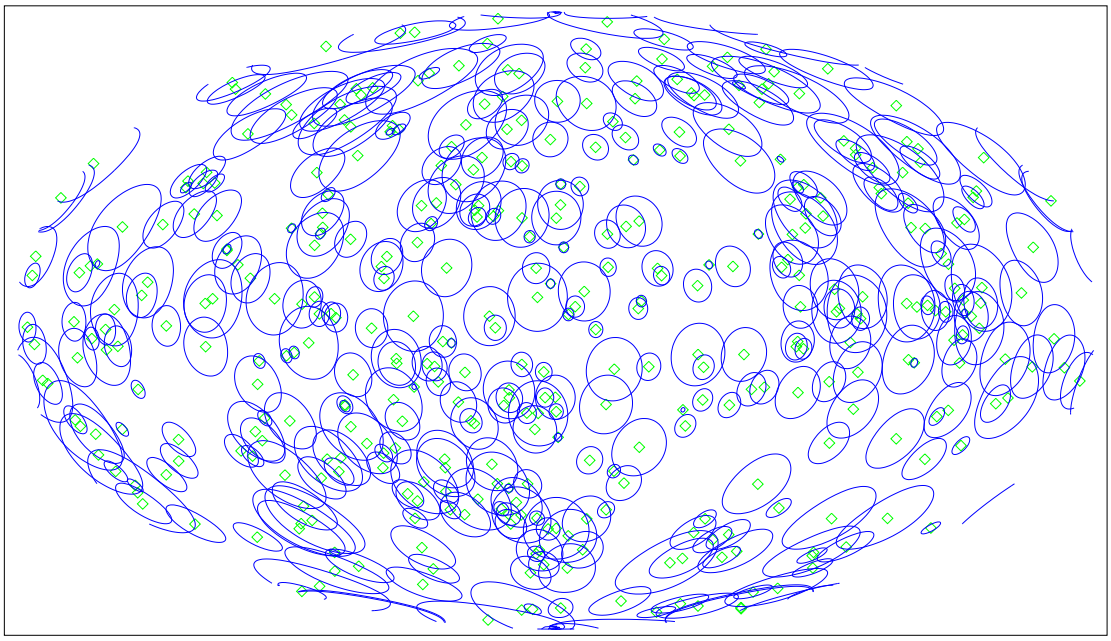

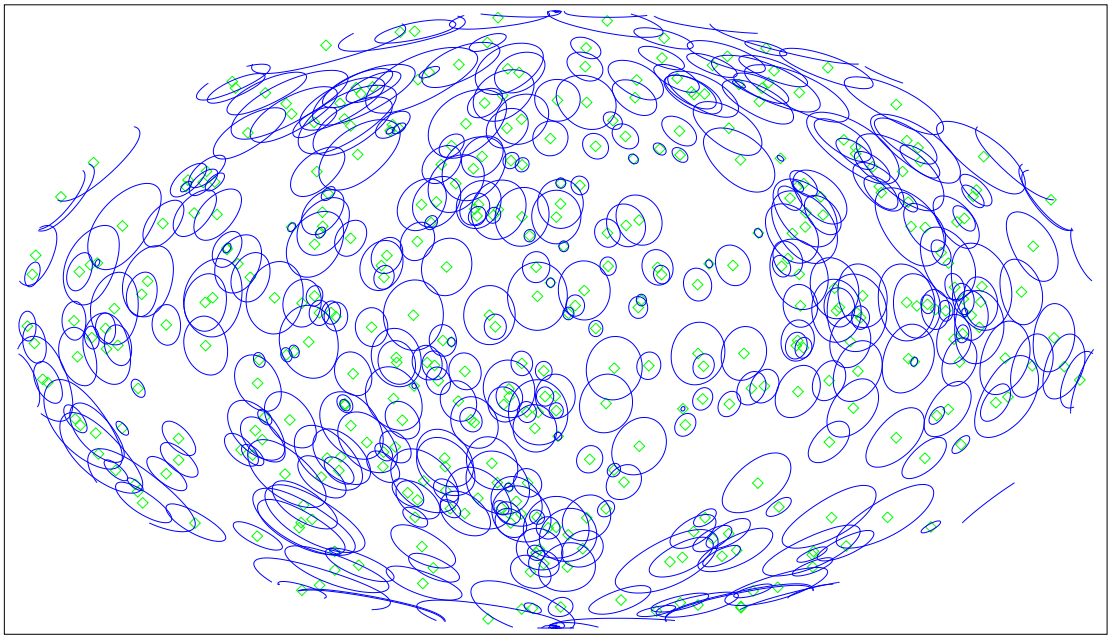

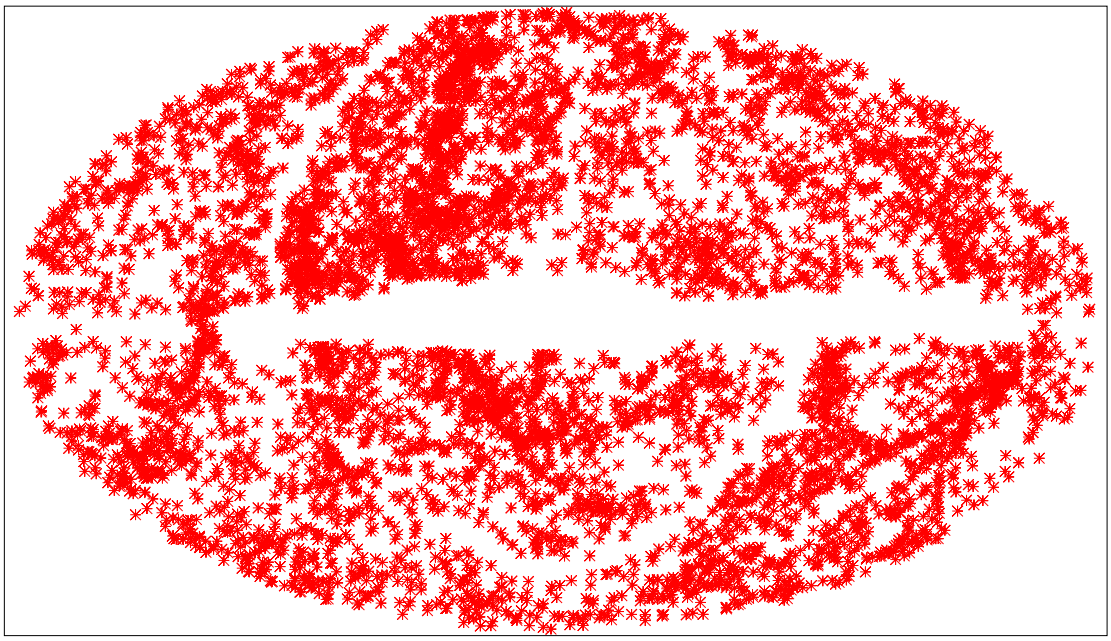

Figure 2.3: All sky Aitoff plot in Galactic coordinates (centred on (l,b)=(0,0)) of PSCz galaxies within $v \leq 8000$ km s^{-1}. Overlay shows BATSE S-GRBs as green diamonds with blue circles showing 1σ statistical errors.

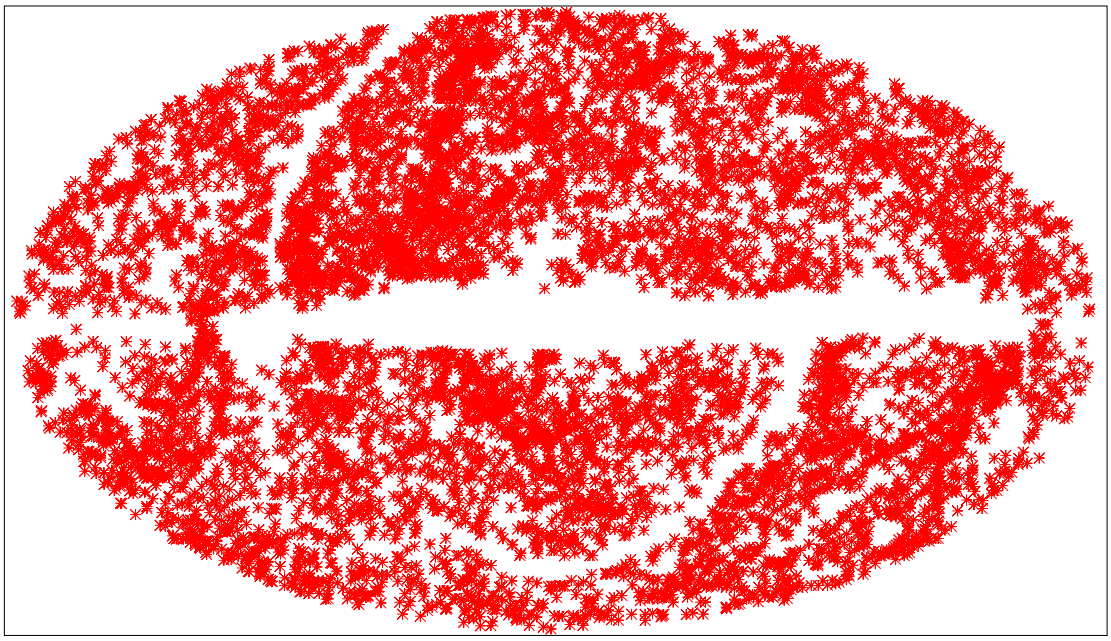

Figure 2.4: All sky Aitoff plot in Galactic coordinates (centred on (l,b)=(0,0)) of PSCz galaxies within $v \leq 11000$ km s^{-1}. Overlay shows BATSE S-GRBs as green diamonds with blue circles showing 1σ statistical errors.

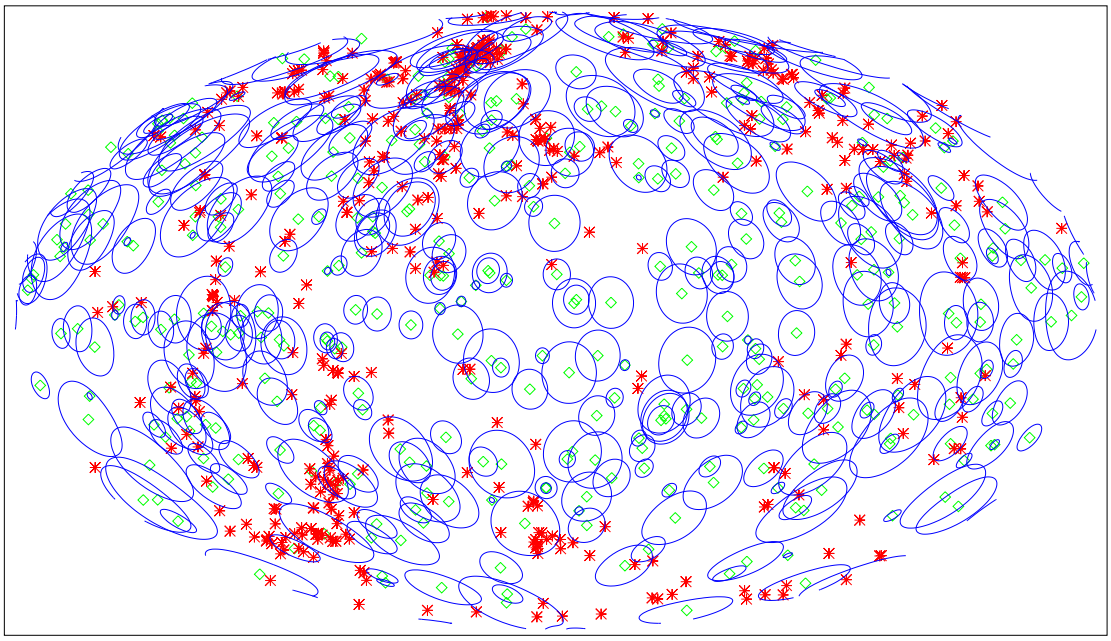

Figure 2.5: All sky Aitoff plot in Galactic coordinates (centred on (l,b)=(0,0)) of PSCz galaxies of T-type ≤ 4 with recession velocities ≤ 2000 km s^{-1}. Overplotted in green diamonds is a distribution of pseudo-bursts, 10% of which are correlated with the galaxies as described in the text. The blue circles are the 1σ statistical errors of the pseudo-bursts, drawn randomly from the real burst population.

In order to examine quantitatively any correlation between bursts and galaxies, the cross correlation function between the short bursts and galaxy samples was computed as follows. For each burst we measured the angular distance, θ, to each galaxy, and repeated this procedure for a set of 10,000 pseudobursts randomly distributed throughout the sky taking into account the known BATSE sky exposure map (Hakkila et al. 2003). The two point angular cross-correlation function, $\omega(\theta)$, can then be estimated as the excess pair count (within an angular bin size, for example 2°) between bursts and PSCz galaxies as compared to between pseudobursts and galaxies (appropriately normalised for sample size) as shown in equation 2.1:

$$\omega(\theta) = \frac{NP_{BG}(\theta)}{NP_{RG}(\theta)} \times \frac{N_{RG}}{N_{BG}} - 1 \tag{2.1}$$

where $NP_{BG}(\theta)$ is the number of burst–galaxy pairs at angle θ, $NP_{RG}(\theta)$ is the number of pseudoburst–galaxy pairs at angle θ, N_{BG} is the total possible burst–galaxy pairs, and N_{RG} is the total possible pseudoburst–galaxy pairs.

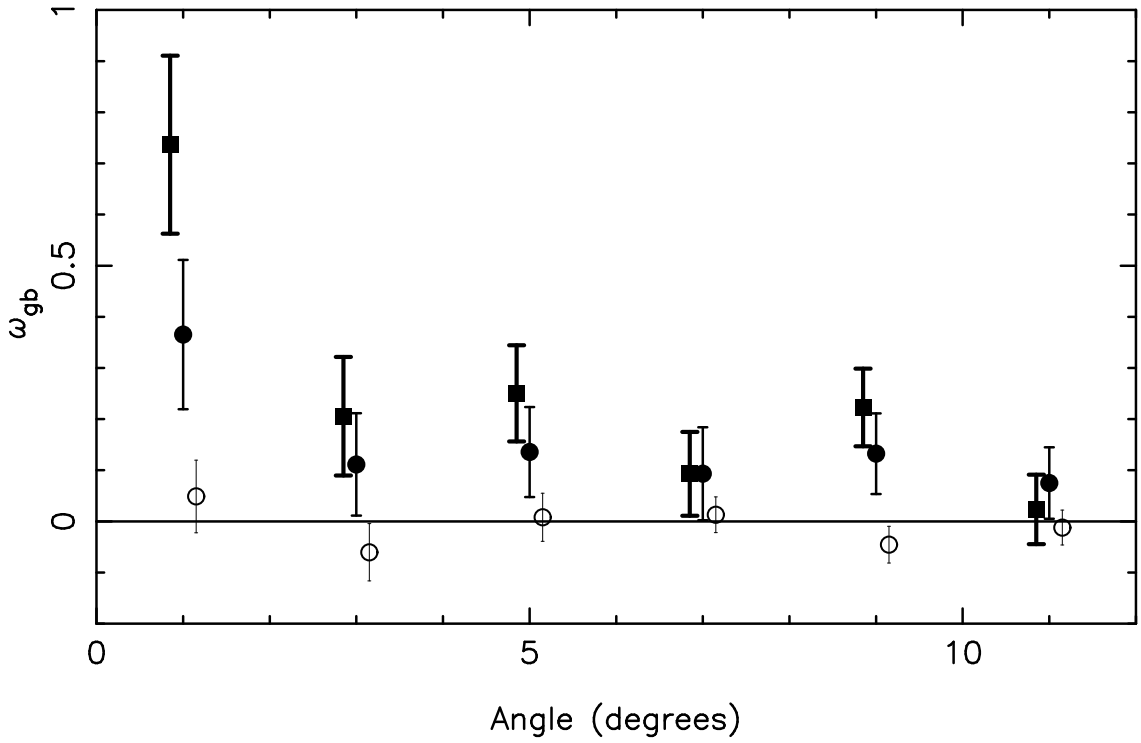

Figure 2.6: Cross correlation plot for short bursts v PSCz galaxies reproduced from Tanvir et al. (2005). The cross correlation function ω_{gb} ($\omega(\theta)$ in main text) is plotted in 2° bins for 400 BATSE short bursts with nearby galaxies from the PSCz catalogue (recession velocities $v < 2000$ km s^{-1} $\approx$ 28 Mpc distant). Filled circles show the correlation with all galaxy types (1,072 galaxies), and bold square symbols represent the same function but with galaxies restricted to earlier morphological types (T-type $\leq$ 4, Sbc and earlier, 709 galaxies). Open circles show the same function for long-duration bursts compared with all galaxy types. Points from the different functions have been offset slightly in angle for clarity.

A cross correlation plot with PSCz galaxies ($v < 2000$ km s^{-1}) is shown in Figure 2.6. Note that this velocity cut extends out to 25 Mpc - 30 Mpc, encompassing the local supercluster, and specifically the Virgo, Fornax and Ursa-Major clusters[2]. Also shown on the same plot are correlation functions between short bursts and galaxy types restricted to morphological T-type $\leq$ 4 (Sbc and earlier, a sub-division which splits our galaxy sample approximately in half by overall numbers), and between long bursts and all galaxy types. The 1σ error bars in each bin were determined from Monte Carlo simulations. The figure shows that the short bursts exhibit a clear ($> 3\sigma$) positive correlation at low angles with all galaxies, and the long bursts exhibit no detectable correlation signal.

[2]Throughout this work we use $H_0 = 71$km s^{-1} Mpc^{-1}. Due to individual peculiar velocities, recession velocity is not always an exact distance proxy.

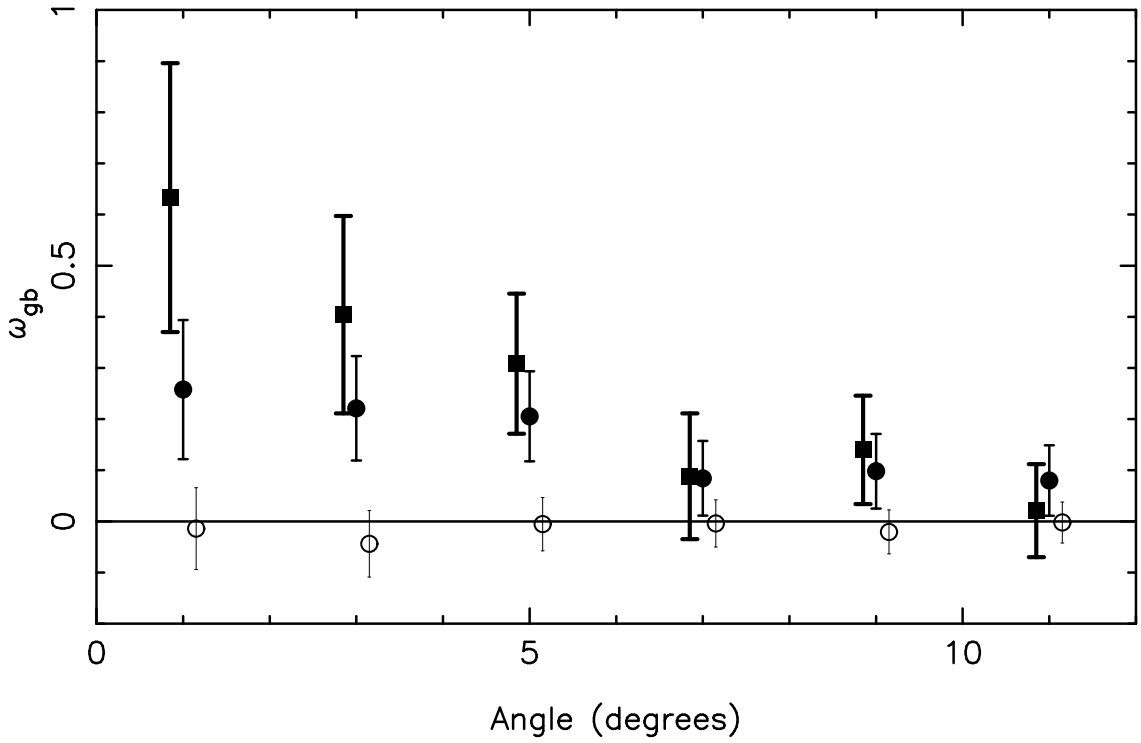

Figure 2.7: Cross correlation plot for short bursts v RC3 galaxies reproduced from Tanvir et al. (2005). The cross correlation function ω_{gb} ($\omega(\theta)$ in main text) is plotted in 2° bins for 400 BATSE short bursts with nearby galaxies from the RC3 catalogue (recession velocities $v < 2000$ km s$^{-1} \approx 28$ Mpc distant). Symbols are as for Figure 2.6.

Being an infra-red survey, the PSCz naturally contains a majority of infra-red bright galaxies (later types including those with young stars and relatively high dust content). It is of course possible that any correlation is somehow an artefact of the choice of galaxy catalogue. We have therefore also measured correlations with a second catalogue, the Third Reference Catalogue of Bright Galaxies (RC3) (de Vaucouleurs et al. 1991). Although there is some overlap, this catalogue contains more galaxies (particularly early types), but is more heterogeneous and biased against low galactic latitudes than the PSCz. Sample results are shown in Figure 2.7, confirming that a statistically significant correlation (at a slightly reduced level) is also seen with the RC3, and the overall behaviour is very similar. For the rest of the discussion, we will restrict our results to the PSCz comparison.

2.2.2 Quantifying correlation – Defining an improved measure, Φ

However, the cross-correlation function is not ideal for our purposes as errors in different bins are not independent, and it makes no direct use of known burst properties such as the individual error circles. In order to optimise the search for a quantifiable correlation signal, we define a correlation measure Φ as the sum of all burst-galaxy pairs weighted by the probability that they could be seen at the observed separation (or greater) if they were truly associated, and further weighted inversely by the burst error-circle size, as shown in equation 2.2.

$$\Phi = \sum_{i}^{Allbursts} \sum_{j}^{Allgalaxies} \frac{1}{\epsilon_i} \int_{\theta_{ij}}^{\infty} \frac{1}{\sqrt{2\pi}\epsilon_i} \exp\left[\frac{-\theta^2}{2\epsilon_i^2}\right] d\theta \tag{2.2}$$

where θ_{ij} is the separation between the ith burst and the jth galaxy, and ϵ_i is the error circle (statistical and systematic: model 1 in Briggs et al. (1999)) of the ith burst position. Thus, for any combination of burst/galaxy sample we can compute a single number Φ to serve as a direct measure of the cross-correlation of that particular sample pairing.

2.2.3 Calibrating and testing Φ

To quantify the significance of an observed value of Φ, we also compute Φ_0, which is the mean of a large number of simulated random burst distributions (each with the same number of positions as the number of bursts under consideration, the same positional errors, and distributed on the sky according to the known BATSE sky exposure map (Hakkila et al. 2003)) correlated against the same set of galaxy positions. Φ/Φ_0 can then be calibrated against a number of artificial burst samples with increasing correlation fraction. Figure 2.8 shows the result of calculating Φ/Φ_0 for a number of simulated burst distributions with respect to the sample of T–type ≤ 4 PSCz galaxies with recession velocities $v < 2000$ km s^{-1}. Pseudo-burst samples were produced in a similar manner to the Φ_0 set discussed above, but this time a particular percentage of the burst sample were selected to lie within a certain offset from randomly chosen galaxies. Each particular burst offset was calculated by choosing a random positional error from the real burst distribution, adding the appropriate systematic error (in quadrature), and finally choosing a

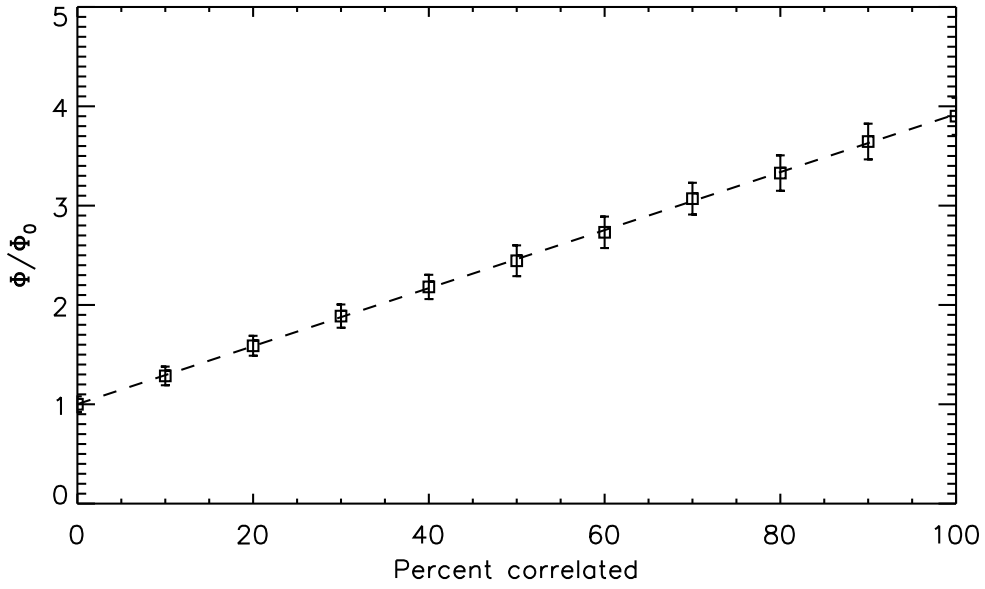

Figure 2.8: Calibration plot of Φ/Φ_0 plotted for simulated burst samples of increasing correlation with PSCz T$\leq$4 galaxies within $v < 2000$ km s^{-1}. Error bars represent one standard deviation of scatter calculated from the dispersion of the individual simulation measures. The dotted line shows the best fit linear regression straight line through the data points.

random fraction and direction of this positional error (assuming the error circles to be Gaussian) to displace the burst in RA and DEC from its generating galaxy position. Thus we produced sets of pseudo-bursts consistent with particular chosen percentages arising from galaxies in the galaxy samples: from hereon in this will be referred to as the 'level of correlation' or 'percentage correlation' for conciseness. For each percentage correlation point, a large number of pseudo-burst distribution simulations were carried out (101 in each case) and the resulting calibration curve plotted.

From Figure 2.8 we can see that Φ/Φ_0 is a linear function of correlation percentage, with well determined mean values at each test point. The individual dispersion of each point is quite significant however, and will be the main source of error in the determination of the degree of correlation in the (necessarily) single measure of correlation of the real burst sample. Given the linearity of the calibration, for computational efficiency of the tests for each combination of burst/galaxy distributions we calculate Φ_0 and Φ_{100} only for a number of simulations (501) for each pairing,

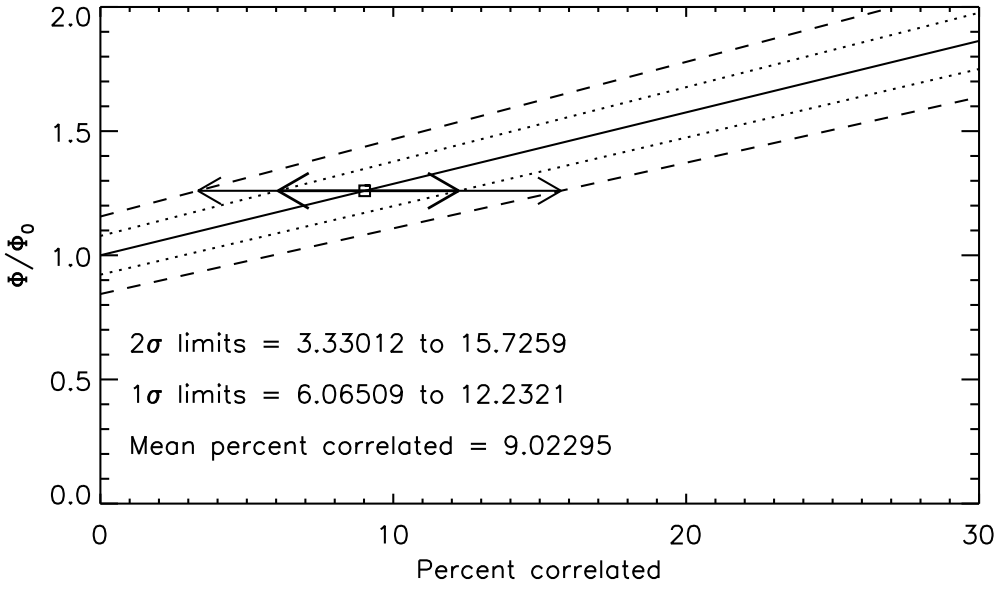

Figure 2.9: Proportion of short bursts correlated with galaxies within $v < 2000$ km s^{-1} according to Φ. In this case, the galaxy sample is restricted to morphological T-type ≤ 4 and within recession velocity $v = 2000$ km s^{-1}. The bold diagonal line represents the value of Φ/Φ_0 (see main text) as a function of the proportion of bursts in the simulated sample whose positions were seeded by the galaxy positions. The dotted (dashed) lines show the 1σ (2σ) deviations around this line according to the simulations. The level of Φ/Φ_0 for the real data is illustrated by the horizontal arrows, which span the 1σ and 2σ ranges. Thus the possibility of no correlation is rejected at more than the 3σ level, and a correlated fraction around 9% is indicated (95% confidence (2σ) limits $\approx 3.2\%$ to $\approx 15.5\%$).

and assume the calibration to be linear between these limits, as shown for example in Figure 2.9.

We can then use Φ to estimate the percentage of bursts in any sample correlated with any galaxy sample. By plotting the 1 and 2 σ confidence limits on a Φ calibration plot for each particular burst/galaxy sample, we can then overplot the individual Φ/Φ_0 measure for the data and estimate the percentage correlation of the burst distribution with the galaxy sample. For example, Figure 2.9 shows that the observed signal from the S-GRB sample with respect to the $v < 2000$ km s^{-1} sphere of PSCz galaxies of T-type ≤ 4 could be explained by a correlated component representing between 6% and 12% of BATSE bursts (1σ range).

To further test the linearity, accuracy and reliability of this estimation, we

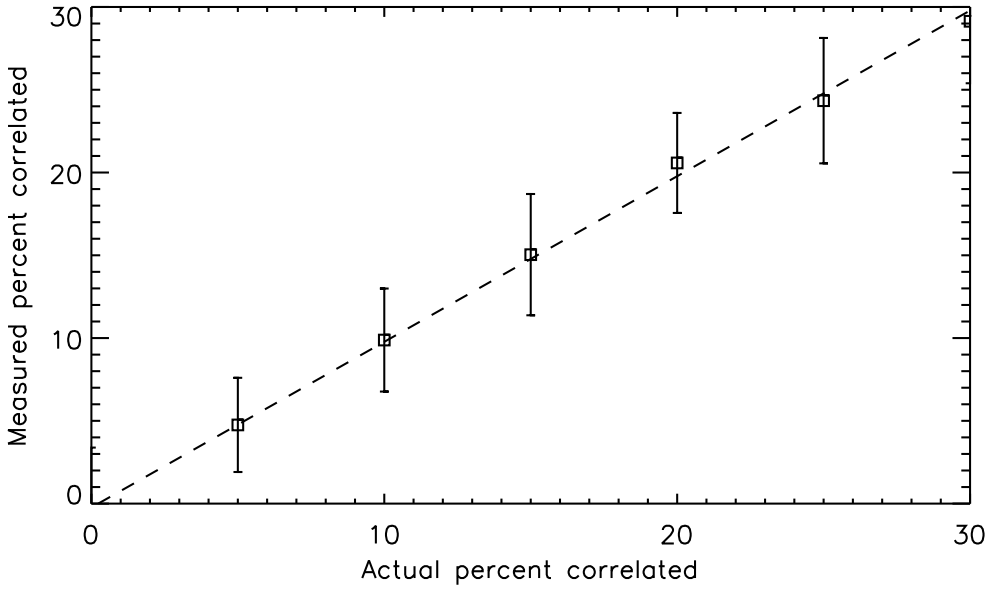

Figure 2.10: Measured versus input test correlations of pseudo-burst samples with respect to PSCz galaxies (T-type ≤ 4) within $v < 2000$ km s^{-1}.

challenged each calibration plot with a number of pseudo-burst samples of known correlation. Figure 2.10 shows the measured correlation as a function of input correlation for pseudo-burst samples with respect to the $v < 2000$ km s^{-1} galaxy sphere again. The error bars on each point represent the standard deviation of 101 individual challenges. From this figure we can see that Φ provides a reliable and consistent measure of actual correlation, though with reasonably broad scatter on individual measurements. Repeating these tests on spheres of galaxies of increasing radius (Figures 2.11 to 2.13), we see that as we increase the radius of investigation the scatter on each individual measurement becomes broader and overlaps more severely with neighbouring points. This is to be expected as the number of galaxies in each sample increases, and detectable structure in the distributions becomes more and more 'washed-out' (see for example Figures 2.1 to 2.4). This effect obviously restricts the radius to which we can investigate burst/galaxy correlations, though in practice there is a further more fundamental restriction: the galaxy catalogues are magnitude limited and by the time we reach recession velocities of $v < 11000$ km s^{-1} or more there are far fewer galaxies appearing in the samples than we would expect for the increase in volume sampled.

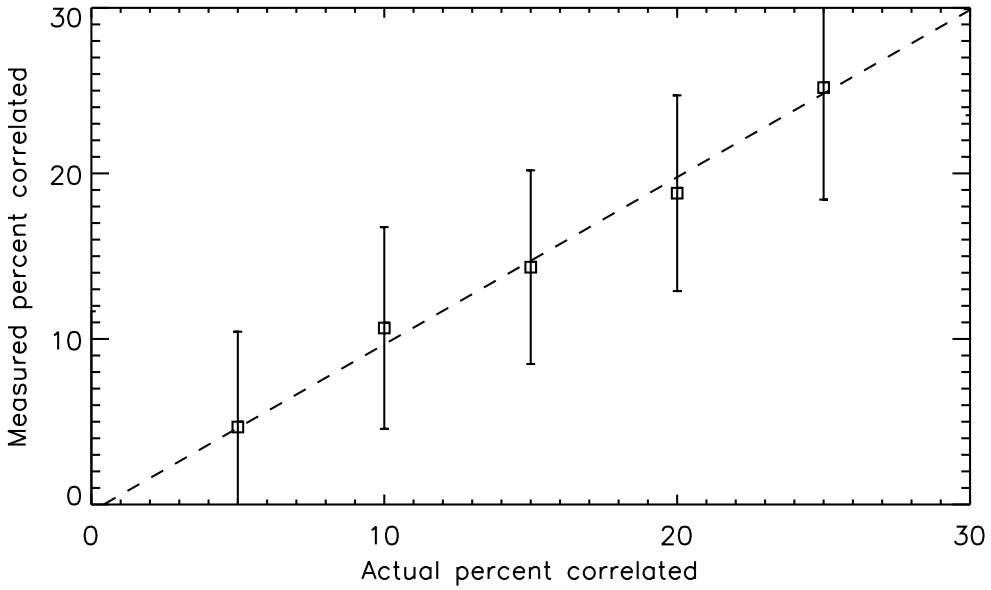

Figure 2.11: Measured versus input test correlations of pseudo-burst samples with respect to PSCz galaxies (T-type ≤ 4) within $v < 5000$ km s^{-1}.

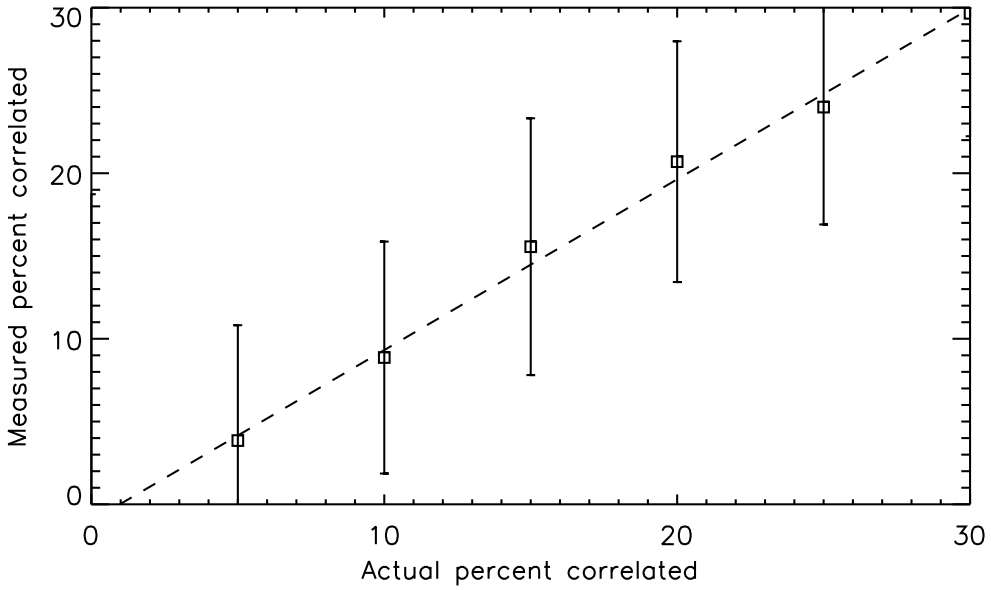

Figure 2.12: Measured versus input test correlations of pseudo-burst samples with respect to PSCz galaxies (T-type ≤ 4) within $v < 8000$ km s^{-1}.

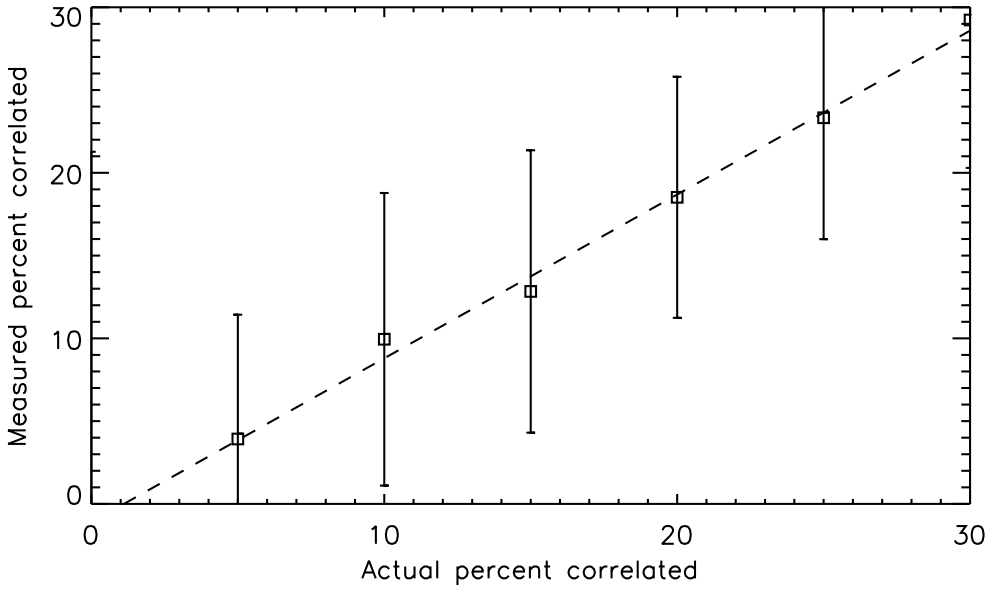

Figure 2.13: Measured versus input test correlations of pseudo-burst samples with respect to PSCz galaxies (T-type ≤ 4) within $v < 11000$ km s^{-1}.

2.2.3.1 Sensitivity of Φ: individual pairings or large scale structure?

It is interesting to ask whether our analysis is more sensitive to individual burst/galaxy correlations, or to correlation with large scale structure on the sky. In order to address this question, we repeated our correlation analyses but this time in calculation of Φ_{100}, for each correlated pseudo-burst we removed the galaxy from which its position was generated. Thus Φ_{100} then measures the correlation between pseudo-bursts and the large scale structure around the generating host. The resulting structure-based Φ_{100} values for the PSCz galaxy shells are shown in Table 2.1.

PSCz galaxy shell recession velocity (km s^{-1})	$\Phi_{100,\mathrm{incl}}$ incl. host (arbitrary units)	$\Phi_{100,\mathrm{excl}}$ excl. host (arbitrary units)	$\Phi_{100,\mathrm{excl}}/\Phi_{100,\mathrm{incl}}$ (%)
$\leq$2000	1875	1684	90%
2000–5000	2873	2663	93%
5000–8000	2354	2151	91%
8000–11000	1810	1616	89%

Table 2.1: Values of Φ_{100} for PSCz galaxy samples measured including and excluding the host of the pseudo-bursts in correlated simulations.

As this table shows, $\geq$ 89% of the correlation signal measured by Φ_{100} is generated from galaxies other than the specific hosts of the pseudo-bursts. It would therefore seem likely that correlation between the real BATSE bursts and galaxy distributions is mainly due to large scale structure on the sky rather than correlation with individual hosts. Given the size of the BATSE error boxes, this is certainly not surprising, but means that our analysis is unlikely to be sensitive to individual galaxy properties. However, given the often large error boxes of individual bursts, sensitivity to structure is actually an advantage. Our technique effectively measures the correlation between two 2-dimensional signals, and is statistical in its nature - the signal is produced from the sums of contributions of many burst-galaxy candidate pairs and thus enhances any inherently weak individual correlation measurements at the expense of sensitivity to individual pair properties. This therefore precludes our ability to identify any individual burst/galaxy associations, or to investigate any dependency of the correlations on galaxy properties such as mass or star formation

rate. Indeed, some preliminary analyses performed by weighting Φ by estimated individual galactic properties such as estimated SFR showed no significant change from the unweighted results.

2.2.3.2 Radial variation: applying analysis to concentric *shells* of galaxies

To counter the dilution of the structure signal, and because the distributions of both bursts and galaxies within our concentric spheres obviously have radial variations as well, we can investigate correlations between the burst samples and concentric shells (as opposed to spheres) of galaxies. The results of applying the same tests to galaxy sample shells of recession velocity radii of $2000 - 5000,\ 5000 - 8000$ and $8000 - 11000$ km s^{-1} are shown in Figures 2.14 to 2.16.

Comparing these results to Figures 2.11 to 2.13, we can see that the overlap between neighbouring data points in the shell challenge plots is less severe, particularly at the larger radii. More importantly though, using comparisons with shells rather than spheres allows us to investigate the radial variation of the correlations in a differential as well as cumulative manner, and to correct for any potential cross-talk between neighbouring shells (see the following section). These differential distributions will be important in later Chapters for model fitting comparisons when comparing plausible luminosity functions for burst progenitors.

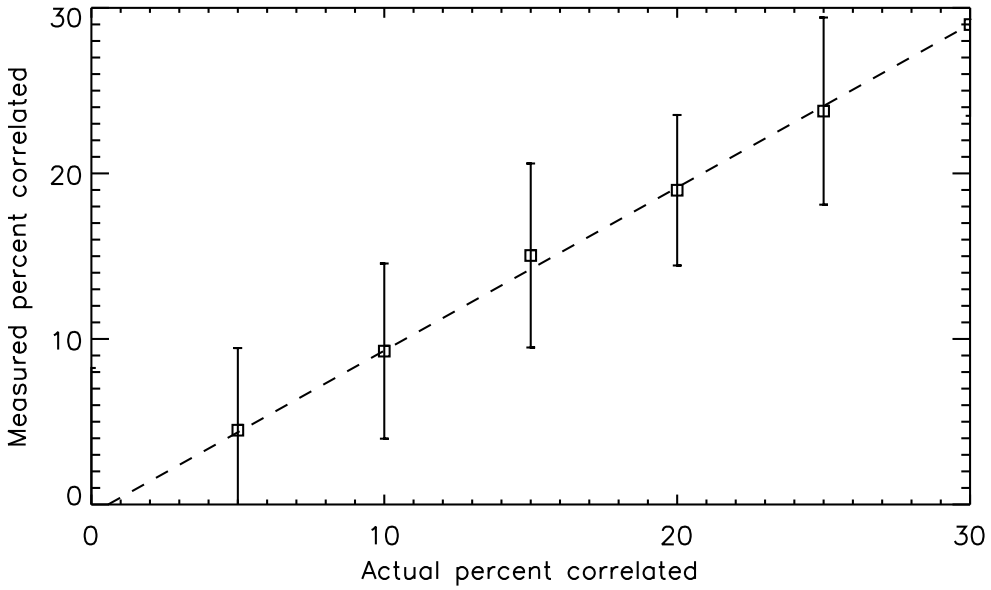

Figure 2.14: Measured versus input test correlations of pseudo-burst samples with respect to PSCz galaxies (T-type ≤ 4) within $2000 < v < 5000$ km s^{-1}.

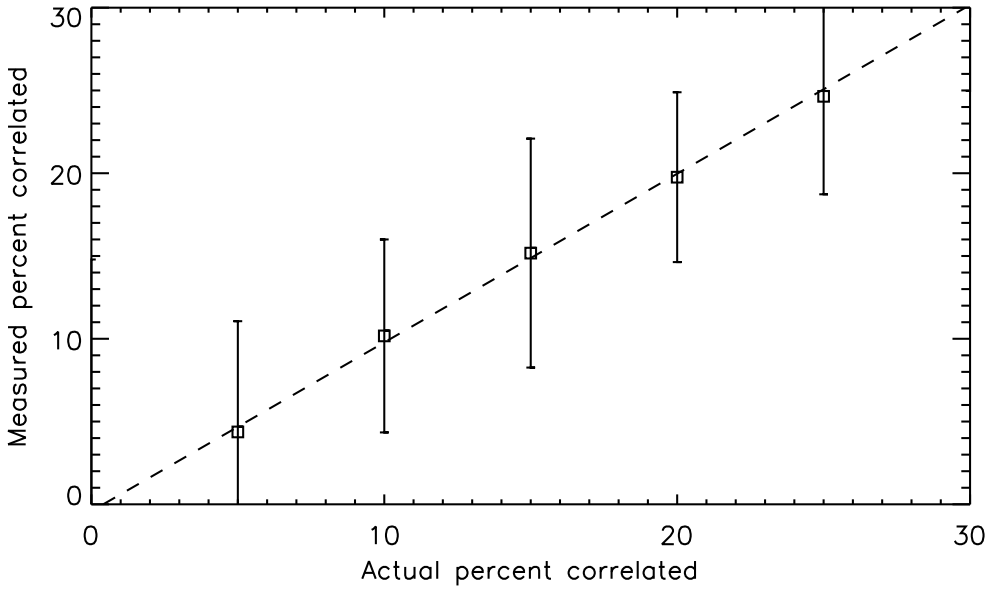

Figure 2.15: Measured versus input test correlations of pseudo-burst samples with respect to PSCz galaxies (T-type ≤ 4) within $5000 < v < 8000$ km s^{-1}.

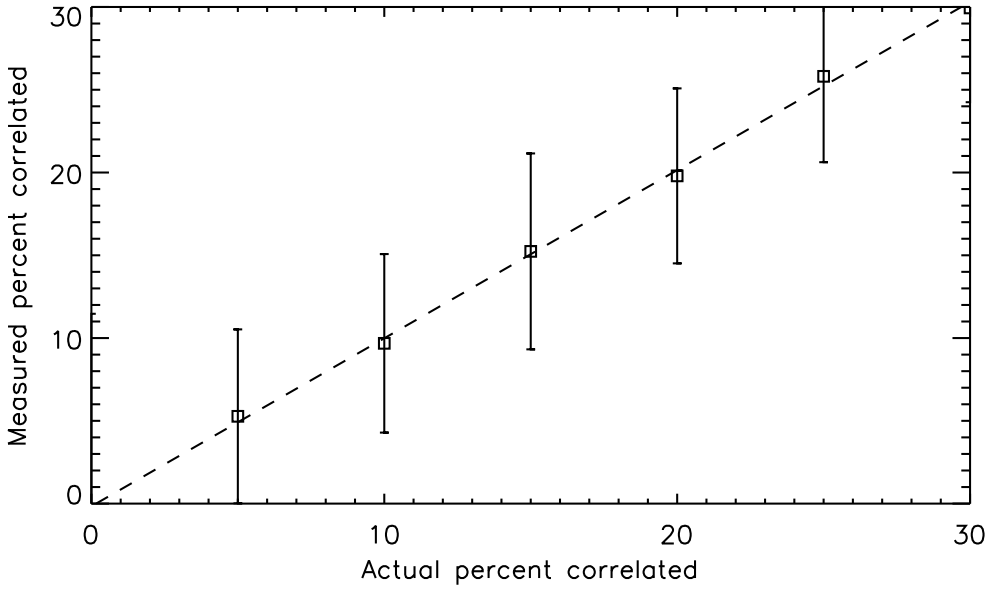

Figure 2.16: Measured versus input test correlations of pseudo-burst samples with respect to PSCz galaxies (T-type ≤ 4) within $8000 < v < 11000$ km s^{-1}.

2.2.4 Applying Φ to real burst samples

2.2.4.1 Cumulative correlation with concentric *spheres* of galaxies

We now turn to applying Φ as a correlation estimator to the real BATSE short GRB sample tested against real galaxy samples. Figure 2.9 earlier showed the measured correlation component of S-GRBs with respect to PSCz galaxies (T-type ≤ 4) with recession velocities $v < 2000$ km s^{-1}. From that Figure, we can see that the null hypothesis of zero correlation is rejected at the 3σ level, with a measured correlation level of $9\% \pm 3\%$, equivalent to 36 ± 12 bursts from the 400 BATSE S-GRB sample having possibly occurred within ~ 28 Mpc. In fact, this is likely to be an underestimate, as our catalogue certainly does not contain all the galaxies in this volume, just the infrared-bright ones, and there remains a thin zone of avoidance around the Galactic plane, and a region unsurveyed by *IRAS* that the PSCz survey does not cover (amounting to about 16% of the sky).

Burst correlation with respect to the whole galaxy sample is shown in Figure 2.17, from which we can see that the correlation levels in the final two spheres at ~ 112 Mpc and beyond become increasingly unconstrained, presumably due to

the dilution of any structure signal detectable in the galaxy sample. Choosing to divide the galaxy sample at T-type ≤ 4 splits the closest galaxy sample spheres into halves of approximately equal numbers. If we then measure the correlations of S-GRBs against these two galaxy samples, we obtain the results shown in Figures 2.18 and 2.19. From these two graphs, we see that the percentage of S-GRBs correlated with galaxies of T-type > 4 within ~ 70 Mpc is about half that of the sample when correlated against galaxies of T-type ≤ 4, and beyond this distance it falls to zero within (once again) increasingly poor constraints. Burst correlation with PSCz galaxies of T-type ≤ 4, however, rises to a level of $20\% \pm 8\%$ (1σ) within ≈ 112 Mpc, where it remains constant and continues to be more pronounced and better constrained than with either the all T-type or T-type > 4 samples out to the highest radii considered.

Above we showed that our technique is more sensitive to large scale structure than individual burst-galaxy correlations, and thus this increased signal probably reflects the tendency for clustering on the sky in the PSCz to increase among earlier type rather than later type galaxies, rather than reflecting a specific association of S-GRBs with early type galaxies. The T-type $\leq$ 4 sample remains dominated by spiral galaxies, with only $\approx 20\%$ of the sample consisting of T-types < 0. We note, however, that the vast majority of long GRBs are seen associated with faint, irregular type field galaxies (Fruchter et al. 2006) and none have yet been associated with early type galaxies or observed in clusters (Bornancini et al. 2004). Our results are thus at least consistent with local short bursts being associated with a variety of galaxy types, including those in clusters and quite different from long burst hosts.

As discussed above, Lazzati, Ghirlanda & Ghisellini (2005) attempted to analyse the likely contribution of SGR giant flares to the BATSE S-GRB population by searching the catalogue for bursts with spectra well modelled by a harder thermal spectrum than the non-thermal power law of classic S-GRBs. However, the sample of short bursts for which they could model spectra with sufficient accuracy was small. Rather than attempt such detailed spectral modelling leading to very small sample sizes, if we divide the bursts by spectral hardness into a harder and softer 50%, then any dependency of correlation on spectral hardness should be detectable via an increased correlated fraction in one half or the other of the sample. We therefore split the total sample in half by the ratio of observed fluence in BATSE energy channels 1 ($20 - 50$ keV) and 3 ($100 - 300$ keV), and compared correlations between these samples and PSCz galaxies (T-type ≤ 4) with a number (20) of entirely random halvings of the S-GRB sample. Figure 2.20 shows the results

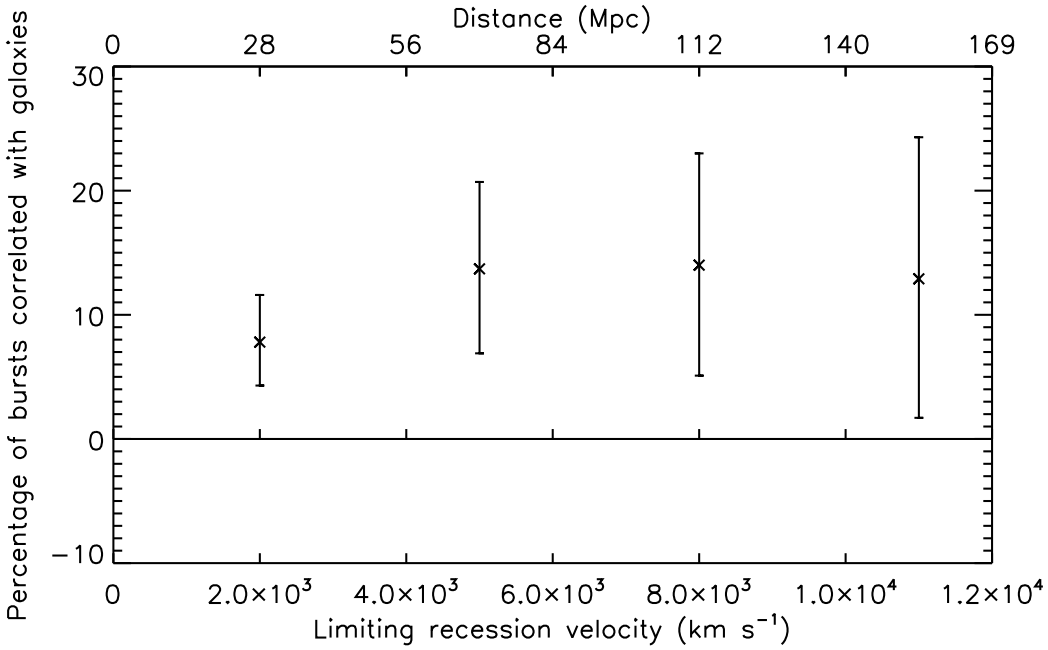

Figure 2.17: Percentage of short bursts correlated with concentric spheres of PSCz galaxies of all type versus sphere limiting recession velocity according to Φ. Error bars show 1σ limits.

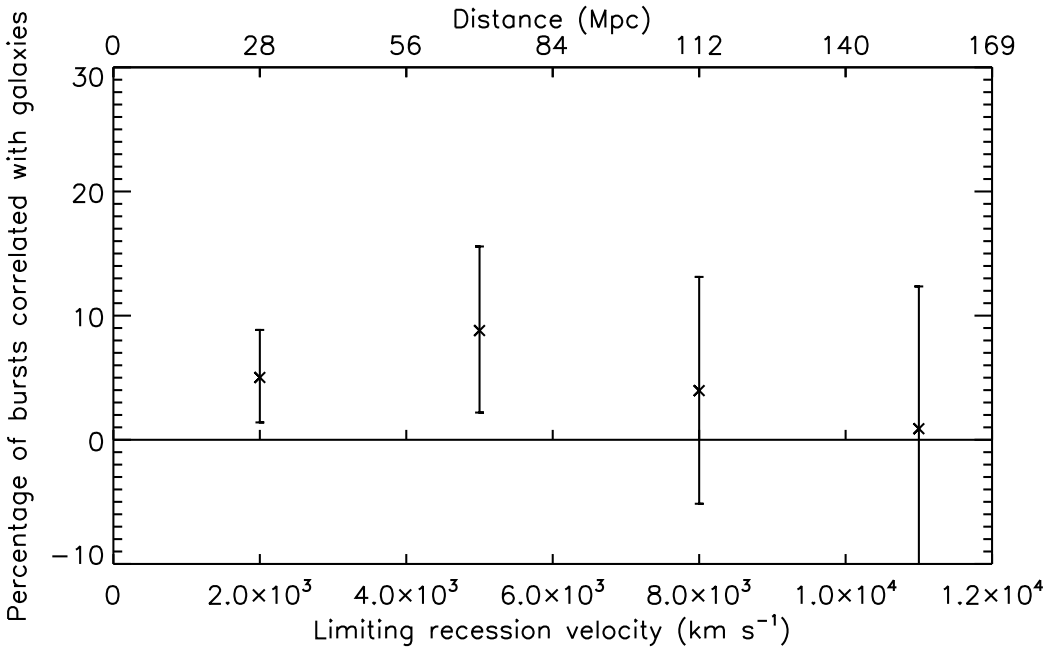

Figure 2.18: Percentage of short bursts correlated with T-type > 4 PSCz galaxy spheres versus sphere limiting recession velocity according to Φ. Error bars show 1σ limits.

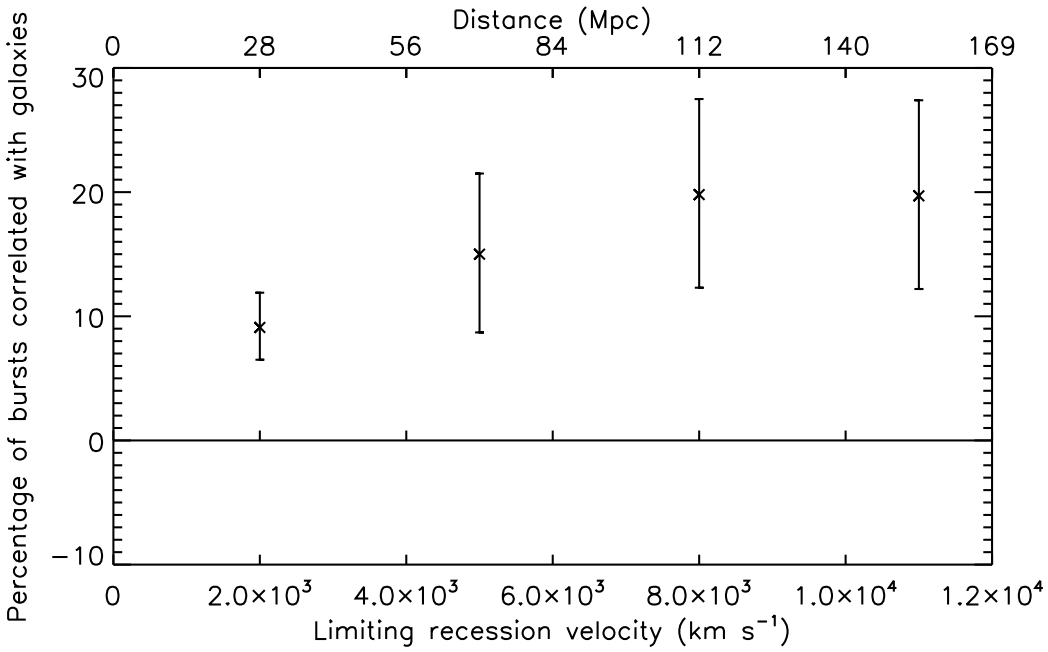

Figure 2.19: Percentage of short bursts correlated with T-type ≤ 4 PSCz galaxy spheres versus sphere limiting recession velocity according to Φ. Error bars show 1σ limits.

of these comparisons, from which we conclude that we can detect no discernible difference in correlation fractions between harder and softer halves of the S-GRB sample compared to random selections.

2.2.4.2 Differential correlation with concentric *shells* of galaxies

As mentioned before, the distributions of both bursts and galaxies projected on the sky within our concentric spheres must have a radial variation as well. Results therefore from examining correlations between the burst samples and concentric shells (as opposed to spheres) of galaxies with recession velocity radii of $0 - 2000,\ 2000 - 5000,\ 5000 - 8000$ and $8000 - 11000$ km s^{-1} are shown in Figure 2.21.

From Figure 2.21, it can be seen that correlation with the earlier T-types remains at an effectively constant level of $\approx$ 8% with respect to the galaxy shells out to ~ 112 Mpc (though constraints become poorer with increasing radius). The correlation level then drops abruptly to zero in the final shell (155–170 Mpc). It is interesting to note that, as we shall see in Chapter 4, this final shell is the only

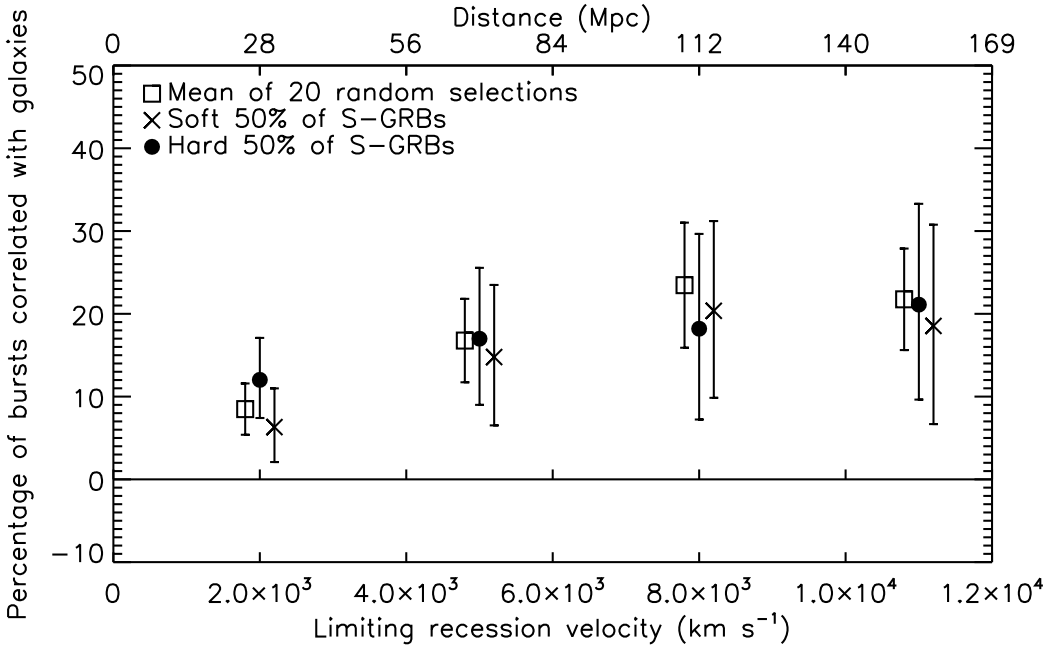

Figure 2.20: Percentage of short bursts selected by spectral hardness correlated with T-type ≤ 4 PSCz galaxy spheres compared with that of 20 equal number random selections. Error bars show 1σ limits on the measured correlations for the individual samples, and the 1σ dispersion of the 20 random samples.

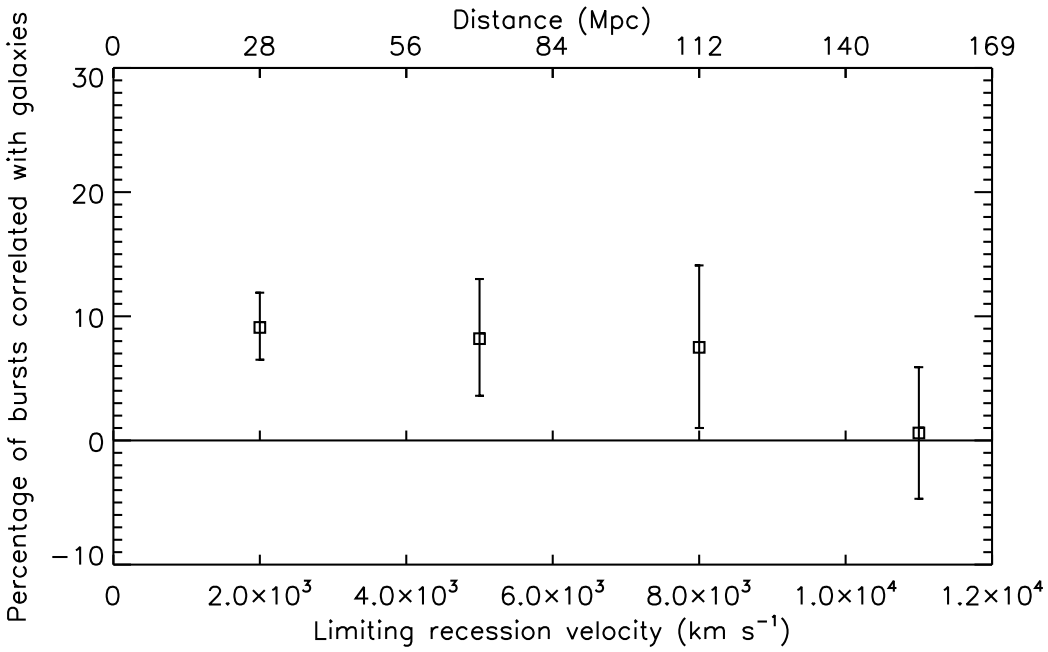

Figure 2.21: Percentage of short bursts correlated with PSCz galaxy shells versus shell outermost recession velocity according to Φ. Open squares represent correlation measured against PSCz galaxies of T-type ≤ 4, and error bars show 1σ limits.

shell which demonstrates any correlation with long duration GRBs. Since these two results demonstrate changes in opposite directions, they are unlikely to be due to any systematic effect such as a decreasing galaxy volume density in the catalogue samples with distance. It is therefore suggestive that we can no longer see the population of short bursts that correlates with nearby galaxies by the time we reach 155 Mpc, due presumably to them being of lower luminosity than their more distant cousins, an observation we discuss briefly below and in more detail in Chapter 3.

There is inevitably some "cross-talk" correlation between shells, both real where galaxy clustering extends across our artificial shell boundaries, and statistical. By analysing the correlation between artificial burst samples created with 100% correlation in one shell and galaxy distributions in neighbouring shells, we can estimate the cross-talk contamination between shells. Iterating around the measured correlation values using these correction factors, we can then produce cross-talk corrected measurements as shown in Figure 2.22. As can be seen, this correction is small within the errors of our measurements and does not significantly affect the results. It is however important in demonstrating the consistency between the measurements in shells, and the cumulative measurements in spheres, where by comparing the val-

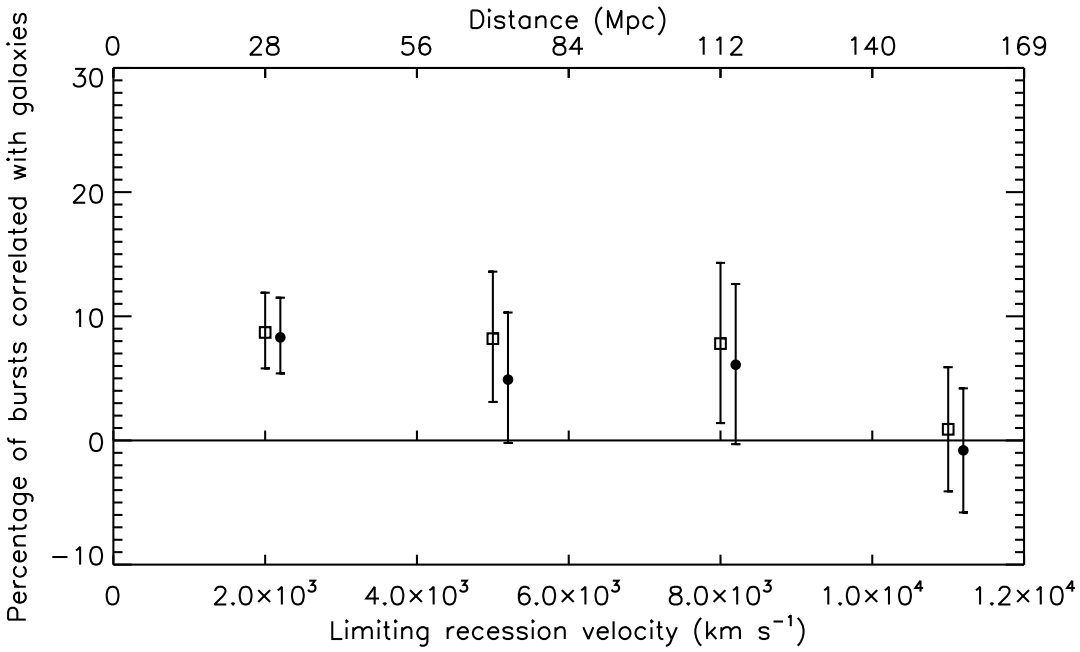

Figure 2.22: Cross-talk corrected correlation between BATSE short duration GRBs and galaxies in concentric shells of increasing galactic recession velocity from the PSCz catalogue. Open squares represent measured correlation values, and filled circles cross-talk corrected values. Data points have been separated along the x axis for clarity.

ues in Figures 2.19 and 2.22 we see that adding the successive cross-talk corrected shell values reproduces well the cumulative sphere distribution.

2.3 Summary and Discussion

We have presented analyses of the correlation of all short duration GRBs in the BATSE catalogue with galaxies in the nearby universe. These results indicate that 20% $\pm$ 8% (1σ limits) of BATSE short GRBs originated within the local Universe ($z < 0.027 \approx 112$ Mpc). These results are in broad agreement with previously reported upper limits for the proportion of BATSE short bursts originating at low redshifts (Popov & Stern 2006; Nakar et al. 2006; Hurley et al. 2005; Dar 2005), particularly in the light of the recent revision to the distance to SGR 1806-20, but are more robust and highly constrained. They also naturally explain the intriguing finding that short-burst positions on the sky show evidence for a weak auto-correlation signal (Magliocchetti, Ghirlanda & Celotti 2003). Recently, Ghirlanda et al. (2006)

have claimed angular correlations at scales $\leq 3^\circ$ between S-GRBs and X-ray selected galaxy clusters within $z \leq 0.45$. When they compared the burst/cluster correlation signal with both the cluster autocorrelation function and the galaxy/cluster cross-correlation function, they found a better match with the latter suggesting that the S-GRB correlation is with the structure traced by the clusters, rather than the clusters themselves. This is certainly consistent with our results, though at first sight the redshift limit used by Ghirlanda et al. (2006) would seem to be too large to be comparable. However, it must be remembered that their comparison is with one large sphere of clusters, and hence measures the cumulative correlation within that sphere - the correlation signal may be coming from much closer structure. In fact, when they restricted their cluster sample to those within $z < 0.1$ they found an increased correlation signal as our results would suggest. Furthermore, when compared to models of the autocorrelation of galaxies within $z < 0.05$ ($\sim$ 210 Mpc, comparable to our 155 Mpc limit), the match showed further slight improvement.

When we analyse the correlations with respect to shells rather than spheres of galaxies, we find that the percentage of bursts exhibiting correlation with each shell remains constant at a level of about 8% out to 112 Mpc and then drops to zero. This is consistent with us reaching the detection limit of the burst sample responsible for the correlation signal. A possible explanation of our result is that we are detecting a low-redshift population of short bursts associated with SGRs. SGRs being magnetars - usually associated with the remnants of short-lived massive stars and therefore expected to follow the Star Formation Rate - it may seem surprising that a stronger correlation is seen with galaxy samples containing a reasonable percentage of galaxies with little recent star formation. However the T-type $\leq$ 4 sample remains dominated by spiral galaxies, with only $\approx$ 20% of the sample consisting of T-types < 0 (lenticulars and earlier). Furthermore, our correlation measures are more sensitive to large scale structure than individual galaxy properties and thus reflect the tendency for the earlier type galaxies in the PSCz to exhibit more clustering than the later types. The fact that the level of correlation halves with the later type sample though is at least consistent with short bursts being associated with a different variety of hosts compared to the longs. We note as well, that if magnetars can be produced via white dwarf–white dwarf mergers (King, Pringle & Wickramasinghe 2001), then as we have shown recently it is quite plausible to produce magnetars in relatively old stellar populations (Levan et al. 2006b).

It is therefore not impossible, and we suggest quite likely, that at least some nearby short duration GRBs are produced by giant flares from SGRs. We know that

SGR giant flares exist, having observed three directly in our own galaxy in the last 30 years of observation. Therefore, even though this rate is ill-constrained by few observations, it would be remarkable if we did not detect others from galaxies within nearby volumes, and it is likely that they would dominate the local population of short bursts. Hurley et al. (2005) estimate that SGR flares of similar energy to the 27th December 2004 event from SGR1806-20 could have been observed by BATSE out to about $30d_{15}$ Mpc. If we assume all our correlation comes from SGR giant flares, then to be visible out to 112 Mpc (the limits of our observed correlations with galaxy shells) there would need to be a population of flares $(112/30d_{15})^2 \approx 14d_{15}^{-2}$ times brighter, which is not unreasonable given that the observed luminosity of the December 27th event is a lower limit, and also magnetic fields an order of magnitude or so greater than that calculated for SGR1806-20 are considered plausible for magnetars. Assuming a constant space density of the local bursts between 28 and 112 Mpc, the number of observable bursts would increase with the cube of the radius. To double the level of correlation seen between these two radii therefore requires a rate of higher energy flares only $2 \times (28/112)^3 \approx 0.03$ times that of the December 27th event, which is negligible within our errors at the lower radii.

Though we can explain the correlations reasonably well via a small population of bright SGR giant flares, our observations cannot rule out the possibility that local short bursts are produced in compact object mergers as is commonly suggested for classic short GRBs. Compact object mergers can have relatively long lifetimes and are thus likely to occur in older stellar populations, and are likely to be more energetic when they occur. The definitive association of a highly energetic local short burst with an old elliptical galaxy would certainly favour the compact object model. It is also possible that in the future these two progenitor populations could be distinguished either by associated gravitational wave signatures, or by the detection of the pulsating tail of nearby extra-galactic SGR flares, as may just be possible by *Swift* (Hurley et al. 2005). The question thus remains: given that a local population of S-GRBs exists, can the likely numbers be explained by a single population of bursts, or is something more complicated required? We will return to this question in detail in Chapter 3 where we will investigate plausible Luminosity Functions for different S-GRB progenitors.

Chapter 3

Luminosity Functions of Short GRBs: one population or two?

3.1 Introduction

We recall that the leading progenitor model for S-GRBs is the merger of two compact objects, neutron star-neutron star (NS-NS) or neutron star-black hole (Nakar 2007) binaries. The Luminosity Function (LF) of BATSE S-GRBs has been investigated previously assuming a single progenitor population (e.g. Schmidt 2001a; Ando 2004; Guetta & Piran 2005, 2006; Hopman et al. 2006) in order to determine the intrinsic rate and most likely LF parameters. In a refinement to their previous work, Guetta & Piran (2006) noted that a second population of bursts may be necessary to explain some features of their model fits and the comparison with *Swift* bursts, particularly at lower redshifts. NS binaries may be either 'primordial', where they are formed following the SN explosion of both partners in an existing massive star binary system, or 'dynamically formed' via gravitational interactions and exchanges in globular clusters between single neutron stars and those in binaries with low mass main sequence stars. Dynamically formed NS binaries thus have an extra delay time to formation in addition to their merger timescale leading to longer overall times to merge. Hopman et al. (2006) considered both primordial and dynamically formed NS binaries, and suggested that the early observed redshift distribution of S-GRBs favoured dynamical formation. Further to that work, Salvaterra et al. (2007) suggested that the more recent *Swift* cumulative redshift distribution is better encompassed by including both formation routes with different abundances above and below $z \sim 0.3$. Recently, in an analysis of a large number of models of compact ob-

ject merger scenarios from population synthesis models, O'Shaughnessy, Belczynski & Kalogera (2008) have shown that the observed S-GRB redshift distribution could be reproduced by a reasonable fraction of those models, though this analysis was insensitive to the low end of the redshift distribution on which our work here is focused. Nakar, Gal-Yam & Fox (2006) find the high rate of observed S-GRBs within 1 Gpc to imply that a single population of NS binaries responsible for all S-GRBs must be dominated by long merger times, inconsistent with the observed NS binary population. However, they also point out that a non-unimodal luminosity function, such as produced by two separate populations of progenitor, remains a plausible possibility for S-GRBs.

There are indeed other possible progenitors for S-GRBs. At much closer distances still, the initial spike in a giant flare from a Soft Gamma Repeater (SGR) in a relatively nearby galaxy would also appear as a S-GRB. For example, the December 27th 2004 event from SGR1806-20 would have been visible by BATSE out to $\sim 30d_{15}-50d_{15}$ Mpc where d_{15} is the distance to SGR 1806-20 in units of 15 kpc (Hurley et al. 2005; Palmer et al. 2005; Taylor & Granot 2006; Nakar 2007). Though this is the brightest giant flare detected so far, it is quite possible that some giant flares may be brighter still and therefore visible to greater distances. Thus, even after recent observations which have lowered the distance estimate to SGR 1806-20 (Bibby et al. 2008), it is entirely plausible that some fraction of S-GRBs are extragalactic SGR giant flares. Several studies have estimated the likely contributions of SGR flares to BATSE S-GRBs as discussed in more detail in the previous Chapter. Ofek (2007) points out that the fraction cannot be less than $\sim 1\%$ without being inconsistent with the observed Galactic SGR giant flare rate, and calculates an upper limit of 16% (95% confidence limits). This limit is based on a conservative measure of probable positional coincidences between S-GRBs localised by the Third Interplanetary Network (IPN)[1] and bright star forming galaxies within 20 Mpc. This limit is, however, sensitive to their estimate of the completion of the galaxy sample and may be higher still.

In Chapter 2, we showed via a correlation analysis using the full sample of BATSE S-GRBs localised to better than 10°, that $9\% \pm 3\%$ of BATSE S-GRBs were likely associated with local galaxies within ≈ 28 Mpc, and up to $20\% \pm 8\%$ with hosts within ≈ 155 Mpc. Additionally, a handful of recently detected S-GRBs have

[1]The IPN is a network of spacecraft equipped with gamma-ray detectors. By timing the arrival of burst signals at several spacecraft, accurate localisation boxes can be found. IPN3 has been functioning since 1990 - for further details regarding the network and current participating craft see http://www.ssl.berkeley.edu/ipn3/.

localisations consistent with origins in nearby galaxies (Ofek et al. 2006, 2007; Frederiks et al. 2007b; Mazets et al. 2008; Levan et al. 2008). Overall, the *Swift* redshift distribution of S-GRBs (Berger 2007) peaks closer than that of long GRBs (Jakobsson et al. 2006b), though there is evidence that some S-GRBs may occur at higher redshifts (Levan et al. 2006a), and that there may be a local population of underluminous long GRBs (e.g. Pian et al. 2006; Soderberg et al. 2006b; Liang & Zhang 2006; Liang et al. 2007; Chapman et al. 2007). Can a suitable LF describing a single progenitor population (presumably compact object mergers) produce a nearby ($z \leq 0.03$) as well as cosmological distribution of S-GRBs, or is it necessary to include an intrinsically different (possibly SGR giant flares) lower luminosity population as well?

Here we attempt to answer this question by considering first single, and then dual population LFs. The intrinsic rates in the models will be assumed from both the observed Galactic SGR flare rates and the modelled NS-NS merger rates in order to investigate the LF parameters. Obviously there are significant uncertainties in these rates: the Galactic giant flare rate in particular is estimated from only 3 observed events. Regardless of these uncertainties and the exact form of luminosity functions chosen, we find that a single progenitor population described by a unimodal (i.e. with a single peak or knee) LF cannot produce sufficient local events, whereas a dual population reproduces the likely local S-GRB distribution as well as the overall number counts.

3.2 Methods

The number of S-GRBs, N, observed above a threshold p in time T and solid angle Ω is given by Equation 3.1, where $\Phi(L)$ is the S-GRB LF, $R_{GRB}(z)$ is the comoving event rate density at redshift z, $dV(z)/dz$ is the comoving volume element at z and z_{max} for a burst of luminosity L is determined by the detector flux threshold (1 photon cm^{-2} s^{-1} for BATSE for S-GRBs) and the luminosity distance of the event.

$$N(>p) = \frac{\Omega T}{4\pi} \int_{L_{min}}^{L_{max}} \Phi(L) dL \int_0^{z_{max}} \frac{R_{GRB}(z)}{1+z} \frac{dV(z)}{dz} dz \tag{3.1}$$

We are of course dealing with detector limited and not bolometric luminosities. Following Schmidt (2001a) and Guetta & Piran (2005) we assume a constant median spectral index of -1.1 in the BATSE energy range of 50-300 keV to derive a simplified

K correction and conversion to photon flux.

3.2.1 Intrinsic rates

The S-GRB rate per unit volume, $R_{\rm GRB}(z)$ is given by Equation 3.2 where $N_{\rm GRB}$ is the number of S-GRBs per progenitor, $\rho_{\rm progenitor}$ is the intrinsic ($z = 0$) progenitor formation rate and $F(z)$ describes the volume evolution of this rate with z.

$$R_{\rm GRB}(z) = N_{\rm GRB} \times \rho_{\rm progenitor} \times F(z)\ {\rm Mpc}^{-3} \tag{3.2}$$

For NS-NS mergers, a burst is produced only once at merger, and we therefore assume $N_{\rm GRB} = 1$. This is of course an upper limit: any beaming of S-GRBs, or a GRB production efficiency per merger of less than 100%, would effectively reduce this number, and reduce the number of bursts observable from the NS-NS merger population. This limit is therefore conservative in the sense that it maximises the possible fraction of bursts produced by mergers in our analysis. The intrinsic NS-NS merger rate is taken as 10^{-5} yr^{-1} per Milky Way equivalent galaxy (Star Formation Rate, SFR $\approx 4{\rm M}_{\odot}$ yr^{-1}, e.g. Diehl et al. (2006)) from the population synthesis models of Kalogera et al. (2007). Mergers, of course, occur some time after the formation of the binary itself. Thus the merger rate at redshift z, is dependent not on the SFR at the same z, but on the earlier SFR at higher redshift. $F(z)$ is therefore given by the convolution of the SFR as a function of redshift with a distribution of delay times from binary formation to merger. The population syntheses of Belczynski et al. (2006) suggest a merger delay time (formation plus coalescence) distribution $dP_m/d(\log(t)) \sim constant$ ($\equiv dP_m/dt \propto 1/t$) between 10^7 and 10^{10} years, with a narrow peak at the very shortest times, and we thus assume a delay time probability distribution where $dP_m/d(\log(t))$ is flat between 10^7 and 10^{10} years and zero outside this range, for simplicity and comparison with previous LF analyses. We note, however, that using a delay model including a narrow early 'spike' (with an order of magnitude higher value between 15 and 30 Myr) makes little difference to the derived LF parameters as can be seen from some examples in Tables 3.1-3.3.

SFR as a function of z is parameterised according to the SF2 model of Porciani & Madau (2001), normalised to a local SFR of 1.3×10^{-2} ${\rm M}_{\odot}{\rm yr}^{-1}{\rm Mpc}^{-3}$ (Gallego et al. 1995) as given in Equation 3.3.

$$\mathrm{SFR}(z) = 1.3 \times 10^{-2} \left(\frac{23 e^{3.4z}}{e^{3.4z} + 22} \right) \ \mathrm{M}_{\odot} \ \mathrm{yr}^{-1} \ \mathrm{Mpc}^{-3} \tag{3.3}$$

An alternative analysis is that the merger rate should be proportional to Stellar Mass Density (SMD), which must be representative of star formation history. We therefore also investigate merger rates which follow a simple single exponential fit to the SMD out to $z \sim 5$ derived from the FORS deep field (Drory et al. 2005) as:

$$\mathrm{SMD}(z) = 10^{8.75} \exp(-\ln(2) z) \ \mathrm{M}_{\odot} \ \mathrm{Mpc}^{-3} \tag{3.4}$$

Over the last 30 years of observations, there have been 3 giant flares from 4 known SGRs in the Milky Way and Magellanic Clouds. The observed local rate of giant flares per Galactic SGR is therefore $\approx 3 \times 10^{-2}$ yr^{-1}, and their short active lifetimes of $\sim 10^4$ years (Duncan & Thompson 1992; Kouveliotou et al. 1998; Kouveliotou 1999) imply $N_{\mathrm{GRB}} \sim 300$ in the SGR case. Magnetars are commonly believed to form in a fraction of core collapse supernovae, and hence their formation should follow the SFR as a function of z. Given the the association of the 4 known SGRs with young stellar populations, this therefore implies a formation rate via core collapse supernovae of 4×10^{-4} yr^{-1}.

However, it is also plausible that magnetars may form via the Accretion Induced Collapse (AIC) of White Dwarf (WD) binaries which contain at least one sufficiently massive and magnetized member (Levan et al. 2006b). In older galaxies with relatively little star formation, this would be the dominant formation route and therefore makes it possible for SGRs to be associated with all types of galaxies, not just those with a relatively high SFR. Following Levan et al. (2006b), the rate of magnetar formation via WD-WD mergers in a Milky Way equivalent galaxy is estimated as 3×10^{-4} yr^{-1}. We therefore assume $F(z)$ for SGRs follows both SFR(z) for magnetar production from supernovae and either the delayed SFR or SMD to allow for production by WD binary mergers.

3.2.2 Luminosity functions

Luminosity functions for SGR giant flares and NS-NS mergers are not well known. A lognormal LF approximates the shape of the theoretical NS-NS merger luminosity distribution (Rosswog & Ramirez-Ruiz 2003), but other functional forms are equally plausible: for example Guetta & Piran (2005) assumed a broken power law for their

LF calculations, and the luminosities of many other astronomical populations are well described by a Schechter function (Schechter 1976).

Given only 3 events, it is not possible to constrain the SGR giant flare LF to any great degree. The 3 observed events have peak luminosities of $\sim 10^{44}$, $\sim 10^{46}$ and $\sim 10^{47}$ erg s^{-1} (Tanaka et al. 2007) (including a correction for the lower distance estimate of SGR 1806-20 found by Bibby et al. (2008)). The more common short duration bursts from SGRs, with luminosities[2] up to 10^{41} erg s^{-1} seem to follow a power law distribution in energy, $dN \propto E^{-\gamma}dE$ where $\gamma \sim 1.4 - 1.8$ (Cheng et al. 1996; Göğüş et al. 2000) similar to that found in earthquakes and solar flares. Intermediate bursts with energies and luminosities between the short bursts and giant flares are also seen, and it is possible therefore that this distribution continues to higher energies and includes the giant flares themselves, particularly since Göğüş et al. (2000) found no evidence for a high energy cutoff in their work. However, Cheng et al. (1996) did find evidence of a cutoff around 5×10^{41} erg, and furthermore the intermediate bursts are generally seen following giant flares and may be some form of aftershock rather than representing part of a continuous spectrum of flare activity. Theory suggests that the common bursts are produced by the release of magnetic energy gated by a small scale fracturing of the crust sufficient only to relieve crustal stresses, whereas the giant flares are the result of large scale cracking sufficient to allow external field reconfiguration to a new equilibrium state (Thompson & Duncan 1993, 1995). Assuming the latter is a physically distinct process discontinuous (in terms of energy release) from the short bursts, then it must have some minimum energy release, and a maximum defined by the total destruction of the external field via the Flowers-Ruderman instability (Flowers & Ruderman 1977) where entire hemispheres of the magnetar flip with respect to each other (Eichler 2002). Having only the 3 observed events to go on, a lognormal LF is once again plausible for giant flare luminosities. The possibility of a continuous luminosity distribution between the short, intermediate and giant flares is not ruled out however, and we therefore also consider a single power law LF as well.

To summarise, we consider the possibility that short GRBs may be produced via two different progenitor routes, both NS-NS mergers and SGR giant flares, each population with intrinsically different luminosities. The forms chosen for the luminosity functions examined are as follows:

[2]Henceforth 'luminosity' is used as shorthand for 'peak luminosity' unless stated otherwise.

1. Lognormal distribution

$$\frac{dN}{d\log L} \propto \exp\left(\frac{-(\log L - \log L_0)^2}{2\sigma^2}\right) \tag{3.5}$$

2. Schechter function

$$\frac{dN}{dL} \propto \left(\frac{L}{L_0}\right)^{-\alpha} \exp\left(-L/L_0\right) , \quad L \geq L_{min} \tag{3.6}$$

3. Power Law

$$\frac{dN}{dL} \propto \left(\frac{L}{L_0}\right)^{-\alpha} , \quad L_{min} \leq L \leq L_0 \tag{3.7}$$

where $L_{min} = 10^{42}$ erg s^{-1} for normalisation and convergence of the Schechter function. The Power Law distribution is normalised to the observed Galactic rate between $L_{GFmin} = 10^{44}$ erg s^{-1} and L_0, but the distribution is analysed down to L_{min} to investigate the possible extension of the power law to lower luminosity flares. L_0, and α or σ are the free parameters to be estimated.

3.2.3 Constraining the models

The C_{max}/C_{min} table from the current BATSE catalogue (Paciesas et al. 1999) provides peak count rate for bursts in units of the threshold count rate at 64 ms, 256 ms and 1024 ms timescales. Not all bursts are included and in addition the BATSE threshold was varied historically. Therefore in order to analyse a coherent set of bursts in a manner consistent with previous LF analyses (e.g. Schmidt 2001a; Guetta & Piran 2005) we restricted the table to only those S-GRBs recorded when the 64ms timescale threshold was set to 5.5σ above background in at least 2 detectors in the $50 - 300$ keV range. The all sky equivalent period (including correction for BATSE's sky coverage) this table of peak luminosities on the 64 ms timescale represents is estimated as ~ 1.8 years.

We then examined the differential distributions of predicted overall counts first from various single, and then combined populations of burst progenitor. By varying the parameters of the chosen luminosity functions, we compared the predicted overall counts (dN/dp) to the observed differential distribution from the C_{max}/C_{min} table. For each set of LF parameters, the redshift distribution of S-GRBs was calculated,

and the nearby distributions compared with the observed correlated distributions from Tanvir et al. (2005). Note that we use the cross-talk corrected correlations measured against galaxies in concentric *shells* (as opposed to *spheres*) of recession velocity in order to obtain a local differential distribution for the model fitting. χ^2 minimisation was then used to optimise the LF parameters by fitting simultaneously to the overall count rate and the local distributions. We assumed a Poissonian error distribution on the overall count rate, whereas we used the explicit Monte Carlo derived error distribution on the local correlated fraction. Note that the greater number of data points in the number count fits means that the combined χ^2 values are dominated by the goodness of fit to the count rate distribution. To explicitly ask whether any of our chosen single LFs can remain consistent with the BATSE number counts while being forced to produce a local distribution of bursts, we also find the best fits constrained by the correlated fraction alone, and the best fits among distributions forced to produce at least the lower limit of the measured local burst distribution within 112 Mpc (i.e the bottom of the error bar on the third data point in the upper panels of Figures 3.1 to 3.4).

In order to check the plausibility and consistency of the best fit models, we further compared the derived redshift distribution to that of S-GRBs observed by *Swift*. We caution that this sample is neither uniformly selected nor complete. Previous studies have analysed the early *Swift* distributions (e.g. Guetta & Piran 2006; Hopman et al. 2006; Nakar, Gal-Yam & Fox 2006; Salvaterra et al. 2007; O'Shaughnessy, Belczynski & Kalogera 2008), and it is clearly useful to compare our models to the current best known redshift distribution in order to check that the predictions are not unrealistic. We stress that the *Swift* distribution was not part of the statistical analysis. S-GRB redshifts have so far only been found from host galaxy associations, the identification of which is not always unambiguous. Furthermore, even the classification of some bursts as either short or long is controversial since their durations change substantially depending on whether or not emission from the long-soft tails (seen in a number of bursts) is included. Nevertheless, about a dozen probable short-hard bursts have reasonably secure redshifts. Specifically we include the following 10 S-GRBs: GRBs 050509B, 050724, 051221a, 060801, 061006, 061201, 061210, 061217 (see Berger (2007) and references therein), 070714B (Graham et al. 2007) and 071227 (D'Avanzo et al. 2007). In order to produce the predicted *Swift* redshift distribution, the *Swift* BAT threshold for S-GRBs was assumed to be twice that of BATSE (Band 2006b).

3.3 Results

3.3.1 Single population Luminosity Functions

NS Merger LF	Parameters ($l_0 \equiv \log L_0$)	Local χ^2/dof	C_{max}/C_{min} χ^2/dof	Overall χ^2/dof
Schechter (*flat*)	$l_0 = 51.75$ $\alpha = 1.25$	11.93	1.01	1.31
Schechter (*spike*)	$l_0 = 51.8$ $\alpha = 1.25$	11.93	1.03	1.33
Schechter (*SMD*)	$l_0 = 50.45$ $\alpha = 0.9$	11.87	1.05	1.34
Lognormal (*SMD*)	$l_0 = 48.9$ $\sigma = 0.75$	11.82	1.09	1.38
Lognormal (*flat*)	$l_0 = 46.4$ $\sigma = 1.5$	11.88	1.18	1.46
Lognormal (*spike*)	$l_0 = 46.6$ $\sigma = 1.45$	11.89	1.19	1.47

Table 3.1: Results of single population Luminosity Functions fit simultaneously to the BATSE number counts and the local distribution, presented in order of decreasing overall goodness of fit (i.e. increasing overall χ^2/dof). The LFs follow merger delay time (formation plus coalescence) distributions either *flat* in log space ($dP_m/d(\log(t)) = constant$), or with a narrow *spike* at early times, or the *SMD* profile of Equation 3.4. The number of degrees of freedom (dof) for the local, C_{max}/C_{min} and overall distributions are 1, 22 and 26 respectively. l_0 is in units of $\log(\text{erg s}^{-1})$, σ in dex and α is dimensionless.

Table 3.1 lists the best fit parameters found from fitting distributions produced by single population NS merger LFs simultaneously to both the overall number counts and the local population as described above. The table is ordered in decreasing overall goodness of fit (i.e. increasing combined χ^2/dof). As mentioned previously, the combined χ^2 is dominated by the fit to the overall BATSE number counts and, as expected, all our chosen single population LFs produce good fits to the C_{max}/C_{min} data leading to acceptable overall fits as measured by the combined χ^2. However, none of the single progenitor population LFs reproduce the local burst population expected from the correlation results (column 3 in Table 3.1 lists

the χ^2/dof results considering the fit to the local distribution only). For example, Figure 3.1 shows the results from a single Schechter function LF which can be seen to produce effectively no S-GRBs within 300 Mpc.

In order to ascertain whether a single merger population can produce the local bursts and remain consistent with the C_{max}/C_{min} data, we then fit single LF populations to the local distribution alone, with no constraints placed on goodness of fit to the overall number counts. As can be seen from Table 3.2, single Schechter function LFs can produce a local population, but the associated number count distribution is an extremely poor match to the C_{max}/C_{min} data. With only four data points to constrain the local distribution there is obviously some ambiguity as to its exact shape, and in order to allow some flexibility in this shape and the fraction of local bursts demanded by the fits, we also chose to constrain the single LFs to only have to produce a fixed number of bursts within a certain radius. We chose the lower limit of the correlated bursts within ~ 112 Mpc, i.e. the third data point in the local distribution panels in the Figures. Table 3.3 shows results from these fits, where it can be seen once again that even with this relaxed local constraint, the single population LFs are still unable to match the number count distribution while producing a local burst population. The inability of either of these local constraints to produce a distribution which fits the number counts is effectively a consequence of the intrinsic S-GRB rate calculated in Equation 3.2 from the assumed merger rates: not enough bursts in total can be produced. In order to produce a large enough fraction of the observed bursts locally, the maximum burst luminosity must be unrealistically low, leading to an extremely unrealistic redshift distribution as demonstrated in Figure 3.2 and therefore not enough bursts overall. The fit to the C_{max}/C_{min} data can be improved to reasonable χ^2 levels by increasing the intrinsic merger rate by a large factor (≥ 500), but the overall redshift distribution still remains as unrealistic as in Figure 3.2.

NS Merger LF	Parameters ($l_0 \equiv \log L_0$)	Local χ^2/dof	C_{max}/C_{min} χ^2/dof	Overall χ^2/dof
Schechter (*flat*)	$l_0 = 51.1$ $\alpha = 2.2$	0.76	> 100	> 100
Schechter (*spike*)	$l_0 = 51.0$ $\alpha = 2.2$	0.76	> 100	> 100
Schechter (*SMD*)	$l_0 = 53.0$ $\alpha = 2.15$	1.08	> 100	> 100
Lognormal (*spike*)	$l_0 = 43.1$ $\sigma = 1.35$	5.30	> 100	> 100
Lognormal (*flat*)	$l_0 = 43.1$ $\sigma = 1.3$	5.38	> 100	> 100
Lognormal (*SMD*)	$l_0 = 43.0$ $\sigma = 1.4$	6.43	> 100	> 100

Table 3.2: Results of single population Luminosity Functions constrained to fit the local distribution, presented in order of decreasing goodness of fit. Details as for Table 3.1.

NS Merger LF	Parameters ($l_0 \equiv \log L_0$)	Local χ^2/dof	C_{max}/C_{min} χ^2/dof	Overall χ^2/dof
Schechter (*flat*)	$l_0 = 48.15$ $\alpha = 0.55$	17.2	> 100	> 100
Schechter (*spike*)	$l_0 = 48.15$ $\alpha = 0.5$	16.8	> 100	> 100
Schechter (*SMD*)	$l_0 = 48.2$ $\alpha = 0.5$	16.5	> 100	> 100
Lognormal (*spike*)	$l_0 = 48.1$ $\sigma = 0.1$	28.4	> 100	> 100
Lognormal (*flat*)	$l_0 = 48.1$ $\sigma = 0.1$	28.3	> 100	> 100
Lognormal (*SMD*)	$l_0 = 48.0$ $\sigma = 0.3$	21.5	> 100	> 100

Table 3.3: Results of single population Luminosity Functions constrained only to produce at least the lower limit of the local distribution within 112 Mpc (see text). Results presented in the same order as Table 3.2, with details as for Table 3.1.

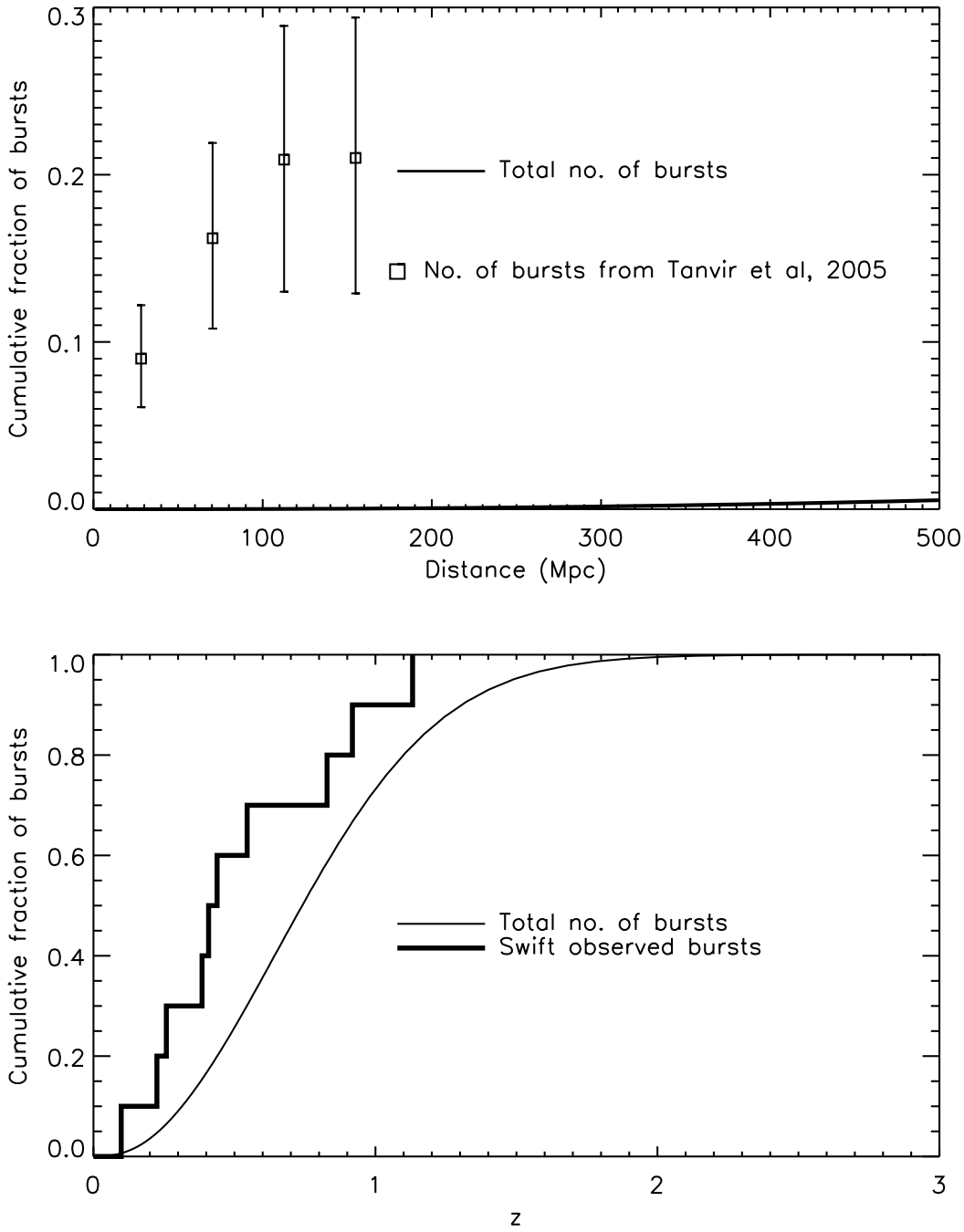

Figure 3.1: Burst distributions from the best fit merger single population Schechter function LF following a $dP_m/d(\log(t)) = constant$ merger time delay distribution. Top panel shows predicted S-GRB distribution within 500 Mpc compared to the local burst fraction measured in Tanvir et al. (2005), bottom panel shows the predicted burst distribution out to $z = 3$ normalised and compared to the *Swift* distribution discussed in the text.

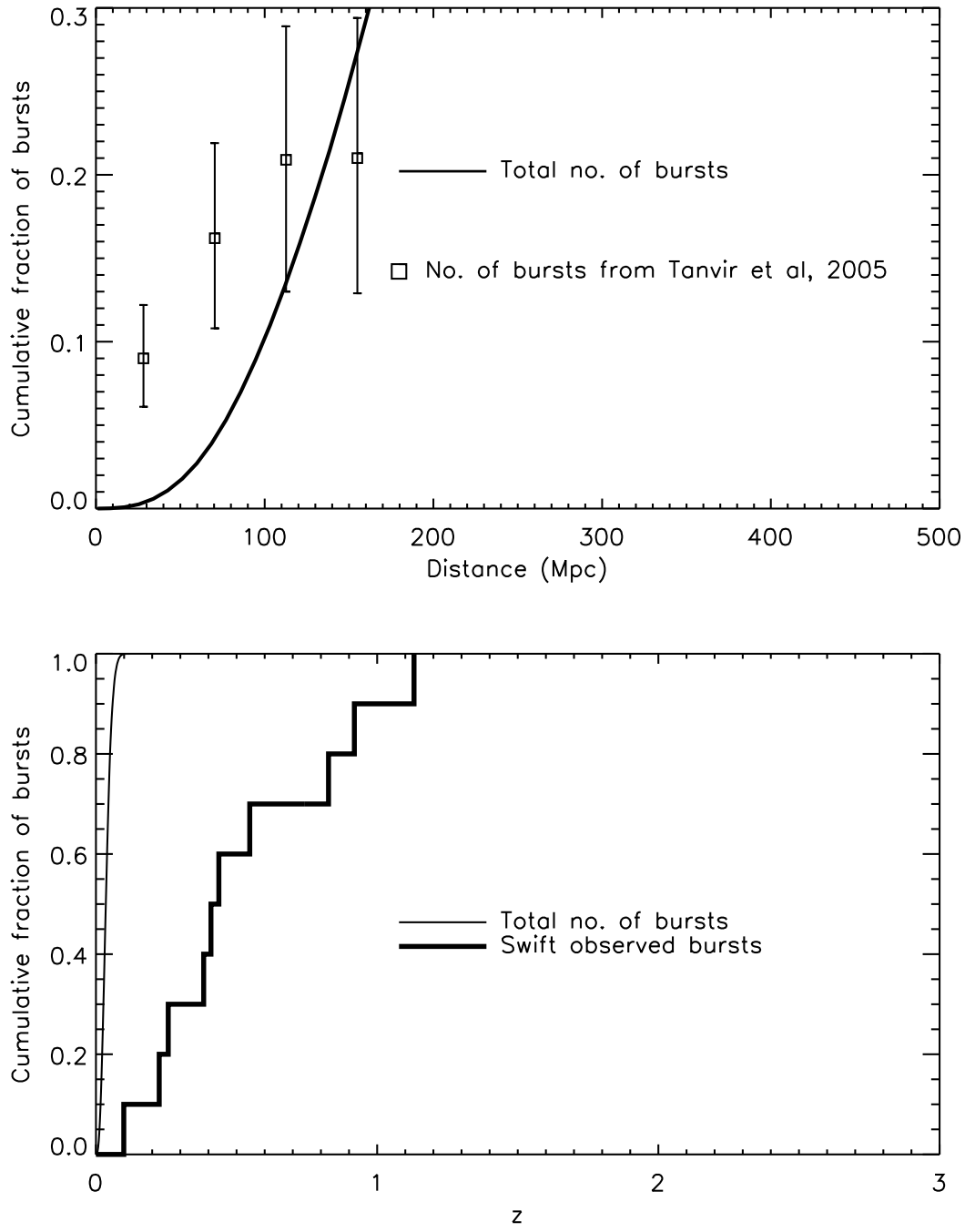

Figure 3.2: Burst distributions from the best fit of the same merger single Schechter function LF as Figure 3.1 constrained only to produce at least the lower limit of the local burst population within ~ 112 Mpc (data point 3). Note the unrealistic wider redshift distribution produced by this fit. Panel Details as for Figure 3.1.

3.3.2 Dual population Luminosity Functions

In contrast, Table 3.4 shows best fit LF parameters for various combinations of dual NS merger and SGR giant flare luminosity function models, along with their respective minimum χ^2 values. Note that the number of degrees of freedom to consider for the local distribution model is a non-trivial issue: there are only 4 local data points to fit, and we are now using 2 LFs with 2 free parameters each. However, as can be seen from Tables 3.2 and 3.3, and the examples of Figures 3.3 and 3.4, the local bursts are only ever reproduced by the lower luminosity LF, and we can therefore continue to assume the local distribution $dof = 1$. By minimising the combined χ^2 values, all the dual LFs tested reproduced the local distribution well while retaining overall number count fits comparable to those of the single LFs. Furthermore, the best fit LF parameters of the dual models are reasonable, and the overall redshift distribution is much more realistic.

For example, a dual lognormal LF, with merger rates following either a delayed merger model (Figure 3.3) or the SMD model of Equation 3.4 (Figure 3.4), produces a good fit to the expected local population while remaining consistent with the early *Swift* redshift distribution. The upper panels of Figures 3.3 and 3.4 show the comparison of these models to the local S-GRB distribution determined by our BATSE cross-correlation analysis, and are typical in that all the dual populations reproduce this local population well. Since these data were used to constrain the fit, a good agreement is to be expected, but it is still interesting to note that the merger population contributes only a small fraction to these local bursts. The lower panels show the overall predicted redshift distribution.

As mentioned before, the intrinsic Galactic rates used to normalise the LFs are not well constrained. Hence in Table 3.4 we also show the results of varying the intrinsic SGR flare rate up and down by an order of magnitude for the dual lognormal (SMD) fit of Figure 3.4. The production of a local S-GRB population is robust against this change, and the overall fit remains good. As may be expected, an increase in the intrinsic flare rate leads to the best fit SGR LF being moved down in luminosity, thus removing a greater fraction of the total flares from observability. Likewise, a lower intrinsic rate generates a higher (and narrower) LF distribution, though in both cases the LF parameters remain entirely plausible.

Figure 3.5 shows the best fit LFs and associated contours of χ^2 with respect to L_0 for the dual population from Figure 3.4. Despite the uncertainties in the underlying Galactic rates of the models, the best fit parameters obtained for this

and the other dual LFs are plausible given the known properties of SGR giant flares and classic S-GRB luminosities. We note that the slopes of the SGR flare power law LFs obtained (1.25 - 1.35) are shallower than the slopes found for ordinary SGR burst fluence distributions (1.4 - 1.8) (Cheng et al. 1996; Göğüş et al. 2000).

The results of all dual population fits are shown in Figures 3.7 to 3.12, including those with increased (Figure 3.11) and decreased (Figure 3.12) intrinsic Galactic flare rates.

NS Merger LF	LF Parameters ($l_0 \equiv \log L_0$)	SGR Giant Flare LF	LF Parameters ($l_0 \equiv \log L_0$)	Local χ^2/dof	C_{max}/C_{min} χ^2/dof	Overall χ^2/dof
Schechter (*flat*)	$l_0 = 52.3$ $\alpha = 1.3$	Power law (*flat*)	$l_0 = 46.7$ $\alpha = 1.25$	2.03	1.15	1.04
Schechter (*flat*)	$l_0 = 52.3$ $\alpha = 1.3$	Lognormal (*flat*)	$l_0 = 45.2$ $\sigma = 0.6$	1.45	1.20	1.06
Lognormal (*SMD*)	$l_0 = 48.35$ $\sigma = 1.05$	Lognormal (*SMD*)	$l_0 = 45.3$ $\sigma = 0.55$	1.66	1.31	1.16
Lognormal (*flat*)	$l_0 = 47.2$ $\sigma = 1.2$	Power law (*flat*)	$l_0 = 46.7$ $\alpha = 1.35$	2.06	1.69	1.49
Lognormal (*flat*)	$l_0 = 47.05$ $\sigma = 1.2$	Lognormal (*flat*)	$l_0 = 45.2$ $\sigma = 0.6$	1.55	1.72	1.50
Lognormal (*SMD*)	$l_0 = 48.6$ $\sigma = 0.9$	Lognormal (*SMD*) ($10 \times MW$)	$l_0 = 44.1$ $\sigma = 0.8$	1.57	1.36	1.20
Lognormal (*SMD*)	$l_0 = 48.6$ $\sigma = 0.9$	Lognormal (*SMD*) ($0.1 \times MW$)	$l_0 = 46.3$ $\sigma = 0.2$	3.13	1.28	1.20

Table 3.4: Results of dual population Luminosity Functions fit simultaneously to the BATSE number counts and the local distribution, presented in order of decreasing overall goodness of fit (i.e. increasing overall χ^2/dof). The LFs follow merger delay time (formation plus coalescence) distributions either *flat* in log space ($dP_m/d(\log(t)) = constant$) or the *SMD* profile of Equation 3.4. Also shown are two results normalised using order of magnitude different observed Galactic (MW) rates. The number of degrees of freedom (dof) for the local, C_{max}/C_{min} and overall distributions are 1, 20 and 24 respectively. l_0 is in units of log(erg s^{-1}), σ in dex and α is dimensionless.

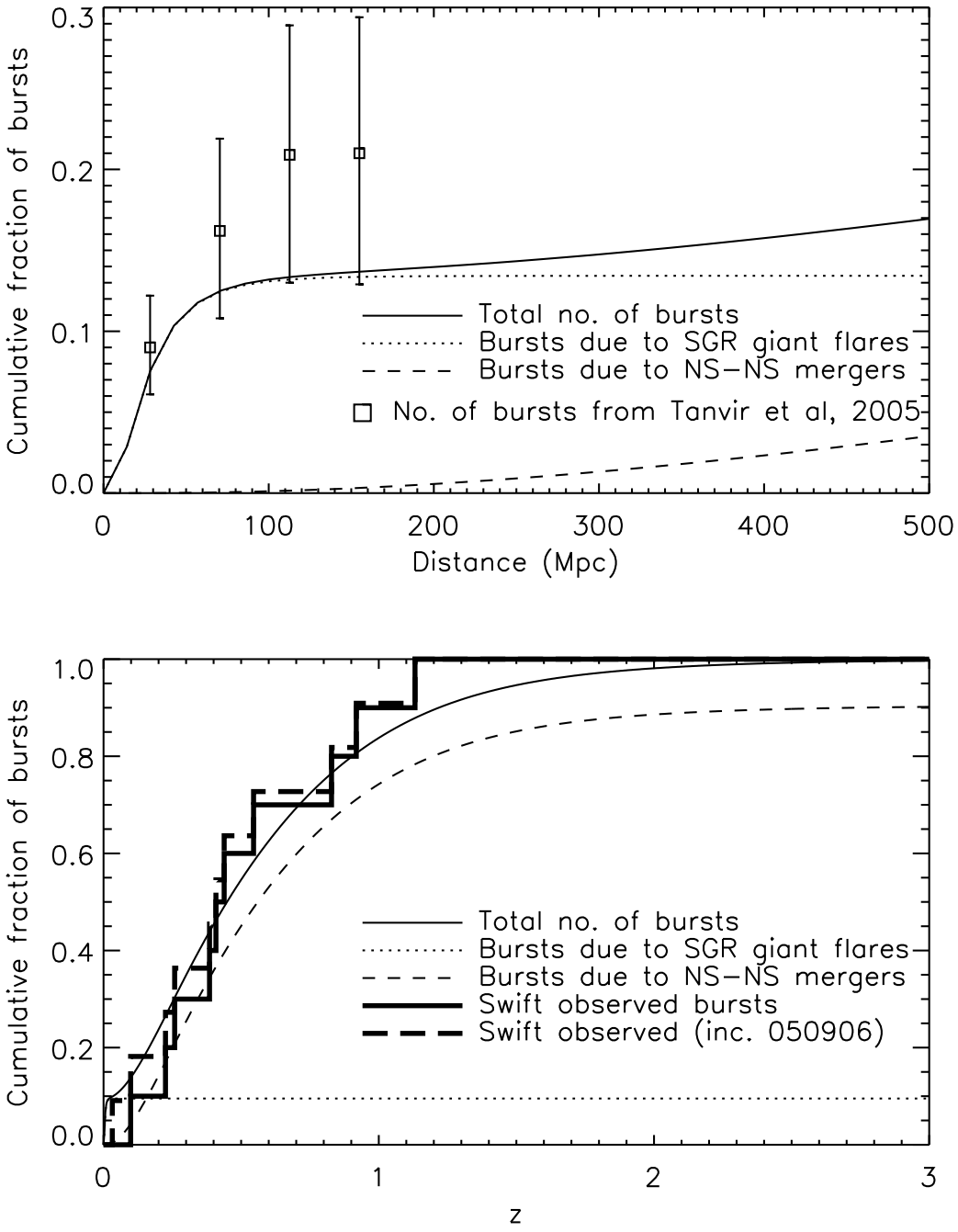

Figure 3.3: Burst distributions from dual lognormal LF (following $dP_m/d(\log(t)) =$ *constant* merger time delay distribution) populations. Panel Details as for Figure 3.1.

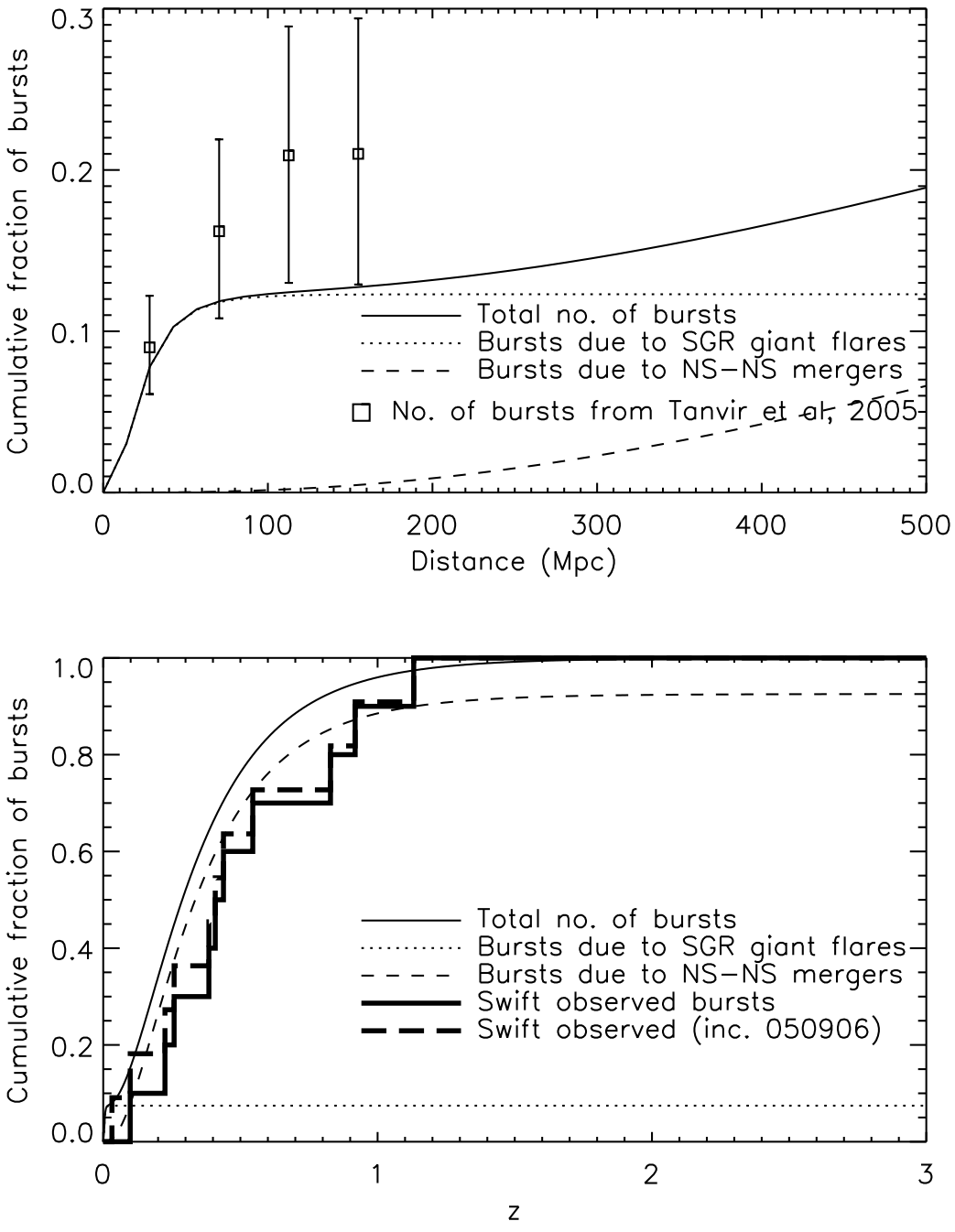

Figure 3.4: Burst distributions from dual lognormal LF (following SMD) populations. Panel Details as for Figure 3.1.

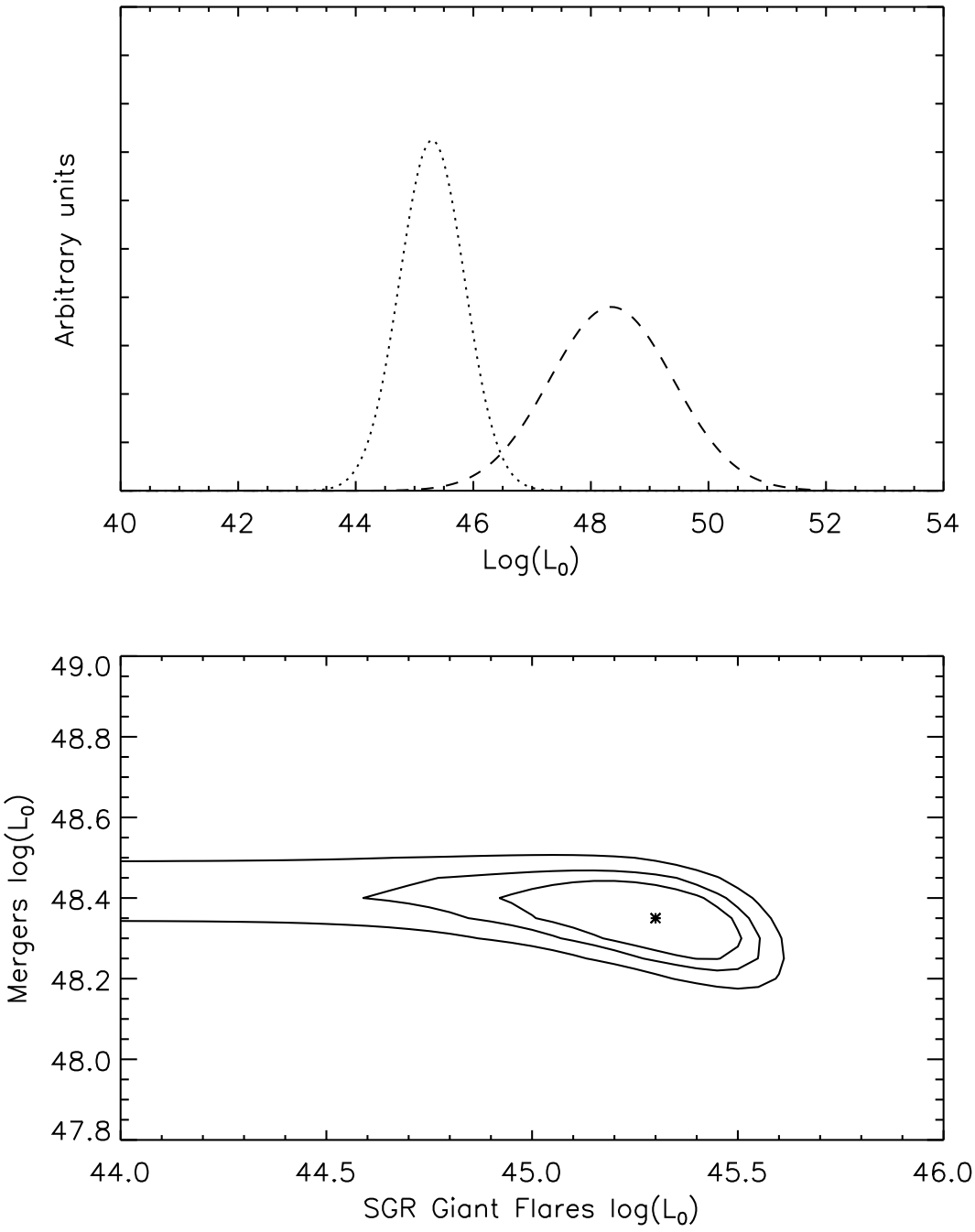

Figure 3.5: Best fit dual population LFs from Figure 3.4. The LFs (top panel: dotted line SGR giant flares, dashed line mergers) are lognormal with intrinsic merger rate components following the SMD model of Equation 3.4. The bottom panel shows contours of χ^2 in $\log(L_0)$ space. Contours shown represent 0.6, 0.9 and 0.99 confidence limits with the minimum χ^2 value plotted as an asterisk.

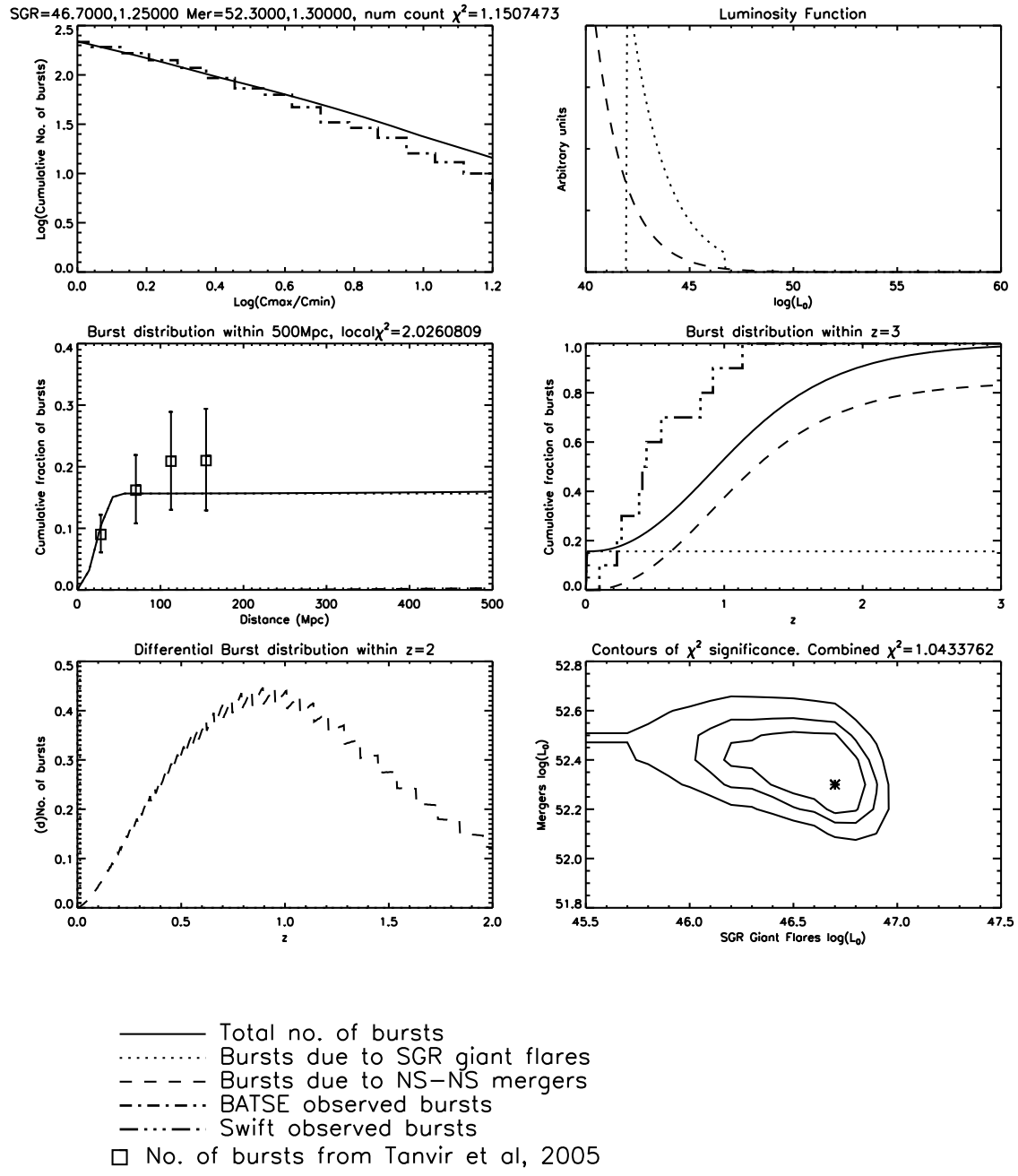

Figure 3.6: **Power Law (SGR flares) and Schechter (mergers) with merger rates following the delayed Star Formation Rate** model of Equation 3.3 fit to BATSE overall number counts and the local burst distribution. Top left: the overall best fit distribution to BATSE number counts (shown cumulative but calculated differentially), Top Right: the best fit LF; Middle Left: the local burst distribution within 500 Mpc compared to local correlation results; Middle Right: cumulative burst distribution within $z = 3$ compared to the *Swift* redshift distribution (but shown here calculated with BATSE threshold limits); Bottom Left: differential burst distribution within $z = 2$ (note that the slight ringing or sawtooth shape is an artefact of the numerical integration procedure used to integrate the Schechter function); Bottom Right: contours of χ^2 significance levels for the overall best fit LF parameters (contours show 0.6, 0.9 and 0.99 significance levels with best fit values plotted as an asterisk).

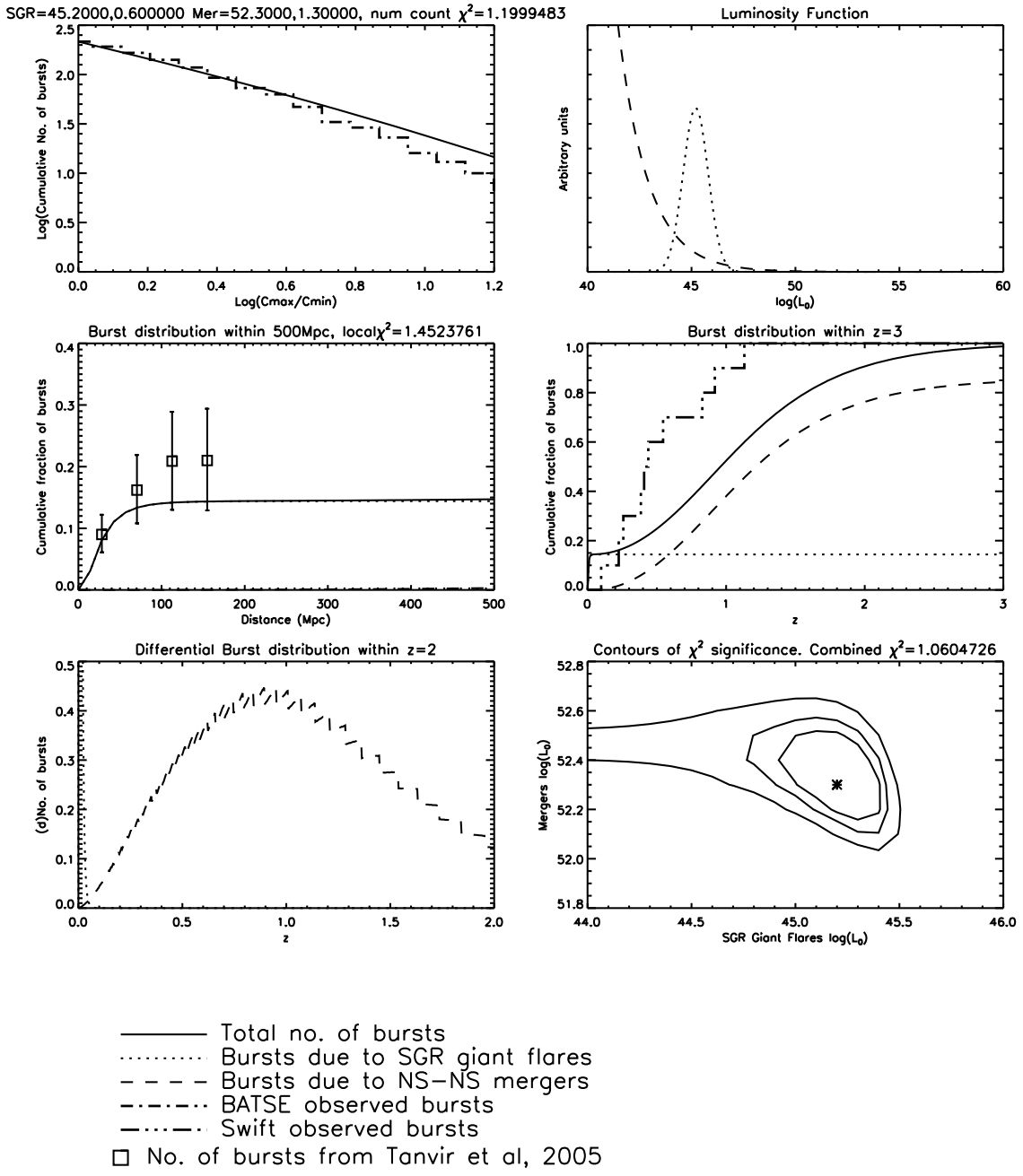

Figure 3.7: **Lognormal (SGR flares) and Schechter (mergers) with merger rates following the delayed Star Formation Rate** model of Equation 3.3 fit to BATSE overall number counts and the local burst distribution. Panel details as for Figure 3.6.

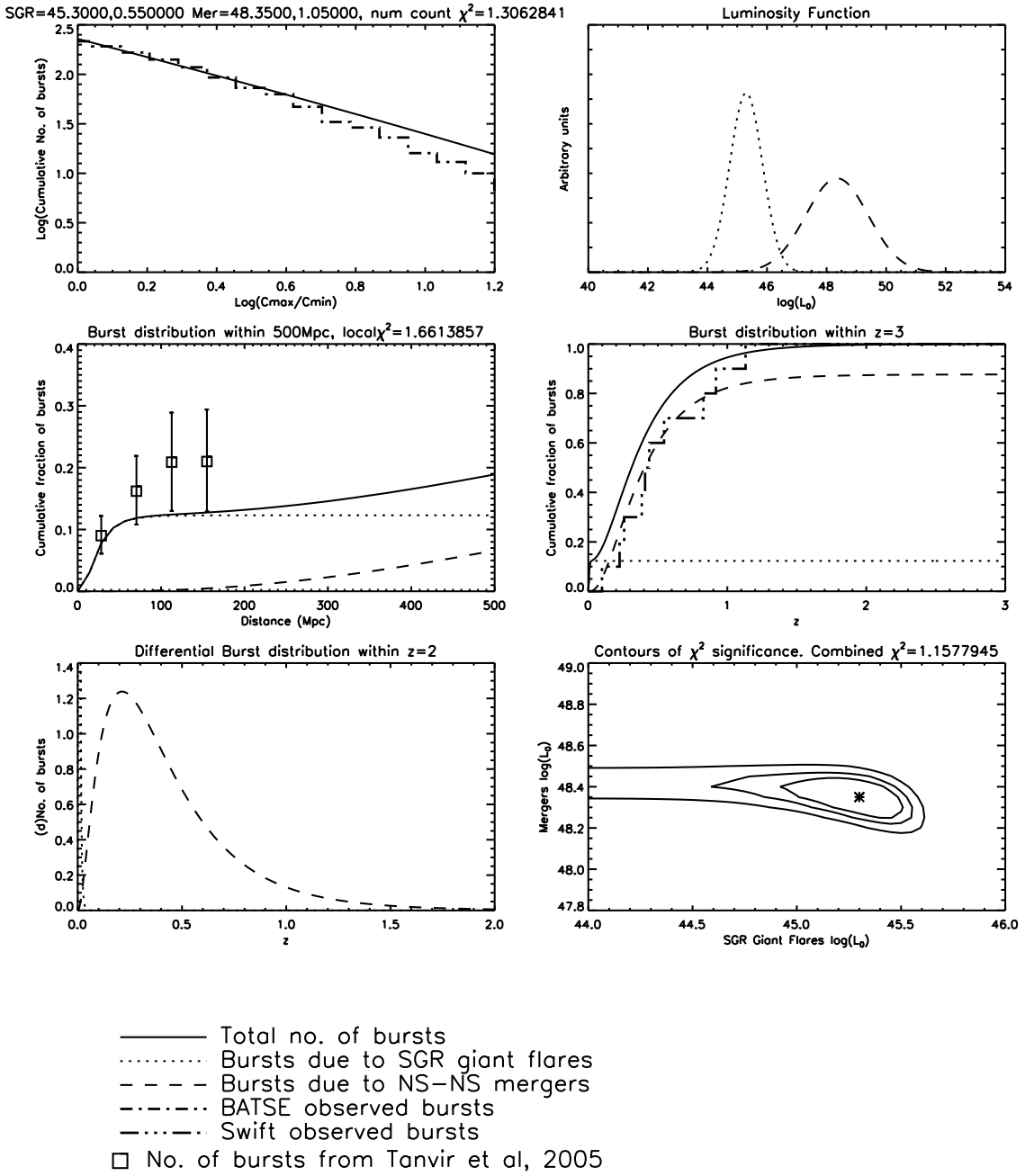

Figure 3.8: **Dual lognormal LF with merger rates following the Stellar Mass Density** model of Equation 3.4 fit to BATSE overall number counts and the local burst distribution. Panel details as for Figure 3.6.

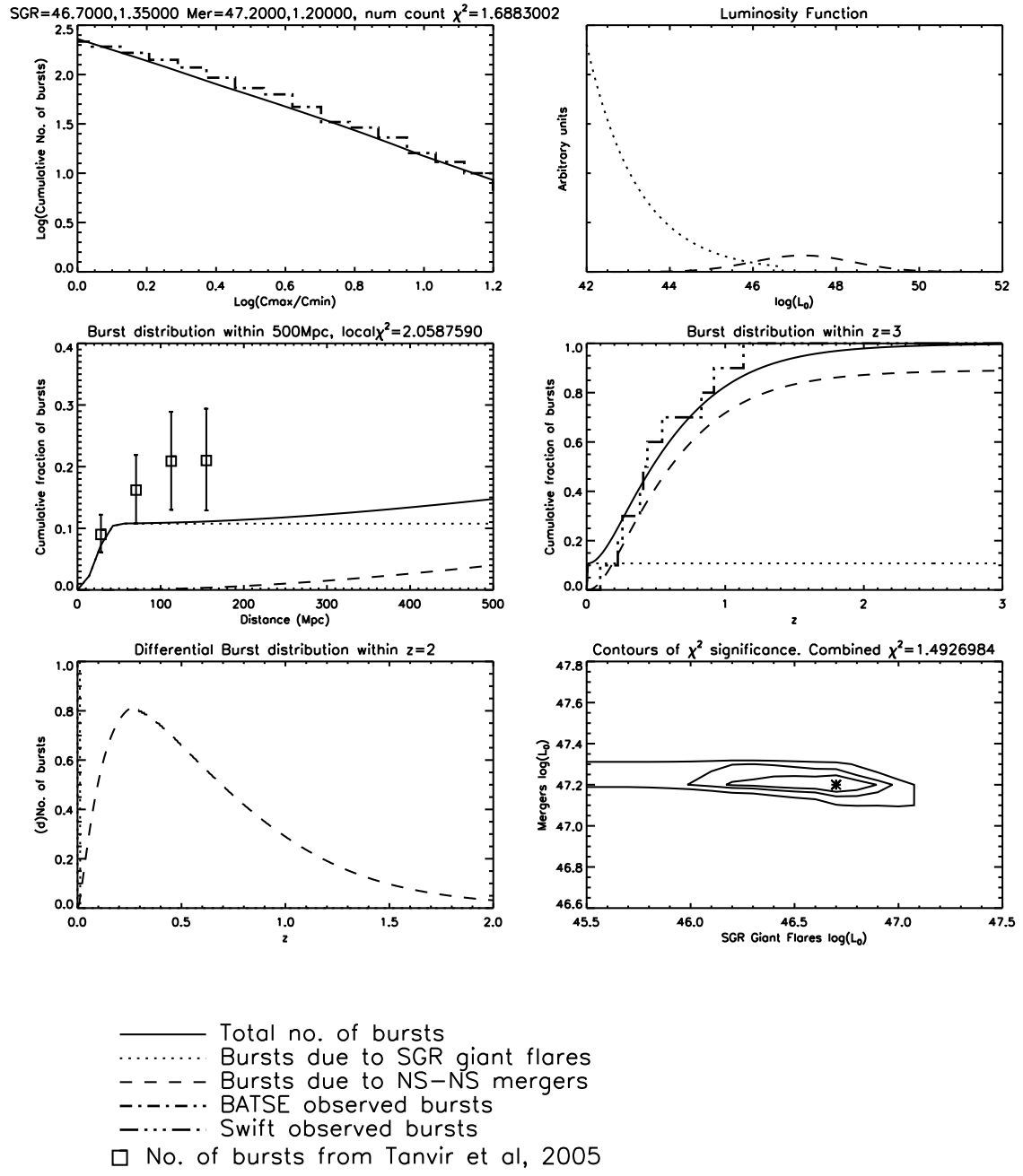

Figure 3.9: **Power Law (SGR flares) and lognormal (mergers) with merger rates following the delayed Star Formation Rate** model of Equation 3.3 fit to BATSE overall number counts and the local burst distribution. Panel details as for Figure 3.6.

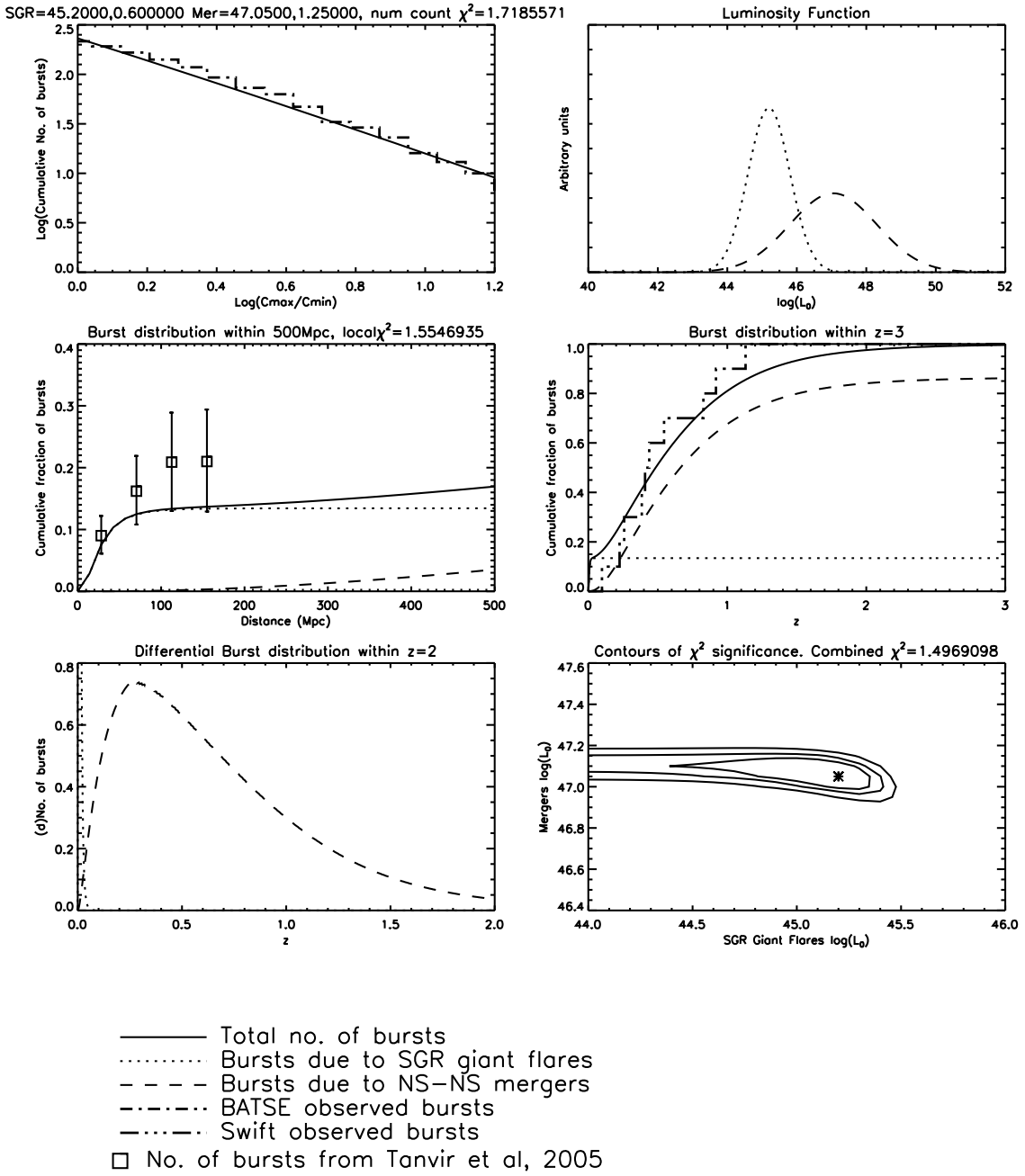

Figure 3.10: **Dual lognormal LF with merger rates following the delayed Star Formation Rate** model of Equation 3.3 fit to BATSE overall number counts and the local burst distribution. Panel details as for Figure 3.6.

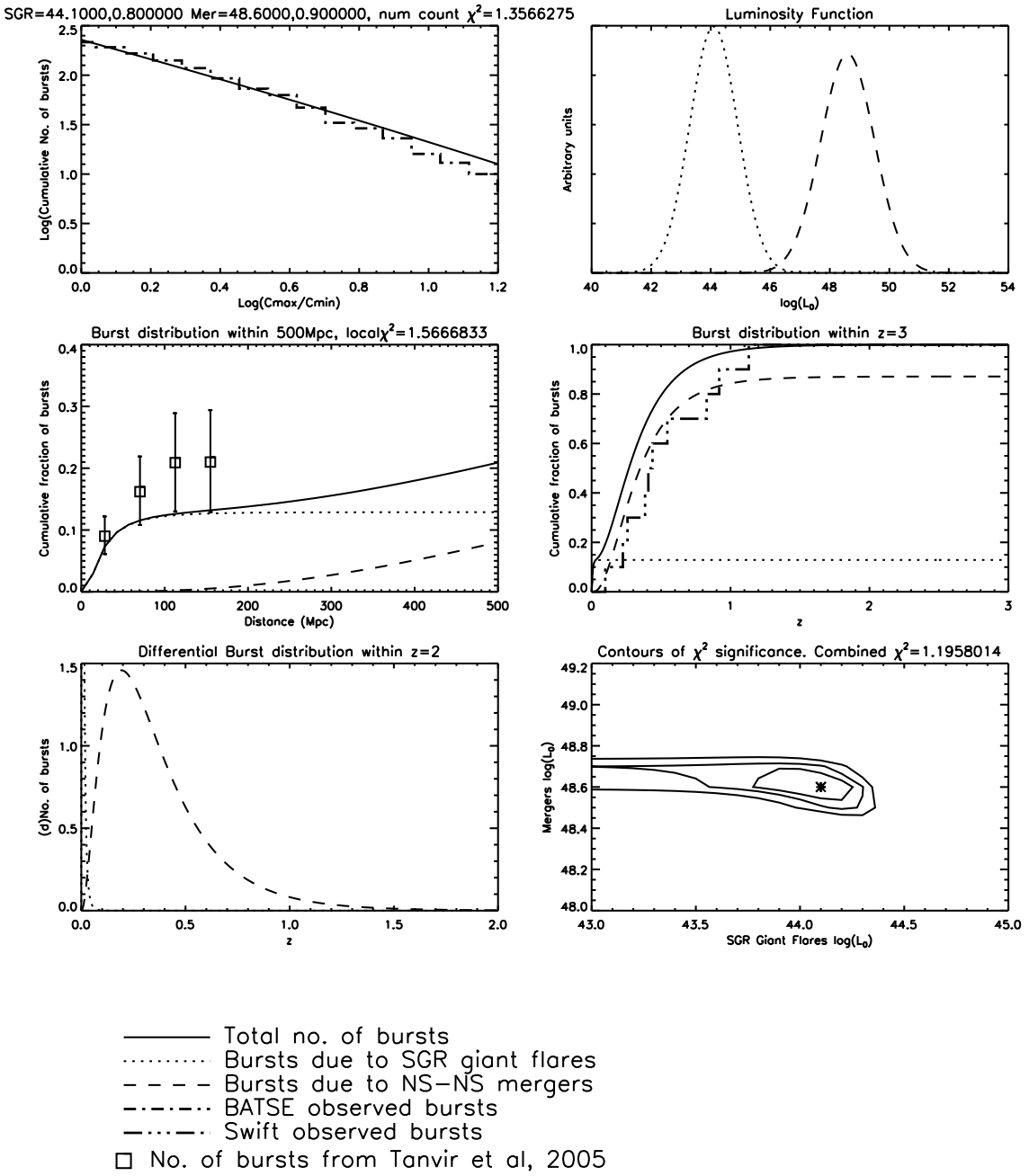

Figure 3.11: **Dual lognormal LF with merger rates following the SMD** model of Equation 3.4, and an intrinsic flare rate of 10× the observed Galactic flare rate. Panel details as for Figure 3.6.

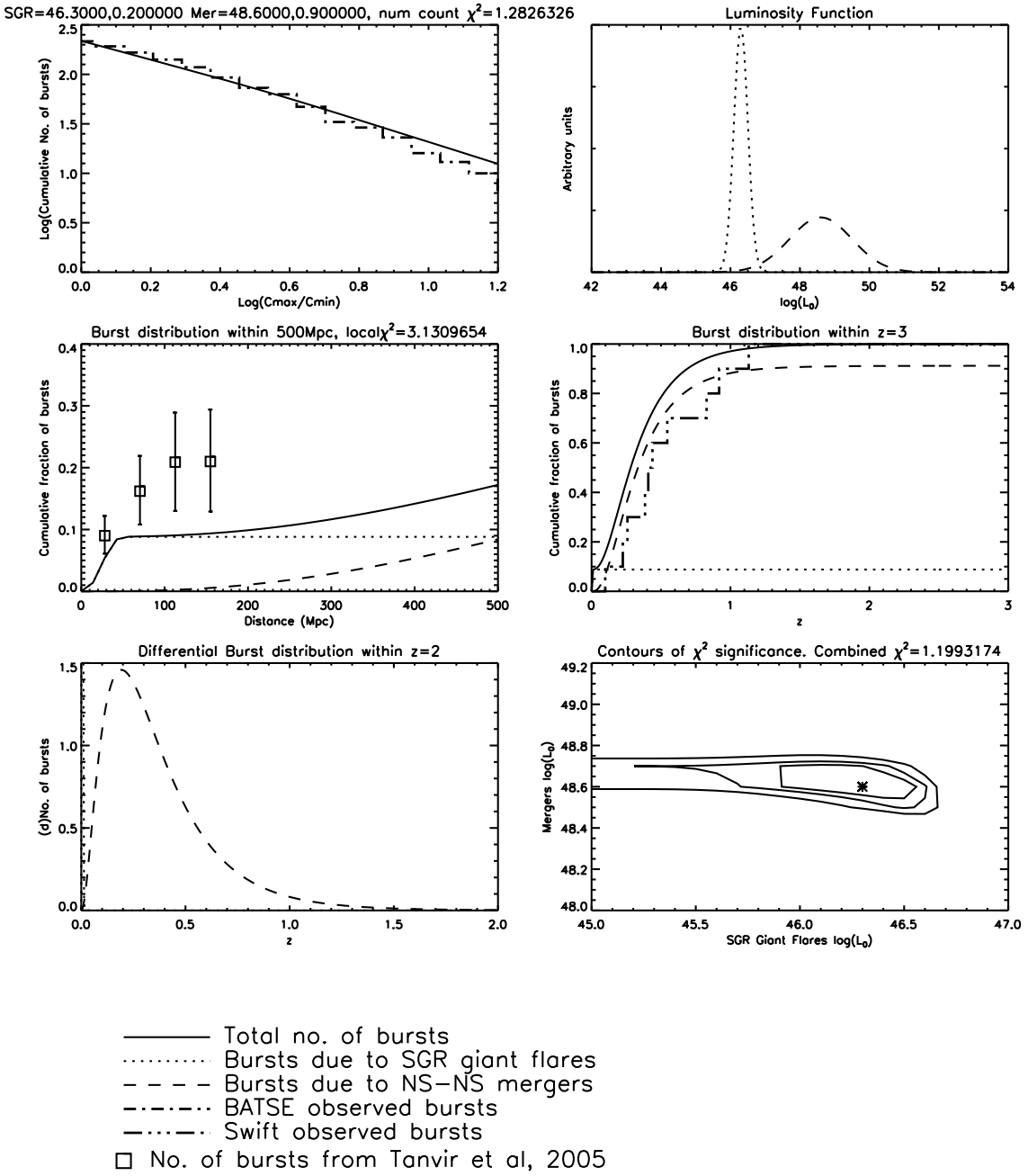

Figure 3.12: **Dual lognormal LF with merger rates following the SMD** model of Equation 3.4, and an intrinsic flare rate of 0.1× the observed Galactic flare rate. Panel details as for Figure 3.6.

3.3.3 Observed Luminosity Distributions

The above results constrain the intrinsic LF of the test populations, and having found the best fit LF parameters it is then interesting to examine the evolution of the ***observed*** LF of the SGR giant flares with distance.

Figures 3.13 to 3.15 show the observed differential luminosity distributions of the nearby bursts in discrete spheres of increasing radii (i.e. cumulative in terms of distance) using the best fit intrinsic LF parameters for the low luminosity (postulated SGR flare) population from Table 3.4. In all spheres, we see the sharp low-luminosity cutoff due to the threshold of the BATSE detection model used in the analysis. By about 30 Mpc, the observed LF is peaking at a luminosity of $\sim 10^{46}-10^{47}$ erg s^{-1} for all models tested, remaining constant with distance after that. By about 114 Mpc (nearer for the power law intrinsic LF), we are seeing no more low luminosity bursts (as would be expected from Figures 3.6 to 3.8) and the observed LF remains constant thereafter.

This evolution clearly shows the balance between the increasing total number of bursts with volume offset by the decreasing probability of the occurrence of bursts sufficiently luminous to be observed at that distance in the ***intrinsic*** LF. We see that no matter which of the functional shapes of intrinsic LF considered, beyond about 30 Mpc the most probable flares that may be detected have luminosities at around the level of the 2004 SGR 1806-20 event. This can perhaps be seen most clearly in the surface plot of observed differential distributions (with respect to distance and luminosity) of the lognormal model shown in Figure 3.16.

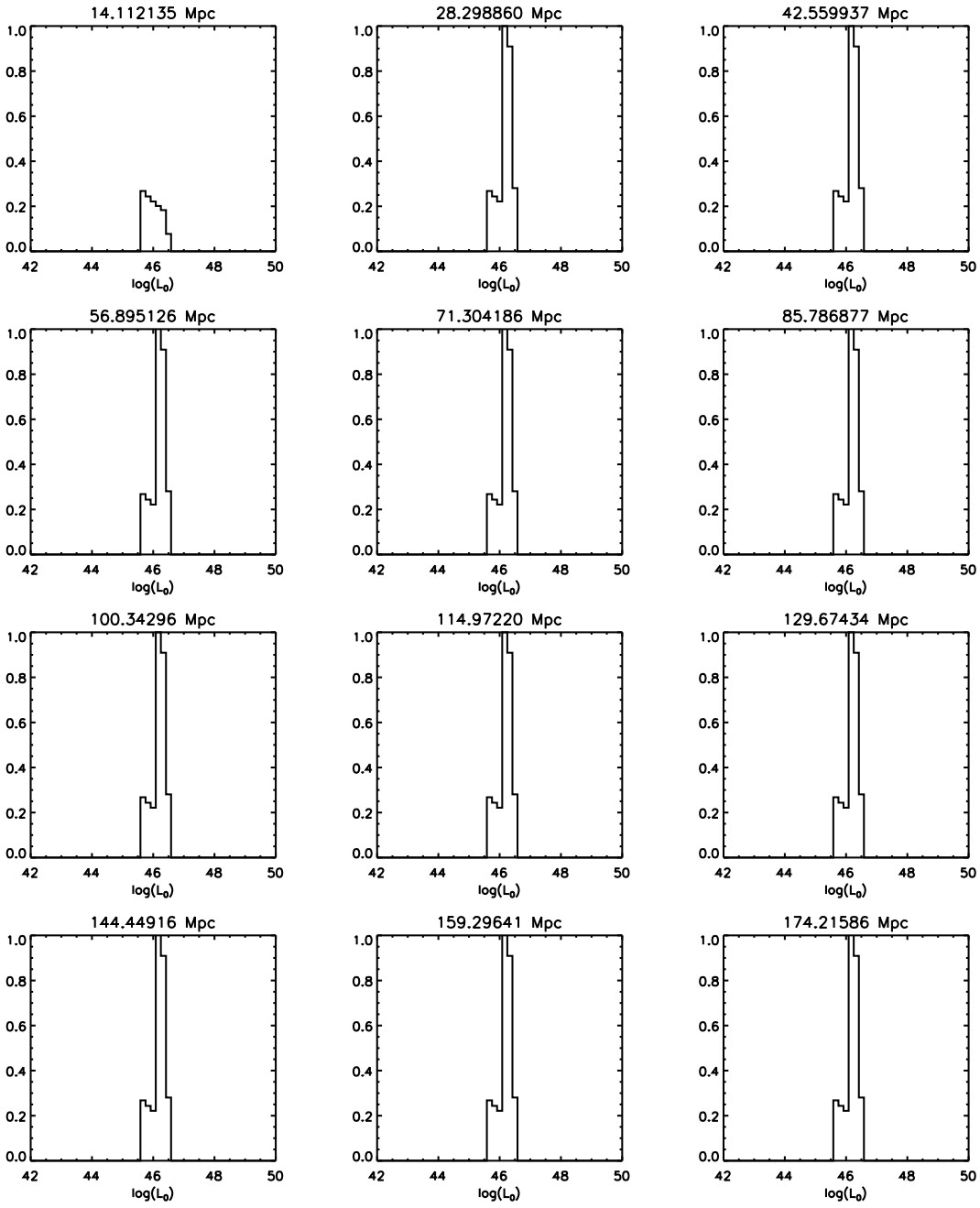

Figure 3.13: Observed LFs of SGR flare luminosities generated by the best fit power law (following delayed SFR) intrinsic LF. Panels show differential (with respect to luminosity) distributions for concentric radii spheres (i.e. cumulative with respect to distance) increasing left to right, top to bottom, normalised to maximum number of flares.

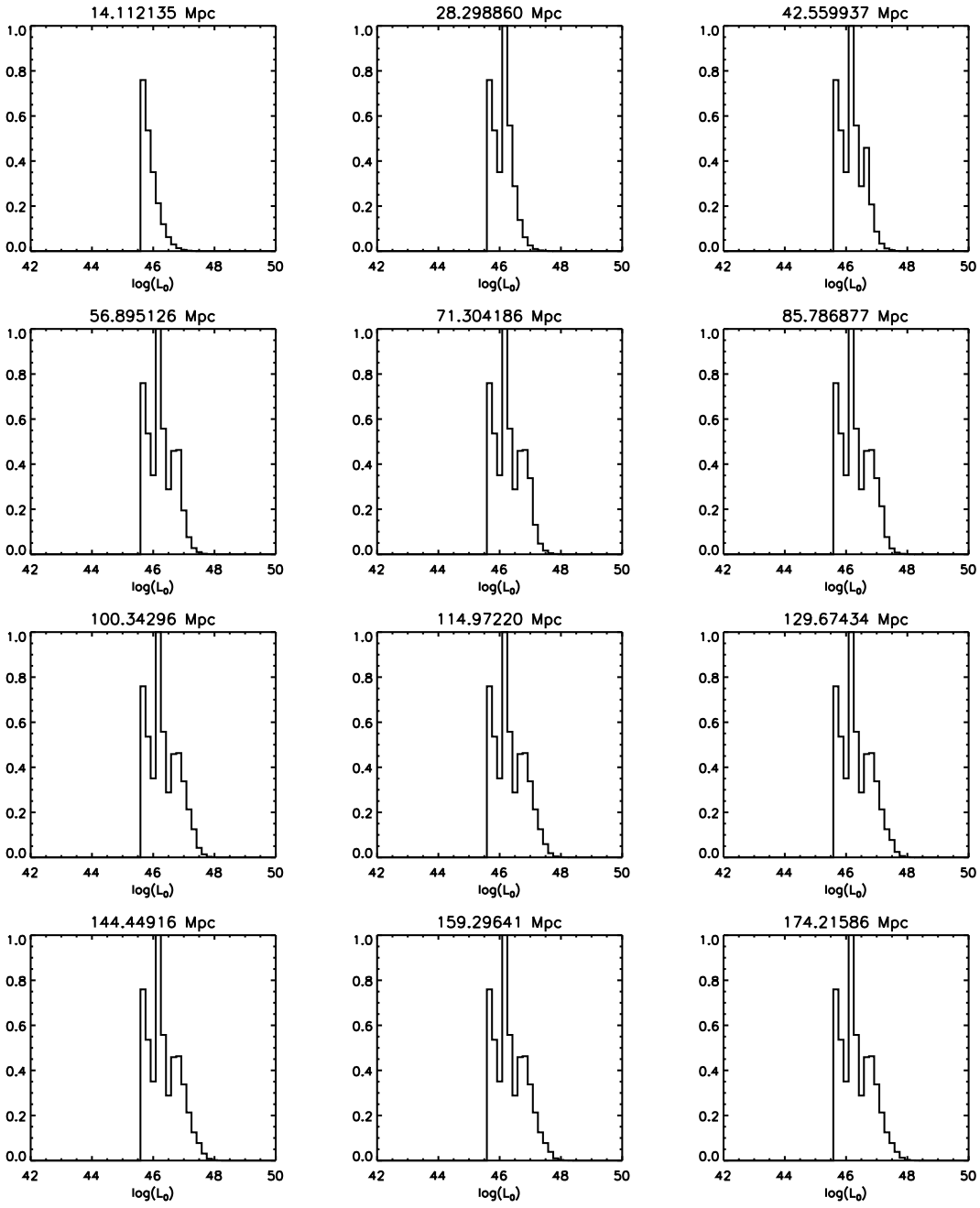

Figure 3.14: Observed LFs of SGR flare luminosities generated by the best fit log-normal (following delayed SFR) intrinsic LF. Panel details as in Figure 3.13.

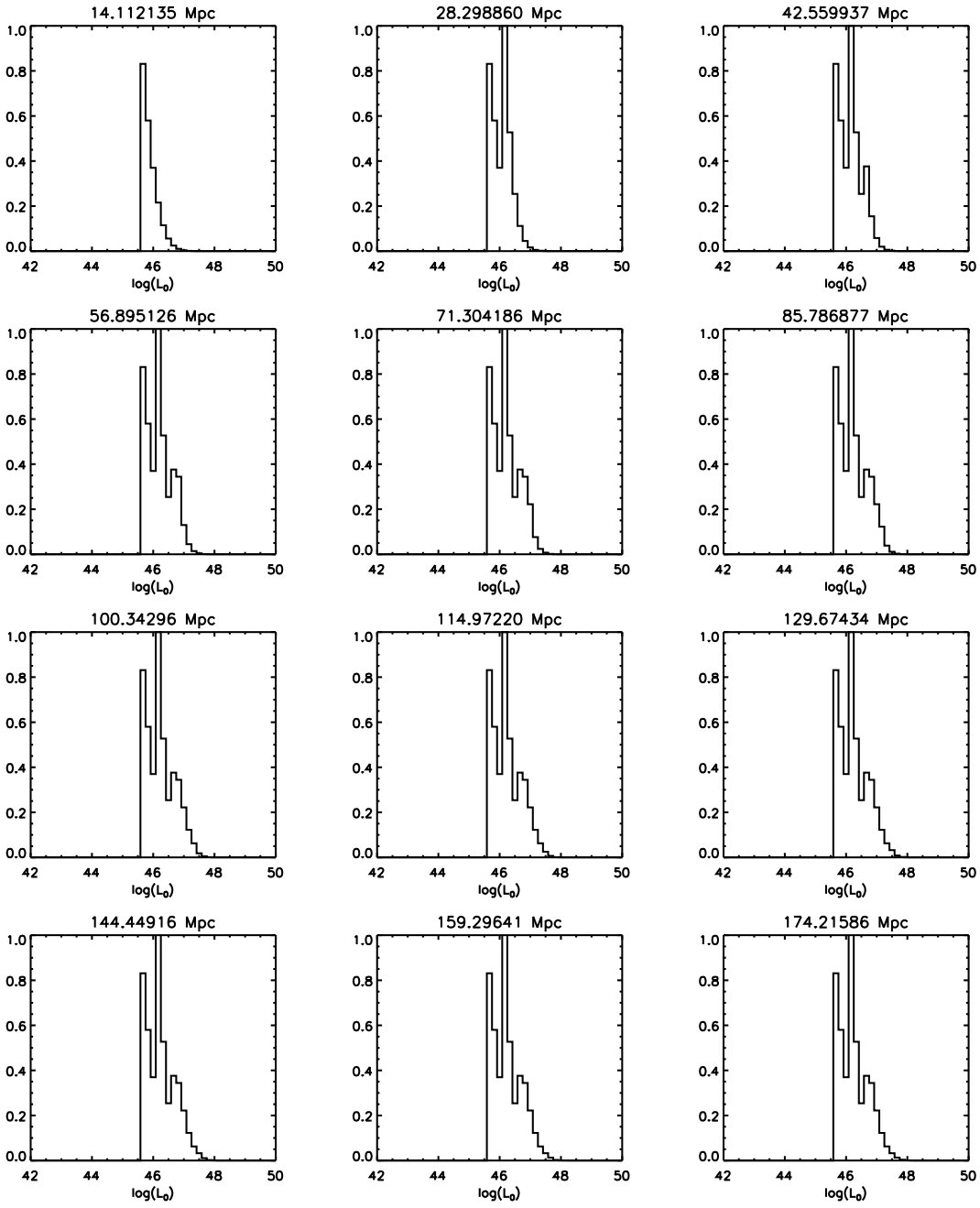

Figure 3.15: Observed LFs of SGR flare luminosities generated by the best fit log-normal (following SMD) intrinsic LF. Panel details as in Figure 3.13.

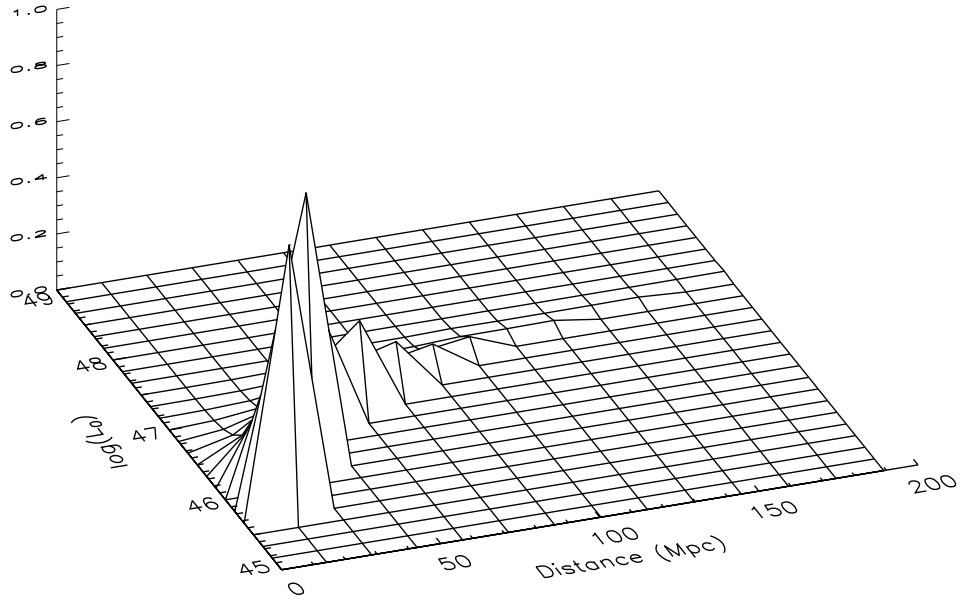

Figure 3.16: Surface plot of differential observed luminosities of SGR flare generated by the best fit lognormal (following delayed SFR) intrinsic LF. The distributions are differential with respect to both luminosity and distance, and normalised to the maximum number of flares.

3.4 Discussion

Figures 3.3 and 3.4 raise two issues worth remarking on. Firstly, they suggest that a combined (local) flare and (cosmological) merger population is sufficient to reproduce adequately the *Swift* z-distribution without the need for further cosmological populations as suggested, for example, in Salvaterra et al. (2007). Secondly, the lower panels of the figures imply Swift should have triggered on about one SGR flare to date (this would rise by a factor of ~ 2 if the redshift completeness for such flares were greater than for S-GRBs as a whole, as is likely given that low-redshift host galaxies are more easily identified). We note that a possible candidate is GRB 050906, the *Swift* BAT error circle of which (Figure 3.17) contains a relatively local galaxy, IC328 (Levan & Tanvir 2005), which may be considered likely to host many SGRs being both massive and actively star forming. At the distance of IC328, ≈ 130 Mpc, the inferred isotropic-equivalent energy release of GRB 050906 would have been $\sim 1.5 \times 10^{46}$ ergs in the 15–150 keV range, which is certainly comparable to the total energy release (> 30 keV) of the SGR 1806-20 giant flare of $\sim 4 \times 10^{46}$ ergs (Levan et al. 2008). However, the association of GRB 050906 with IC328 cannot be made with certainty, since the galaxy lies at the edge of the 2.6 arcmin (90% confidence) radius BAT error circle, and this circle contains other galaxies at higher redshifts too. Nevertheless, galaxies such as IC328 are rare in GRB error boxes, and Levan et al. (2008) estimate a $< 1\%$ likelihood of this alignment occurring by chance. If we assume that GRB 050906 is associated with IC328 and include this burst in the *Swift* redshift distribution (long-dashed histogram in Figures 3.4 and 3.3), then the agreement with the dual LF models is better still.

Though not *Swift* detections, there are two further recent S-GRB events which are candidate extragalactic SGR flares: GRB 051103 whose IPN error box (Figure 3.18) includes the outskirts of M81 at 3.5 Mpc (Golenetskii 2005), and GRB 070201 whose error box similarly overlaps a spiral arm of M31 (Figure 3.19) at only $\sim$ 0.77 Mpc (Perley & Bloom 2007; Pal'Shin 2007; Mazets et al. 2008). In terms of their duration and light curve shape, both share similar characteristics with SGR giant flares (Frederiks et al. 2007b; Mazets et al. 2008; Ofek et al. 2008), and furthermore the non-detection of gravitational waves by LIGO from GRB 070201 (LIGO Scientific Collaboration 2007) excludes a merger progenitor within M31 with $> 99\%$ confidence. If both these events were due to extragalactic SGRs then this brings to three the number of giant flares with peak luminosity $> 10^{47}$erg s^{-1} seen locally in just a few years. As can be seen from Figure 3.16, this level of luminosity is certainly

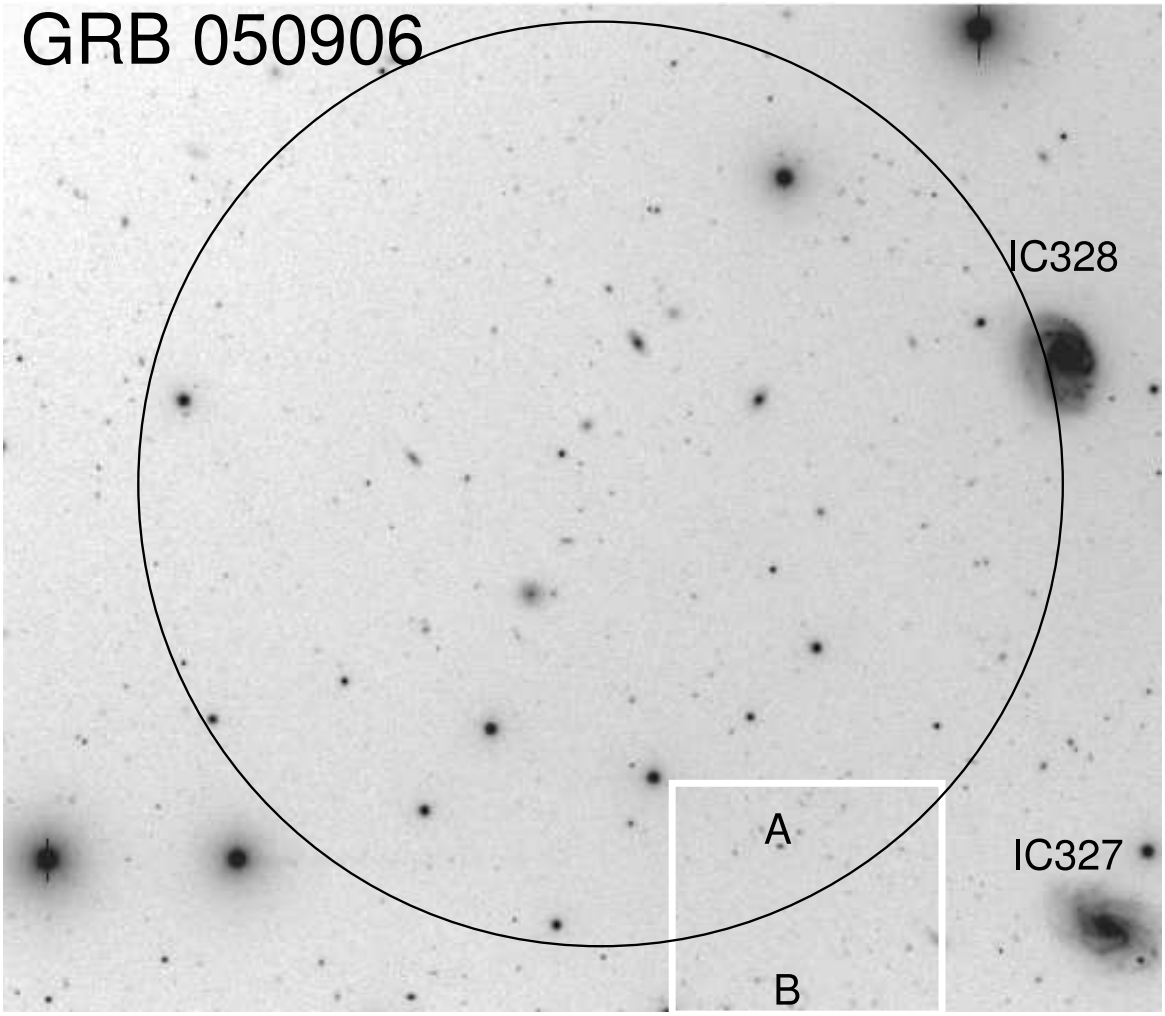

Figure 3.17: The *Swift* BAT error box of GRB 050906. IC328 can be seen on the edge of the 2.6 arcmin radius BAT error circle. The white box indicates two further galaxies, A and B, which have spectroscopic redshifts of $z = 0.43$, hence demonstrating the alternative possible association of this burst with a higher redshift cluster. Figure reproduced from Figure 1 of Levan et al. (2008).

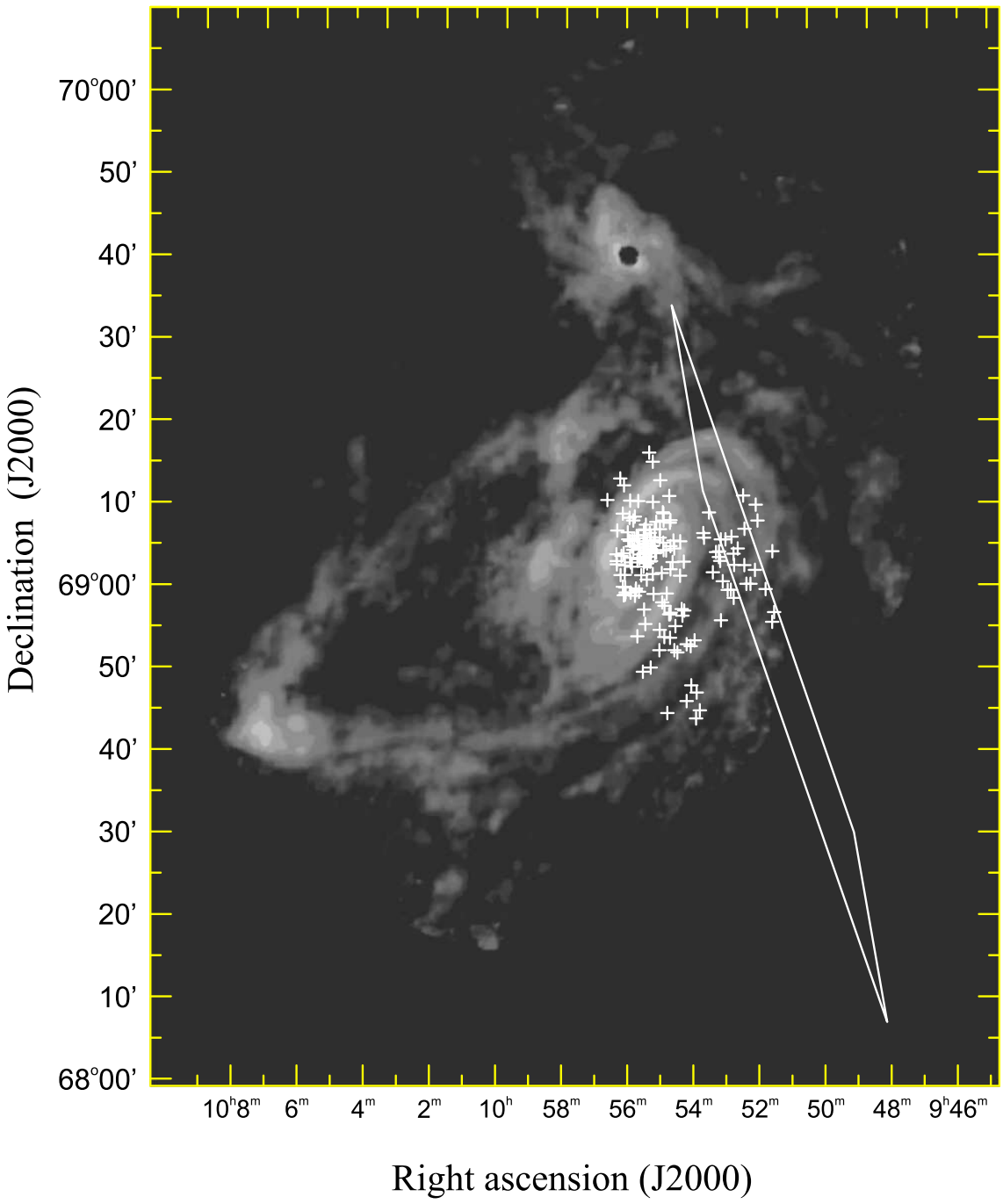

Figure 3.18: The IPN error box of GRB 051103 in relation to the M81 group in 21cm HI emission. Figure reproduced from Figure 4 of Frederiks et al. (2007b), the white crosses are Chandra observed X-ray sources.

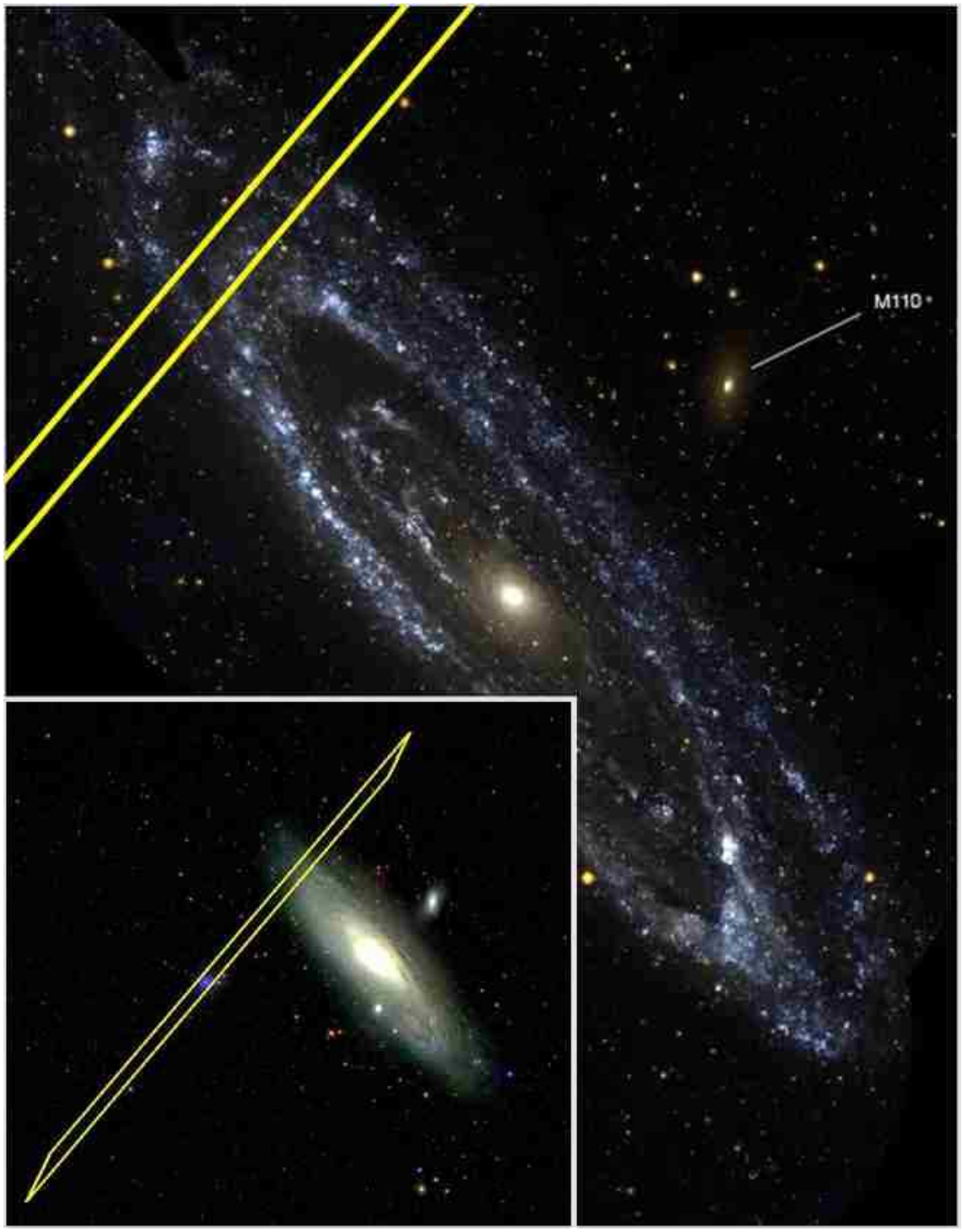

Figure 3.19: The IPN error box of GRB 070201 in relation to M31 in UV light as observed by *GALEX* (inset shows full error box superimposed on SDSS image of M31). Figure reproduced from Figure 1 of LIGO Scientific Collaboration (2007).

larger than the most probable observed luminosities our models would predict for flares within this distance.

Levan et al. (2008) estimated that a Galactic SGR giant flare rate of $\sim 5 \times 10^{-4}$ yr^{-1} would be sufficient to produce ~ 10 extragalactic flares per year similar to the SGR 1806-20 event within a sphere of radius 100 Mpc. Using a power law LF (constrained by a search for positional coincidences between galaxies within 20 Mpc and the IPN error boxes of a sample of 47 S-GRBs), Ofek (2007) estimated the rate of extragalactic flares with energy $> 3.7 \times 10^{46}$erg (the energy of the 2004 SGR1806-20 event (Hurley et al. 2005)) to be $\sim 0.5 \times 10^{-4}$ yr^{-1} per SGR, and the 95% confidence lower limit of the Galactic rate to be 2×10^{-4} yr^{-1} per SGR. Integrating the best fit lognormal (following SMD) intrinsic LF enables us to estimate the rate of flares with peak luminosity $> 10^{47}$ erg s^{-1} to be between these two values at $\sim 1 \times 10^{-4}$ yr^{-1} per SGR. We can then use this predicted intrinsic rate to investigate the likelihood of having observed two extragalactic SGR flares with such luminosity within the 17 years of IPN3 observation.

Considering a local volume within 5 Mpc (encompassing both M31 and M81/82), then the SFR of galaxies within this volume as listed by Ofek (2007) (with revised distance estimates (Karachentsev et al. 2004)) can be estimated to be about 22× that of the Milky Way. Adopting our predicted flare rate, the probability of observing two (one) or more such flares within this volume during the 17 years of IPN3 observation is 1% (14%). This indicates we have been witness to a rather rare coincidence, and is perhaps suggestive that not both GRB 051103 and GRB 070201 are SGR flares.

3.5 Summary and Conclusions

We have examined a selection of plausible Luminosity Functions, singly and in combination, for both neutron star mergers and SGR giant flares as progenitors of short Gamma-ray Bursts. Assuming observed and theoretical Galactic intrinsic rates, merger delay time distributions, Star Formation Rate and Stellar Mass Density parameterisations, we exclude both lognormal and Schechter type LFs for a single NS merger population of progenitor as being unable to produce a nearby S-GRB population while remaining consistent with overall BATSE number counts. Indeed, given that even a Schechter function (dominated by low luminosity events) cannot reproduce the likely local population, it is hard to conceive of any unimodal LF

which could and still be consistent with the higher redshift distribution. We suggest that at least a bimodal LF, and therefore likely a dual population model, is necessary to account for the local population. Given the uncertainties in the intrinsic rates assumed, we cannot sensibly choose between the LF combinations, but we point out that the best fit LF parameters in all dual populations considered are in reasonable agreement with the known properties of SGR giant flares and classic S-GRBs, even when the intrinsic rate of Galactic SGR flares is varied by an order of magnitude in either direction. To put this another way, as is well known a single population Luminosity Function provides a good fit to overall BATSE number counts, but we find that a separate, lower luminosity population of progenitors is both required, and is sufficient, to reproduce a local S-GRB population. Furthermore, the properties of this population are in agreement with those observed from Galactic SGR giant flares.

In addition, all dual populations (except those where the merger population is described by a Schechter function) produce a redshift distribution in reasonable agreement with that of S-GRBs in the *Swift* era - which we emphasise played no part in the fitting procedure for our modelling - without the need for additional cosmological populations. This agreement is improved further by inclusion of the plausibly low-redshift ($z \approx 0.031$) *Swift*-detected GRB 050906 in the overall *Swift* redshift distribution. Conversely however, our results imply that it is unlikely that both GRB 051103 and GRB 070201 (neither of which triggered *Swift*) are nearby extra-galactic SGR flares. The non-detection by LIGO of gravitational waves coincident with GRB 070201 excludes a NS-NS merger event within 3.5 Mpc as the source of this burst at the 90% confidence level (LIGO Scientific Collaboration 2007), thus providing further tentative evidence in favour of GRB 070201 being more likely as a candidate SGR giant flare.

Chapter 4

Are there more nearby Long GRBs in the BATSE Catalogue than just GRB 980425?

4.1 Introduction

In the preceding two Chapters, we have concentrated exclusively on the short ($T_{90} <$ 2s) class of GRBs. In this Chapter, we turn to the long GRBs (L-GRBs, $T_{90} \geq 2$s) which constitute $\sim 75\%$ of the BATSE catalogue. Previously, we used this set of all BATSE long bursts purely as a control, where they were shown as a whole to exhibit no measurable correlation with local galaxies. However, is it possible that there is a sub-sample of these L-GRBs that may be identified with a local population? In this Chapter we will first briefly review some of the observed properties of L-GRBs and empirical relations among those properties which may be used to extract plausible subsets of L-GRBs for separate investigation. We then present correlation results using the methods of the previous Chapters to constrain the fraction of L-GRBs which may have occurred within ~ 155 Mpc.

Historically, owing to their extended afterglows and greater relative ease of localisation, long GRBs are the better monitored and understood class. Accurate redshifts have been obtained spectroscopically both by studying the absorption of their afterglows, and by virtue of their precise localisations on host galaxies. In particular, the (typically less than 5) arcsecond localisation of L-GRBs by the XRT onboard *Swift* has meant that redshifts have been obtained for almost a third of

Swift detected bursts (Burrows et al. 2008). The mean redshift of *Swift* L-GRBs was measured in late 2005 for an unbiased sample of 16 long GRBs as $z = 2.8$ (Jakobsson et al. 2006b), and the highest redshift so far is $z = 6.295$ (Haislip et al. 2006; Kawai et al. 2006). At the other end of the scale, *Swift* has also detected the second lowest redshift GRB so far, GRB 060218 with $z = 0.0331$.

Furthermore, even before *Swift*, sufficient L-GRBs were well-localised and well-studied enough for several empirical correlations between their observed properties to be proposed. For example, *BeppoSAX* L-GRBs with robust redshift and spectral measurements were found to show a correlation between spectral peak energy and overall isotropic energy release - the E_p/E_{iso} or Amati relation (Amati et al. 2002) - where spectrally softer bursts are less isotropically energetic. This correlation has since been extended to include *HETE-2* bursts, X-ray Flashes (Sakamoto et al. 2005; Lamb, Donaghy & Graziani 2004), and *Swift* bursts (Amati 2006b). Correcting E_{iso} for beaming factors calculated from observed jet break times, Ghirlanda, Ghisellini & Lazzati (2004) also found a correlation between Ep and this beaming corrected energy output. However, neither of these two relations are without controversy, with several authors arguing that the exact form of correlations are strongly dependent on selection and instrumental effects (e.g. Friedman & Bloom 2005b; Nakar & Piran 2005; Band & Preece 2005; Butler, Kocevski & Bloom 2008).

Long duration GRBs ($T_{90} > 2$s) also exhibit a spectral lag-luminosity relationship (Norris, Marani & Bonnell 2000; Salmonson & Galama 2002; Norris 2002) where there is anti-correlation between overall luminosity and the time delay between the observation of equivalent temporal features in different energy bands (observed pulses in general appearing earlier at higher energies). Furthermore, GRBs with long spectral lags (and hence low luminosity) tend to have smoother light curves with broader features, and lower peak fluxes (Norris, Scargle & Bonnell 2001). Isotropic-equivalent peak luminosity has also been shown to correlate with light curve variability, originally for a relatively small number of bursts (Reichart et al. 2001; Fenimore & Ramirez-Ruiz 2000) but recently confirmed by Guidorzi et al. (2005) for a larger sample, though with a larger scatter in the data. Though the exact form and tightness of the correlation is currently a matter of some debate (Reichart & Nysewander 2005; Guidorzi et al. 2006; Li & Paczyński 2006), there appears little doubt that the luminosity of long GRBs correlates with variability.

The two closest Gamma-ray Bursts detected so far are GRB 980425 (Galama et al. 1998) and GRB 060218 (Cusumano et al. 2006; Mirabal & Halpern 2006), both long duration GRBs of exceptionally low intrinsic luminosity. Indeed GRB980425 is

usually taken as the archetypal low-luminosity, low variability, soft spectrum GRB. Though an outlier to the E_p/E_{iso} relationship in the sense of being too spectrally hard for its isotropic luminosity, it is still softer than the majority of BATSE long bursts. These two bursts and the further example of the low-redshift, low-luminosity GRB 031203 (Gotz et al. 2003; Prochaska et al. 2004; Watson et al. 2004), are extensively reviewed by Kaneko et al. (2007), and their light curves are shown in Figure 4.1. These three light curves are unfortunately from three separate instruments, which makes detailed comparisons difficult (given different energy ranges and sensitivities of detectors etc.), however broadly speaking they can be seen to be relatively featureless, single peaked FRED (Fast Rise Exponential Decay) type light curves. This similarity in shape will be used in our burst sample selections below.

Thus these three bursts, along with the correlations discussed above, suggest that GRBs observed to be under-luminous with smooth light curves are drawn from a relatively nearby population. Further support is given to this argument by the fact that the proportion of long-lag bursts increases from negligible among BATSE bright bursts to $\sim 50\%$ at trigger threshold (Norris 2002). In addition, if there is a separate population of intrinsically low-luminosity L-GRBs, then their proportion will naturally increase towards lower observational thresholds (e.g. Coward 2005). Similar arguments based on analyses of detector sensitivities, and the detection rates of bursts known to be local, also suggest that a sub-class of low-luminosity bursts may be much more prevalent in the local Universe than their higher luminosity cousins (Soderberg et al. 2006b; Liang et al. 2007; Cobb et al. 2006b).

During nine years of operation, BATSE detected 2704 GRBs, of which $\approx 75\%$ were long. Very few of these bursts have identified hosts or redshifts, but if some originated within similar distances to GRB 980425 and GRB 060218 then it should be possible to estimate this fraction statistically via their distribution on the sky, using the same technique with which in Chapter 2 we found $\approx 20\%$ of BATSE short bursts to be correlated with galaxy samples within ≈ 112 Mpc (Tanvir et al. 2005). If indeed there is a large population of under-luminous, smooth long GRBs, then restricting the long burst sample to those with light curve properties similar to GRB 980425 should enhance any correlation signal.

We therefore consider below the correlation between BATSE long bursts and the two galaxy catalogues used in the preceding analyses of S-GRBs: the PSCz galaxy redshift survey (Saunders et al. 2000) and as a check once again against possible catalogue biases, the Third Reference catalogue of Bright Galaxies (RC3) (de Vaucouleurs et al. 1991).

GRB 980425 (BATSE & *BeppoSAX*)

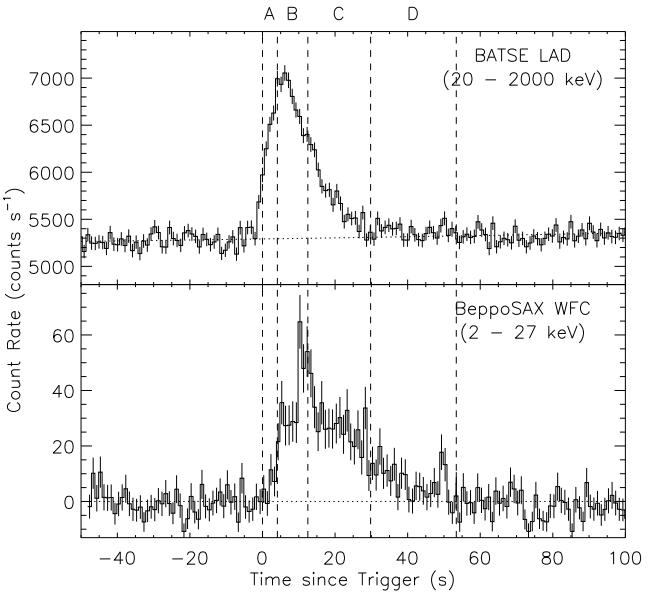

GRB 031203 (*INTEGRAL*)

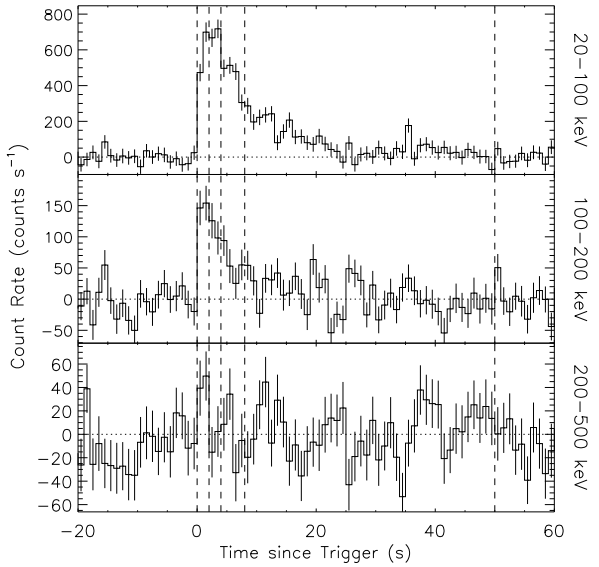

GRB 060218 (*Swift* BAT & XRT)

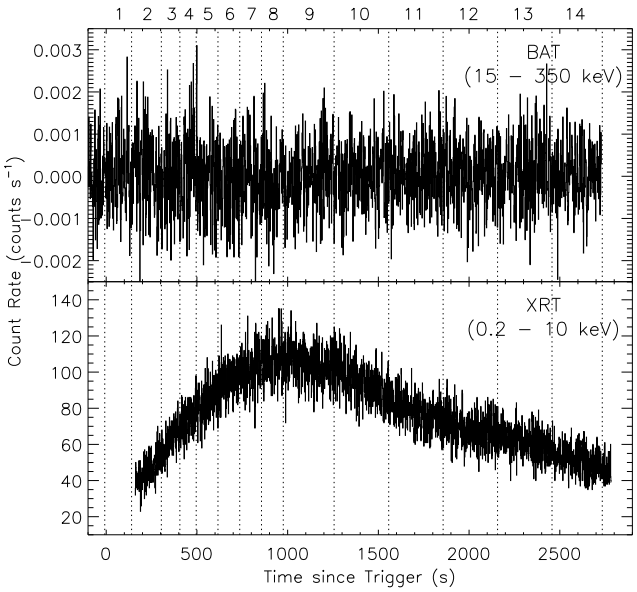

Figure 4.1: Light curves of the three closest L-GRBs to date: top panel GRB 980425, middle GRB 031203, and bottom GRB 060218. Figures from Kaneko et al. (2007).

4.2 Methods

The long burst sample consists of the 1437 long GRBs with location errors $\leq 10^{\circ}$ and measured fluences in the current BATSE catalogue (4B(R) Paciesas et al. (1999), including web supplement). Our galaxy samples are drawn from two galaxy catalogues, the *IRAS* PSCz galaxy redshift survey (Saunders et al. 2000) and the Third Reference Catalogue of Bright Galaxies (RC3) (de Vaucouleurs et al. 1991). Using the measured heliocentric recession velocities of galaxies in these catalogues, we made samples of galaxies within concentric spheres of recession velocity $v < 2000,\ 5000,\ 8000$ and 11000 km s^{-1} (corresponding to radii of $28(z = 0.0067)$, 70(0.017), 113(0.027) and 155(0.037) Mpc respectively). Following the method described in Chapter 2 and Tanvir et al. (2005), we define the statistic Φ for each galaxy sample compared with the long GRBs as shown in Equation 2.2.

To reiterate, the closest known bursts (GRBs 980425, 060218 and 031203) were under-luminous and spectrally soft with smooth single-peaked light curves. In order to select a burst sub-sample with properties similar to these bursts, three separate selections were performed on the L-GRB sample, based on observed fluence, spectral softness, and overall light curve shape. First, as argued above, since long-lag (and therefore likely under-luminous) bursts increase from a negligible proportion of BATSE bright bursts to $\sim 50\%$ at trigger threshold (Norris 2002), we ordered the L-GRBs by total burst fluence and selected the low-fluence half. Similarly, to select for spectrally soft bursts, we split the total sample in half by the ratio of observed fluence in BATSE energy channels 1 $(20 - 50$ keV) and 3 $(100 - 300$ keV). We did not attempt further cuts on the data based on fluence or spectral hardness since this would not be justified for several reasons. Firstly, the number of bursts selected in finer cuts would be very small for statistical analysis. Secondly the low fluence bursts (for example) will obviously contain bursts that are dim due to being further away and these cannot be distinguished from the nearby bursts - we aimed purely to increase the fraction of nearby bursts in the samples as predicted by the correlations guiding the cuts. Thirdly, given the overall lack of correlation in the sample as a whole, any measured correlation is likely to be very weak and further cuts beyond the median would be statistically dubious. The third selection for bursts of a smooth, single-peaked nature was made by visual examination of the light curves of the entire L-GRB sample. We emphasise that this selection was based on simple pre-agreed criteria to select smooth, single peaked curves broadly similar to the known local bursts, not to attempt detailed selection with respect to

small scale variation. To further minimise any subjectivity involved, selection was performed independently by two observers and then arbitrated by a third. Finally, the bursts common to all three selections (177) were then used to form a low-fluence, spectrally-soft, single-peaked sub-sample.

4.3 Results

Figure 4.2 shows plots of correlation (expressed as the percentage of bursts in each sample correlated with galaxy distribution) between BATSE long GRBs and concentric spheres of galaxy samples from both the PSCz and RC3 catalogues. The results show a high degree of consistency, confirming that the correlation measurements are not dependent on a chance choice of galaxy catalogue. In practice, each volume sample in the RC3 catalogue contained between 1.5 and 2 times the number of galaxies in the equivalent PSCz sample. This inevitably leads to increased dispersion in the values of Φ measured with the PSCz samples compared to the RC3 samples, though we still consider the completeness and homogeneity of the PSCz sample to make it a more appropriate comparison set.

As can be seen, long burst correlation (particularly with the PSCz samples) remains formally consistent with zero out to the largest radii considered of $v \leq 11000$ km s^{-1} (≈ 155 Mpc), confirming that nearby long GRBs are indeed rarely observed events. However, the most probable level of correlation increases with distance, but this could not be reliably investigated beyond the radii considered due to the flux-limited nature of the galaxy catalogues meaning that there are just too few galaxies in the catalogues at larger radii to be useful.

Turning now to the sub-samples with properties similar to known local bursts, Figure 4.3 shows correlations with concentric *shells* (as opposed to *spheres*) of galaxies with recession velocity radii of $0-2000,\ 2000-5000,\ 5000-8000$ and $8000-11000$ km s^{-1}. From this figure it can be seen that each of the low-fluence, spectrally-soft, and smooth light curve sub-samples exhibits broadly equivalent, marginally increased correlations in the second and fourth shells, compared to the mean of 20 random burst 50% sub-samples. Furthermore, a combined set containing only those bursts (177) common to all three individual sub-samples exhibits increased correlation of $16\% \pm 8\%$ ($\equiv 28 \pm 14$ bursts) in the $2000-5000$ km s^{-1} shell, and $19\% \pm 11\%$ ($\equiv 34 \pm 19$ bursts) in the outermost shell.

Returning to examine concentric *spheres* of galaxies, Figure 4.4 shows the

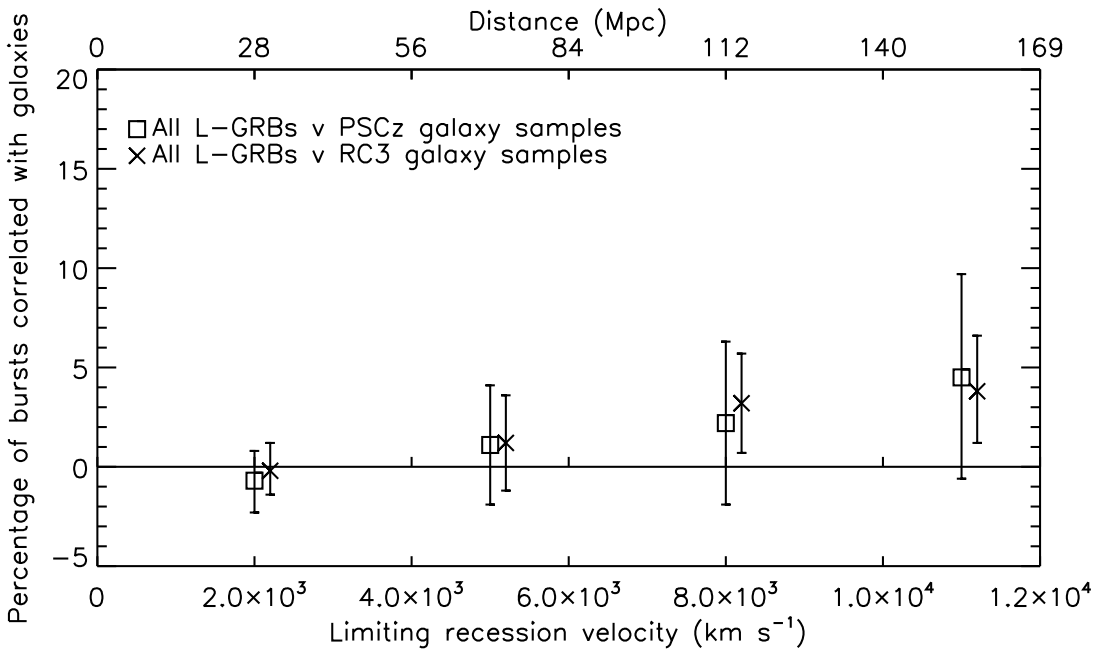

Figure 4.2: Measured correlation (expressed as the percentage of bursts in each sample correlated with galaxy distribution) versus galactic recession velocity for concentric spheres of galaxy samples from both the PSCz and RC3 catalogues. Data points have been separated along the x axis for clarity, and error bars represent 1σ errors.

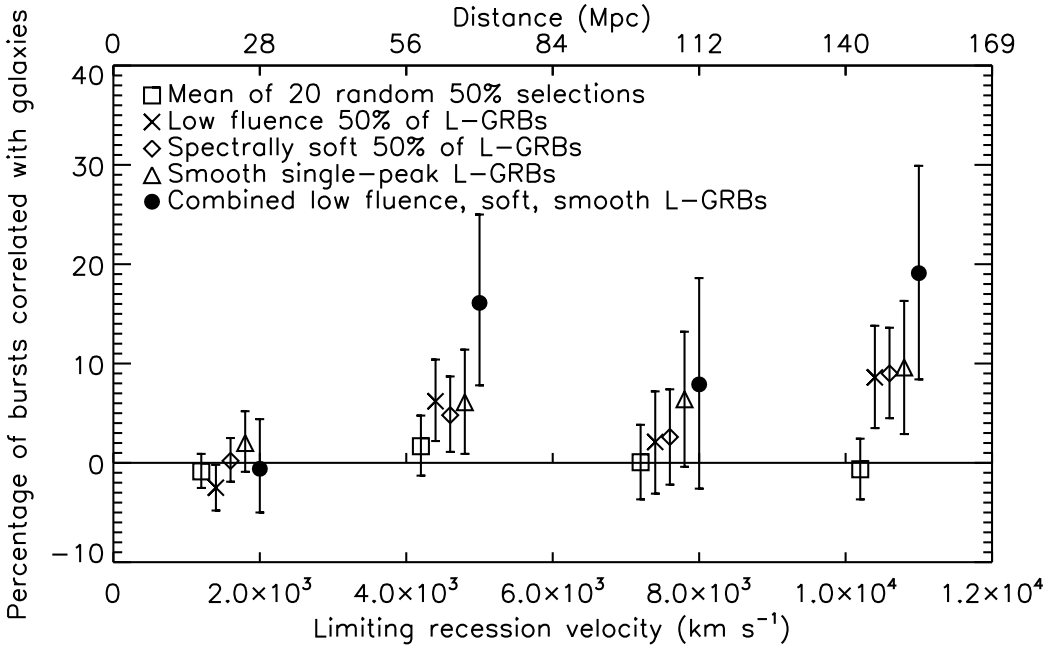

Figure 4.3: Measured correlation between BATSE long duration GRBs and galaxies in concentric shells of increasing galactic recession velocity from the PSCz catalogue, compared with that of 20 random burst 50% sub-samples. Error bars on the random sample data points represent the dispersion (1σ) of the sample correlations.

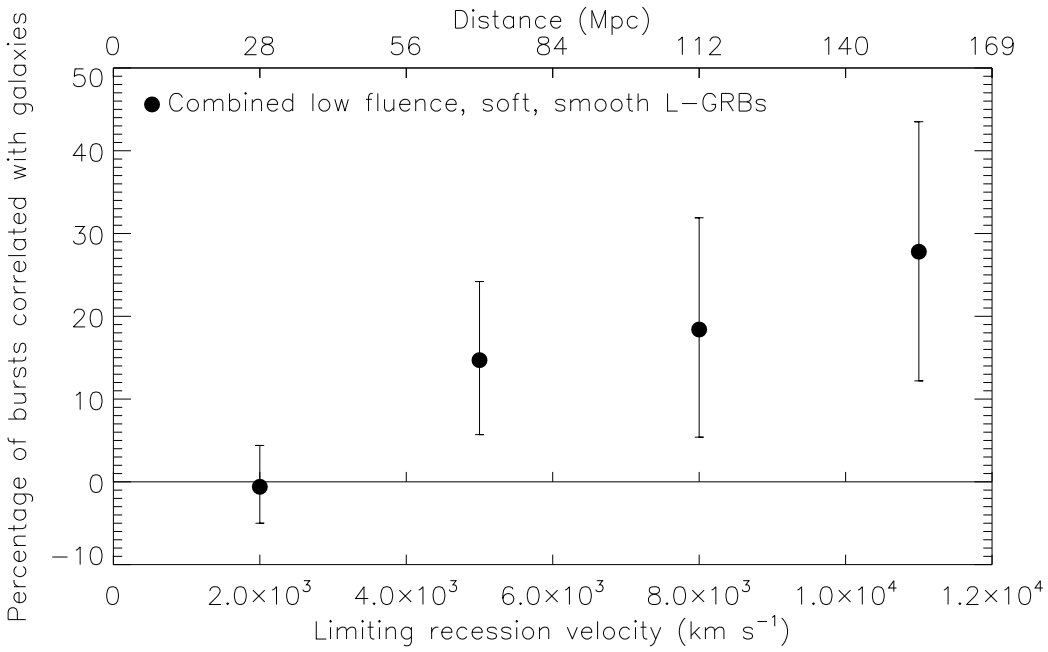

Figure 4.4: Measured correlation between the combined low-fluence, spectrally soft, single-peaked L-GRBs and galaxies in concentric spheres from the PSCz catalogue.

cumulative correlation versus radius of the combined sub-sample of L-GRBs, where it can be seen that $28\% \pm 16\%$ of low-fluence, spectrally-soft bursts with smooth single-peaked light curves are correlated with galaxies within ≈ 155 Mpc, equivalent to a total of 50 ± 28 bursts in the 9 years of BATSE operation.

It is possible of course that this is a result of an entirely random and somewhat fortuitous selection of burst sub-sample. To investigate this, we have made 20 random selections of an equivalent number of bursts from the whole L-GRB sample and investigated their correlations. Figure 4.5 shows a comparison between the mean correlations of these random samples and our soft, smooth, low fluence sample. The random samples are seen to maintain a mean correlation very close to zero in all spheres. We can therefore be reasonably confident that our correlated sub-sample is not a statistical fluke, though we caution that the errors on the low level correlations in the limited size burst sample are large, and none of our individual measured correlation points are beyond 2σ of zero correlation.

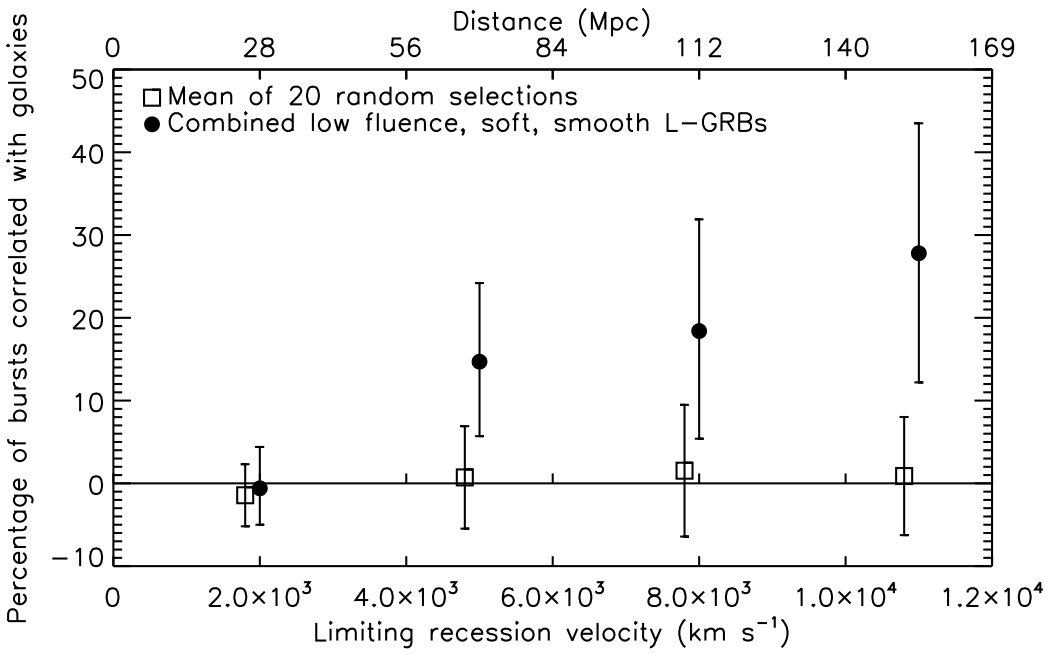

Figure 4.5: Measured correlation between the combined low-fluence, spectrally soft, single-peaked L-GRBs and galaxies in concentric spheres from the PSCz catalogue, compared with that of 20 random sub-samples of equal numbers of bursts. Error bars on the random sample data points represent the dispersion (1σ) of the sample correlations.

4.4 Discussion

4.4.1 Two populations of long bursts?

Our results confirm that nearby long GRBs as a whole are indeed rare events, with correlation remaining consistent with zero out to ≈ 155 Mpc, but with a 10% upper limit (1σ), equivalent to 144 bursts. Restricting the L-GRB sample to those with properties similar to known nearby bursts increased the measured correlation to $28\% \pm 16\%$ of the sub-sample ($\equiv 50 \pm 28$ bursts) within the same radius. It is worth emphasising that this means the 177 burst sub-sample contains a *lower* limit (1σ) of 22 bursts correlated with local large scale structure, almost one quarter more than the 1σ *upper* limit (18) expected from just applying the whole sample correlation rate to the sub-sample. The local rate density of under-luminous L-GRBs implied by our result is in agreement with those calculated via detector sensitivity and luminosity function arguments. For example, Soderberg et al. (2006b) argue that sub-energetic bursts are ~ 10 times[1] more abundant than typical bright GRBs based on the sensitivities of *BeppoSAX*, *HETE-2* and *Swift* to GRB 980425 and GRB 060218. Similarly Pian et al. (2006) (using BATSE, *HETE-2* and *Swift* sensitivities) found a local rate density at least 100 times greater than that estimated from cosmological bursts alone. In addition Cobb et al. (2006b) estimate an event ratio ~ 100 between low and high luminosity bursts based on assuming the *Swift* population of high-luminosity bursts to be complete to its mean redshift. Coward (2005) showed that a simulated distribution of L-GRBs produced by assuming a dual population of lower and higher luminosity bursts was compatible with the observed redshift distribution, and led to an estimate of ≈ 220 Gpc^{-3}yr^{-1} for the rate density of low-luminosity bursts. Furthermore, Liang et al. (2007) suggest that in order to avoid over-predicting the number of intermediate luminosity GRBs observed at low redshifts, the high-luminosity and low-luminosity bursts must be characterised by separate luminosity functions. They choose models of the same functional form (smoothed broken power-law), but with the coefficients of each separately constrained to produce GRB rates consistent with those observed. Finally, Guetta & Della Valle (2007) estimate a local GRB rate of $200 - 1800$ Gpc^{-3}yr^{-1} using a luminosity function consistent with the luminosities of local bursts. Figure 4.6 shows our results plotted with respect to predicted rates of Low-Luminosity GRBs

[1]Note that this rate includes a beaming correction factor of ~ 100 to obtain the 'true' rate of cosmological bursts. Therefore, in terms of observable bursts, this implies LL bursts are about 1000 times more abundant than their HL counterparts.

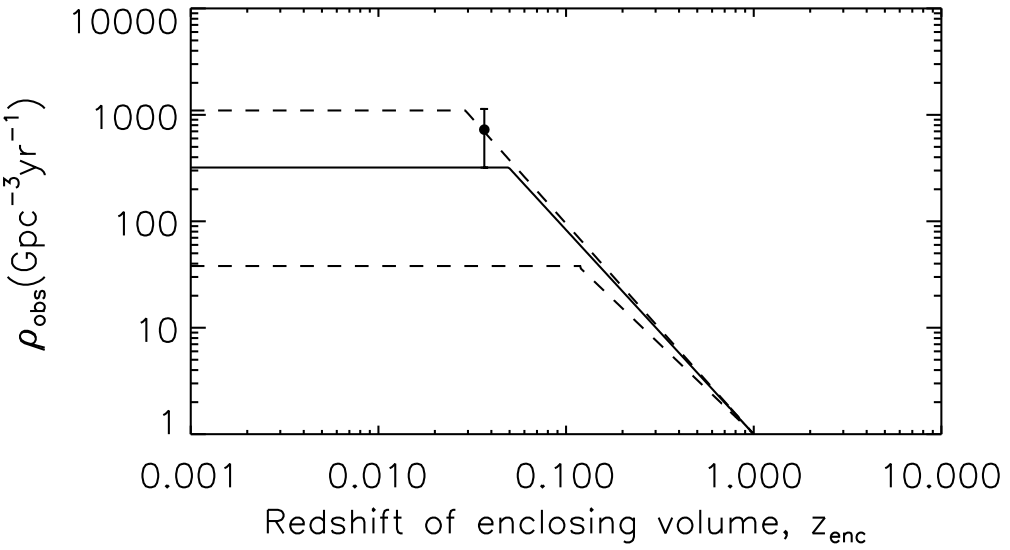

Figure 4.6: The observed burst rate, $\rho_{\rm obs}$, within the enclosed volume out to redshift $z_{\rm enc}$. The filled circle shows the observed burst rate within our investigated total volume. The area enclosed by the dashed lines represents the upper and lower limits of the predicted observed rate for Low-Luminosity GRBs as a function of enclosing volume (after Figure 5(b) of Liang et al. (2007)).

from Liang et al. (2007). The results presented here are therefore consistent with the suggestion that there are separate low and high luminosity L-GRB populations with different luminosity functions, and we will return to this question in greater detail in Chapter 5.

4.4.2 Comparison with supernova searches

GRB 980425 was the first GRB to be observationally associated with a supernova (Galama et al. 1998), and GRB 060218 (Cusumano et al. 2006) is the most striking recent example. These nearby SN associated L-GRBs share similar properties (low-fluence, spectrally soft and smooth single-peaked light curves) as argued by Bloom et al. (1998), and it may therefore seem that a search for temporal and spatial correlation between bursts and supernovae would provide a means of identifying individual GRB hosts, particularly at low redshift. However the heterogeneity and inherent incompleteness of SN catalogues (due for example to the difficulty of SN detection in dusty environments, biased surveys and magnitude limitations) make

it difficult to use them to identify GRB host galaxies. Recent observations also suggest that not all long GRBs are necessarily accompanied by an observable supernova (Fynbo et al. 2006; Gal-Yam et al. 2006; Della Valle et al. 2006), and of course, not all Ib/c SNe produce GRBs (e.g. Soderberg et al. 2006b). Nevertheless several groups have attempted searches for spatial and temporal coincidences of GRBs with SNe (for example Wang & Wheeler (1998); Kippen et al. (1998); Norris, Bonnell & Watanabe (1999)). Results obtained vary depending particularly on any restrictions imposed on the burst or SN properties in the analyses, and generally the statistics remain too poor to draw any firm conclusions from these and other studies. In addition, it has been suggested recently that the host galaxies of SNe type Ic without GRBs may be systematically different from those with GRBs, particularly in terms of metallicity (Modjaz et al. 2008).

It is therefore apparent that using SNe searches to identify possible nearby GRBs is fraught with difficulty. Soderberg et al. (2006b) estimate that only $\sim 3\%$ of Ib/c SNe give rise to detectable low-luminosity GRBs comparable to GRBs 980425 and 060218. During the lifetime of the BATSE experiment, the Asiago supernova catalogue (Barbon et al. 1999)[2] contains only 33 events classified as Ib, Ibc or Ic within the volume considered here. Given further that most supernova searches, particularly in the 1990s, concentrated on targeting relatively bright galaxies, untypical of GRB hosts, we should expect that few, if any, GRB-SN were discovered by chance in these surveys. Our approach, independent of any assumed correlation other than that GRBs must occur in or near a host galaxy, is therefore justified and enables the placing of limits to the number of observed nearby L-GRBs based on location with respect to potential host galaxy distributions alone.

4.5 Summary and Conclusions

We have analysed the correlations of the entire BATSE catalogue of long GRBs with measured fluences localised to better than 10° (1437 bursts) with galaxy samples out to ≈ 155 Mpc from two independent galaxy catalogues. We find that correlation between the L-GRB set as a whole and samples from both galaxy catalogues remains within 1 standard deviation (σ) of zero out to the highest radii considered. However, selecting a sub-sample of bursts with properties similar to those of the known local L-GRBs significantly increased correlation with large scale structure on the sky to

[2]http://web.pd.astro.it/supern/snean.txt

a level of $28\% \pm 16\%$ ($\equiv 50 \pm 28$ bursts) within the same radius.

The cumulative correlation rate out to ≈ 155 Mpc suggests that BATSE most likely observed between 2 and 9 long GRBs per year similar to, and from within similar distances to the closest known GRBs to date. This implies an observed local L-GRB rate density within 155 Mpc of 700 ± 360 Gpc^{-3}yr^{-1} (to BATSE detection limits, and assuming the BATSE sky exposure fraction to be of the order of 0.5). This is in reasonable agreement with 230^{+490}_{-190} Gpc^{-3}yr^{-1} as calculated by Soderberg et al. (2006b) via combined analyses of the sensitivities of *BeppoSAX*, *HETE-2*, *Swift*. It is also in good agreement with observed rates of Low-Luminosity GRBs predicted from luminosity function arguments (Coward 2005; Liang et al. 2007; Guetta & Della Valle 2007).

Comparison between datasets from different missions and detectors is difficult (see for example Berger et al. (2005); Band (2006b)). However if we naively assume the *Swift* GRB catalogue to be similar to the BATSE catalogue, and compare our expected number of local L-GRBs with a uniformly selected sample of *Swift* L-GRBs with redshifts (Jakobsson et al. 2006a,b, as discussed in Section 5.2.3.2 of Chapter 5), then we would expect this sample of 65 bursts (to 1 April 2008) to contain 2 ± 1 within 155 Mpc. In fact, the sample contains one burst (GRB 060218) within this distance which is certainly consistent with our expectations given the small numbers involved.

It may be argued that since we are looking for nearby bursts, these would be more likely to have measured redshifts than the bursts in general, though all three nearest GRBs were significantly underluminous events. Comparing to the entire August 2008 *Swift* sample of 314 long GRBs, our results suggest it contains a 1σ upper limit of 31 bursts with redshift $z < 0.0367$ from overall correlations, or more precisely 11 ± 6 from the correlations of our subsample of bursts with properties similar to known local bursts (assuming that the subsample contains all the local correlations). Similarly, comparing to the total sample of *Swift* L-GRBs with measured redshifts (110 bursts), then we would expect 4 ± 2.

In the next Chapter, we will see that the best fit dual population Luminosity Functions to these correlations and either the number counts or overall *Swift* redshift distribution predict slightly lower rates leading to only 1 or 2% of *Swift* L-GRBs (3 to 6 bursts) being predicted to occur within 155 Mpc. This suggests that the number of local L-GRBs expected to be detected by *Swift* is likely to be at the low end of our correlation results derived from the BATSE distributions. So far, only GRB 060218

has been identified as occurring within our considered volume, but we may expect a few more low-redshift long bursts to be identified in the future, particularly among spectrally-soft, under-luminous bursts with little variability.

Chapter 5

Luminosity Functions of Long GRBs: two populations too?

5.1 Introduction

In Chapter 4 we showed that a sub-sample of BATSE long duration GRBs with properties similar to the known local bursts exhibit a correlation rate with local galaxies of $28\% \pm 16\%$ compared to $4.5\% \pm 5\%$ of the population as a whole. From the observations of low-luminosity nearby L-GRBs such as GRB 980425 and GRB 060218, estimates have been calculated of the likely intrinsic rates of such bursts (e.g. Soderberg et al. 2006b; Pian et al. 2006). Luminosity function arguments (e.g. Liang et al. 2007; Guetta & Della Valle 2007) suggest that this is not just a result of the selection effect of only being able to see low luminosity bursts nearby: if these bursts came from the low luminosity tail of a single overall LF, then we should have observed more intermediate redshift bursts of intermediate luminosity. How well do the correlation results of our work fit in with this other evidence?

Unfortunately, there are not theoretical models with clear predictions for two (or more) distinct luminosity populations for L-GRBs; nor is there a locally observed phenomenon which may be responsible for a nearby population of L-GRBs in the same way as the SGR Giant Flares for the S-GRBs. There are plausible channels via which GRBs of differing luminosity may be produced (see for example the *Type I* and *Type II* collapsars discussed in Section 1.2.3 of Chapter 1, and speculations regarding strange stars in Chapter 6). These models do not as yet provide estimates of intrinsic rates, and hence we do not have as good a handle from first principles on the possible rates of any separate progenitor populations as we had for investigating

plausible LFs for the S-GRB population in Chapter 3. However, as mentioned above there are estimates of the intrinsic rates of both cosmological L-GRBs and the nearby low luminosity bursts. Schmidt (2001b) found a rate of cosmological L-GRBs of ~ 0.5 Gpc^{-3}yr^{-1}, and very similar rates of ~ 0.44 Gpc^{-3}yr^{-1} (Guetta, Piran & Waxman 2005) and ~ 1.1 Gpc^{-3}yr^{-1} (Guetta & Della Valle 2007; Liang et al. 2007) have also been calculated. Note that these are isotropic equivalent rates, with no account taken of beaming to infer "true" rates. However, this makes no difference to our calculations here - we are interested in the intrinsic rates of observable L-GRBs alone as opposed to the total rate.

Local rates of low luminosity L-GRBs have been estimated as being at least 100 times greater than the cosmological rates, both from the the analysis of the sensitivities of detectors to the known local bursts (Soderberg et al. 2006b; Pian et al. 2006) and luminosity function arguments (Coward 2005; Liang et al. 2007; Guetta & Della Valle 2007), as well as arguments based on the completeness (to its mean redshift) of the *Swift* population of high luminosity bursts (Cobb et al. 2006b). In particular, Guetta & Della Valle (2007) estimate a local GRB rate of $200-1800$ Gpc^{-3}yr^{-1} using a luminosity function consistent with the luminosities of local bursts; Coward (2005) and Liang et al. (2007) suggest intrinsic low luminosity burst rates of 220 Gpc^{-3}yr^{-1} and 325^{+352}_{-177} Gpc^{-3}yr^{-1} respectively from LF arguments based on there being separate populations of high (HL) and low (LL) luminosity L-GRBs. Our rate of low luminosity L-GRBs calculated from the correlation analyses of 700 ± 360 Gpc^{-3}yr^{-1} is consistent with these other estimates, as can be seen for example in Figure 4.6 of Chapter 4.

We therefore proceed to investigate whether the local distribution of L-GRBs found from the results of our correlation analyses can be produced by a single progenitor population LF, or whether once again a two population model LF is preferred.

5.2 Methods

The overall method we employ is the same as that of Chapter 3, with Equation 3.1 still defining the number of bursts observed with respect to time and threshold. The simplified K correction for the long bursts is based on assuming a constant median spectral index of -1.6 for L-GRBs (Schmidt 2001b; Guetta, Piran & Waxman 2005).

5.2.1 Intrinsic Rates

The intrinsic rate of L-GRBs per unit volume, $R_{\mathrm{GRB}(z)}$ is given by Equation 5.1 where ρ_0 is the intrinsic ($z = 0$) L-GRB rate and $F(z)$ once again describes the volume evolution of this rate with z.

$$R_{\mathrm{GRB}}(z) = \rho_0 \times F(z)\ \mathrm{Mpc}^{-3} \tag{5.1}$$

A variety of rates for ρ_0 for both the high and low luminosity burst populations are investigated as follows. For single (assumed HL) populations, we consider a rate of $\rho_0 = 1\ \mathrm{Gpc}^{-3}\mathrm{yr}^{-1}$ consistent with the values from the literature discussed above, and a rate 100 times greater than this to allow for larger numbers of potentially local bursts from the low luminosity tail of the LF. For dual populations, we consider rate combinations as follows: $\rho_0^{HL} = 1\ \mathrm{Gpc}^{-3}\mathrm{yr}^{-1}$ and $\rho_0^{LL} = 700\ \mathrm{Gpc}^{-3}\mathrm{yr}^{-1}$ from the correlation results of Chapter 4; $\rho_0^{HL} = 1.12\ \mathrm{Gpc}^{-3}\mathrm{yr}^{-1}$ and $\rho_0^{LL} = 325\ \mathrm{Gpc}^{-3}\mathrm{yr}^{-1}$ from the results of Liang et al. (2007); and $\rho_0^{HL} = 23\ \mathrm{Gpc}^{-3}\mathrm{yr}^{-1}$ and $\rho_0^{LL} = 230\ \mathrm{Gpc}^{-3}\mathrm{yr}^{-1}$ from the results of Soderberg et al. (2006b). We note that this last ρ_0^{HL} from Soderberg et al. (2006b) includes a correction factor ~ 100 for beaming of the HL bursts, but provides a useful intermediate rate for the purposes of our investigations. In contrast to the S-GRB case, $F(z)$ is no longer complicated by factors such as delay rates or multiple production pathways, and we assume that L-GRBs simply follow the Star Formation Rate as a function of z, given once again by the parameterisation of Equation 3.3.

5.2.2 Luminosity Functions

Once again, the luminosity functions of L-GRBs are not well known. We investigate, as for the S-GRBs, both lognormal and Schechter type functions for both the HL and postulated LL populations. Cosmological L-GRBs have been investigated previously (e.g. Liang et al. 2007; Guetta & Della Valle 2007) using a broken power law LF, and we therefore also include a broken power law LF in the analysis. These LFs are defined in the equations overpage:

1. Lognormal distribution

$$\frac{dN}{d\log L} \propto \exp\left(\frac{-(\log L - \log L_0)^2}{2\sigma^2}\right) \tag{5.2}$$

2. Schechter function

$$\frac{dN}{dL} \propto \left(\frac{L}{L_0}\right)^{-\alpha} \exp\left(-L/L_0\right) , \quad L \geq L_{min} \tag{5.3}$$

3. Broken Power Law

$$\frac{dN}{dL} \propto \begin{cases} \left(\frac{L}{L_0}\right)^{-\alpha_1}, & L < L_0 \\ \left(\frac{L}{L_0}\right)^{-\alpha_2}, & L \geq L_0 \end{cases} \tag{5.4}$$

where $L_{min} = 10^{42}$ erg s^{-1} for normalisation and convergence of the Schechter function.

The broken power law LF (Equation 5.4) contains 3 free parameters (L_0, α_1 and α_2), but to allow for feasible computation we constrain the slopes α_1 and α_2 as follows. Guetta & Piran (2007) found a consistent higher luminosity slope $\alpha_2 = 2$ for a series of different R_{GRB} models compared to both BATSE and early *Swift* peak flux distributions, and we therefore fix $\alpha_2 = 2$ in the analysis of single LF distributions using Equation 5.4. When considering dual population LFs described by broken power laws, we follow the results of Liang et al. (2007) who found a best fit of $\alpha_1 = 0$ for a separate low luminosity population of bursts constrained by the properties of the known local L-GRBs. We therefore fix $\alpha_1 = 0$ for the low luminosity population, and $\alpha_2 = 2$ for the high luminosity population when considering dual population broken power law LFs.

5.2.3 Constraining the models

5.2.3.1 Constraints via number counts

We first proceed to constrain the LF models in an almost identical manner to section 3.2.3 of Chapter 3. The C_{max}/C_{min} table from the current BATSE catalogue (Paciesas et al. 1999) is again used to provide a distribution of peak count rate, this time for a population restricted to only those L-GRBs (743) recorded

when the 1024ms timescale threshold was set to 5.5σ above background in at least 2 detectors in the $50 - 300$ keV range. The all sky equivalent period (including correction for BATSE's sky coverage) this table of peak luminosities on the 1024 ms timescale represents is estimated as ~ 1.97 years, and the BATSE limiting photon flux for L-GRBs is assumed to be 0.25 photons cm^{-2} s^{-1}.

The cross-talk corrected correlations for the low-luminosity, soft, single peaked sub-sample from Chapter 4 were then used to define the local distribution of L-GRBs in terms of the percentage of bursts correlated with galaxies from the *PSCz* catalogue in concentric shells (differential distribution) and spheres (cumulative distribution) of recession velocity. χ^2 minimisation was again used to optimise the LF parameters by fitting to the overall count rate and the local distributions, simultaneously and individually as before.

As for the S-GRB models, the plausibility of the best fit models was checked by comparison to the wider redshift distribution of L-GRBs. This distribution, for both pre-*Swift* and *Swift* samples, was obtained from the updated [1] (to 1 April 2008: Jakobsson P, private communication) data presented in Jakobsson et al. (2006a,b). For comparison with *Swift* data, we assume the BAT to be twice as sensitive as BATSE to long duration GRBs (Band 2006b).

5.2.3.2 Constraints via the *Swift* redshift distribution

The *Swift* redshift distribution of L-GRBs used for comparison in the section above is a much larger and more robust sample than for the S-GRBs. The sample is carefully selected to consist of those bursts with observing conditions favourable for redshift determination and in that sense should represent a more complete and relatively unbiased sample with respect to redshift. The criteria used for example include fast and accurate localisation (XRT position distributed within 12 hours of burst) and favourable sky positioning with respect to the Sun position as well as low Galactic extinction values. For a full description of the sample and selection criteria see Jakobsson et al. (2006a,b).

We can therefore sensibly constrain our models using this *Swift* distribution. However, our number count distribution is based on the BATSE sample of L-GRBs, not *Swift*. The *Swift* thresholding algorithm is complex and varying, and thus an equivalently uniform number count distribution for *Swift* is somewhat difficult to

[1] http://www.astro.ku.dk/~pallja/GRBsample.html

calculate simply and reliably. Therefore, we instead choose as a second independent analysis to investigate the LF models constrained to fit the overall *Swift* redshift distribution and our local correlations without regard to number count distribution with respect to threshold.

The *Swift* redshift distribution used is determined using 65 bursts observed between December 2004 and April 2008, a period of 3.29 years during which *Swift* observed a total of 283 L-GRBs. We can then bin this sample in 20 redshift bins in order to obtain a differential redshift distribution for comparison to our model predictions. The *Swift* BAT has a (partially coded) Field of View of ~ 2 sr (Sakamoto et al. 2008) and hence observes approximately 1/6 of the entire sky at any one time. The redshift sample therefore represents an equivalent all sky observing period of ~ 0.13 years.

5.3 Results

5.3.1 Constraints via number counts

5.3.1.1 Single population Luminosity Functions

Table 5.1 lists the best fit parameters found from fitting distributions produced by single population LFs simultaneously to both the overall number counts and the local population as described above. The table is ordered in decreasing overall goodness of fit (i.e. increasing combined χ^2/dof). Intrinsic GRB rates of both 1.0 $\mathrm{Gpc^{-3}yr^{-1}}$ (consistent with the estimated intrinsic rates of cosmological L-GRBs from previous work (e.g. Guetta & Della Valle 2007; Liang et al. 2007)), and a rate 100 times greater than this were investigated. As can be seen from the table, all the single LFs tested using the lower estimated intrinsic rates produce good fits to the overall number counts, but are unable to produce any local bursts (see for example Figure 5.1). Increasing the intrinsic L-GRB rate by a factor of 100 does not help produce the local population, and furthermore all the LFs tested utilising this higher rate produce poorer fits to the overall number counts.

As with the short GRBs, it is appropriate to ask the specific question as to whether a single population can produce the local bursts at all. We therefore again perform fits of single LF populations to the local distribution alone, and to a limited fraction of local bursts within 112 Mpc: the results of these fits are presented in

Single LF	Intrinsic rate ($\mathrm{Gpc^{-3}yr^{-1}}$)	Parameters ($l_0 \equiv \log L_0$)	Local χ^2/dof	C_{max}/C_{min} χ^2/dof	Overall χ^2/dof
Schechter	1	$l_0 = 51.85$ $\alpha = 1.0$	6.88	1.17	1.25
Lognormal	1	$l_0 = 49.1$ $\sigma = 1.2$	6.87	1.54	1.27
Broken power law ($\alpha_2 = 2.0$)	1	$l_0 = 51.2$ $\alpha_1 = 0.95$	6.88	1.48	1.48
Schechter	100	$l_0 = 51.85$ $\alpha = 1.3$	6.85	2.22	2.14
Lognormal	100	$l_0 = 46.0$ $\sigma = 1.5$	6.66	3.94	3.59
Broken power law ($\alpha_2 = 2.0$)	100	$l_0 = 52.2$ $\alpha_1 = 1.05$	6.88	4.93	4.44

Table 5.1: Results of single population L-GRB Luminosity Functions fit simultaneously to number counts and the local distribution, presented in order of decreasing overall goodness of fit (i.e. increasing overall χ^2/dof). The number of degrees of freedom (dof) for the local, C_{max}/C_{min} and overall distributions are 1, 22 and 26 respectively. l_0 is in units of $\log(\mathrm{erg\ s^{-1}})$, σ in dex and αs are dimensionless.

Tables 5.2 and 5.3. Unsurprisingly with no constraints on the overall number counts distribution, the properties of the fits to the local distributions are independent of the two intrinsic rates chosen. However, even with the higher rate far too few bursts are produced overall to significantly improve the number count fit.

Figures 5.2 and 5.3 show examples from Tables 5.2 and 5.3 of how single LF populations can produce the local distribution only at the expense of unrealistic overall redshift distributions, leading to the extremely poor fits to the overall number counts, since just not enough L-GRBs are produced in total.

Single LF	Intrinsic rate ($\mathrm{Gpc^{-3}yr^{-1}}$)	Parameters ($l_0 \equiv \log L_0$)	Local χ^2/dof	C_{max}/C_{min} χ^2/dof	Overall χ^2/dof
Schechter	1	$l_0 = 49.5$ $\alpha = 1.7$	2.40	> 100	> 100
Lognormal	1	$l_0 = 46.1$ $\sigma = 1.0$	2.75	> 100	> 100
Broken power law ($\alpha_2 = 2.0$)	1	$l_0 = 50.5$ $\alpha_1 = 2.0$	3.85	> 100	> 100
Schechter	100	$l_0 = 49.5$ $\alpha = 1.7$	2.40	> 100	> 100
Lognormal	100	$l_0 = 46.1$ $\sigma = 1.0$	2.75	> 100	> 100
Broken power law ($\alpha_2 = 2.0$)	100	$l_0 = 50.5$ $\alpha_1 = 2.0$	3.85	> 100	> 100

Table 5.2: Results of single population L-GRB Luminosity Functions constrained to fit the local distribution from the correlation analyses, presented in the same order as Table 5.1. Details as for Table 5.1.

Single LF	Intrinsic rate ($\mathrm{Gpc^{-3}yr^{-1}}$)	Parameters ($l_0 \equiv \log L_0$)	Local χ^2/dof	C_{max}/C_{min} χ^2/dof	Overall χ^2/dof
Schechter	1	$l_0 = 48.2$ $\alpha = -0.55$	4.51	> 100	> 100
Lognormal	1	$l_0 = 48.4$ $\sigma = 0.1$	4.37	> 100	> 100
Broken power law ($\alpha_2 = 2.0$)	1	$l_0 = 50.0$ $\alpha_1 = 1.85$	5.13	> 100	> 100
Schechter	100	$l_0 = 48.2$ $\alpha = -0.55$	4.51	> 100	> 100
Lognormal	100	$l_0 = 48.4$ $\sigma = 0.1$	4.37	> 100	> 100
Broken power law ($\alpha_2 = 2.0$)	100	$l_0 = 50.0$ $\alpha_1 = 1.85$	5.13	> 100	> 100

Table 5.3: Results of single population L-GRB Luminosity Functions constrained only to produce at least the lower limit of the local distribution within 112 Mpc (see text). Results presented in the same order as Table 5.2, with details as for Table 5.1.

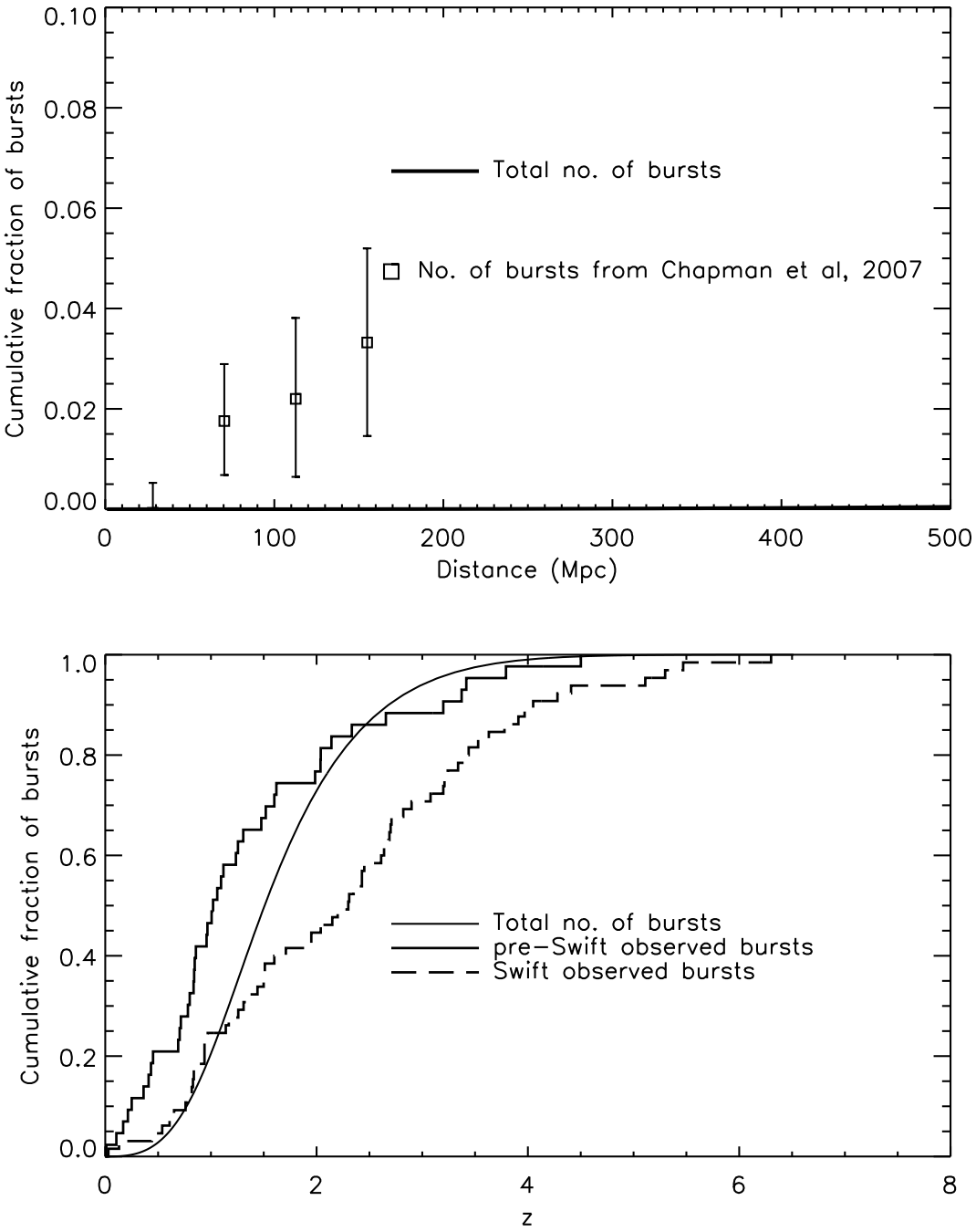

Figure 5.1: Burst distributions from the best fit single population Schechter function LF using an intrinsic rate of 1.0 $\mathrm{Gpc}^{-3}\mathrm{yr}^{-1}$ fit simultaneously to the number counts and the local burst distribution. Top panel shows predicted L-GRB distribution within 500 Mpc compared to the local burst fraction measured in Chapman et al. (2007), bottom panel shows the predicted burst distribution out to $z = 7$ normalised and compared to the *Swift* and pre-*Swift* distributions discussed in the text.

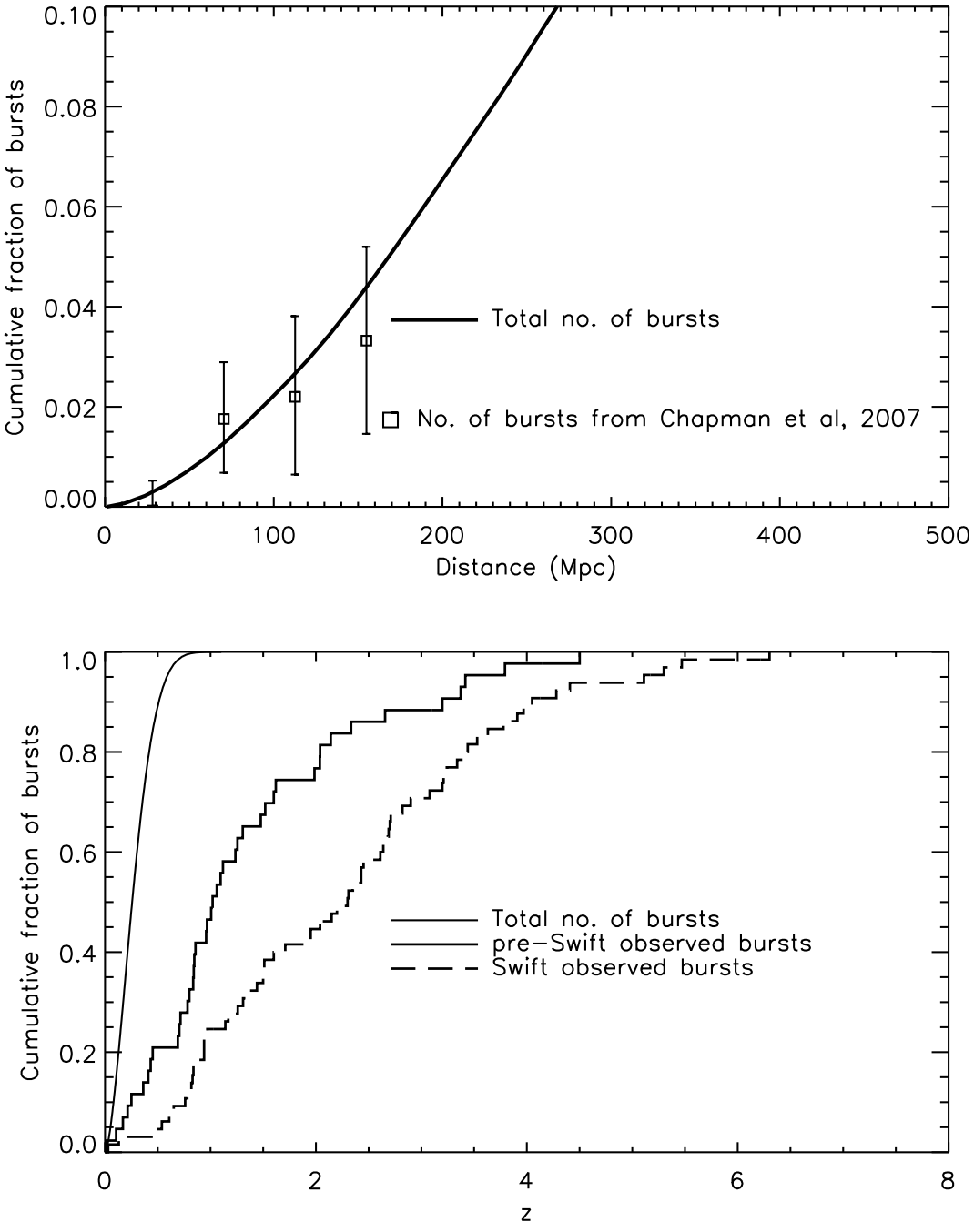

Figure 5.2: Burst distributions from the best fit single population Schechter function LF using an intrinsic rate of 1.0 $\mathrm{Gpc}^{-3}\mathrm{yr}^{-1}$ constrained to fit the local burst distribution. Panel details as for Figure 5.1.

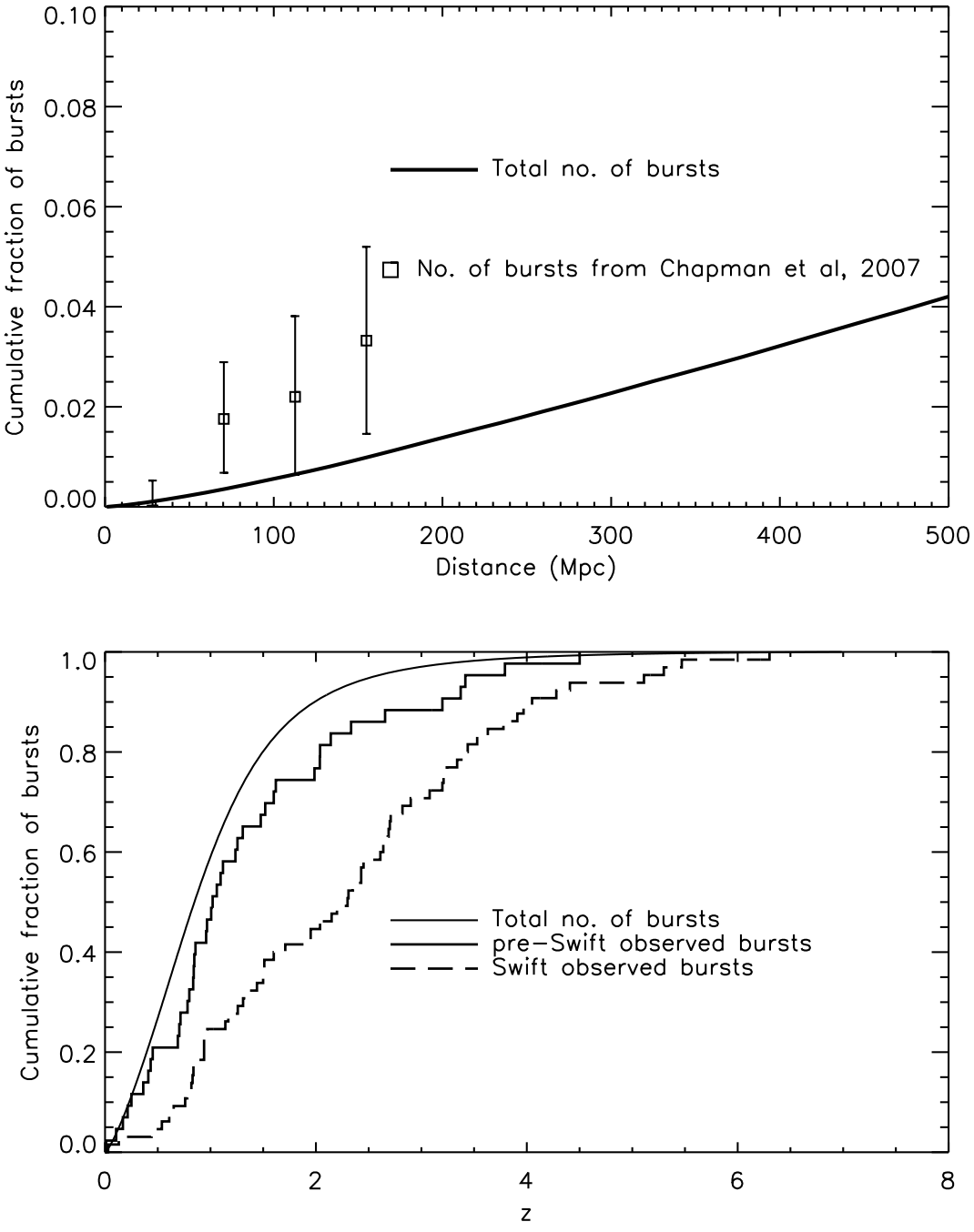

Figure 5.3: Burst distributions from the best fit broken power law LF using an intrinsic rate of 100.0 $\mathrm{Gpc^{-3}yr^{-1}}$ constrained only to produce at least the lower limit of the local distribution within 112 Mpc. Panel details as for Figure 5.1.

5.3.1.2 Dual population Luminosity Functions

In Chapter 3 we showed that for the short GRBs, good fits could be obtained to both the overall number counts and the local distributions by using a dual population of higher and lower luminosity LFs. Table 5.4 shows results for dual LF models for the long duration GRBs presented in descending order of goodness of combined fit, and Figures 5.4 to 5.10 show plots of the fits and distributions obtained. All dual LF models tested produce good fits to the overall number counts and local population as measured by the combined χ^2 values. The poorest fit quantitatively to the local distribution itself is produced by the dual broken power law models, as seen qualitatively by comparing Figures 5.9 and 5.10 to, for example, the dual Schechter LF populations of Figure 5.6 or the lognormal LL and Schechter HL models of Figure 5.5. It would seem that the shallow decay of luminosities beyond the break in the LL luminosity function is probably unrealistic. The next poorest fit to the local distribution is obtained from the dual Schechter LF population utilising the intrinsic rates from Soderberg et al. (2006b), which as mentioned above assume an intrinsic HL rate corrected for beaming and therefore has the lowest ratio of low luminosity to high luminosity intrinsic rates. In contrast, the best 3 fits to the local distribution (Figures 5.8, 5.5 and 5.6) come from populations using the intrinsic LL rate of 700 $\mathrm{Gpc^{-3}yr^{-1}}$ from our correlation studies and the HL rate from the literature of 1.0 $\mathrm{Gpc^{-3}yr^{-1}}$. Though these parameters are uncertain, these results would certainly seem to corroborate the idea that low luminosity L-GRBs are substantially more prevalent in terms of intrinsic rates than their high luminosity counterparts.

Furthermore, the wider redshift distributions of the best overall fits are realistic, and compare particularly well with the low redshift regime ($z \lesssim 1.5$) of the *Swift* redshift distribution. This can be seen clearly from Figures 5.11 and 5.12 which show the redshift distribution out to $z = 2$ of the dual Schechter LF models with higher LL/HL intrinsic rate ratios. Beyond $z \sim 1.5$, the predicted rate diverges from the *Swift* sample, in a similar manner to that found by previous workers (e.g. Guetta & Piran 2007). There could be several reasons for this. The BAT energy window on *Swift* makes it likely to be more sensitive to high redshift bursts (Band 2006a), and our simplified K correction model may be inadequate to account for this. More detailed spectral modelling of L-GRBs for input to the luminosity functions would hopefully improve this fit. In addition, our number count analysis has been based on BATSE threshold levels with an estimation of *Swift* sensitivity as being simply

twice that of BATSE for L-GRBs. In reality, *Swift* has a complex triggering algorithm and further work to model fits to the *Swift* peak flux distributions is required. Alternatively of course, it may be that L-GRBs do not follow the globally averaged SFR, particularly such a simple parameterisation as that of Equation 3.3 (Guetta & Piran 2007). Models including more complex SFR parameterisations (Gorosabel et al. 2004), or the effects of other factors such as metallicity (Natarajan et al. 2005) would seem to reproduce the *Swift* higher redshift fractions better, but do not appear to be as good a match to the lower redshift regime as of July 2008 [2].

[2]http://www.astro.ku.dk/∼pallja/GRBsample.html

High Luminosity LF (ρ_0 Gpc^{-3}yr^{-1})	LF Parameters ($l_0 \equiv \log L_0$)	Low Luminosity LF (ρ_0 Gpc^{-3}yr^{-1})	LF Parameters ($l_0 \equiv \log L_0$)	Local χ^2/dof	C_{max}/C_{min} χ^2/dof	Overall χ^2/dof
Schechter (1.12)	$l_0 = 52.2$ $\alpha = 1.05$	Schechter (325)	$l_0 = 46.7$ $\alpha = -1.5$	5.38	1.13	1.16
Schechter (1)	$l_0 = 52.3$ $\alpha = 1.05$	Lognormal (700)	$l_0 = 47.2$ $\alpha = 0.1$	3.31	1.28	1.20
Schechter (1)	$l_0 = 52.3$ $\alpha = 1.05$	Schechter (700)	$l_0 = 46.7$ $\alpha = -1.5$	4.12	1.25	1.21
Schechter (23)	$l_0 = 52.4$ $\alpha = 1.25$	Schechter (230)	$l_0 = 46.6$ $\alpha = -1.5$	6.00	1.24	1.29
Lognormal (1)	$l_0 = 48.9$ $\alpha = 1.30$	Lognormal (700)	$l_0 = 47.2$ $\alpha = 0.1$	3.26	1.84	1.67
Broken power law (1.12), $\alpha_2 = 2$	$l_0 = 51.9$ $\alpha_1 = 1.0$	Broken power law (325), $\alpha_1 = 0$	$l_0 = 46.6$ $\alpha_2 = 1.9$	6.00	2.00	1.97
Broken power law (1), $\alpha_2 = 2$	$l_0 = 51.9$ $\alpha_1 = 1.0$	Broken power law (700), $\alpha_1 = 0$	$l_0 = 46.3$ $\alpha_2 = 1.9$	5.76	2.09	1.99

Table 5.4: Results of dual population Luminosity Functions for L-GRBs fit simultaneously to number counts and the local distribution, presented in order of decreasing goodness of fit (i.e. increasing overall χ^2/dof). The number of degrees of freedom (dof) for the local, C_{max}/C_{min} and overall distributions are 1, 20 and 24 respectively. l_0 is in units of log(erg s^{-1}), σ in dex and αs are dimensionless.

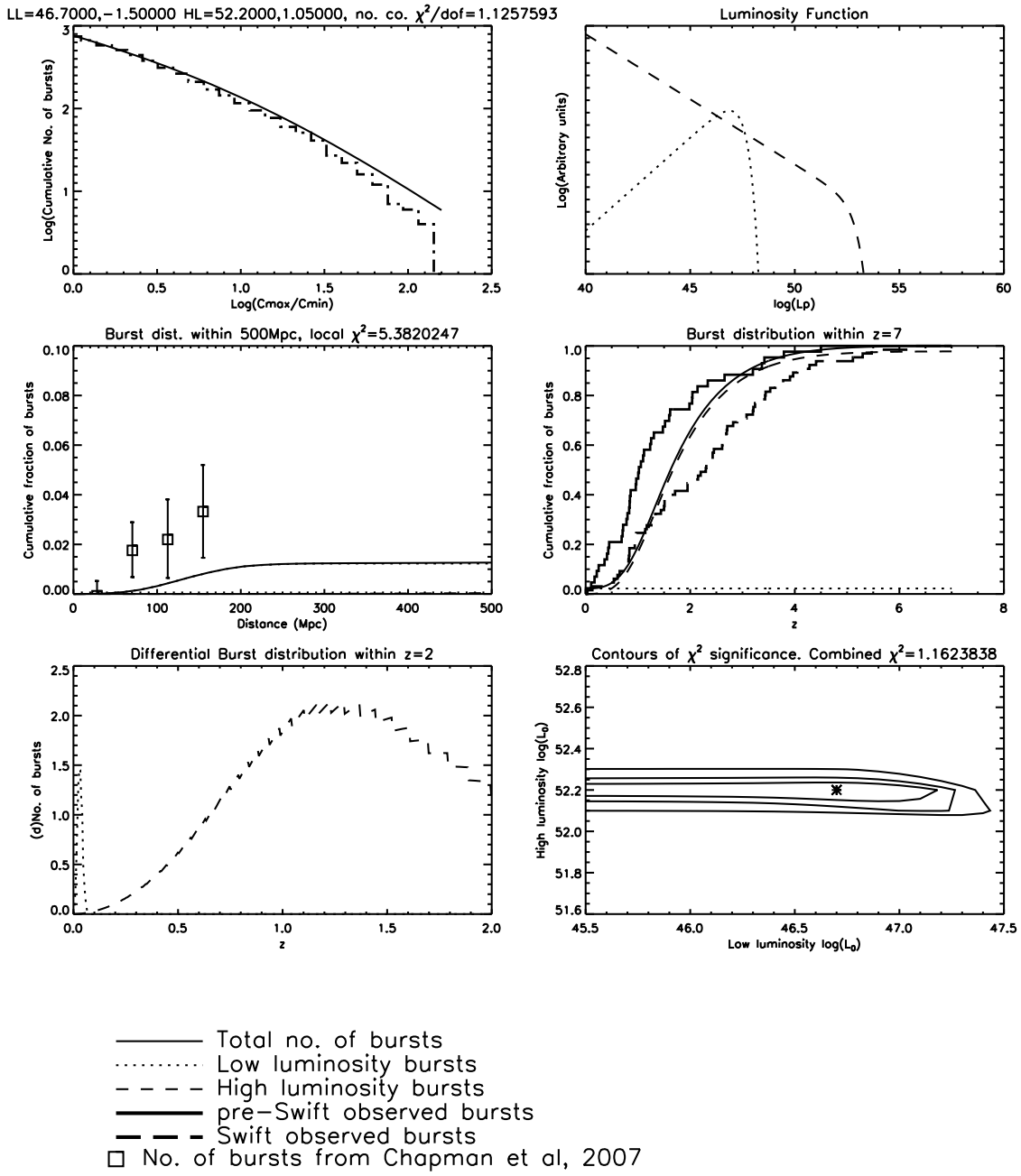

Figure 5.4: **Dual population Schechter function LFs using intrinsic rates 1.12 $\mathbf{Gpc^{-3}yr^{-1}}$ (HL) and 325 $\mathbf{Gpc^{-3}yr^{-1}}$ (LL) from Liang et al. (2007)**: results from best fit simultaneously to BATSE overall number counts and the local burst distribution. Top left: the overall best fit distribution to BATSE number counts (shown cumulative but calculated differentially); Top Right: the best fit LFs; Middle Left: the local burst distribution within 500 Mpc compared to local correlation results; Middle Right: cumulative burst distribution within $z = 7$ (calculated with *Swift* threshold limits) compared to the *Swift* and pre-*Swift* redshift distributions; Bottom Left: differential burst distribution within $z = 2$ (note that the slight ringing or sawtooth shape is an artefact of the numerical integration procedure used to integrate the Schechter function); Bottom Right: contours of χ^2 significance levels for the overall best fit LF parameters (contours show 0.6, 0.9 and 0.99 significance levels with best fit values plotted as an asterisk).

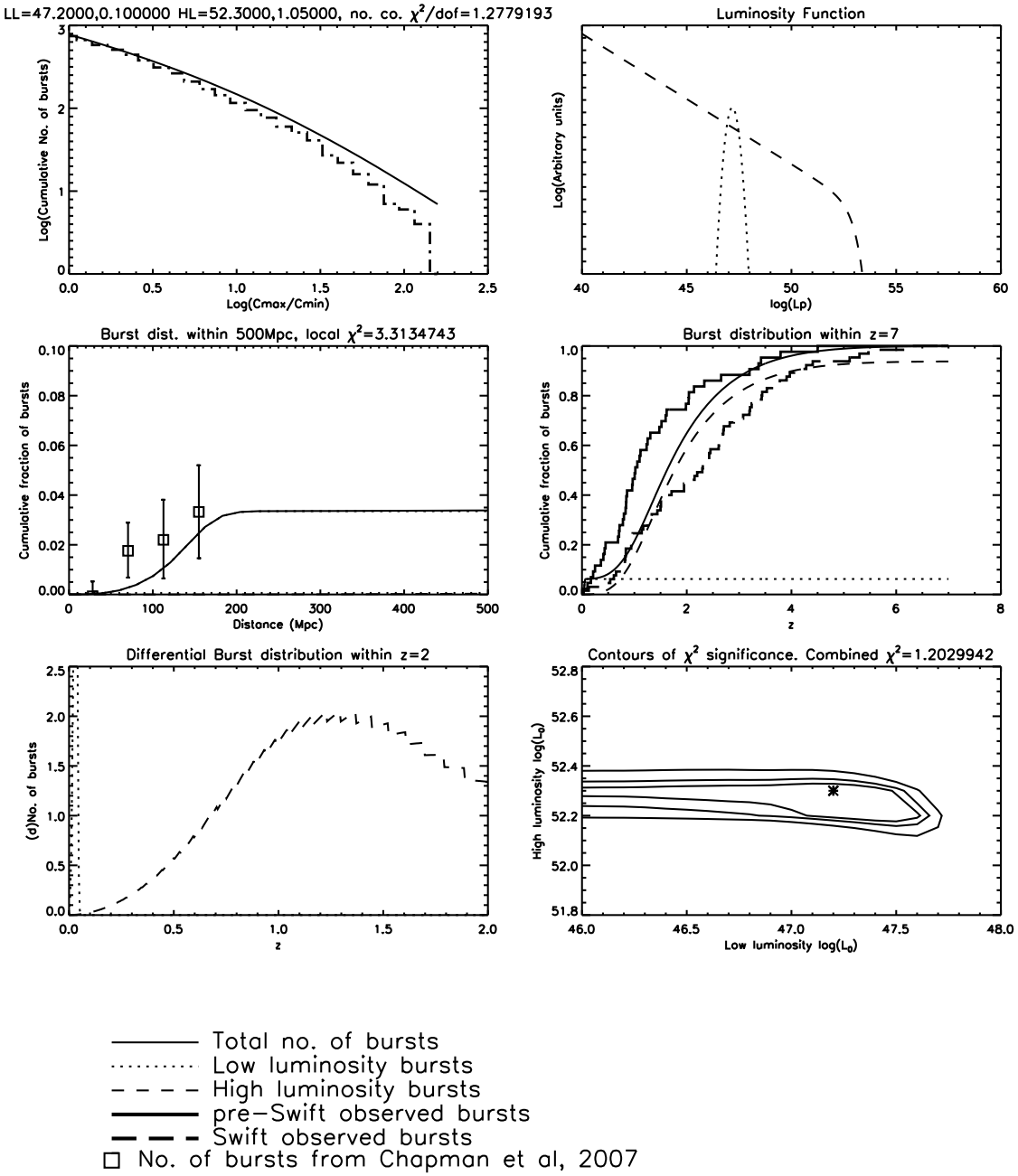

Figure 5.5: **Lognormal LL and Schechter HL LFs using intrinsic rates of 1 $\mathbf{Gpc^{-3}yr^{-1}}$ (HL) and 700 $\mathbf{Gpc^{-3}yr^{-1}}$ (LL)**: results from best fit simultaneously to BATSE overall number counts and the local burst distribution. Panel details as for Figure 5.4.

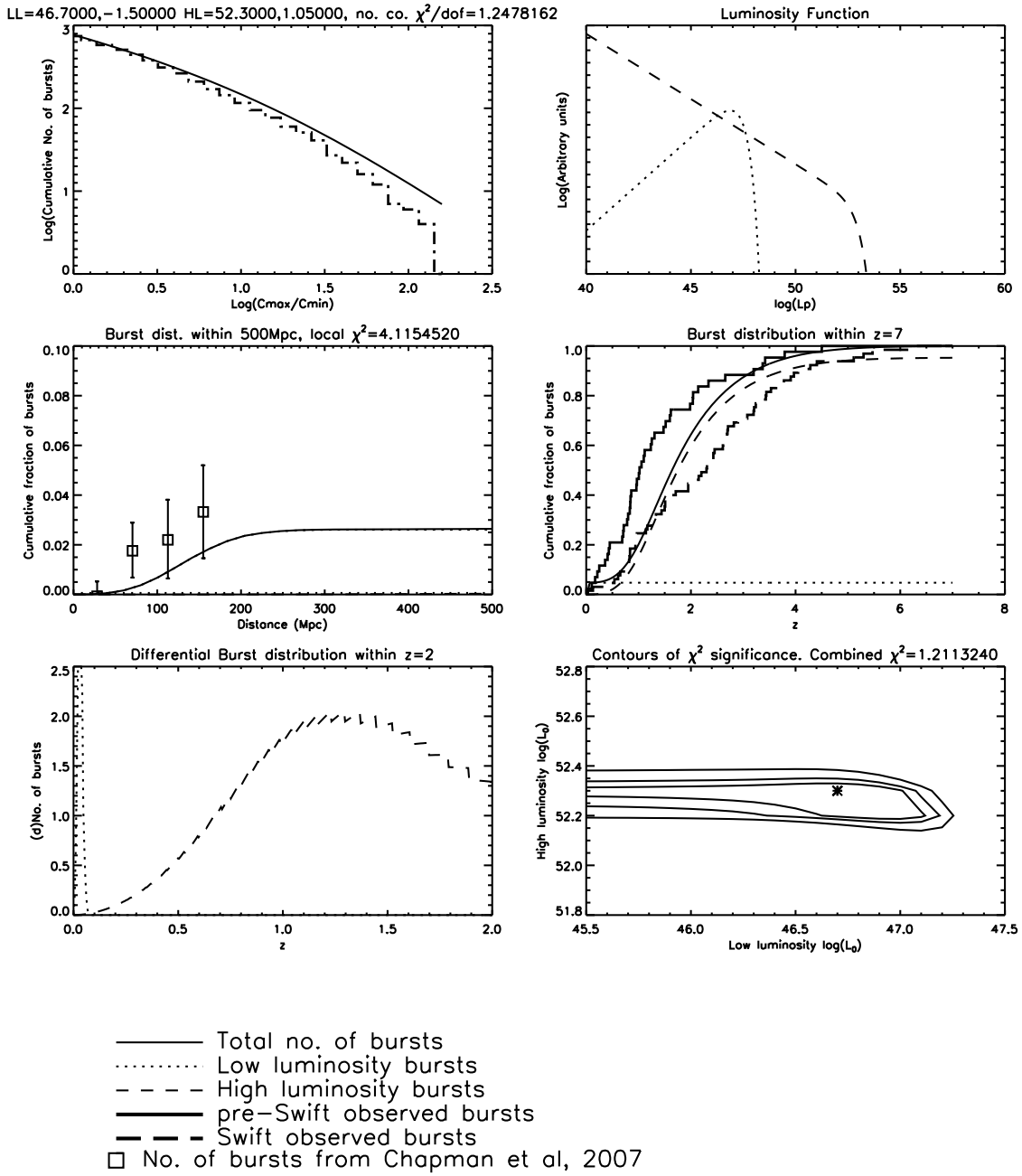

Figure 5.6: **L-GRB Dual population Schechter function LFs using intrinsic rates of** 1 **Gpc^{-3}yr^{-1} (HL) and** 700 **Gpc^{-3}yr^{-1} (LL)**: results from best fit simultaneously to BATSE overall number counts and the local burst distribution. Panel details as for Figure 5.4.

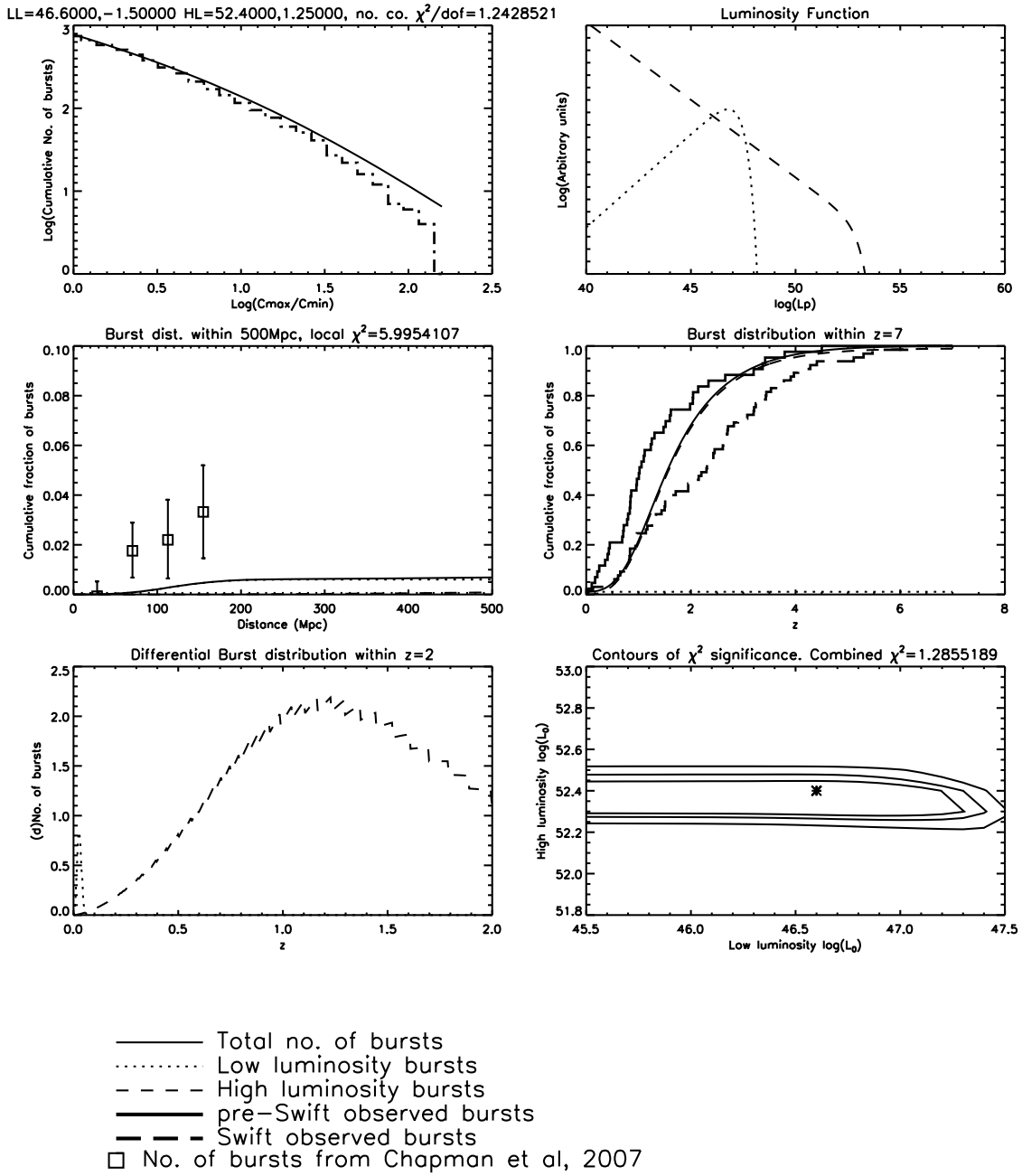

Figure 5.7: **L-GRB Dual population Schechter function LFs using intrinsic rates from Soderberg et al. (2006b)**: results from best fit simultaneously to BATSE overall number counts and the local burst distribution. Panel details as for Figure 5.4.

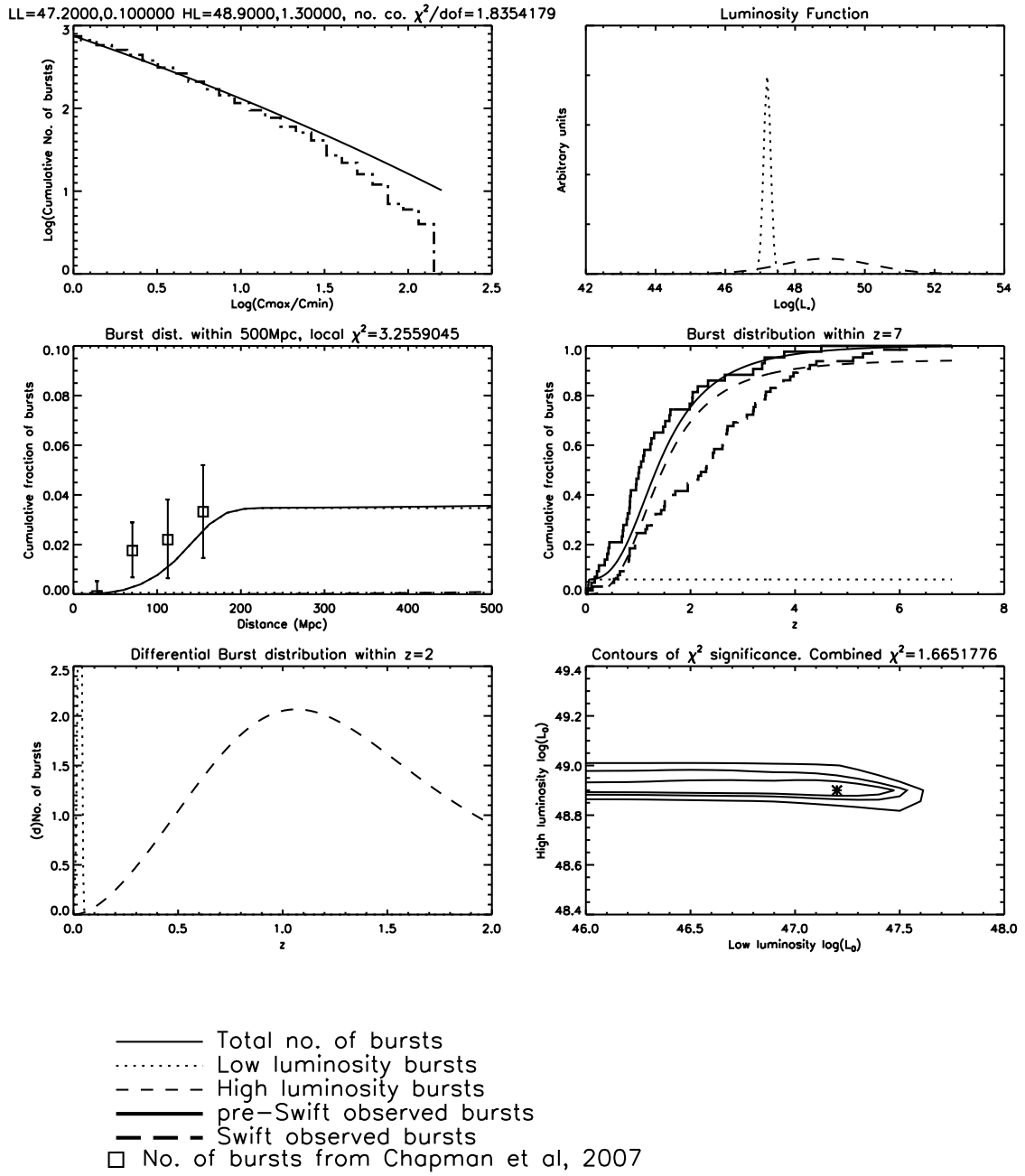

Figure 5.8: **Dual Lognormal LF results using intrinsic rates of** 1 $\mathbf{Gpc^{-3}yr^{-1}}$ **(HL) and** 700 $\mathbf{Gpc^{-3}yr^{-1}}$ **(LL)**: results from best fit simultaneously to BATSE overall number counts and the local burst distribution. Panel details as for Figure 5.4.

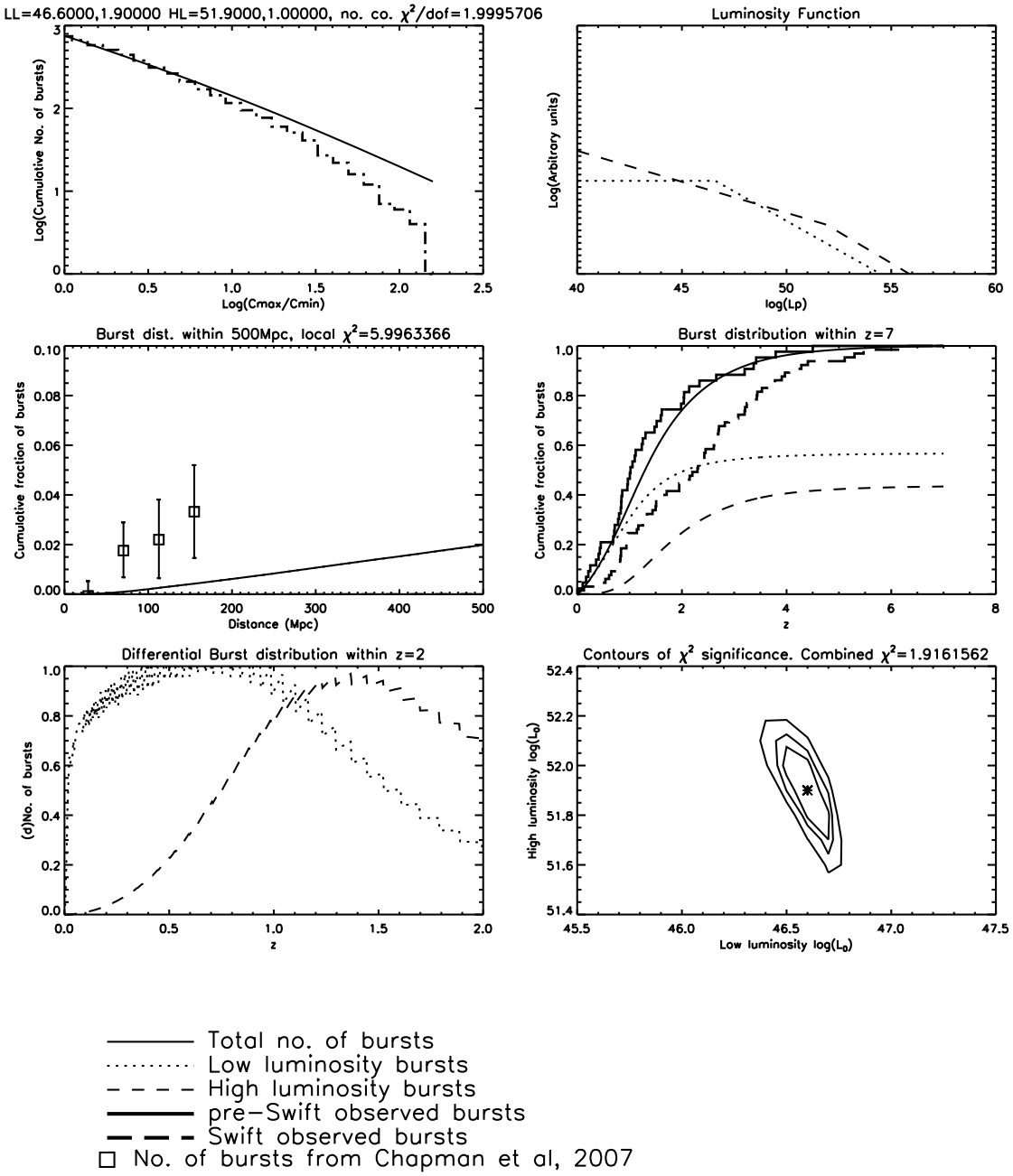

Figure 5.9: **L-GRB Dual population broken power law LFs using intrinsic rates from Liang et al. (2007)**: results from best fit simultaneously to BATSE overall number counts and the local burst distribution. Panel details as for Figure 5.4.

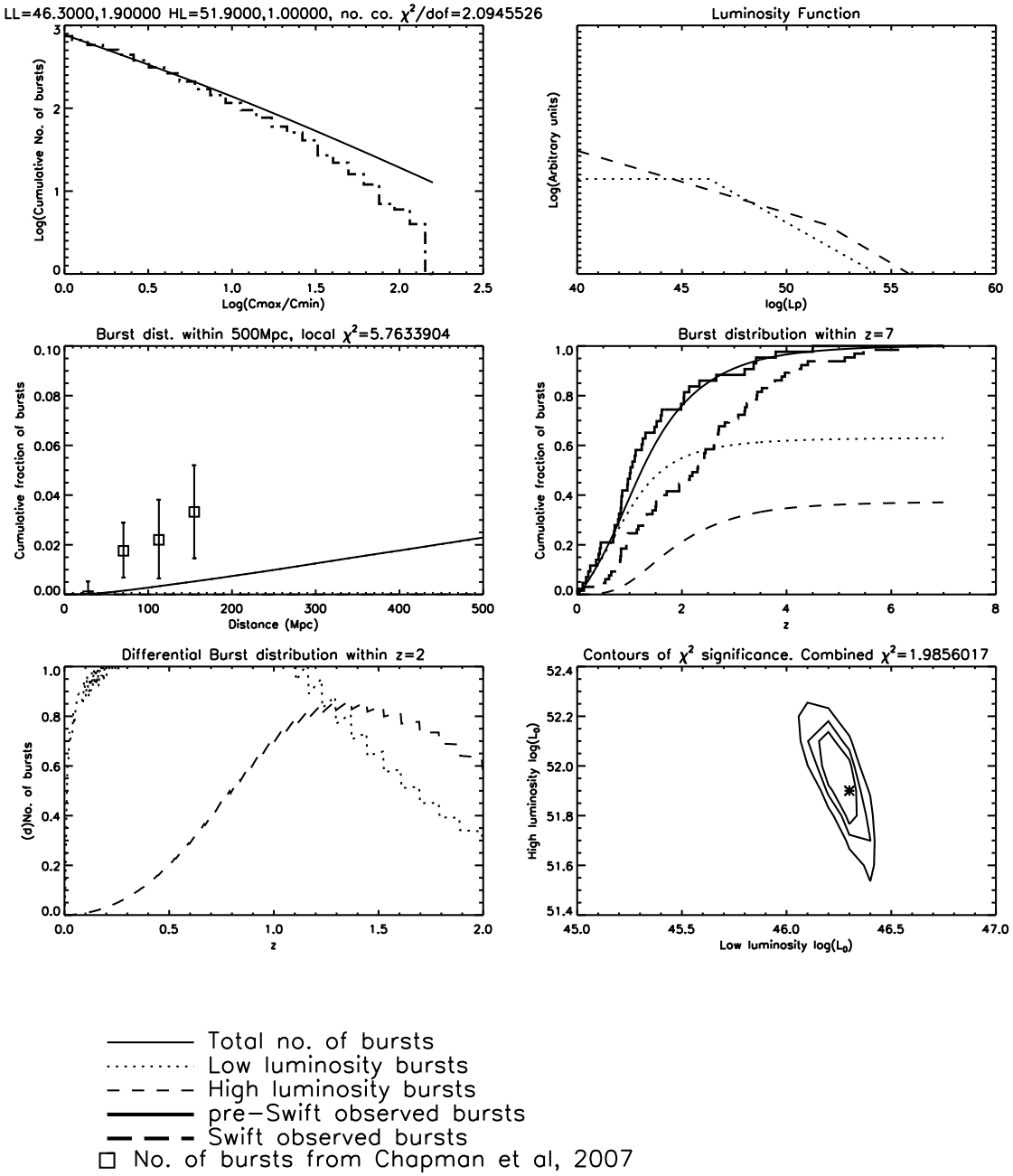

Figure 5.10: **L-GRB Dual population broken power law LFs using intrinsic rates of** 1 **Gpc^{-3}yr^{-1} (HL) and** 700 **Gpc^{-3}yr^{-1} (LL)**: results from best fit simultaneously to BATSE overall number counts and the local burst distribution. Panel details as for Figure 5.4.

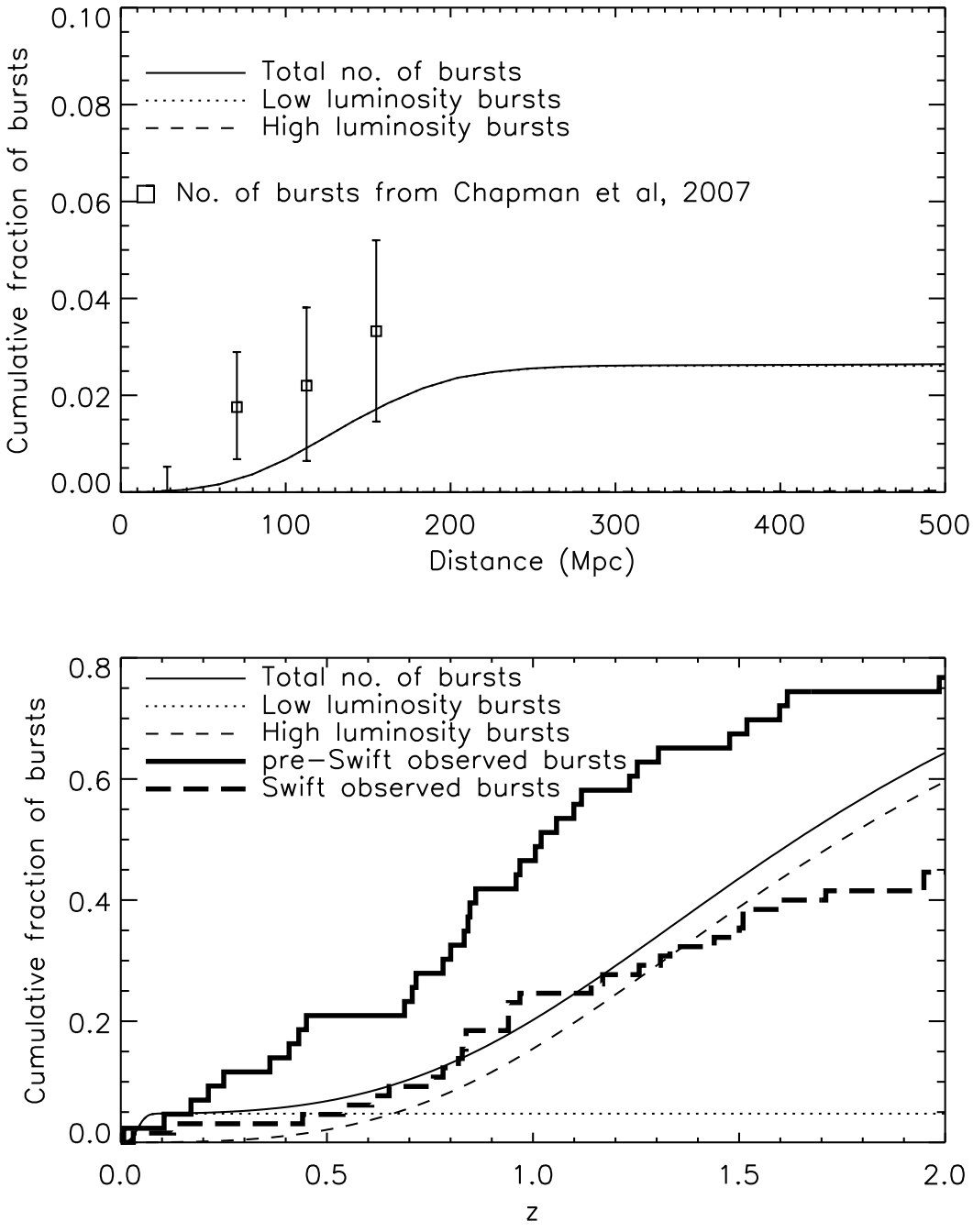

Figure 5.11: Redshift distribution within $z = 2$ of dual Schechter L-GRB LF using intrinsic rates of 1 $\mathrm{Gpc^{-3}yr^{-1}}$ (HL) and 700 $\mathrm{Gpc^{-3}yr^{-1}}$ (LL). Top panel shows predicted L-GRB distribution within 500 Mpc, and the bottom panel shows the predicted burst distribution out to $z = 2$ normalised and compared to the *Swift* and pre-*Swift* distributions discussed in the text The model distribution is calculated using a *Swift* threshold limit assumed to be half that of BATSE.

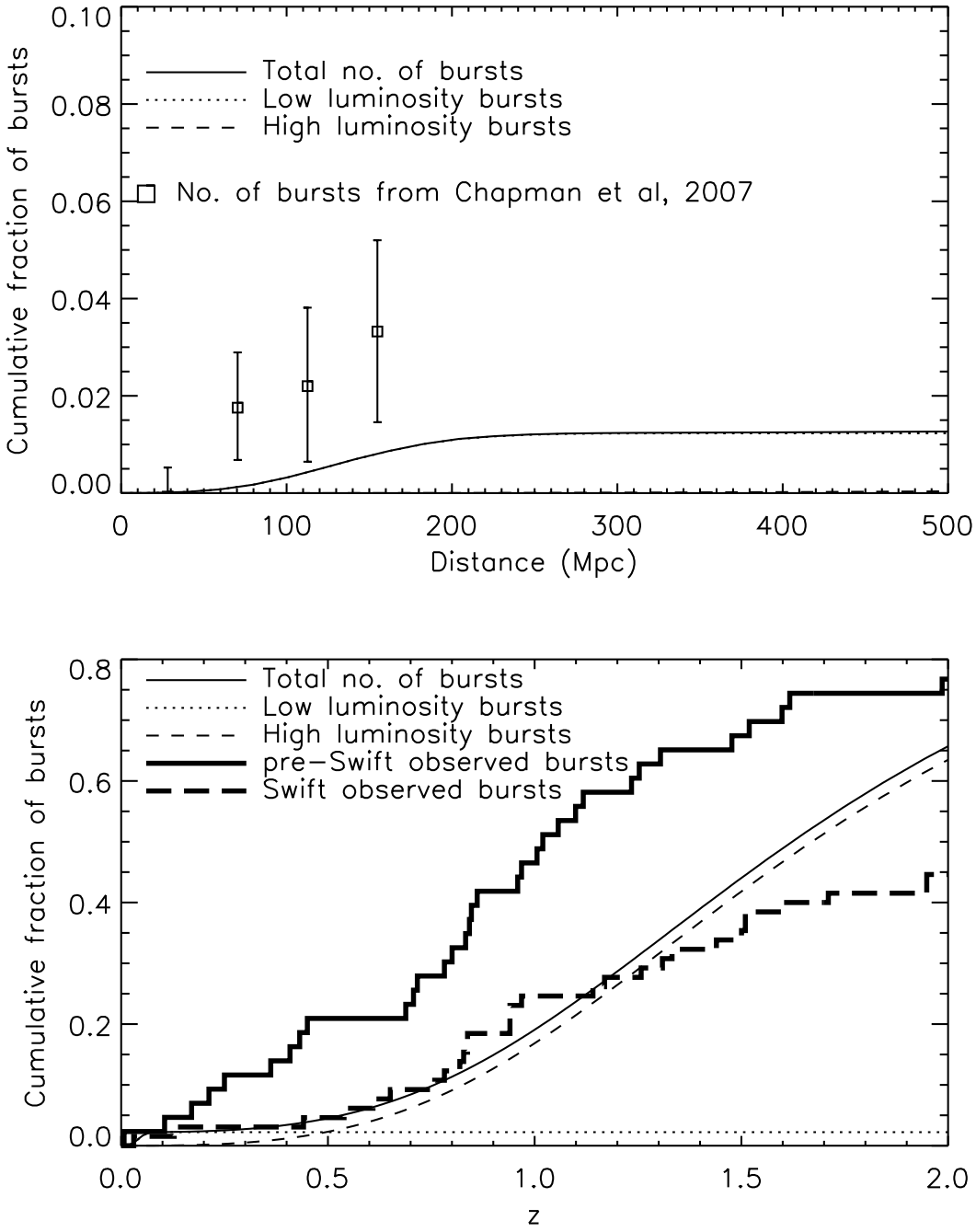

Figure 5.12: Redshift distribution within $z = 2$ of dual Schechter L-GRB LF using intrinsic rates of 1.12 $\mathrm{Gpc^{-3}yr^{-1}}$ (HL) and 325 $\mathrm{Gpc^{-3}yr^{-1}}$ (LL) from Liang et al. (2007). Panel details as for Figure 5.11.

5.3.2 Constraints via overall redshift distribution

5.3.2.1 Single population Luminosity Functions

Given the uncertainties regarding the appropriateness of applying an adjusted version of the BATSE number count distribution to the *Swift* sample, we can alternatively compare the predicted redshift distributions from our LF models directly to the overall *Swift* redshift distribution, both alone and in conjunction with the predicted local fraction from the correlation results. Table 5.5 shows the results of constraining single LF models by the redshift distribution alone.

Single LF	Intrinsic rate ($\mathrm{Gpc^{-3}yr^{-1}}$)	Parameters ($l_0 \equiv \log L_0$)	Local χ^2/dof	Redshift χ^2/dof	Overall χ^2/dof
Lognormal	1	$l_0 = 46.5$ $\sigma = 2.9$	6.88	0.96	1.10
Schechter	1	$l_0 = 53.3$ $\alpha = 1.2$	6.88	1.04	1.17
Broken power law ($\alpha_2 = 2.0$)	1	$l_0 = 53.3$ $\alpha_1 = 1.0$	6.88	1.14	1.25
Schechter	100	$l_0 = 52.7$ $\alpha = 1.3$	6.87	2.62	2.45
Lognormal	100	$l_0 = 44.1$ $\sigma = 2.2$	6.83	2.77	2.57
Broken power law ($\alpha_2 = 2.0$)	100	$l_0 = 50.0$ $\alpha_1 = 1.0$	6.85	6.53	5.61

Table 5.5: Results of single population L-GRB Luminosity Functions constrained to fit the *Swift* redshift distribution presented in order of decreasing goodness of fit (i.e. increasing overall χ^2/dof). The number of degrees of freedom (dof) for the local, redshift and overall distributions are 1, 17 and 21 respectively. l_0 is in units of $\log(\mathrm{erg\ s^{-1}})$, σ in dex and αs are dimensionless.

From this Table, we can see that all single LF models using an intrinsic L-GRB rate of 1.0 $\mathrm{Gpc^{-3}yr^{-1}}$ produce good fits to the overall *Swift* distribution, though once again produce no local bursts leading to a poor fit to the local distribution. Combined χ^2 measurements for both the overall redshift and local fits are dominated once again by the greater number of data points and smaller errors in the overall redshift distribution, and are therefore also reasonable for these models. In fact, the

combined fits to both the local and overall distributions produce identical best fit parameters.

Increasing the intrinsic L-GRB rate by a factor of 100 to 100 $\mathrm{Gpc}^{-3}\mathrm{yr}^{-1}$ produces more low redshift bursts at the expense once again of a poorer fit to the *Swift* distribution beyond $z \sim 1$, but still no local bursts within ~ 300 Mpc as can be seen for example in Figures 5.14 and 5.16. The qualitative differences at the low-z end of the distribution between the higher and lower intrinsic rates can be seen by comparing those Figures with Figures 5.13 and 5.15.

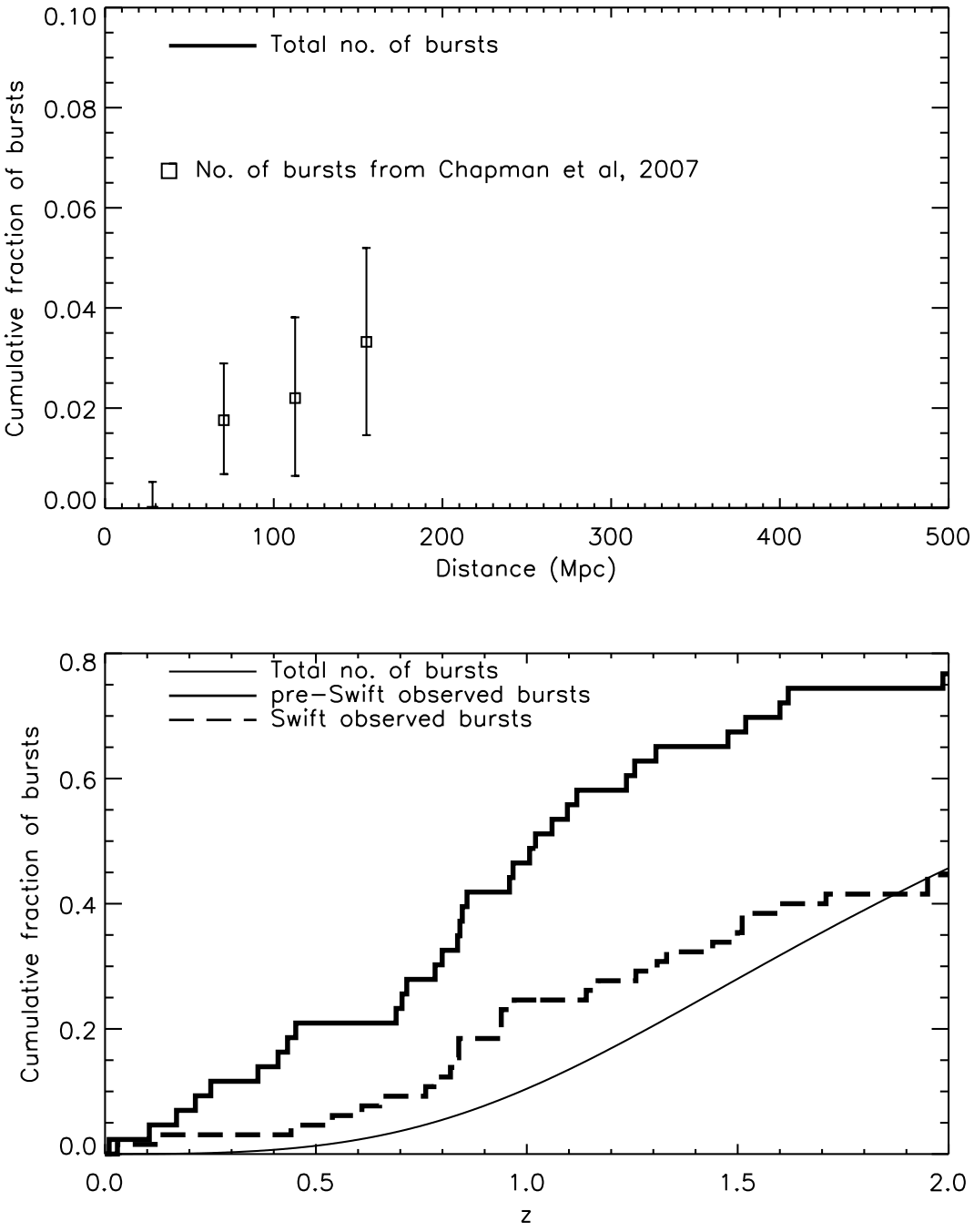

Figure 5.13: Redshift distribution within $z = 2$ of single Schechter L-GRB LF constrained to *Swift* redshift distribution only using intrinsic rate of 1 $\mathrm{Gpc}^{-3}\mathrm{yr}^{-1}$. Top panel shows predicted L-GRB distribution within 500 Mpc, and the bottom panel shows the predicted burst distribution out to $z = 2$ normalised and compared to the *Swift* and pre-*Swift* distributions discussed in the text The model distribution is calculated using a *Swift* threshold limit assumed to be half that of BATSE.

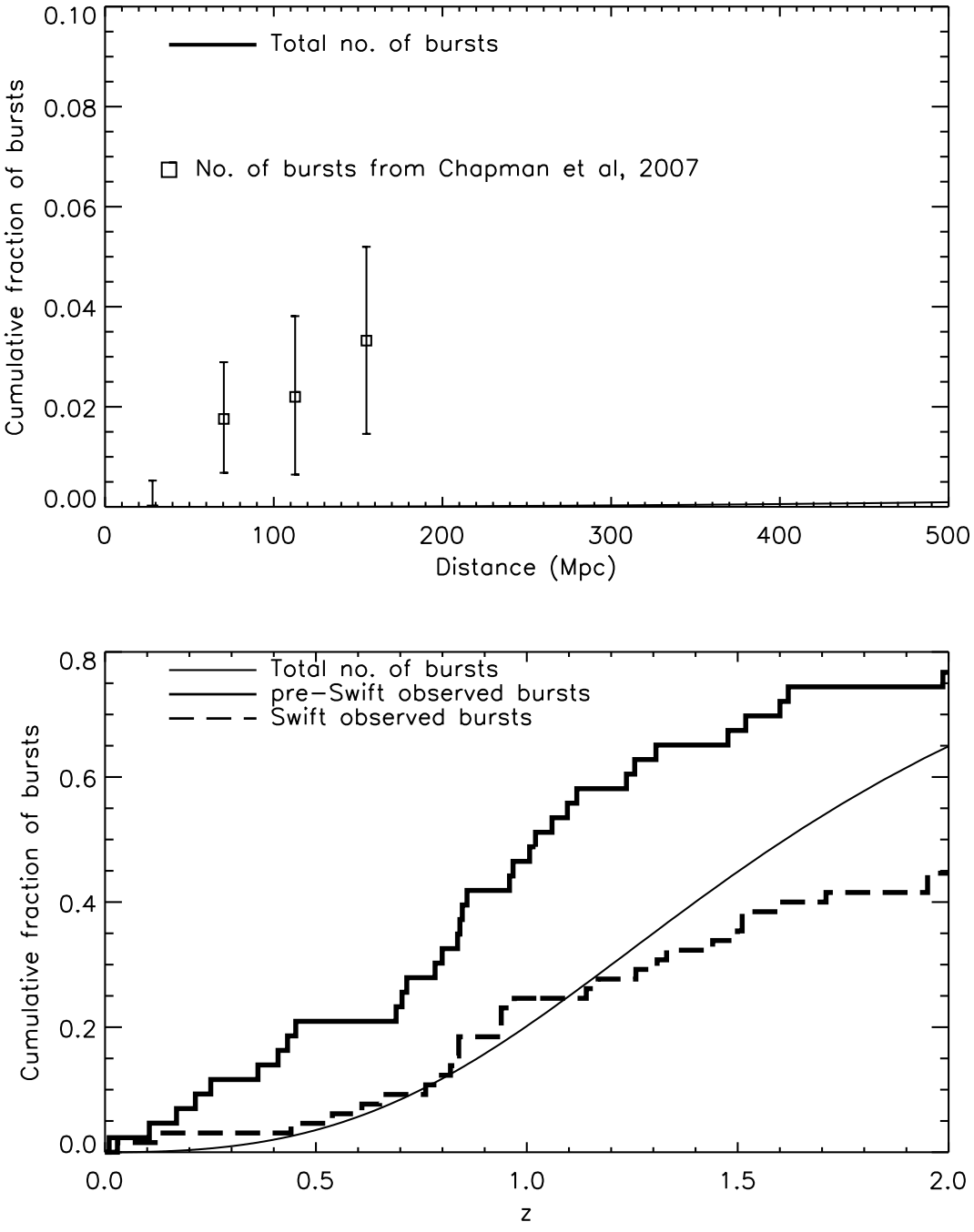

Figure 5.14: Redshift distribution within $z = 2$ of single Schechter L-GRB LF constrained to *Swift* redshift distribution only using intrinsic rate of 100 $\mathrm{Gpc}^{-3}\mathrm{yr}^{-1}$. Panel details as for Figure 5.13.

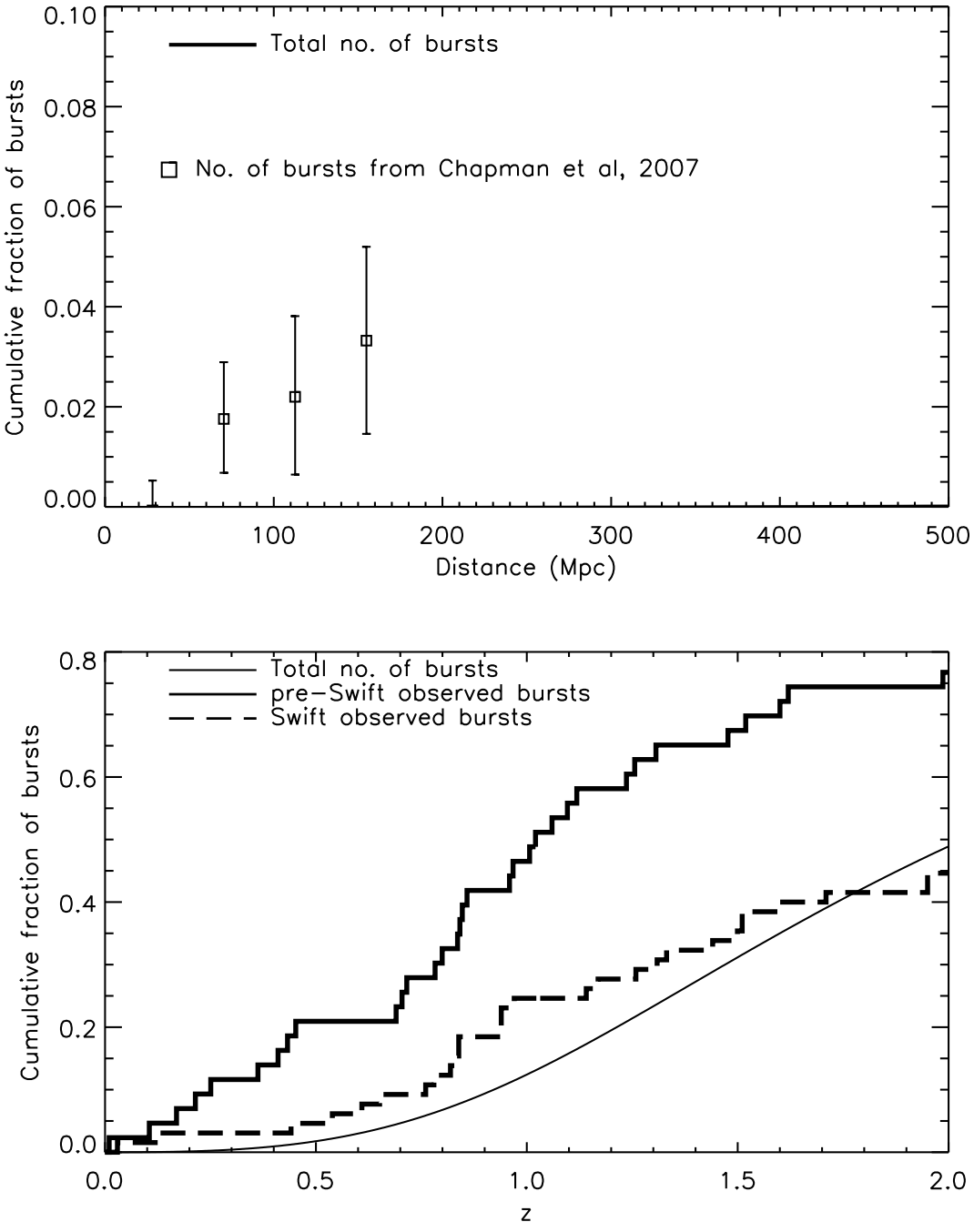

Figure 5.15: Redshift distribution within $z = 2$ of single Lognormal L-GRB LF constrained to *Swift* redshift distribution only using intrinsic rate of 1 $\mathrm{Gpc}^{-3}\mathrm{yr}^{-1}$. Panel details as for Figure 5.13.

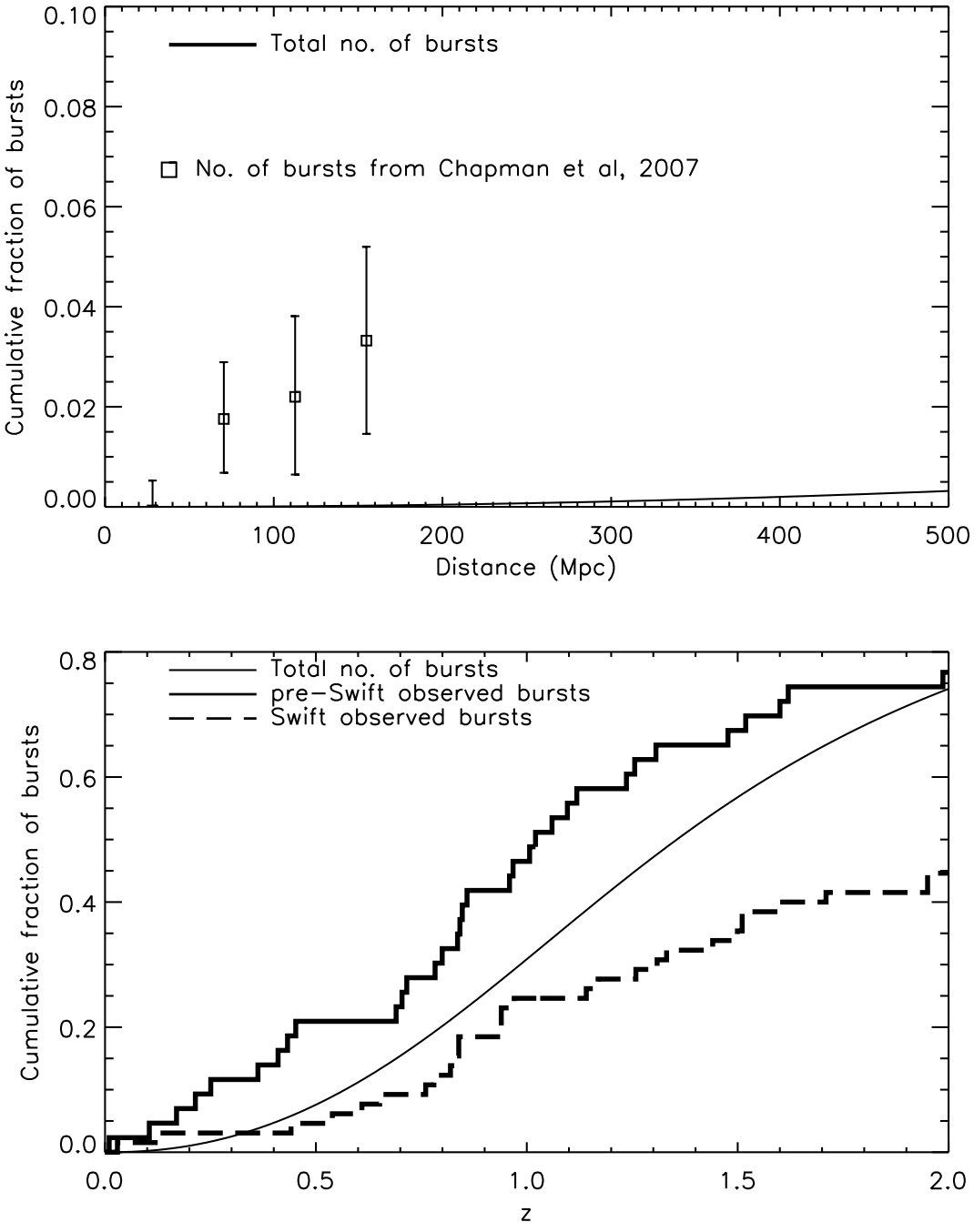

Figure 5.16: Redshift distribution within $z = 2$ of single Lognormal L-GRB LF constrained to *Swift* redshift distribution only using intrinsic rate of 100 $\mathrm{Gpc}^{-3}\mathrm{yr}^{-1}$. Panel details as for Figure 5.13.

5.3.2.2 Dual population Luminosity Functions

We therefore move on to consider the effects of including a second, low luminosity population of L-GRBs. Table 5.6 presents the results of populations produced by the dual LFs of section 5.2.2 above constrained simultaneously by the overall *Swift* redshift distribution and the distribution of local bursts from the correlation analysis. Two sets of intrinsic progenitor rates are used for the dual populations: 1.12 $\mathrm{Gpc^{-3}yr^{-1}}$ (HL) and 325 $\mathrm{Gpc^{-3}yr^{-1}}$ (LL) from the results of Liang et al. (2007), and 1.0 $\mathrm{Gpc^{-3}yr^{-1}}$ (HL, from previous analyses from the literature (e.g. Guetta & Della Valle 2007)) and 700 $\mathrm{Gpc^{-3}yr^{-1}}$ (LL, following from the results of Chapter 4). From this table and Figures 5.17 to 5.23 we can see that all dual LF models produce reasonable fits to the *Swift* redshift distribution, along now with a nearby population produced solely by the low luminosity progenitors.

None of the dual LF models reproduce the very closest (within ~ 100 Mpc or so) population of bursts expected from our correlation results though, and indeed the fits generally underproduce the local bursts in total. It is difficult to distinguish between this being a real effect or possibly the result of the rather coarse redshift binning necessary to maintain reasonable counts for the χ^2 analysis from the still limited number of bursts with known redshifts. Future results from *Swift* and *Fermi* (formerly *GLAST*) in the next few years will produce a larger sample of bursts with well constrained redshifts (including, hopefully, more nearby bursts) and the binning resolution should be able to be increased sufficiently to settle the issue.

Nevertheless, the dual LF models do produce a nearby population of bursts. In particular, the dual Schechter and dual Lognormal models (using an intrinsic HL rate of 700 $\mathrm{Gpc^{-3}yr^{-1}}$ implied by the correlation results) produce best fits within 1σ of the two outermost spheres considered in the correlation analysis (see the top panels of Figures 5.24 and 5.25). From Figure 5.20 we see that the dual Schechter LF model reproduces the overall *Swift* redshift distribution extremely well, though it overproduces the lowest redshift bursts by about a factor of two (see bottom panel of Figure 5.24). In contrast, the dual Lognormal model is a much closer fit to the low end of the redshift distribution (bottom panel Figure 5.25), while overproducing intermediate redshift bursts between redshifts of about 1.5 and 4.

It is interesting to note the difference in the number count distributions of the best fits to the overall redshift distribution with those of the BATSE distribution as shown in the top left panels of Figures 5.17 to 5.23. Although a downward shift of the distribution as a whole is seen as expected (due to the shorter all sky equivalent

observation period in the *Swift* sample), the slope of the distribution is also markedly different. The significantly shallower slope implies that the *Swift* sample contains a comparatively greater fraction of brighter (in terms of instrument threshold) bursts than the BATSE sample. It is not obvious why this should be the case, and it is likely that this is indicative of the inadequacy of our simplistic assumption of *Swift* being twice as sensitive as BATSE to long bursts, and/or the simplistic K correction assumed. Further work involving a detailed analysis of the *Swift* observed fluence distribution, along with a more accurate description of the *Swift* triggering algorithm and spectral response is required to investigate this further.

High Luminosity LF (ρ_0 Gpc^{-3}yr^{-1})	LF Parameters ($l_0 \equiv \log L_0$)	Low Luminosity LF (ρ_0 Gpc^{-3}yr^{-1})	LF Parameters ($l_0 \equiv \log L_0$)	Local χ^2/dof	Redshift χ^2/dof	Overall χ^2/dof
Broken power law (1), $\alpha_2 = 2$	$l_0 = 53.2$ $\alpha_1 = 1.0$	Broken power law (700), $\alpha_1 = 0$	$l_0 = 46.4$ $\alpha_2 = 2.0$	6.12	0.85	1.00
Broken power law (1.12), $\alpha_2 = 2$	$l_0 = 53.0$ $\alpha_1 = 1.0$	Broken power law (325), $\alpha_1 = 0$	$l_0 = 47.2$ $\alpha_2 = 2.2$	5.75	0.89	1.01
Schechter (1)	$l_0 = 52.8$ $\alpha = 1.05$	Schechter (700)	$l_0 = 47.0$ $\alpha = -1.4$	4.57	1.39	1.34
Schechter (1.12)	$l_0 = 52.7$ $\alpha = 1.05$	Lognormal (325)	$l_0 = 47.4$ $\alpha = 0.1$	5.46	1.57	1.53
Schechter (1.12)	$l_0 = 52.8$ $\alpha = 1.05$	Schechter (325)	$l_0 = 47.6$ $\alpha = 0.05$	5.85	1.59	1.56
Lognormal (1)	$l_0 = 48.9$ $\alpha = 1.55$	Lognormal (700)	$l_0 = 47.2$ $\alpha = 0.05$	4.35	1.95	1.77
Lognormal (1.12)	$l_0 = 48.8$ $\alpha = 1.55$	Lognormal (325)	$l_0 = 47.3$ $\alpha = 0.05$	5.44	2.03	1.89

Table 5.6: Results of dual population Luminosity Functions for L-GRBs fit simultaneously to the *Swift* redshift distribution and local distribution, presented in order of decreasing goodness of fit (i.e. increasing overall χ^2/dof). The number of degrees of freedom (dof) for the local, redshift and overall distributions are 1, 15 and 19 respectively. l_0 is in units of log(erg s^{-1}), σ in dex and αs are dimensionless.

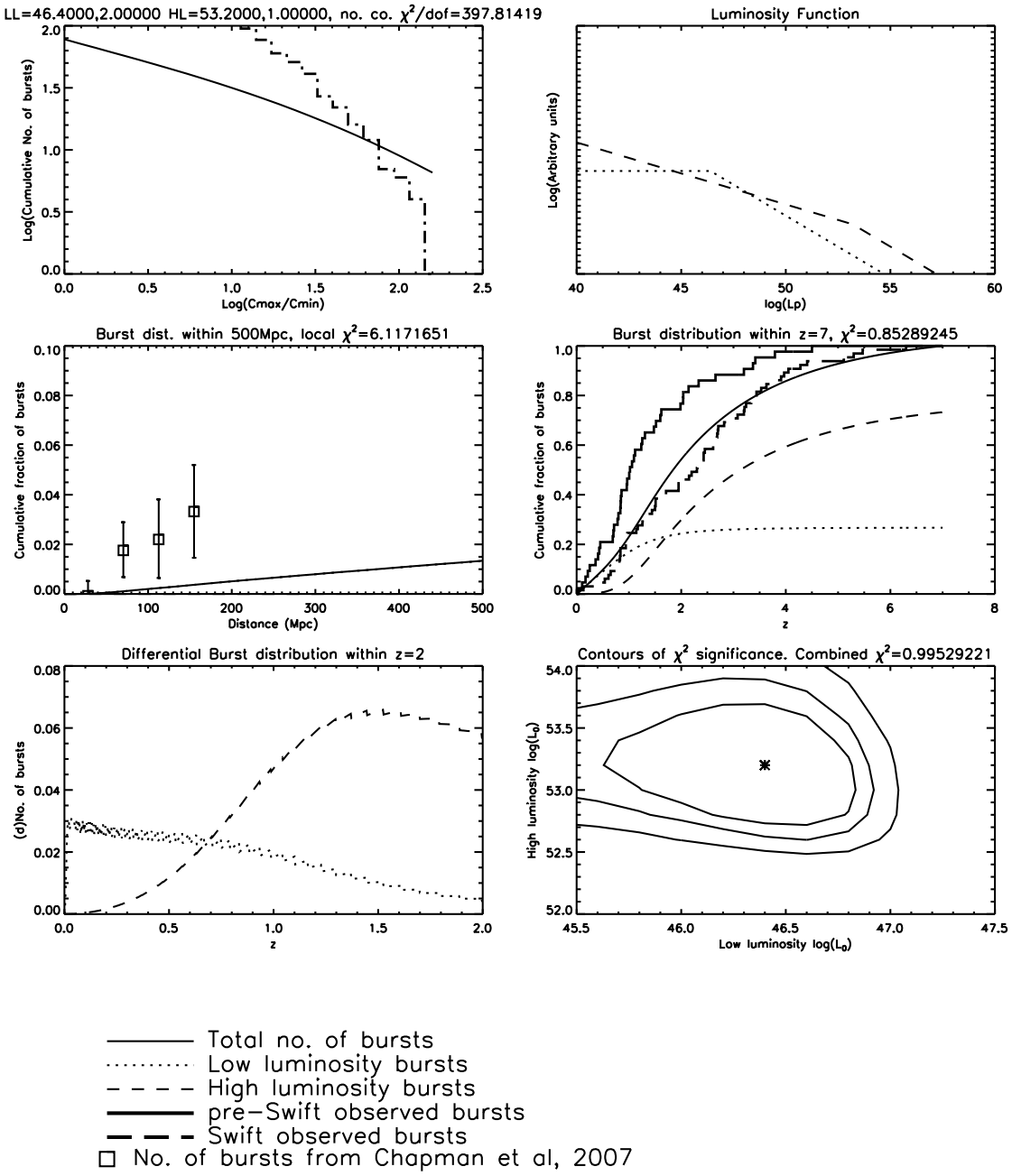

Figure 5.17: **L-GRB Dual population broken power law LFs using intrinsic rates of** 1 $\mathbf{Gpc^{-3}yr^{-1}}$ **(HL) and** 700 $\mathbf{Gpc^{-3}yr^{-1}}$ **(LL)**: results from best fit simultaneously to the *Swift* redshift distribution and the local burst distribution. Top left: number count distribution compared to BATSE number counts; Top Right: the best fit LFs; Middle Left: the local burst distribution within 500 Mpc compared to local correlation results; Middle Right: cumulative burst distribution within $z = 7$ (calculated with *Swift* threshold limits) compared to the *Swift* and pre-*Swift* redshift distributions; Bottom Left: differential burst distribution within $z = 2$; Bottom Right: contours of χ^2 significance levels for the overall best fit LF parameters (contours show 0.6, 0.9 and 0.99 significance levels with best fit values plotted as an asterisk).

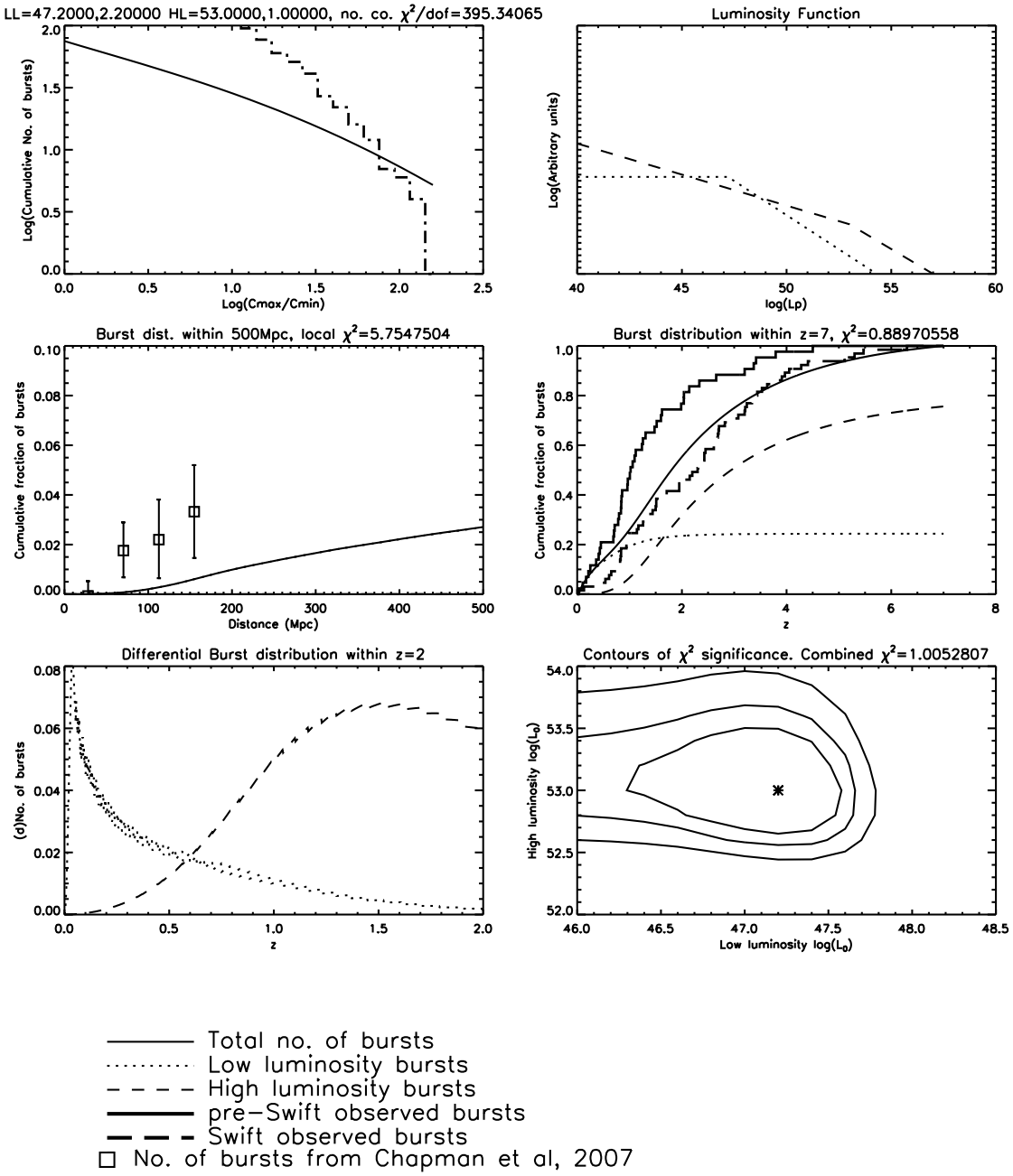

Figure 5.18: **L-GRB Dual population broken power law LFs using intrinsic rates from Liang et al. (2007)**: results from best fit simultaneously to the *Swift* redshift distribution and the local burst distribution. Panel details as for Figure 5.17.

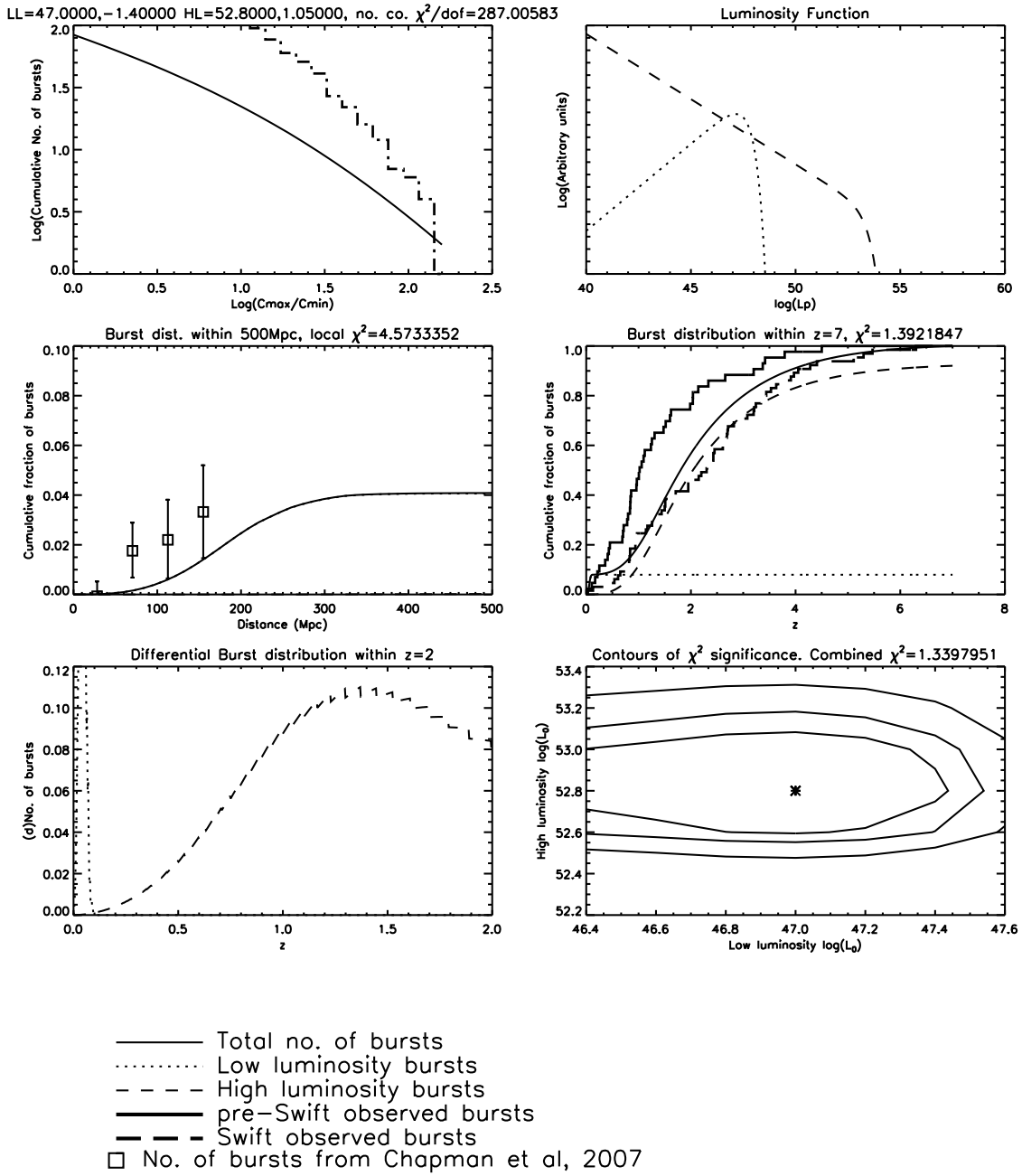

Figure 5.19: **L-GRB Dual population Schechter function LFs using intrinsic rates of** 1 **Gpc^{-3}yr^{-1} (HL) and** 700 **Gpc^{-3}yr^{-1} (LL)**: results from best fit simultaneously to the *Swift* redshift distribution and the local burst distribution. Panel details as for Figure 5.17.

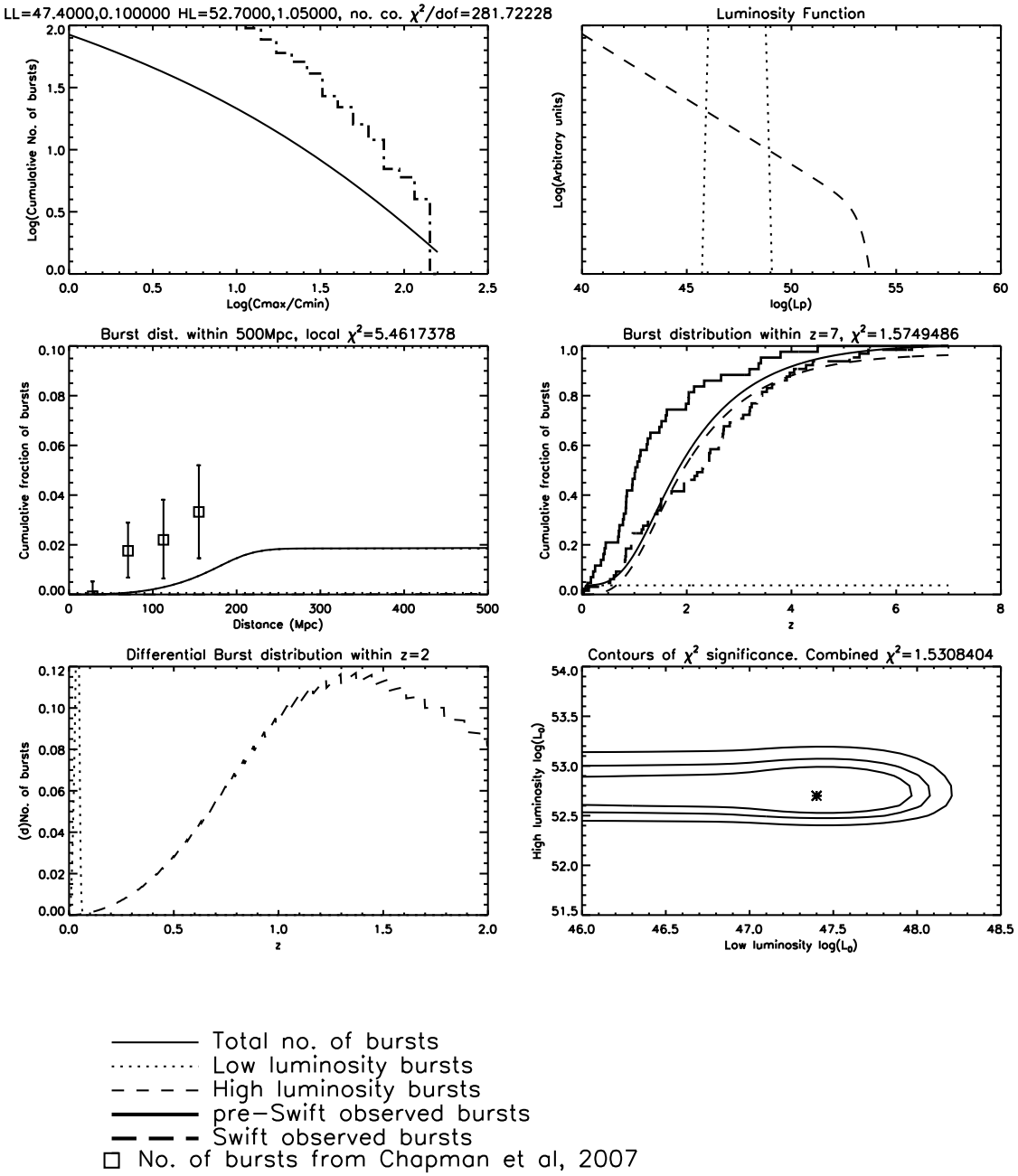

Figure 5.20: **L-GRB Lognormal (LL) and Schechter (HL) LFs using intrinsic rates from Liang et al. (2007)**: results from best fit simultaneously to the *Swift* redshift distribution and the local burst distribution. Panel details as for Figure 5.17.

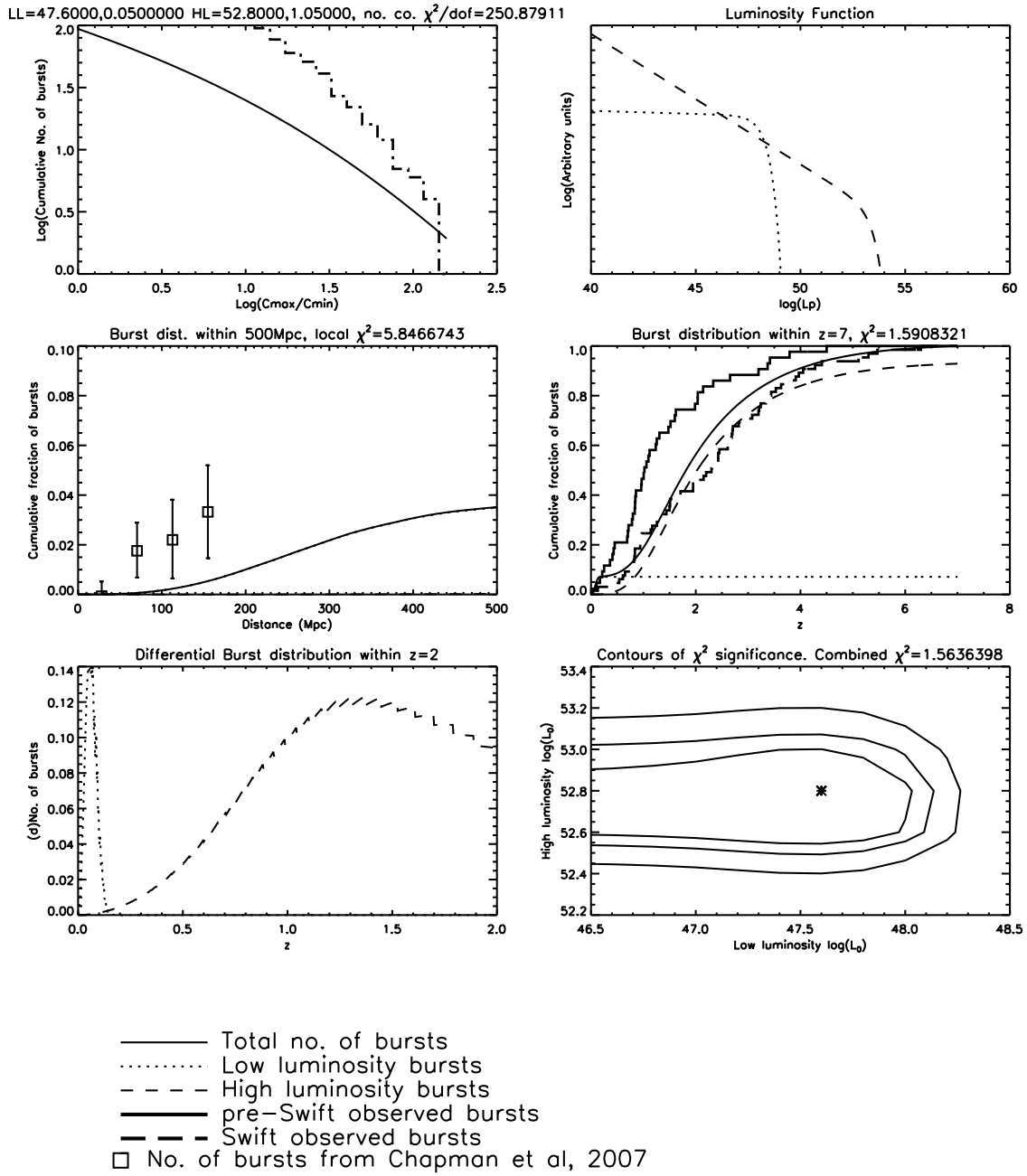

Figure 5.21: **Dual population Schechter function LFs using intrinsic rates 1.12 $\mathbf{Gpc^{-3}yr^{-1}}$ (HL) and 325 $\mathbf{Gpc^{-3}yr^{-1}}$ (LL) from Liang et al. (2007)**: results from best fit simultaneously to *Swift* redshift distribution and the local burst distribution. Panel details as for Figure 5.17.

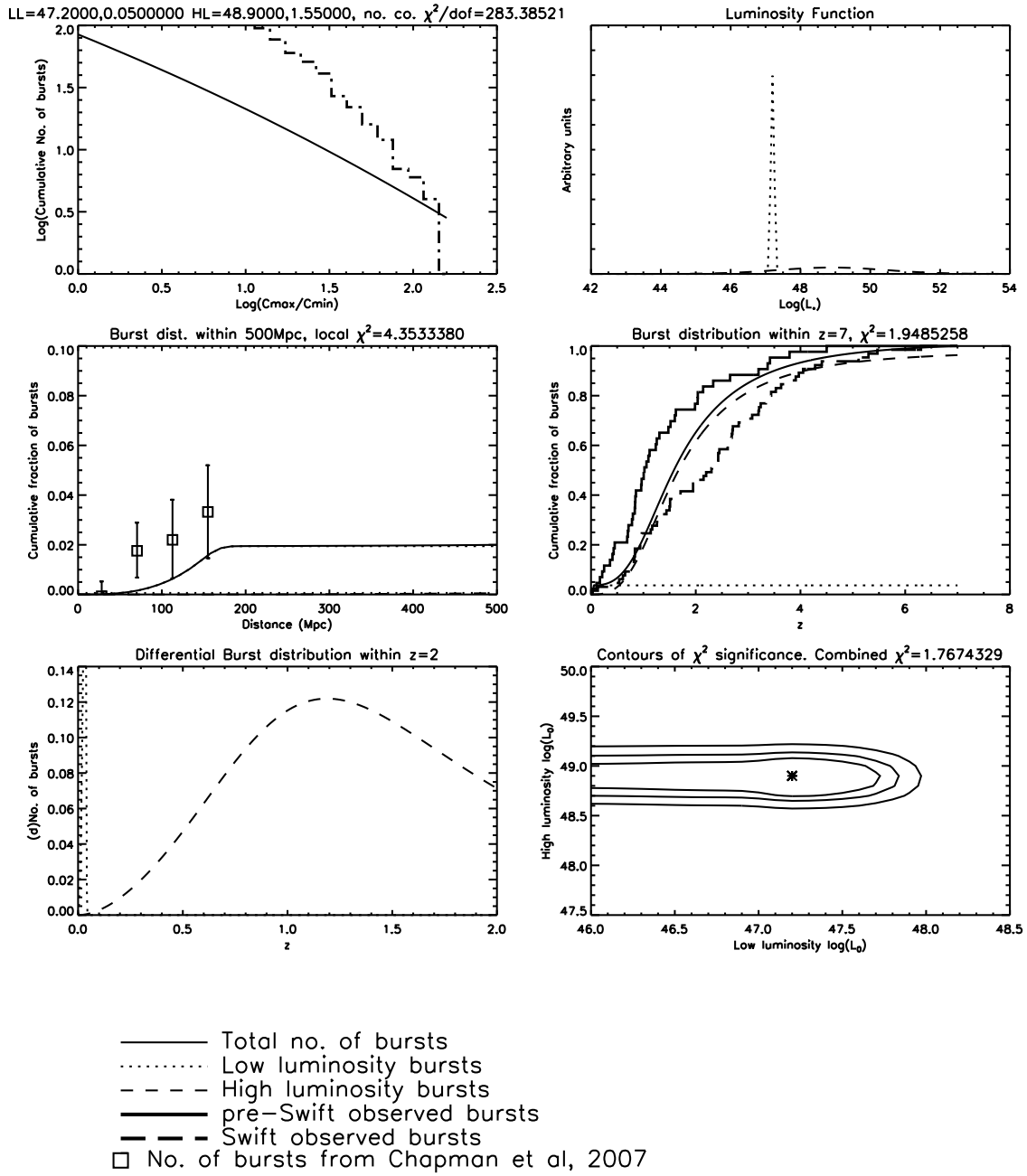

Figure 5.22: **L-GRB Dual population Lognormal using intrinsic rates of 1 $\mathbf{Gpc^{-3}yr^{-1}}$ (HL) and 700 $\mathbf{Gpc^{-3}yr^{-1}}$ (LL)**: results from best fit simultaneously to the *Swift* redshift distribution and the local burst distribution. Panel details as for Figure 5.17.

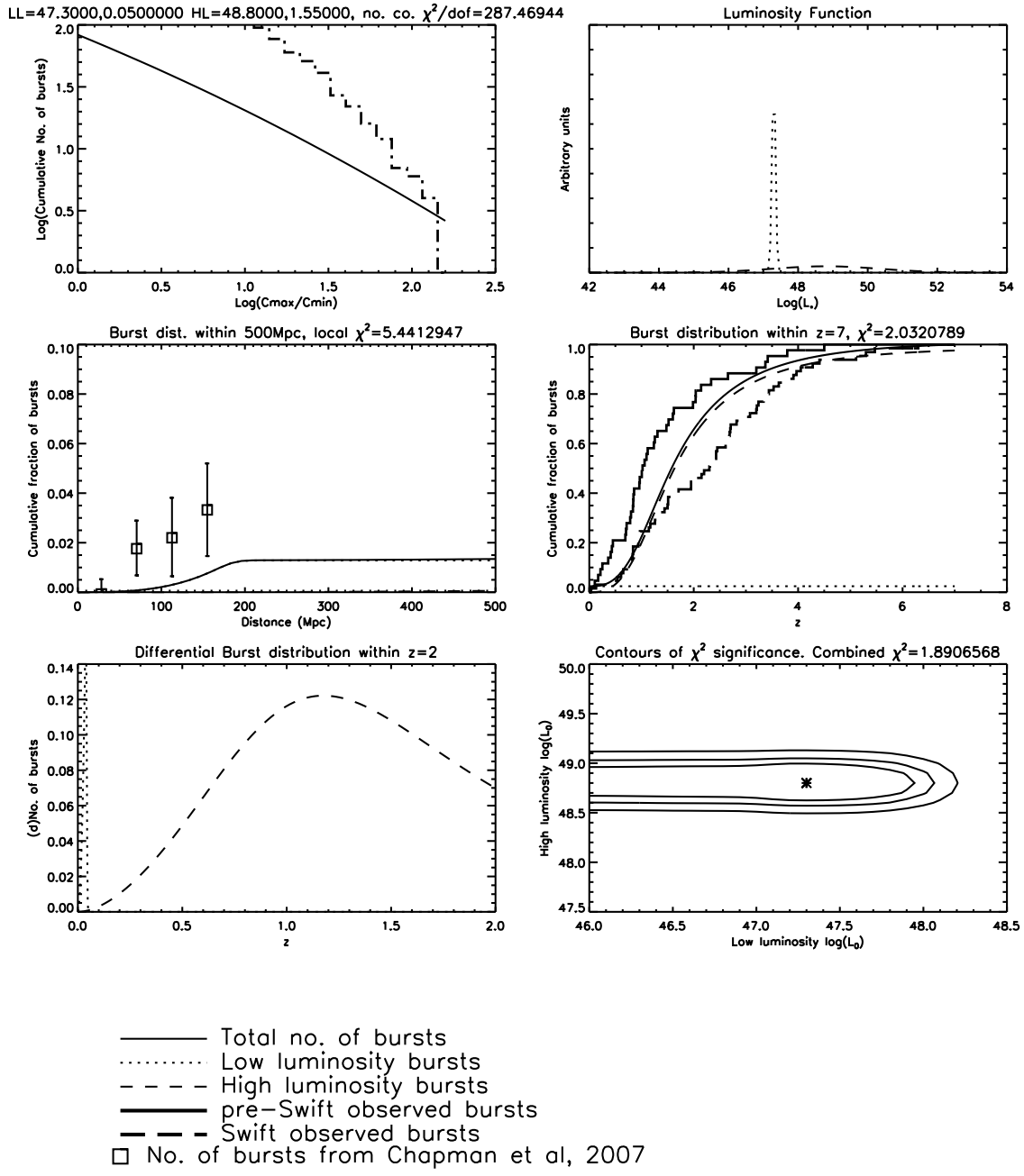

Figure 5.23: **L-GRB Dual population Lognormal LFs using intrinsic rates from Liang et al. (2007)**: results from best fit simultaneously to the *Swift* redshift distribution and the local burst distribution. Panel details as for Figure 5.17.

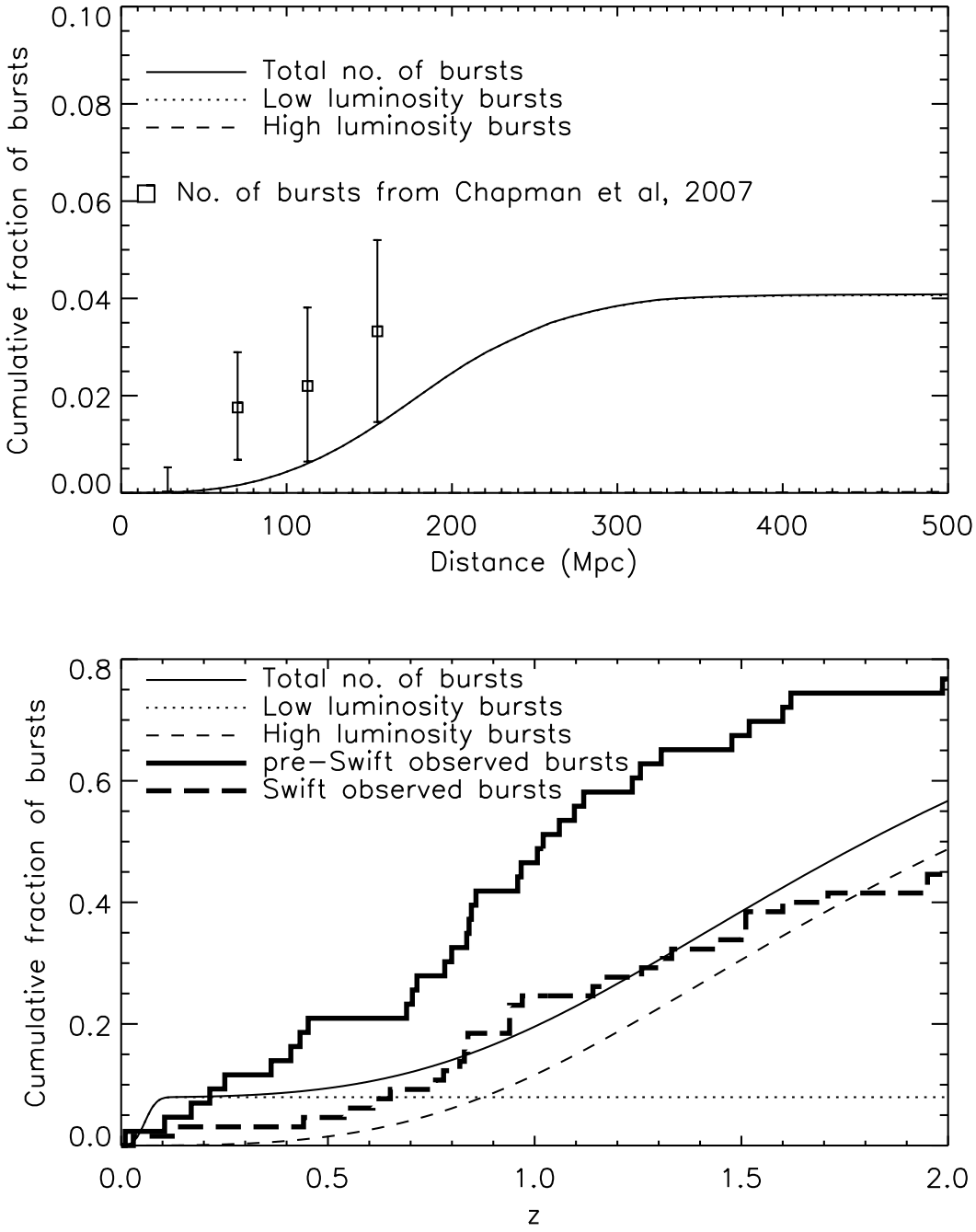

Figure 5.24: Redshift distribution within $z = 2$ of dual Schechter function LFs using intrinsic rates of 1 $\mathrm{Gpc^{-3}yr^{-1}}$ (HL) and 700 $\mathrm{Gpc^{-3}yr^{-1}}$ (LL) fit simultaneously to the *Swift* redshift distribution and the local burst distribution. The top panel shows the predicted L-GRB distribution within 500 Mpc, and the bottom panel shows the predicted burst distribution out to $z = 2$ normalised and compared to the *Swift* and pre-*Swift* distributions discussed in the text. The model distribution is calculated using a *Swift* threshold limit assumed to be half that of BATSE.

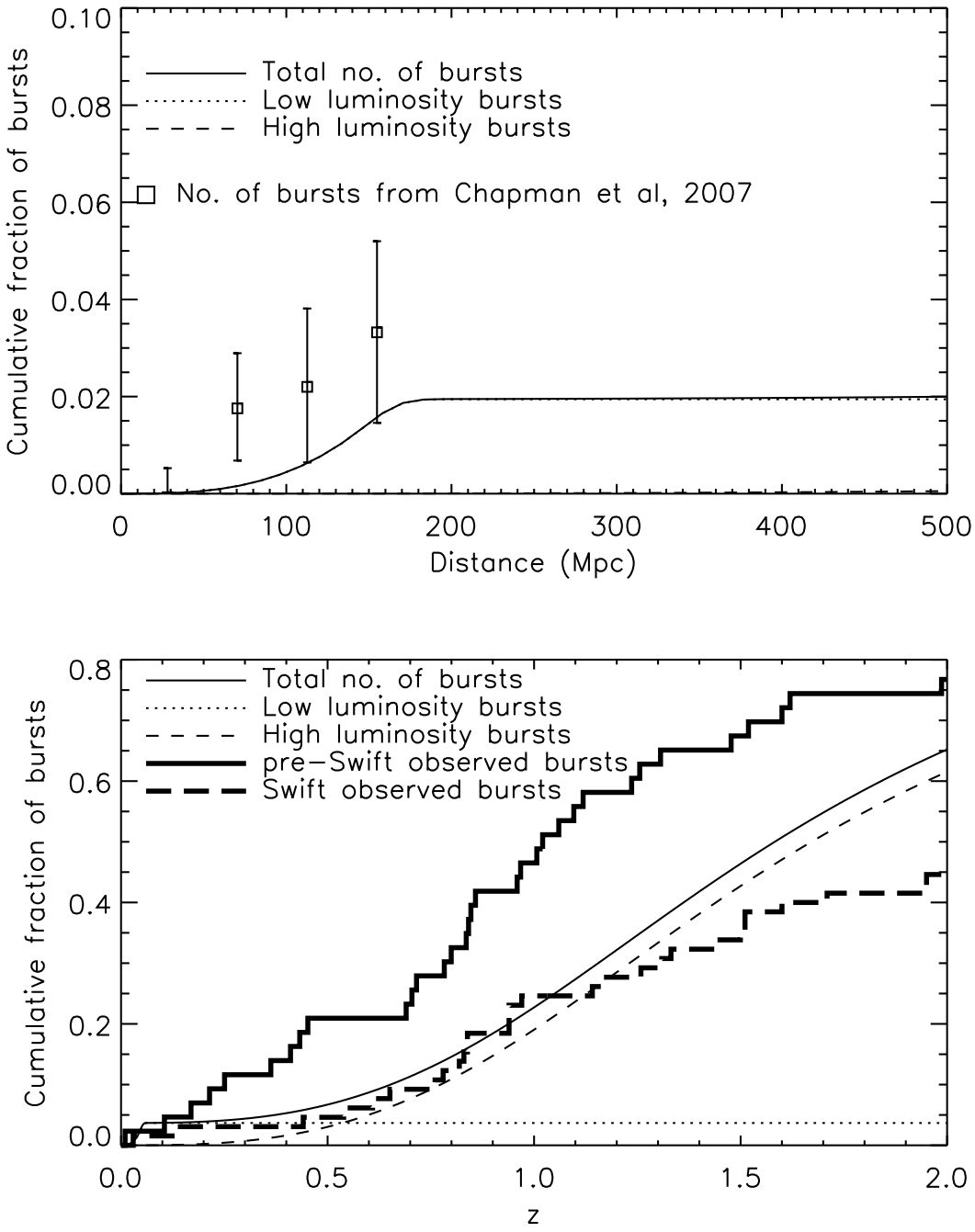

Figure 5.25: Redshift distribution within $z = 2$ of dual Lognormal L-GRB LFs fit simultaneously to *Swift* redshift distribution and the local burst distribution using intrinsic rates of 1 $\mathrm{Gpc}^{-3}\mathrm{yr}^{-1}$ (HL) and 700 $\mathrm{Gpc}^{-3}\mathrm{yr}^{-1}$ (LL). Panel details as for Figure 5.24.

5.4 Summary and Conclusions

By investigating a variety of plausible single population LFs and intrinsic rates for L-GRBs, we find that a nearby distribution at the levels found by the correlation analyses of Chapter 4 cannot be produced from the low luminosity tail of a single population of progenitors while maintaining compatibility with overall number counts and a realistic overall redshift distribution.

In a similar manner to the work of Chapter 3 for the short GRBs, we find that a separate, low luminosity population of L-GRBs is necessary to reproduce a local population. Without clear predictions from theoretical models for distinctly separate LL and HL progenitors (though plausible production routes do exist as discussed in Chapters 1 and 6), we can only assume intrinsic rates for the two burst populations from observations, our correlation analyses, and previous LF studies. However, we find that these rates, particularly those with high ratios of LL to HL bursts, produce burst distributions that match well with the *Swift* redshift distribution below about $z \lesssim 1.5$. At higher redshifts the predictions (constrained by the threshold-adjusted BATSE number counts) are not such a good match to the *Swift* observations, though they remain much more realistic than those of single population LFs forced to produce a local distribution of bursts, and remain within the bounds of pre-*Swift* observations.

Since the *Swift* redshift distribution for L-GRBs is a much larger and more robust sample than for the shorts, we can also use this to constrain the LF models instead of the number count distribution. We then find that the dual LFs are able to reproduce extremely well this overall redshift distribution while producing an acceptable local distribution as well. As mentioned at the end of Chapter 4, the local rates predicted by the best fit LFs are at the low end of our correlation results: around 2% of *Swift* L-GRBS predicted to occur within 155 Mpc when the LFs are constrained by the adjusted BATSE number count distribution, and only around 1% when constrained by the *Swift* overall redshift distribution. The latter is perhaps not surprising, since the observed distribution is itself part of the fit. Taken at face value for even the whole of the August 2008 *Swift* catalogue, this implies only about 3–6 *Swift* L-GRBs to have been observed within 155 Mpc, which compares reasonably well to the one (GRB 060218) identified for certain. As mentioned before, *Swift* is more sensitive to higher redshift bursts, and our assumptions regarding its spectral sensitivity and the associated K correction may very well be inadequate to account for this completely. Nevertheless, we would still expect a few more local bursts to

be identified or detected in the future.

We thus find that both when the models are constrained by number counts, or by overall redshift distribution, the expected population of local bursts from our correlation analysis is only produced by a separate, lower luminosity population of L-GRBs. As for the S-GRBs, the uncertainties regarding intrinsic progenitor rates and inadequate theoretical models do not allow us to choose sensibly between the specific luminosity function models investigated, but our results clearly suggest that single LF models are inadequate to produce a local burst distribution while maintaining consistency with the wider redshift distribution observed so far.

Ideally, we would like to fit using all three constraints simultaneously: the local distribution, an observed fluence distribution, and the overall redshift distribution. However, this requires further investigation into the *Swift* triggering algorithm, spectral response, and observed count rates. Future work improving the spectral modelling of L-GRBs and applying this to *Swift* specific threshold distributions should hopefully allow us to investigate whether these dual LF models are then consistent with all three constraints. This would also allow investigation into whether the basic assumption that L-GRBs follow the globally averaged SFR with no evolution is an adequate assumption, or whether (for example) formation models with some dependency on metallicity are preferred.

Chapter 6

Conclusions and Discussion

The focus of this work has been on the existence and nature of nearby populations of Gamma-ray Bursts, both long and short. Traditional correlation analysis and a novel correlation estimator have been used to estimate the fraction of BATSE bursts which show angular cross-correlation on the sky with samples of galaxies within 155 Mpc from local galaxy catalogues. The correlation estimator employed is sensitive to large scale structure rather than individual burst/galaxy pairings, and this precludes us from drawing conclusions about the properties of the potential host galaxy populations, other than their propensity to trace large scale structure. For the short duration GRBs, where alternative progenitor models exist, plausible luminosity function models have been investigated to both explain the observed correlations and elicit the likelihood of whether (and at what level) two populations of S-GRBs may exist. For the long GRBs, separate progenitor models with well known observational or theoretical properties do not exist, but observations of nearby bursts and previous luminosity function analyses suggest that there may well be a separate population of low luminosity L-GRBs. Bursts known to be nearby share several similar properties, and these were used to select and examine the correlations of a subset of BATSE L-GRBs with properties similar to the known local bursts. This subset was indeed found to exhibit an increased level of correlation with the nearby galaxy samples compared to that of the L-GRB population as a whole. We have then once again examined plausible single and dual luminosity function models for different luminosity L-GRB populations. We speculate later in this Chapter regarding the possible origins of separate populations of lower and higher luminosity L-GRBs.

6.1 Short GRBs

In Chapter 2 we showed that $9\% \pm 3\%$ of the BATSE short bursts with localisations better than 10° are correlated with galaxies of morphological T-type ≤ 4 from the *IRAS* PSCz catalogue with recession velocities ≤ 2000 km s^{-1} (within ~ 28 Mpc). The null hypothesis of zero correlation is thus rejected at a 3σ confidence level. Correlation with galaxies continues to increase to a level of $20\% \pm 8\%$ out to recession velocities of 8000 km s^{-1} (~ 112 Mpc) and remains constant at this level out to the furthest distances we were able to examine of 155 Mpc.

The most widely accepted model for S-GRBs is that of binary neutron star mergers. The initial short, hard spike of a giant flare from a Soft Gamma Repeater occurring in a sufficiently nearby galaxy would also have appeared to BATSE as a short GRB. Thus there are two possible models for S-GRBs, and in Chapter 3 we investigated the ability of plausible Luminosity Functions (combined with observed and theoretical rates of progenitor occurrence) to reproduce both the overall BATSE number counts and a local population as measured from the correlation analysis. We found that only dual Luminosity Functions consisting of a lower and higher luminosity population were able to reproduce the observed local S-GRB population while remaining consistent with overall number counts. The properties of the best fit LFs agreed well with the observed and expected luminosities of the two progenitor populations. Furthermore, the overall redshift distribution predicted by dual LF models was reasonably consistent with the current redshift distribution of *Swift* short GRBs, despite this taking no part in the analysis. We caution however, that this early redshift distribution is uncertain, contains several bursts with redshifts measured solely from plausible host associations, and may well suffer from selection effects.

From the results in Chapter 3, particularly comparing Figures 3.1, 3.4 and 3.3, we can see that the nearby population of shorts identified by the correlation analysis is naturally explained by a population of extragalactic SGR giant flares. In fact, the results imply that this nearby population can only be explained by a separate low luminosity burst population – even the most low luminosity dominated single population model produces effectively no events within ~ 100 Mpc. If this low luminosity population is indeed due to SGR giant flares and not neutron star mergers, then it is not encouraging news for current gravitational wave detectors. Overall our best fit LF models suggest that up to $\sim 15\%$ of *Swift* S-GRBs should arise from extragalactic SGR giant flares within 100 Mpc, and about 5% from within

20 Mpc. LIGO may currently be able to detect optimally placed and oriented binary mergers out to around 20 Mpc, and our results predict effectively no S-GRBs produced by NS mergers within this distance. Nevertheless, even sensitivity out to this kind of distance is useful in order to rule out a merger origin for a candidate nearby short burst, as LIGO was able to do with with $> 99\%$ confidence for GRB 070201, whose location error box overlapped M31. Advanced LIGO, offering an order of magnitude increase in sensitivity along with increased bandwidth and tunability, is expected to be able to detect the merger of two 1.4 $M_{\odot}$ neutron stars out to a distance of around 300 Mpc [1]. Our LF models suggest approximately 2% of BATSE S-GRBs, equivalent to an event rate of 2 to 4 bursts per year (full sky) could have originated from NS mergers within this sort of distance, and this rate is therefore more encouraging for possible positive, rather than purely null results.

The recently launched *GLAST*, NASA's Gamma-ray Large Area Space Telescope (now renamed *Fermi*), will be sensitive to much higher gamma-ray energies than *Swift*, and hence it should be more sensitive to the spectrally harder short GRBs. However, the all-sky GLAST Burst Monitor (GBM) will only be able to localise bursts to within a few degrees on the sky compared to *Swift*'s few arcsecond localisation capabilities. The Large Area Telescope (LAT) has arcminute localisation capability, but only for bursts within a much narrower field of view (~ 2 sr). It is to be hoped that significant synergy will exist between *Fermi* and *Swift*, and with luck, several bursts a year should be observable by both satellites. Thus we may hope that *Swift* may be able to search promptly for, and localise, X-ray afterglows from GBM/LAT detected bursts which may not have triggered the BAT, thus increasing the number of S-GRBs observed. In a complementary manner, LAT/GBM should be able to provide significantly enhanced spectral information for *Swift* detected bursts, which, coupled with (non-)detections of gravitational radiation should greatly increase our capabilities for distinguishing between extra-galactic SGR giant flares and binary NS merger events.

There may even be a chance that LOFAR (the LOw Frequency ARray) currently being deployed in Europe could detect the radio signals from an extragalactic SGR giant flare. Though recently descoped, the "minimum" LOFAR configuration of 36 base stations will have a sensitivity of 0.6 mJy in a one hour integration at 210 MHz (2 polarisations, 4 MHz bandwidth) (Jarvis M, private communication). The 2004 Giant Flare from SGR 1806-20 had an observed flux density of 152 mJy at 1.4 GHz ~ 7 days after outburst, with evidence for a spectrum consistent with a

[1] http://www.ligo.caltech.edu/

power law of $S_\nu \propto \nu^{-0.66}$ below 5 GHz, and an early decay rate $\propto t^{-1.6}$ (Gaensler et al. 2005). Though it is a bold extrapolation, if we assume this spectral model is valid down to 210 MHz, and the decay rate constant to (say) day 1, then the flare could have been as bright as ~ 10 Jy around outburst. Thus, assuming a distance of ~ 10 kpc to SGR 1806-20, then a flare such as this may possibly be detected by LOFAR out to $\sim 1-2$ Mpc, certainly encompassing M31. Longer integrations and larger bandwidths would push this detectability distance further, but the main uncertainty is the level of early radio emission from giant flares. In addition, bright flares such as the 2004 event are unfortunately rather rare, with our best fit LF models predicting an event rate of flares with peak luminosity $> 10^{47}$ erg s^{-1} to be $\sim 1 \times 10^{-4}$ yr^{-1} per SGR.

6.2 Long GRBs

In Chapter 4, correlation analysis of the BATSE long population as a whole with local galaxies showed results consistent with zero out as far as 155 Mpc, though the relatively large 1σ errors do admit the possibility of up to 10% exhibiting some correlation (the most probable rate being $\sim 4.5\%$, equivalent to around 75 bursts during BATSE's lifetime).

The three L-GRBs known to be local share similar properties of being spectrally soft, of low luminosity and with smooth single-peaked light curves. In addition, empirical relations of L-GRBs as a whole are consistent with these properties implying that low luminosity bursts are spectrally softer and less variable than high luminosity bursts. It is therefore plausible that subsets of the BATSE L-GRB population sharing these properties are likely to contain a greater proportion of potentially nearby bursts. We therefore extracted subsets of L-GRBs based on these properties and indeed found their correlation with local galaxies to increase. In particular, a combined subset of bursts common to our three selection criteria exhibited a correlated fraction of $28\% \pm 16\%$ within a sphere of 155 Mpc, equivalent to 50 ± 28 bursts in the nine years of BATSE operation (Figure 4.4). Though this result is statistically marginal, taken at face value it represents a local rate density of L-GRBs within 155 Mpc of 700 ± 360 Gpc^{-3}yr^{-1} (to BATSE detection limits, and assuming the BATSE sky exposure fraction to be of the order of 0.5). This rate density is in reasonable agreement with that found by other workers via complementary techniques (Soderberg et al. 2006b; Liang et al. 2007; Guetta & Della

Valle 2007).

It may be thought that the preponderance of low-luminosity bursts in the local Universe is nothing other than a selection effect - we can only observe these bursts within a nearby volume. Though this selection effect obviously exists and is present in the data, the lack of intermediate luminosity bursts detected at intermediate redshifts implies this is not the whole story. Previous studies of L-GRB luminosity functions have indeed shown that a single LF for L-GRBs cannot produce sufficient low and high luminosity bursts without significantly overproducing bursts of intermediate luminosity which we would expect to observe, but don't. The rate density predicted by our correlation analysis is consistent with the rate densities predicted assuming a separate low-luminosity population, and we consider our evidence therefore to support the two population case (see Figure 4.6).

Furthermore, though there are not two clearly separate (and known to exist) progenitor populations with well delineated intrinsic properties for L-GRBs, we can still perform luminosity function modelling as for the short bursts by assuming progenitor rates from observations of both the cosmological and known nearby bursts. Constraining these models via overall BATSE number counts and the correlation fractions for the low-luminosity, soft, single-peaked sub-sample of L-GRBs from Chapter 4, we found once again that a variety of single LF models tested could not reproduce the local distribution while remaining consistent with overall number counts. Dual LF models however, with plausible intrinsic rates for low and high luminosity bursts, were able to produce good fits to both. In addition, the wider redshift distribution of the burst population from dual LF models is realistic and matches well the *Swift* L-GRB redshift distribution below $z \sim 1.5$. Above this regime, the *Swift* observations contain a greater fraction of high redshift bursts than the models predict, though the models stay within the bounds of pre-*Swift* observations. When the LF models are constrained via the overall redshift distribution instead of the threshold-adjusted BATSE number counts, we find that dual LF models produce extremely good fits to the *Swift* distribution while still able to produce adequate numbers of local bursts, though the predicted overall number-count distribution is then significantly different to that of the BATSE sample.

With increased numbers of L-GRBs with redshift measurements in the future, we should be able to improve the resolution of the redshift bins in order to constrain the models with greater accuracy. Furthermore, improved modelling of burst spectral properties for input to the luminosity functions, along with detailed analysis of the *Swift* triggering history should allow use of all three constraints (local numbers,

overall redshift distribution, and number counts) to investigate the adequacy of the dual LF models. This may also shed light on whether the simple assumption of L-GRBs following the globally averaged star formation rate is justified, or whether account needs to be taken of a more complex relationship with SFR (including, for example metallicity dependencies).

What could produce two classes of L-GRB, different in terms of luminosity, spectra and variability? Clearly the two types of collapsar discussed in Chapter 1, section 1.2.3 may power bursts of intrinsically different duration: their luminosity properties are therefore also likely to be different. It is also possible that proto-magnetar driven L-GRBs (if they exist) would be likely to power lower luminosity, longer bursts, though their light curve properties may be at odds with the lack of variability expected from low luminosity events. One intriguing, though highly speculative possibility is the production of GRBs by quark (or strange) stars. First postulated in 1984 (Witten 1984), a quark star may form following a phase transition to stable quark matter in the high density and pressure environments of the centre of a neutron star. Conditions may be extreme enough to allow formation of a nugget of strange matter which rapidly grows to encompass the entire star, being an energetically favourable state. Unfortunately we have no evidence that these exotic objects exist. However, if they do exist, then they have been postulated as potential GRB progenitors (Paczyński & Haensel 2005). The important property which they have is that of effectively being a huge quark bag the surface of which is impenetrable to baryons, but allows photons, electrons, positrons, neutrinos and magnetic fields to cross freely. Thus this membrane provides a perfect way for separating the baryons from the huge reservoir of energy available internal to the quark star following its exothermic conversion. The energy is therefore available to drive the ultra-relativistic outflow necessary to form a GRB in a naturally baryon-free manner, which must then be collimated in a similar manner to collapsar and other models - presumably disks and magnetic fields play a strong role here again. The exciting possibility is this: the quark star scenario provides a natural way to drive ultra-relativistic outflows and may thus power the L-GRBs of high luminosity. Low luminosity, nearby GRBs may be caused by more spherical explosions in ordinary core collapse events, producing weak GRBs but potentially very bright supernovae such as in the case of GRB 980425 and SN 1998bw.

6.3 The Final Word

Having finished above on a highly speculative note, it is perhaps worth restating here the four main conclusions of this work:

- A nearby population of short duration GRBs exists, as demonstrated by the correlation of a fraction of BATSE S-GRBs with galaxy distributions on the sky within 155 Mpc.
- This nearby population can only be produced by a separate population of lower luminosity S-GRB progenitors, naturally explained as being giant flares from extragalactic SGRs. The remaining population of S-GRBs are consistent with being produced by binary neutron star mergers.
- A nearby population of under-luminous, spectrally soft, smoothly varying long duration GRBs also exists as shown by correlations on the sky with nearby galaxies.
- Invoking a separate population of low-luminosity L-GRBs, with intrinsic rates several 100 times greater than that of cosmological bursts, reproduces adequately this nearby population while closely matching the overall *Swift* redshift distribution.

References

Amati L., 2003, Chinese Journal of Astronomy and Astrophysics Supplement, 3, 455

Amati L., 2006a, ArXiv Astrophysics e-prints, astro.ph.11189

Amati L., 2006b, MNRAS, 372, 233

Amati L. et al., 2002, A&A, 390, 81

Amati L., Guidorzi C., Frontera F., Della Valle M., Finelli F., Landi R., Montanari E., 2008, ArXiv e-prints, 0805.0377

Ando S., 2004, Journal of Cosmology and Astro-Particle Physics, 6, 7

Avila-Reese V., Firmani C., Ghisellini G., Cabrera J. I., 2008, ArXiv e-prints, 0802.2578

Band D. L., 2006a, in Holt S. S., Gehrels N., Nousek J. A., eds, American Institute of Physics Conference Series Vol. 836, Gamma-Ray Bursts in the Swift Era. p. 704

Band D. L., 2006b, ApJ, 644, 378

Band D. L., Preece R. D., 2005, ApJ, 627, 319

Barbon R., Buondí V., Cappellaro E., Turatto M., 1999, A&AS, 139, 531

Barthelmy S. D. et al., 2008, GRB Coordinates Network, 8113

Belczynski K., Perna R., Bulik T., Kalogera V., Ivanova N., Lamb D. Q., 2006, ApJ, 648, 1110

Berger E., 2007, ApJ, 670, 1254

Berger E., 2008, ArXiv e-prints, 0805.0306

Berger E. et al., 2005, ApJ, 634, 501

Bibby J. L., Crowther P. A., Furness J. P., Clark J. S., 2008, MNRAS, 386, L23

Blandford R. D., Znajek R. L., 1977, MNRAS, 179, 433

Bloom J. S., Frail D. A., Kulkarni S. R., 2003, ApJ, 594, 674

Bloom J. S. et al., 1999, Nat, 401, 453

Bloom J. S., Kulkarni S. R., Harrison F., Prince T., Phinney E. S., Frail D. A., 1998, ApJ, 506, L105

Bornancini C. G., Martínez H. J., Lambas D. G., Le Floc'h E., Mirabel I. F., Minniti D., 2004, ApJ, 614, 84

Briggs M. S. et al., 1996, ApJ, 459, 40

Briggs M. S., Pendleton G. N., Kippen R. M., Brainerd J. J., Hurley K., Connaughton V., Meegan C. A., 1999, ApJS, 122, 503

Bucciantini N., Quataert E., Arons J., Metzger B. D., Thompson T. A., 2008, MNRAS, 383, L25

Burrows A., 1987, ApJ, 318, L57

Burrows A., Lattimer J. M., 1988, Phys. Rep., 163, 51

Burrows D. N. et al., 2008, ArXiv e-prints, 0803.1844

Butler N. R., Kocevski D., Bloom J. S., 2008, ArXiv e-prints, 0802.3396

Butler N. R., Kocevski D., Bloom J. S., Curtis J. L., 2007, ApJ, 671, 656

Castro-Tirado A. J., Gorosabel J., 1999, A&AS, 138, 449

Cavallo G., Rees M. J., 1978, MNRAS, 183, 359

Champion D. J., Lorimer D. R., McLaughlin M. A., Cordes J. M., Arzoumanian Z., Weisberg J. M., Taylor J. H., 2004, MNRAS, 350, L61

Chapman R., Tanvir N. R., Priddey R. S., Levan A. J., 2007, MNRAS, 382, L21

Cheng B., Epstein R. I., Guyer R. A., Young A. C., 1996, Nat, 382, 518

Christensen L., Hjorth J., Gorosabel J., 2004, A&A, 425, 913

Cline D. B., Czerny B., Matthey C., Janiuk A., Otwinowski S., 2005, ApJ, 633, L73

Cline D. B., Matthey C., Otwinowski S., 2000, in Kippen R. M., Mallozzi R. S., Fishman G. J., eds, American Institute of Physics Conference Series Vol. 526, Gamma-ray Bursts, 5th Huntsville Symposium. p. 97

Cline D. B., Matthey C., Otwinowski S., 2001, in Costa E., Frontera F., Hjorth J., eds, Gamma-ray Bursts in the Afterglow Era. p. 56

Cline D. B., Matthey C., Otwinowski S., 2003, Astroparticle Physics, 18, 531

Cobb B. E., Bailyn C. D., van Dokkum P. G., Buxton M. M., Bloom J. S., 2004, ApJ, 608, L93

Cobb B. E., Bailyn C. D., van Dokkum P. G., Natarajan P., 2006a, ApJ, 651, L85

Cobb B. E., Bailyn C. D., van Dokkum P. G., Natarajan P., 2006b, ApJ, 645, L113

Cohen E., Kolatt T., Piran T., 1994, ArXiv Astrophysics e-prints, astro-ph/9406012

Colgate S. A., 1968, Canadian Journal of Physics. Proceedings of the 10th International Conference on Cosmic Rays, Calgary, Alberto, June 19-30, 1967, Vol. 46., p.476, 46, 476

Costa E. et al., 1997, Nat, 387, 783

Coward D. M., 2005, MNRAS, 360, L77

Cusumano G., Barthelmy S., Gehrels N., Hunsberger S., Immler S., Marshall F., Palmer D., Sakamoto T., 2006, GRB Coordinates Network, 4775

Dai X. et al., 2007, ArXiv e-prints, 0712.2239

Dar A., 2005, GRB Circular Network, 2942

D'Avanzo P., Fiore F., Piranomonte S., Covino S., Tagliaferri G., Chincarini G., Stella L., 2007, GRB Coordinates Network, 7152

de Vaucouleurs G., de Vaucouleurs A., Corwin H. G., Buta R. J., Paturel G., Fouque P., 1991, Third Reference Catalogue of Bright Galaxies. Volume 1-3, XII, Springer-Verlag Berlin Heidelberg New York

Della Valle M. et al., 2006, Nat, 444, 1050

Diehl R. et al., 2006, Nat, 439, 45

Donaghy T. Q. et al., 2006, ArXiv Astrophysics e-prints, astro-ph/0605570

Drory N., Salvato M., Gabasch A., Bender R., Hopp U., Feulner G., Pannella M., 2005, ApJ, 619, L131

Duncan R. C., Thompson C., 1992, ApJ, 392, L9

Eichler D., 2002, MNRAS, 335, 883

Eichler D., Livio M., Piran T., Schramm D. N., 1989, Nat, 340, 126

Fan Y.-Z., Xu D., 2006, MNRAS, 372, L19

Fenimore E. E., Ramirez-Ruiz E., 2000, ArXiv Astrophysics e-prints astro-ph/0004176

Flowers E., Ruderman M. A., 1977, ApJ, 215, 302

Frail D. A. et al., 1997, ApJ, 483, L91

Frederiks D. D., Golenetskii S. V., Palshin V. D., Aptekar R. L., Ilyinskii V. N., Oleinik F. P., Mazets E. P., Cline T. L., 2007a, Astronomy Letters, 33, 1

Frederiks D. D., Palshin V. D., Aptekar R. L., Golenetskii S. V., Cline T. L., Mazets E. P., 2007b, Astronomy Letters, 33, 19

Friedman A. S., Bloom J. S., 2005a, Nuovo Cimento C Geophysics Space Physics C, 28, 669

Friedman A. S., Bloom J. S., 2005b, ApJ, 627, 1

Fruchter A. S. et al., 2006, Nat, 441, 463

Fruchter A. S. et al., 1999, ApJ, 519, L13

Fugazza D. et al., 2006, GRB Coordinates Network, 5271

Fynbo J. P. U. et al., 2006, Nat, 444, 1047

Gaensler B. M. et al., 2005, Nat, 434, 1104

Gal-Yam A. et al., 2006, Nat, 444, 1053

Galama T. J. et al., 1998, Nat, 395, 670

Gallego J., Zamorano J., Aragon-Salamanca A., Rego M., 1995, ApJ, 455, L1

Gehrels N. et al., 2006, Nat, 444, 1044

Ghirlanda G., Ghisellini G., 2007, ArXiv Astrophysics e-prints, astro-ph/0702004

Ghirlanda G., Ghisellini G., Lazzati D., 2004, ApJ, 616, 331

Ghirlanda G., Ghisellini G., Lazzati D., Firmani C., 2004, ApJ, 613, L13

Ghirlanda G., Ghisellini G., Nava L., Firmani C., 2005, in Bulik T., Rudak B., Madejski G., eds, American Institute of Physics Conference Series Vol. 801, Astrophysical Sources of High Energy Particles and Radiation. p. 123

Ghirlanda G., Magliocchetti M., Ghisellini G., Guzzo L., 2006, MNRAS, 368, L20

Ghisellini G., 2001, ArXiv Astrophysics e-prints astro-ph/0111584

Göğüş E., Woods P. M., Kouveliotou C., van Paradijs J., Briggs M. S., Duncan R. C., Thompson C., 2000, ApJ, 532, L121

Göğüş E., Woods P., Kouveliotou C., 2008, GRB Coordinates Network, 8118

Golenetskii S., et al., 2005, GRB Circular Network, 4197

Golenetskii S. V., Ilinskii V. N., Mazets E. P., 1984, Nat, 307, 41

Gorosabel J., Castro-Tirado A. J., 1997, ApJ, 483, L83

Gorosabel J., Castro-Tirado A. J., Brandt S., Lund N., 1998, A&A, 336, 57

Gorosabel J. et al., 2005, A&A, 437, 411

Gorosabel J., Lund N., Brandt S., Westergaard N. J., Castro Cerón J. M., 2004, A&A, 427, 87

Gotz D., Mereghetti S., Beck M., Borkowski J., Mowlavi N., 2003, GRB Coordinates Network, 2459

Graham J. F., Fruchter A. S., Levan A. J., Nysewander M., Tanvir N. R., Dahlen T., Bersier D., Pe'Er A., 2007, GRB Coordinates Network, 6836

Guetta D., Della Valle M., 2007, ApJ, 657, L73

Guetta D., Piran T., 2005, A&A, 435, 421

Guetta D., Piran T., 2006, A&A, 453, 823

Guetta D., Piran T., 2007, Journal of Cosmology and Astro-Particle Physics, 7, 3

Guetta D., Piran T., Waxman E., 2005, ApJ, 619, 412

Guidorzi C., Frontera F., Montanari E., Rossi F., Amati L., Gomboc A., Hurley K., Mundell C. G., 2005, MNRAS, 363, 315

Guidorzi C., Frontera F., Montanari E., Rossi F., Amati L., Gomboc A., Mundell C. G., 2006, MNRAS, 371, 843

Haislip J. B. et al., 2006, Nat, 440, 181

Hakkila J., Pendleton G. N., Meegan C. A., Briggs M. S., Kippen R. M., Preece R. D., 2003, in AIP Conf. Proc. 662: Gamma-Ray Burst and Afterglow Astronomy 2001: A Workshop Celebrating the First Year of the HETE Mission. p. 176

Heger A., Fryer C. L., Woosley S. E., Langer N., Hartmann D. H., 2003, ApJ, 591, 288

Hjorth J. et al., 2003, Nat, 423, 847

Hopman C., Guetta D., Waxman E., Portegies Zwart S., 2006, ApJ, 643, L91

Hurley K. et al., 2005, Nat, 434, 1098

Hurley K. et al., 1999a, Nat, 397, 41

Hurley K., Hartmann D. H., Kouveliotou C., Kippen R. M., Laros J., Cline T., Boer M., 1999b, ApJ, 515, 497

Jakobsson P., Fynbo J. P. U., 2007, ArXiv e-prints, 0704.1421

Jakobsson P. et al., 2006a, in Holt S. S., Gehrels N., Nousek J. A., eds, American Institute of Physics Conference Series Vol. 836, Gamma-Ray Bursts in the Swift Era. p. 552

Jakobsson P. et al., 2006b, A&A, 447, 897

Kalogera V., Belczynski K., Kim C., O'Shaughnessy R., Willems B., 2007, Phys. Rep., 442, 75

Kaneko Y. et al., 2007, ApJ, 654, 385

Karachentsev I. D., Karachentseva V. E., Huchtmeier W. K., Makarov D. I., 2004, AJ, 127, 2031

Kawai N. et al., 2006, Nat, 440, 184

King A. R., Pringle J. E., Wickramasinghe D. T., 2001, MNRAS, 320, L45

Kippen R. M. et al., 1998, ApJ, 506, L27

Klebesadel R. W., Strong I. B., Olson R. A., 1973, BAAS, 5, 322

Kobulnicky H. A., Kewley L. J., 2004, ApJ, 617, 240

Kolatt T., Piran T., 1996, ApJ, 467, L41

Kouveliotou C., 1999, Proceedings of the National Academy of Science, 96, 5351

Kouveliotou C. et al., 1998, Nat, 393, 235

Kouveliotou C., Meegan C. A., Fishman G. J., Bhat N. P., Briggs M. S., Koshut T. M., Paciesas W. S., Pendleton G. N., 1993, ApJ, 413, L101

Kulkarni S. R. et al., 1998a, Nat, 393, 35

Kulkarni S. R. et al., 1998b, Nat, 395, 663

Lamb D. Q., 1995, PASP, 107, 1152

Lamb D. Q., Donaghy T. Q., Graziani C., 2004, New Astronomy Review, 48, 459

Lamb D. Q., Graziani C., Smith I. A., 1993, ApJ, 413, L11

Lamb D. Q., Quashnock J. M., 1995, Astrophys. Space. Sci., 231, 19

Lazzati D. et al., 2001, A&A, 378, 996

Lazzati D., Ghirlanda G., Ghisellini G., 2005, MNRAS, 362, L8

Le Floc'h E. et al., 2003, A&A, 400, 499

Lee W. H., Ramirez-Ruiz E., 2006, ApJ, 641, 961

Levan A., Tanvir N., 2005, GRB Circular Network, 3927

Levan A. J. et al., 2006a, ApJ, 648, L9

Levan A. J. et al., 2008, MNRAS, 384, 541

Levan A. J., Wynn G. A., Chapman R., Davies M. B., King A. R., Priddey R. S., Tanvir N. R., 2006b, MNRAS, 368, L1

Li L.-X., Paczyński B., 2006, MNRAS, 366, 219

Liang E., Zhang B., 2006, ApJ, 638, L67

Liang E., Zhang B., Virgili F., Dai Z. G., 2007, ApJ, 662, 1111

Liang E.-W., Racusin J. L., Zhang B., Zhang B.-B., Burrows D. N., 2008a, ApJ, 675, 528

Liang N., Xiao W. K., Liu Y., Zhang S. N., 2008b, ArXiv e-prints, 0802.4262

LIGO Scientific Collaboration, Hurley K., 2007, ArXiv e-prints, 0711.1163

MacFadyen A. I., Woosley S. E., 1999, ApJ, 524, 262

Magliocchetti M., Ghirlanda G., Celotti A., 2003, MNRAS, 343, 255

Manchester R. N., Taylor J. H., 1977, Pulsars / Richard N. Manchester, Joseph H. Taylor. W. H. Freeman, San Francisco :

Marani G. F., Nemiroff R. J., Norris J. P., Bonnell J. T., 1997, ApJ, 474, 576

Mazets E. P. et al., 2008, ApJ, 680, 545

Mazets E. P., Golenetskii S. V., 1981, Astrophys. Space. Sci., 75, 47

Mazets E. P., Golentskii S. V., Ilinskii V. N., Aptekar R. L., Guryan I. A., 1979, Nat, 282, 587

Meegan C. A. et al., 1996, ApJS, 106, 65

Mészáros P., 2002, ARA&A, 40, 137

Metzger B. D., Quataert E., Thompson T. A., 2008, MNRAS, 385, 1455

Metzger M. R., Djorgovski S. G., Kulkarni S. R., Steidel C. C., Adelberger K. L., Frail D. A., Costa E., Frontera F., 1997, Nat, 387, 878

Mirabal N., Halpern J. P., 2006, GRB Coordinates Network, 4792

Modjaz M. et al., 2008, AJ, 135, 1136

Nakar E., 2007, Phys. Rep., 442, 166

Nakar E., Gal-Yam A., Fox D. B., 2006, ApJ, 650, 281

Nakar E., Gal-Yam A., Piran T., Fox D. B., 2006, ApJ, 640, 849

Nakar E., Piran T., 2005, MNRAS, 360, L73

Narayan R., Paczynski B., Piran T., 1992, ApJ, 395, L83

Narayan R., Piran T., Kumar P., 2001, ApJ, 557, 949

Natarajan P., Albanna B., Hjorth J., Ramirez-Ruiz E., Tanvir N., Wijers R., 2005, MNRAS, 364, L8

Nelemans G., Yungelson L. R., Portegies Zwart S. F., Verbunt F., 2001, A&A, 365, 491

Nomoto K., Kondo Y., 1991, ApJ, 367, L19

Norris J. P., 2002, ApJ, 579, 386

Norris J. P., Bonnell J. T., Watanabe K., 1999, ApJ, 518, 901

Norris J. P., Cline T. L., Desai U. D., Teegarden B. J., 1984, Nat, 308, 434

Norris J. P., Marani G. F., Bonnell J. T., 2000, ApJ, 534, 248

Norris J. P., Scargle J. D., Bonnell J. T., 2001, in Ritz S., Gehrels N., Shrader C. R., eds, AIP Conf. Proc. 587: Gamma 2001: Gamma-Ray Astrophysics. p. 176

Norton A. J., Wynn G. A., Somerscales R. V., 2004, ApJ, 614, 349

Ofek E. O., 2007, ApJ, 659, 339

Ofek E. O. et al., 2007, ApJ, 662, 1129

Ofek E. O. et al., 2006, ApJ, 652, 507

Ofek E. O. et al., 2008, ApJ, 681, 1464

O'Shaughnessy R., Belczynski K., Kalogera V., 2008, ApJ, 675, 566

Paciesas W. S. et al., 1999, ApJS, 122, 465

Paczynski B., 1986, ApJ, 308, L43

Paczynski B., 1992, Acta Astronomica, 42, 145

Paczynski B., 1995, PASP, 107, 1167

Paczynski B., 1998, in American Institute of Physics Conference Series. p. 783

Paczyński B., Haensel P., 2005, MNRAS, 362, L4

Palmer D. M. et al., 2005, Nat, 434, 1107

Pal'Shin V., 2007, GRB Coordinates Network, 6098

Panaitescu A., Kumar P., 2001, ApJ, 560, L49

Panaitescu A., Mészáros P., Burrows D., Nousek J., Gehrels N., O'Brien P., Willingale R., 2006, MNRAS, 369, 2059

Perley D. A., Bloom J. S., 2007, GRB Coordinates Network, 6091

Pian E. et al., 2006, Nat, 442, 1011

Piran T., 1999a, Bulletin of the American Astronomical Society, 31, 695

Piran T., 1999b, Phys. Rep., 314, 575

Piran T., 2005, Reviews of Modern Physics, 76, 1143

Podsiadlowski P., Pfahl E., Rappaport S., 2005, in Rasio F. A., Stairs I. H., eds, Astronomical Society of the Pacific Conference Series Vol. 328, Binary Radio Pulsars. p. 327

Popov S. B., Stern B. E., 2006, MNRAS, 365, 885

Porciani C., Madau P., 2001, ApJ, 548, 522

Prochaska J. X. et al., 2006, ApJ, 642, 989

Prochaska J. X. et al., 2004, ApJ, 611, 200

Quashnock J. M., Lamb D. Q., 1993a, MNRAS, 265, L45

Quashnock J. M., Lamb D. Q., 1993b, MNRAS, 265, L59

Racusin J. L., Liang E. ., Burrows D. N., Morris D. C., Zhang B. B., Zhang B., 2008, ArXiv e-prints, 0801.4749

Ramirez-Ruiz E., 2004, MNRAS, 349, L38

Rees M. J., 1998, in Olinto A. V., Frieman J. A., Schramm D. N., eds, Eighteenth Texas Symposium on Relativistic Astrophysics. p. 34

Rees M. J., Meszaros P., 1992, MNRAS, 258, 41P

Rees M. J., Meszaros P., 1994, ApJ, 430, L93

Reichart D. E., Lamb D. Q., Fenimore E. E., Ramirez-Ruiz E., Cline T. L., Hurley K., 2001, ApJ, 552, 57

Reichart D. E., Nysewander M. C., 2005, ArXiv Astrophysics e-prints astro-ph/0508111

Rhoads J. E., 1997, ApJ, 487, L1

Rhoads J. E., 1999, ApJ, 525, 737

Rosswog S., 2005, Nuovo Cimento C Geophysics Space Physics C, 28, 607

Rosswog S., Ramirez-Ruiz E., 2003, MNRAS, 343, L36

Ruderman M., 1975, New York Academy Sciences Annals, 262, 164

Rutledge R. E., Lewin W. H. G., 1993, MNRAS, 265, L51

Sakamoto T. et al., 2008, ApJS, 175, 179

Sakamoto T. et al., 2005, ApJ, 629, 311

Salmonson J. D., Galama T. J., 2002, ApJ, 569, 682

Salvaterra R., Cerutti A., Chincarini G., Colpi M., Guidorzi C., Romano P., 2007, ArXiv e-prints, 0710.3099

Sari R., Piran T., Halpern J. P., 1999, ApJ, 519, L17

Sari R., Piran T., Narayan R., 1998, ApJ, 497, L17

Saunders W. et al., 2000, MNRAS, 317, 55

Schaefer B. E., Xiao L., 2006, ArXiv Astrophysics e-prints, astro-ph/0608441

Schartel N., Andernach H., Greiner J., 1997, A&A, 323, 659

Schechter P., 1976, ApJ, 203, 297

Schmidt G. D. et al., 2003, ApJ, 595, 1101

Schmidt M., 2001a, ApJ, 559, L79

Schmidt M., 2001b, ApJ, 552, 36

Smartt S. J., Vreeswijk P. M., Ramirez-Ruiz E., Gilmore G. F., Meikle W. P. S., Ferguson A. M. N., Knapen J. H., 2002, ApJ, 572, L147

Soderberg A. M. et al., 2006a, ApJ, 650, 261

Soderberg A. M. et al., 2004, Nat, 430, 648

Soderberg A. M. et al., 2006b, Nat, 442, 1014

Sokolov V. V. et al., 2001, A&A, 372, 438

Stairs I. H., 2008, in American Institute of Physics Conference Series Vol. 983, 40 Years of Pulsars: Millisecond Pulsars, Magnetars and More. p. 424

Stanek K. Z. et al., 2003, ApJ, 591, L17

Struble M. F., Rood H. J., 1997, ApJ, 490, 109

Tanaka Y. T., Terasawa T., Kawai N., Yoshida A., Yoshikawa I., Saito Y., Takashima T., Mukai T., 2007, ApJ, 665, L55

Tanvir N. R., Chapman R., Levan A. J., Priddey R. S., 2005, Nat, 438, 991

Tanvir N. R., Varricatt W., 2008, GRB Coordinates Network, 8126

Taylor G. B., Granot J., 2006, Modern Physics Letters A, 21, 2171

Taylor J. H., Weisberg J. M., 1982, ApJ, 253, 908

Tegmark M., Hartmann D. H., Briggs M. S., Hakkila J., Meegan C. A., 1996, ApJ, 466, 757

Thompson C., Duncan R. C., 1993, ApJ, 408, 194

Thompson C., Duncan R. C., 1995, MNRAS, 275, 255

Thompson C., Duncan R. C., 1996, ApJ, 473, 322

Thompson C., Duncan R. C., 2001, ApJ, 561, 980

Thomsen B. et al., 2004, A&A, 419, L21

Troja E. et al., 2007, ApJ, 665, 599

Troja E., King A. R., O'Brien P. T., Lyons N., Cusumano G., 2008, MNRAS, 385, L10

Usov V. V., 1992, Nat, 357, 472

van Paradijs J. et al., 1997, Nat, 386, 686

Vanlandingham K. M. et al., 2005, AJ, 130, 734

Wang C., Lai D., Han J. L., 2006, ApJ, 639, 1007

Wang L., Wheeler J. C., 1998, ApJ, 504, L87

Wang V. C., Lingenfelter R. E., 1995, ApJ, 441, 747

Watson D. et al., 2004, ApJ, 605, L101

Wickramasinghe D. T., Ferrario L., 2000, PASP, 112, 873

Witten E., 1984, Phys. Rev. D, 30, 272

Woods P. M., Göğüş E., Kouveliotou C., 2008, GRB Coordinates Network, 8166

Woods P. M., Thompson C., 2004, ArXiv Astrophysics e-prints astro-ph/0406133

Woosley S. E., 1993, ApJ, 405, 273

Woosley S. E., Bloom J. S., 2006, ARA&A, 44, 507

Zhang B., Mészáros P., 2004, International Journal of Modern Physics A, 19, 2385

Zhang B., Zhang B.-B., Liang E.-W., Gehrels N., Burrows D. N., Mészáros P., 2007, ApJ, 655, L25

Appendix A: Publication List

Chapman R., Levan A. J., Priddey R. S., Tanvir N. R., Wynn G. A., King A. R., Davies M. B., 2007a, in Napiwotzki R., Burleigh M. R., eds, Astronomical Society of the Pacific Conference Series Vol. 372, 15th European Workshop on White Dwarfs. p. 415

Chapman R., Levan A. J., Wynn G. A., Davies M. B., King A. R., Priddey R. S., Tanvir N. R., 2008, in Bassa C., Wang Z., Cumming A., Kaspi V. M., eds, American Institute of Physics Conference Series Vol. 983, 40 Years of Pulsars: Millisecond Pulsars, Magnetars and More. p. 301

Chapman R., Priddey R. S., Tanvir N. R., 2008, in Bassa C., Wang Z., Cumming A., Kaspi V. M., eds, American Institute of Physics Conference Series Vol. 983, 40 Years of Pulsars: Millisecond Pulsars, Magnetars and More. p. 304

Chapman R. et al., 2005, GRB Coordinates Network, 3375, 1

Chapman R., Tanvir N. R., Priddey R. S., Levan A. J., 2007b, MNRAS, 382, L21

Haislip J. B. et al., 2006, Nat, 440, 181

Hurkett C. P. et al., 2006, MNRAS, 368, 1101

Jakobsson P. et al., 2006a, A&A, 460, L13

Jakobsson P., Levan A., Chapman R., Rol E., Tanvir N., Vreeswijk P., Watson D., 2006b, GRB Coordinates Network, 5617, 1

Levan A. J., Jakobsson P., Chapman R., Tanvir N., Rol E., 2006a, GRB Coordinates Network, 5573, 1

Levan A. J. et al., 2007, MNRAS, 378, 1439

Levan A. J. et al., 2006b, ApJ, 648, 1132

Levan A. J. et al., 2008, MNRAS, 384, 541

Levan A. J., Wynn G. A., Chapman R., Davies M. B., King A. R., Priddey R. S., Tanvir N. R., 2006c, MNRAS, 368, L1

Rol E., Tanvir N., Levan A., Adamson A., Fuhrman L., Priddey R., Chapman R., 2005, GRB Coordinates Network, 3372, 1

Rol E. et al., 2007, GRB Coordinates Network, 6221, 1

Tanvir N. et al., 2005a, GRB Coordinates Network, 3028, 1

Tanvir N. R., Chapman R., Levan A. J., Priddey R. S., 2005b, Nat, 438, 991

Appendix B: Publications arising directly from this work

The publications reproduced in the following pages are those arising directly from this work and published in refereed journals (two accepted and one submitted).

Vol 438|15 December 2005|doi:10.1038/nature04310

LETTERS

An origin in the local Universe for some short γ-ray bursts

N. R. Tanvir[1], R. Chapman[1], A. J. Levan[1] & R. S. Priddey[1]

Gamma-ray bursts (GRBs) divide into two classes[1]: 'long', which typically have initial durations of $T_{90} > 2$ s, and 'short', with durations of $T_{90} < 2$ s (where T_{90} is the time to detect 90% of the observed fluence). Long bursts, which on average have softer γ-ray spectra[2], are known to be associated with stellar core-collapse events—in some cases simultaneously producing powerful type Ic supernovae[3–5]. In contrast, the origin of short bursts has remained mysterious until recently. A subsecond intense 'spike' of γ-rays during a giant flare from the Galactic soft γ-ray repeater, SGR 1806–20, reopened an old debate over whether some short GRBs could be similar events seen in galaxies out to ~70 Mpc (refs 6–10; redshift $z \approx 0.016$). Shortly after that, localizations of a few short GRBs (with optical afterglows detected in two cases[11,12]) have shown an apparent association with a variety of host galaxies at moderate redshifts[11–14]. Here we report a correlation between the locations of previously observed short bursts and the positions of galaxies in the local Universe, indicating that between 10 and 25 per cent of short GRBs originate at low redshifts ($z < 0.025$).

The satellite-based γ-ray detector CGRO/BATSE triggered on roughly 500 short-duration bursts during its nine-year lifetime. Unfortunately, the (1σ) positional uncertainties for these bursts were typically many degrees, giving limited information to help identify even their host galaxies, let alone their progenitors. A handful of short GRBs were localized to smaller error boxes by the Interplanetary Network and the Beppo-SAX and HETE-II satellites, but these only showed an absence of bright candidate host galaxies or afterglows[15,16]. Recently, however, afterglow detections for three short GRBs have associated them with galaxies at redshifts $z \approx 0.2$: the X-ray afterglow of GRB 050509B was close to a bright elliptical galaxy at $z = 0.225$, suggesting physical association[13,14]; GRB 050709 produced an optical afterglow locating it to a late-type galaxy at $z = 0.16$ (ref. 11); and GRB 050724 exhibited an afterglow located in another elliptical galaxy at $z = 0.257$ (ref. 12). The energetics of these bursts, and their association with a variety of host galaxies (including those with only old stellar populations) provide support for the view that some fraction of short GRBs arise from the coalescence of neutron-star/neutron-star (NS–NS) binaries[17–19].

On the other hand, the recent observation of the 'hypergiant' flare from SGR 1806–20 (refs 6, 7) re-ignited interest in the idea that some short bursts could be distant SGR flares. Although previous giant flares were bright enough to have been seen by BATSE perhaps as far as the Virgo cluster, the SGR 1806–20 event would have been detectable out to several tens of megaparsecs, appearing very much like a short-hard GRB.

If even a proportion of short bursts originate in nearby galaxies, then despite poor localizations they may show a measurable spatial correlation with the positions of low-redshift galaxies. The PSCz galaxy redshift survey[20] makes an appropriate comparison data set for the all-sky BATSE data because, being IRAS-selected, it suffers less from incompleteness at low Galactic latitudes than other nearby redshift surveys (although other catalogues show similar results, as described in Supplementary Information).

We considered all 400 $T_{90} < 2$ s bursts with localizations better than 10 degrees from the BATSE catalogue (4B(R); ref. 21 together with web supplement cited therein). A cross-correlation plot between these GRBs and the (1,070) PSCz galaxies with heliocentric recession velocity, v, $\leq 2{,}000\ \mathrm{km\ s^{-1}}$ is shown in Fig. 1. This sample includes most galaxies within about 25 Mpc, encompassing the local supercluster, and specifically the Virgo, Fornax and Ursa Major clusters. A clear positive correlation is revealed, which is even stronger when the galaxies are restricted to earlier morphological types (specifically Sbc and earlier; that is, T-type ≤ 4). The figure also shows, as expected, that the long-duration bursts are uncorrelated with these galaxies.

However, the cross-correlation function is not ideal for this

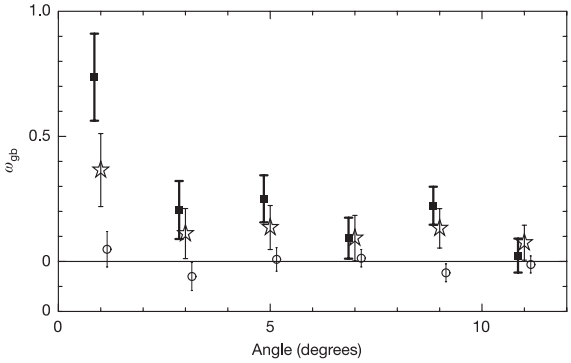

Figure 1 | Angular cross-correlation functions for BATSE short bursts with nearby galaxies from the PSCz catalogue. Two-point angular correlation functions, ω_{gb} (in two-degree bins), are shown for 400 BATSE short bursts ($T_{90} < 2$ s and statistical position uncertainty ≤ 10 degrees) with nearby galaxies from the PSCz catalogue (recession velocities $v \leq 2{,}000\ \mathrm{km\ s^{-1}} \approx 28$ Mpc distant). Filled circles show the correlation with all galaxy types (1,072 galaxies), and bold square symbols represent the same function but with galaxies restricted to earlier morphological types (T-type ≤ 4, Sbc and earlier, 709 galaxies). Open circles show the same function for long-duration bursts compared with all galaxy types. Points from the different functions have been offset slightly in angle for clarity. The short bursts exhibit clear ($>3\sigma$) correlation at low angles with the earlier-type galaxies, and a $>2\sigma$ correlation with all galaxy types. In contrast, as would be expected, the long bursts (1,481 events) show no measurable correlation with local galaxies. The highly anisotropic distribution on the sky of galaxies within this region makes it possible to detect this correlation signal. Uncertainties (error bars represent 1σ) in each bin were determined from Monte Carlo simulations, but true errors are not independent from bin to bin.

[1]Centre for Astrophysics Research, University of Hertfordshire, College Lane, Hatfield AL10 9AB, UK.

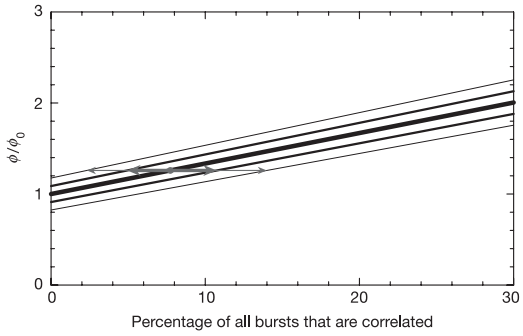

Figure 2 | Proportion of short bursts correlated with galaxies within $v \leq 2{,}000\,\mathrm{km\,s^{-1}}$. This figure summarizes an analysis of many simulated BATSE short-burst samples in which a proportion of bursts are laid down correlated with the PSCz galaxy positions and the remainder are placed at random. In this case, the galaxy sample is restricted to morphological T-type ≤ 4 and within recession velocity $v = 2{,}000\,\mathrm{km\,s^{-1}}$. The bold diagonal line represents the value of Φ/Φ_0 (see main text) as a function of the proportion of bursts in the simulated sample whose positions were seeded by the galaxy positions (random errors based on those in the BATSE catalogue were used to find offsets from these seed positions). The thinner lines show the 1σ and 2σ deviations around this line according to the simulations. The level of Φ/Φ_0 for the real data is illustrated by the horizontal arrow, which spans the 2σ (small arrow) and 1σ (large arrow) ranges. Thus the possibility of no correlation is rejected at more than the 3σ level, and a correlated fraction around ~8% is indicated (95% confidence limits ~2% to ~14%). As discussed in the text, there are reasons for expecting this to be an underestimate. Note that using all T-types produces a consistent, but less well constrained result.

purpose as errors in different bins are not independent, and it makes no direct use of known BATSE instrumental characteristics. In order to optimize the search for a correlation signal, we compute Φ, the sum of all burst-galaxy pairs weighted by the probability that they could be seen at the observed separation (or greater) if they were truly associated, and further weighted inversely by the burst error-circle size:

$$\Phi = \sum_{i}^{\text{All bursts}} \sum_{j}^{\text{All galaxies}} \frac{1}{\varepsilon_i} \int_{\theta_{ij}}^{\infty} \frac{1}{\sqrt{2\pi}\varepsilon_i} \exp\left(\frac{-\theta^2}{2\varepsilon_i^2}\right) \mathrm{d}\theta$$

where θ_{ij} is the separation between the ith burst and the jth galaxy, and ε_i is the error circle (statistical and systematic[22]) of the ith burst position. Further discussion of the BATSE instrumental characteristics[23] is provided in Supplementary Information.

To quantify the significance of the observed value of Φ, we also compute Φ_0, which is the mean of a large number of simulated random burst distributions (each with the same number of positions as the number of bursts under consideration, the same positional errors, and distributed on the sky according to the known BATSE sky exposure map[24]) correlated against the same set of (T-type ≤ 4) PSCz galaxy positions. The spread of simulated results around Φ_0 allows us to test the null hypothesis that there is no correlation between the positions of bursts and galaxies. This null hypothesis is rejected at the 99.9% level, confirming the indications of the cross-correlation function.

Next we attempt to estimate the proportion of bursts that are associated with nearby galaxies. To do this, we constructed many more artificial short-burst data sets, this time with both a random component and a component correlated with the galaxies from the PSCz galaxy catalogue with $v \leq 2{,}000\,\mathrm{km\,s^{-1}}$ and T-type ≤ 4 (that is, with a 'host' selected at random from the catalogue and with positions smeared according to the real error circles from BATSE). Figure 2 shows that the observed signal could be explained by a correlated component representing between 6% and 12% of BATSE bursts (1σ range). In fact, this is likely to be an underestimate, as our catalogue certainly does not contain all the galaxies in this volume, just the infrared-bright ones, and there remains a thin zone of avoidance around the Galactic plane, and a region unsurveyed by IRAS that the PSCz survey does not cover (amounting to about 16% of the sky).

Repeating this procedure in bins of recession velocity $v = 2{,}000$–$5{,}000\,\mathrm{km\,s^{-1}}$ and $v = 5{,}000$–$8{,}000\,\mathrm{km\,s^{-1}}$, we continue to find significant correlations (at nearly the 2σ level in each bin). This provides strong confirmation that the correlation seen in the low-redshift bin was not simply a chance coincidence. The cumulative proportion of correlated bursts as a function of limiting cut-off velocity is shown in Fig. 3. Inevitably it becomes harder to detect correlations as the galaxy (and presumably detected burst) volume density decreases with increasing distance, and the angular size of large-scale structure projected on the sky also reduces. The range of percentage correlated bursts conservatively suggests that a total proportion of between 10% and 25% of BATSE bursts originate within ~100 Mpc.

Our results are broadly consistent (discussed further in Supplementary Information) with previously reported upper limits for the proportion of BATSE short bursts originating at low redshifts[6–10]. They also explain the intriguing finding that short-burst positions on the sky show evidence for a weak auto-correlation signal[25,26].

At first sight, the most likely explanation of our result is that we are detecting a low-redshift population of short bursts associated with SGRs. However, SGRs being the remnants of short-lived massive stars, it is then rather surprising that a stronger correlation is seen with earlier-type galaxies, which include some galaxies with little recent star formation. Furthermore, although a positive correlation signal is seen when restricting the burst sample to only those with $T_{90} < 0.5$ s, a somewhat stronger signal is seen with the $T_{90} > 0.5$ s short bursts, which is again surprising given that the spike from SGR1806–20 had a duration[6] of around 0.2 s.

An alternative possibility is that some or all of the low-redshift short bursts have the same progenitors as the recently discovered short-burst population at redshifts $z > 0.1$. This would have the merit of simplicity, but as we show in Fig. 4, the higher-redshift bursts so far detected would have been rather brighter than any detected by BATSE if they had occurred at $z < 0.02$. Thus a rather broad intrinsic luminosity function, perhaps comparable to that of

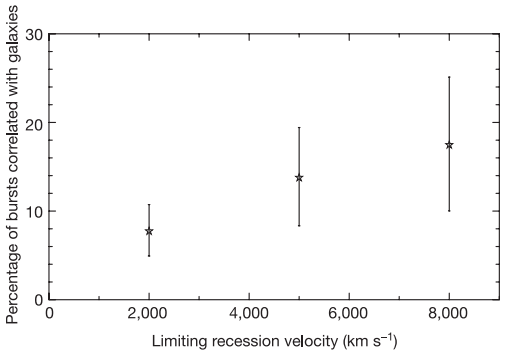

Figure 3 | The percentage of correlated bursts with increasing redshift. This figure shows the results of repeating the analysis of Fig. 2 for two further velocity-limited samples. Both the expected number of correlated bursts and 1σ ranges are shown. We emphasize that these figures are arrived at by comparing the relative values of Φ/Φ_0 for many simulated burst data sets with the real galaxy data set in each case. At higher redshifts the implied proportion of correlated bursts increases, as we would expect, but the statistical constraints also become weaker.

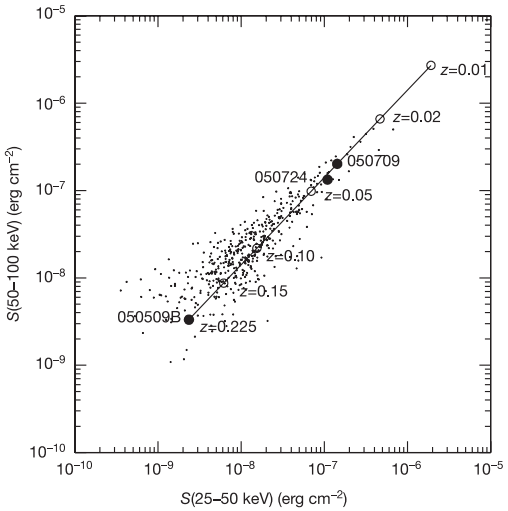

Figure 4 | The positions of GRB 050509B, GRB050709 and GRB050724 (bold points) in the BATSE fluence distribution. The measured γ-ray fluence (S) of GRB 050509b (ref. 14) was very low (9.5×10^{-9} erg cm^{-2} in the 15–150 keV band) and, when converted into the full BATSE passband (25–300 keV), is essentially the faintest burst within this catalogue. As illustrated by the open points, if this burst had occurred within 100 Mpc it would lie in the brightest 1% of bursts, although it would be brighter than any BATSE bursts were it closer than 30 Mpc—the volume in which we measure our most significant correlation. The other two recently claimed short-burst identifications are brighter[29,30], and therefore if they had occurred at lower redshift would certainly have been the brightest in the BATSE sample. This implies that the bursts responsible for the correlation we measure are most probably intrinsically much less luminous than these three, although, as discussed in the text, a broad luminosity function might accommodate both with the same class of progenitor.

the long-duration bursts, is required to accommodate reasonable numbers of both local and cosmological examples within the BATSE sample. A combination of differing progenitor masses and beaming could plausibly give rise to such a broad luminosity function for NS–NS binary mergers[27].

If both cosmological and local short-GRBs arise from NS–NS coalescence, then their association with at least intermediate-age and possibly old stellar populations is to be expected (owing to the inspiral lifetime of such binaries). Furthermore, the rate implied by our work of several bursts per year within 100 Mpc is in good agreement with recent calculations of the rate density of such events, based on the observed double neutron star population in the Milky Way[28]. The presence of such a large local population of NS–NS merger events would be encouraging for their detection prospects with upcoming gravity wave detectors.

Received 15 June; accepted 6 October 2005.

1. Norris, J. P., Cline, T. L., Desai, U. D. & Teegarden, B. J. Frequency of fast narrow gamma-ray bursts. *Nature* **308,** 434–435 (1984).
2. Kouveliotou, C. *et al.* Identification of two classes of gamma-ray bursts. *Astrophys. J.* **413,** L101–L104 (1993).
3. Woosley, S. E. Gamma-ray bursts from stellar mass accretion disks around black holes. *Astrophys. J.* **405,** 273–277 (1993).
4. Hjorth, J. *et al.* A very energetic supernova associated with the gamma-ray burst of 29 March 2003. *Nature* **423,** 847–850 (2003).
5. Stanek, K. *et al.* Spectroscopic discovery of the supernova 2003dh associated with GRB 030329. *Astrophys. J.* **591,** L17–L20 (2003).
6. Hurley, K. *et al.* An exceptionally bright flare from SGR 1806–20 and the origins of short duration γ-ray bursts. *Nature* **434,** 1098–1103 (2005).
7. Palmer, D. *et al.* A giant γ-ray flare from the magnetar SGR 1806–20. *Nature* **434,** 1107–1109 (2005).
8. Nakar, E., Gal-Yam, A., Piran, T. & Fox, D. B. The distances to short-hard GRBs and the SGR connection. *Astrophys. J.* (2005)(in the press); preprint at ⟨http://arxiv.org/astro-ph/0502148⟩.
9. Popov, S. B. & Stern, B. E. Soft gamma repeaters outside the Local group. *Mon. Not. R. Astron. Soc.* (submitted); preprint at ⟨http://arxiv.org/astro-ph/0503532⟩ (2005).
10. Lazzati, D. A certain flare. *Nature* **434,** 1075–1076 (2005).
11. Hjorth, J. *et al.* The optical afterglow of the short γ-ray burst GRB 050709. *Nature* **437,** 859–861 (2005).
12. Berger, E. *et al.* The afterglow and elliptical host galaxy of the short γ-ray burst GRB 050724. *Nature* doi:10.1038/nature04238 (in the press); preprint at ⟨http://arxiv.org/astro-ph/0508115⟩ (2005).
13. Bloom, J. *et al.* Closing in on a short-hard burst progenitor: constraints from early-time optical imaging and spectroscopy of a possible host galaxy of GRB 050509b. *Astrophys. J.* (in the press); preprint at ⟨http://arxiv.org/astro-ph/0505480⟩.
14. Gehrels, N. *et al.* A short γ-ray burst apparently associated with an elliptical galaxy at redshift $z = 0.225$. *Nature* **437,** 851–854 (2005).
15. Klotz, A., Boer, M. & Atteia, J.-L. Observational constraints on the afterglow of GRB 020531. *Astron. Astrophys.* **404,** 815–818 (2003).
16. Gorosabel, J. *et al.* Constraints on the afterglow of the short/hard burst GRB 010119. *Astron. Astrophys.* **383,** 112–117 (2002).
17. Eichler, D., Livio, M., Piran, T. & Schramm, D. N. Nucleosynthesis, neutrinos and gamma-rays from coalescing neutron stars. *Nature* **340,** 126–128 (1989).
18. Mochkovitch, R., Hernanz, M., Isern, J. & Martin, X. Gamma-ray bursts as collimated jets from neutron star/black hole mergers. *Nature* **361,** 236–238 (1993).
19. Rosswog, S., Ramirez-Ruiz, E. & Davies, M. B. High resolution calculations of merging neutron stars III: Gamma-ray bursts. *Mon. Not. R. Astron. Soc.* **345,** 1077–1090 (2003).
20. Saunders, W. *et al.* The PSCz catalogue. *Mon. Not. R. Astron. Soc.* **317,** 55–63 (2000).
21. Paciesas, W. *et al.* The Fourth BATSE Gamma-Ray Burst Catalog (revised). *Astrophys. J. Suppl.* **122,** 465–495 (1999).
22. Briggs, M. S. *et al.* The error distribution of BATSE gamma-ray burst locations. *Astrophys. J.* **122,** 503–518 (1999).
23. Pendleton, G. N. *et al.* The structure and evolution of LOCBURST: The BATSE burst location algorithm. *Astrophys. J.* **512,** 362–376 (1999).
24. Hakkila, J. *et al.* in *Gamma Ray Burst and Afterglow Astronomy 2001* (eds Ricker, G. R. & Vanderspek, R. K.) 176–178 (AIP Astronomy and Astrophysics Vol. 662, Woods Hole, Massachusetts, 2003).
25. Balazs, L. G., Meszaros, A. & Horvath, I. Anisotropy of the sky distribution of gamma-ray bursts. *Astron. Astrophys.* **339,** 1–6 (1998).
26. Magliocchetti, M., Ghirlanda, G. & Celotti, A. Evidence for anisotropy in the distribution of short-lived gamma-ray bursts. *Mon. Not. R. Astron. Soc.* **343,** 255–258 (2003).
27. Rosswog, S. & Ramirez-Ruiz, E. On the diversity of short gamma-ray bursts. *Mon. Not. R. Astron. Soc.* **343,** L36–L40 (2003).
28. Kalogera, V. *et al.* The cosmic coalescence rates of neutron star binaries. *Astrophys. J.* **601,** L179–L182 (2004).
29. Butler, N. *et al.* GRB050709: A possible short-hard GRB localized by HETE. *GRB Circ. Netw.* **3570** (2005).
30. Krimm, H. *et al.* GRB050724: Refined analysis of the Swift-BAT possible short burst. *GRB Circ. Netw.* **3667** (2005).

Supplementary Information is linked to the online version of the paper at www.nature.com/nature.

Acknowledgements We acknowledge the use of the publicly available BATSE Current Burst database. We thank M. Briggs for advice on BATSE instrumental characteristics. N.R.T., A.J.L. and R.S.P. acknowledge support from UK PPARC, and R.C. acknowledges the support of a University of Hertfordshire studentship.

Author Information Reprints and permissions information is available at npg.nature.com/reprintsandpermissions. The authors declare no competing financial interests. Correspondence and requests for materials should be addressed to N.R.T. (nrt@star.herts.ac.uk).

Mon. Not. R. Astron. Soc. **382,** L21–L25 (2007) doi:10.1111/j.1745-3933.2007.00381.x

How common are long gamma-ray bursts in the local Universe?

Robert Chapman,[1]★ Nial R. Tanvir,[2] Robert S. Priddey[1] and Andrew J. Levan[3]

[1]*Centre for Astrophysics Research, University of Hertfordshire, College Lane, Hatfield AL10 9AB*
[2]*Department of Physics and Astronomy, University of Leicester, Leicester, LE1 7RH*
[3]*Department of Physics, University of Warwick, Coventry, CV4 7AL*

Accepted 2007 August 14. Received 2007 June 29; in original form 2007 April 27

ABSTRACT

The two closest gamma-ray bursts so far detected (GRBs 980425 and 060218) were both under-luminous, spectrally soft, long-duration bursts with smooth, single-peaked light curves. Only of the order of 100 GRBs have measured redshifts, and there are, for example, 2704 GRBs in the BATSE (Burst and Transient Source Experiment) catalogue alone. It is therefore plausible that other nearby GRBs have been observed but not identified as being relatively nearby. Here we search for statistical correlations between BATSE long-duration GRBs and galaxy samples with recession velocities $v \leqslant 11\,000\,\mathrm{km\,s^{-1}}$ ($z = 0.0367, \approx$155 Mpc) selected from two catalogues of nearby galaxies. We also examine the correlations using burst subsamples restricted to those with properties similar to the two known nearby bursts. Our results show correlation of the entire long-GRB sample to remain consistent with zero out to the highest radii considered whereas a subsample selected to be low fluence, spectrally soft, with smooth single-peaked light curves (177 bursts), demonstrates increased correlation with galaxies within $\approx$155 Mpc. The measured correlation (28 ± 16 per cent of the sample) suggests that BATSE observed between two and nine long-duration GRBs per year similar to, and from within similar distances to, GRBs 980425 and 060218. This implies an observed local rate density (to BATSE limits) of $700 \pm 360\,\mathrm{Gpc^{-3}\,yr^{-1}}$ within 155 Mpc.

Key words: gamma-rays: bursts.

1 INTRODUCTION

The two closest gamma-ray bursts (GRBs) detected so far are GRB 980425 (Galama et al. 1998) and GRB 060218 (Cusumano et al. 2006; Mirabal & Halpern 2006), both long-duration GRBs of exceptionally low luminosity. Indeed, GRB 980425 is usually taken as the archetypal low-luminosity, low-variability, soft spectrum GRB. During nine years of operation, BATSE (the Burst and Transient Source Experiment on board the *Compton Gamma Ray Observatory*) detected 2704 GRBs. As is well known, there is good evidence for two observed classes of GRB distinguished most clearly by T_{90}, the time taken to collect 90 per cent of a burst's total gamma-ray fluence (Kouveliotou et al. 1993; Norris et al. 1984). Long-duration GRBs (L-GRBs, $T_{90} > 2$ s) show a correlation between spectral peak energy and overall isotropic energy release – the $E_\mathrm{p}/E_\mathrm{iso}$ or Amati relation (Amati et al. 2002) – where softer bursts are less isotropically energetic (although GRB 980425 is an outlier to this relationship in the sense that it is too spectrally hard for its isotropic luminosity, it is still softer than the majority of BATSE long bursts). L-GRBs also exhibit a spectral lag-luminosity relationship (Norris, Marani & Bonnell 2000; Salmonson & Galama 2002; Norris 2002) where there is anticorrelation between overall luminosity and the time-delay between the observation of corresponding light curve features in different energy bands. Furthermore, GRBs with long spectral lags (and hence low luminosity) tend to have smoother light curves with broader features, and lower peak fluxes (Norris, Scargle & Bonnell 2001). Isotropic-equivalent peak luminosity has also been shown to correlate with light curve variability, originally for a relatively small number of bursts (Reichart et al. 2001; Fenimore & Ramirez-Ruiz 2000) but recently confirmed by Guidorzi et al. (2005) for a larger sample, though with a larger scatter in the data. Though the exact form and tightness of the correlation is currently a matter of some debate (Reichart & Nysewander 2005; Guidorzi et al. 2006; Li & Paczyński 2006), there appears little doubt that the luminosity of L-GRBs correlates with variability.

GRBs 980425, 060218 and the next nearest L-GRB with a well-observed SN component to date, GRB 031203 (Gotz et al. 2003; Prochaska et al. 2004; Watson et al. 2004), are comprehensively reviewed by Kaneko et al. (2007). The properties of these nearby bursts, along with the correlations discussed above, suggest that under-luminous L-GRBs are likely to be spectrally soft with smooth, single-peaked light curves. Thus we can use these properties to select those bursts most likely to be of intrinsically low luminosity and therefore drawn from a relatively nearby population. Furthermore, as suggested by arguments based on analyses of detector sensitivities

★Email: r.1.chapman@herts.ac.uk

and luminosity function calculations (Pian et al. 2006; Soderberg et al. 2006; Liang et al. 2007; Cobb et al. 2006), this sub-class of low-luminosity bursts may be many times more prevalent in the local Universe than high-luminosity bursts.

Approximately 75 per cent of the 2704 BATSE GRBs were long, but due to large localization error regions few of these bursts have identified hosts or redshifts. However, if some originated within similar distances to GRB 980425 and GRB 060218 then it should be possible to estimate this fraction statistically via their distribution on the sky, using the same technique we used previously to investigate the distribution of short GRBs (Tanvir et al. 2005). If indeed there is an unidentified population of under-luminous, soft, smooth L-GRBs, then restricting the BATSE sample to those with properties similar to GRB 980425 should enhance any correlation signal.

We therefore consider below the correlation between BATSE long bursts and two galaxy catalogues: the PSCz (Point Source Catalogue Redshift) galaxy survey (Saunders et al. 2000) and the Third Reference Catalogue of Bright Galaxies (RC3) (de Vaucouleurs et al. 1991). The PSCz is based on the *IRAS* Point Source Catalogue, and is less affected by dust extinction in the galactic plane than other redshift surveys, making it an appropriate comparison data set for the all-sky BATSE data set. Though less complete, the RC3 is useful as a further comparison set and a check against any possible catalogue bias.

2 METHODS

The long burst sample consists of the 1437 L-GRBs with location errors $\leqslant 10^{\circ}$ and measured fluences in the current BATSE catalogue [4B(R), Paciesas et al. (1999), including web supplement]. Our galaxy samples are drawn from two galaxy catalogues, the *IRAS* PSCz galaxy survey (Saunders et al. 2000) and the RC3 (de Vaucouleurs et al. 1991). Using the measured heliocentric recession velocities of galaxies in these catalogues, we made samples of galaxies within concentric spheres of recession velocity $v < 2000$, 5000, 8000 and 11 000 km s^{-1} [corresponding to radii of 28(z = 0.0067), 70(0.017), 113(0.027) and 155(0.037) Mpc respectively].[1] Following the method described in Tanvir et al. (2005), we define the statistic Φ for each galaxy sample compared with the L-GRBs as shown in equation (1), where θ_{ij} is the separation between the ith burst and the jth galaxy, and ϵ_i is the error circle of the ith burst position (statistical combined with systematic errors from model 1 of Briggs et al. 1999). For each comparison set (burst sample with galaxy sample), Φ thus provides a measure of the overall correlation between the bursts and galaxies.

$$\Phi = \sum_{i}^{\text{Bursts}} \sum_{j}^{\text{Galaxies}} \frac{1}{\epsilon_i} \int_{\theta_{ij}}^{\infty} \frac{1}{\sqrt{2\pi}\epsilon_i} \exp\left[\frac{-\theta^2}{2\epsilon_i^2}\right] \mathrm{d}\theta \qquad (1)$$

Values of Φ can be calibrated and used to measure the percentage of bursts correlated with each galaxy sample by simulating distributions of known correlation with that galaxy sample. To achieve this we generated a number (501) of distributions of random bursts (each with the same number of positions as the number of bursts under consideration, the same positional errors, and distributed on the sky according to the known BATSE sky exposure map (Hakkila et al. 2003). From these we computed Φ_0 and its associated dispersion. Similarly, we generated 501 100 per cent correlated test distributions for each galaxy sample (this time with 'host' positions chosen randomly from the galaxy sample and pseudo-bursts displaced from these positions assuming Gaussian probability distributions within error circles chosen randomly from the burst sample) which enabled us to calculate Φ_{100}. Calibration plots of Φ/Φ_0 versus percentage correlation with associated errors could then be produced.

To reiterate, the closest known bursts (GRBs 980425, 060218 and 031203) were under-luminous and spectrally soft with smooth single-peaked light curves. In order to select a burst subsample with properties similar to these bursts, three separate selections were performed on the L-GRB sample, based on observed fluence, spectral softness and overall light-curve shape. First, as argued above, because long-lag (and therefore likely under-luminous) bursts increase from a negligible proportion of BATSE bright bursts to $\sim$50 per cent at trigger threshold (Norris 2002), we ordered the L-GRBs by total burst fluence and selected the low-fluence half. Similarly, to select for spectrally soft bursts, we split the total sample in half by the ratio of observed fluence in BATSE energy channels 1 (20–50 keV) and 3 (100–300 keV). We did not attempt further cuts on the data based on fluence or spectral hardness as this would not be justified for several reasons. First, the number of bursts selected in finer cuts would be very small for statistical analysis. Secondly, the low-fluence bursts (for example) will obviously contain bursts that are dim due to being further away and these cannot be distinguished from the nearby bursts – we aimed purely to increase the fraction of nearby bursts in the samples as predicted by the correlations guiding the cuts. Thirdly, given the overall lack of correlation in the sample as a whole, any measured correlation is likely to be very weak and further cuts beyond the median would be statistically dubious. The third selection for bursts of a smooth, single-peaked nature was made by visual examination of the light curves of the entire L-GRB sample. We emphasize that this selection was based on simple pre-agreed criteria to select smooth, single-peaked curves broadly similar to the known local bursts, not to attempt detailed selection with respect to small-scale variation. To further minimize any subjectivity involved, the selection was performed independently by two of us and then arbitrated by a third. Finally, the bursts common to all three selections (177) were then used to form a low-fluence, spectrally soft, single-peaked subsample.

3 RESULTS

Fig. 1 shows plots of correlation (expressed as the percentage of bursts in each sample correlated with galaxy distribution) between BATSE L-GRBs and concentric spheres of galaxy samples from both the PSCz and RC3 catalogues. The results show a high degree of consistency, confirming that the correlation measurements are not dependent on a chance choice of galaxy catalogue. In practice, each volume sample in the RC3 catalogue contained between 1.5 and 2 times the number of galaxies in the equivalent PSCz sample. This inevitably leads to increased dispersion in the values of Φ measured with the PSCz samples compared to the RC3 samples, though we still consider the completeness and homogeneity of the PSCz sample to make it a more appropriate comparison set.

As can be seen, long-burst correlation (particularly with the PSCz samples) remains formally consistent with zero out to the largest radii considered of $v \leqslant 11000$ km s^{-1} ($\approx$155 Mpc), confirming that nearby L-GRBs are indeed rarely observed events. However, the most probable level of correlation increases with distance, but this could not be reliably investigated beyond the radii considered due

[1] Throughout this Letter we use $H_0 = 71$ km s^{-1} Mpc^{-1}. Due to individual peculiar velocities, the recession velocity is not always an exact distance proxy.

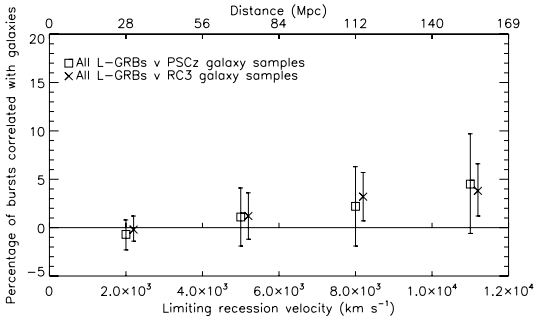

Figure 1. Measured correlation (expressed as the percentage of bursts in each sample correlated with galaxy distribution) versus galactic recession velocity for concentric spheres of galaxy samples. Data points have been separated along the x-axis for clarity, and error bars represent 1σ errors.

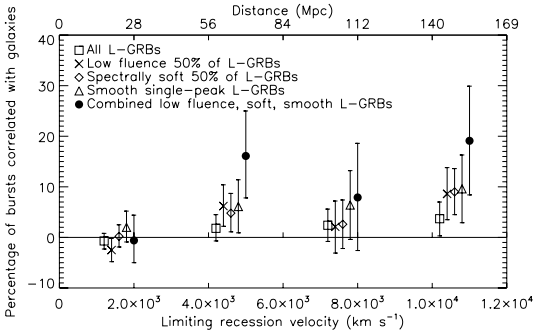

Figure 2. Measured correlation between BATSE L-GRBs and galaxies in concentric shells of increasing galactic recession velocity from the PSCz catalogue. Details as Fig. 1.

to the flux-limited nature of the galaxy catalogues, meaning that there are just too few galaxies in the catalogues at larger radii to be useful.

Turning now to the subsamples with properties similar to known local bursts, Fig. 2 shows correlations with concentric *shells* (as opposed to *spheres*) of galaxies with recession velocity radii of 0–2000, 2000–5000, 5000–8000 and 8000–11 000 km s^{-1}. From this figure it can be seen that each of the low-fluence, spectrally soft, smooth light-curve subsamples exhibit broadly equivalent, marginally increased correlations in the second and fourth shells. Furthermore, a combined set containing only those bursts (177) common to all three individual subsamples exhibited increased correlation of 16 ± 8 per cent ($\equiv 28 \pm 14$ bursts) in the 2000–5000 km s^{-1} shell, and 19 ± 11 per cent ($\equiv 34 \pm 19$ bursts) in the outermost shell.

Returning to examine concentric *spheres* of galaxies, Fig. 3 shows the cumulative correlation versus radius of the combined subsample of L-GRBs, where it can be seen that 28 ± 16 per cent of low-fluence, spectrally soft bursts with smooth single-peaked light-curves are correlated with galaxies within $\approx$155 Mpc, equivalent to a total of 50 ± 28 bursts in the nine years of BATSE operation.

It is interesting to ask whether our analysis is more sensitive to individual burst–galaxy correlations, or to correlation with large-scale structure on the sky. In order to address this question, we repeated our correlation analyses, but this time in calculation of Φ_{100} for each correlated pseudo-burst we removed the galaxy from which its position was generated. Thus Φ_{100} then measures the correlation between pseudo-bursts and the large-scale structure around the generating host. The resulting structure-based Φ_{100} values for the PSCz galaxy shells are shown in Table 1.

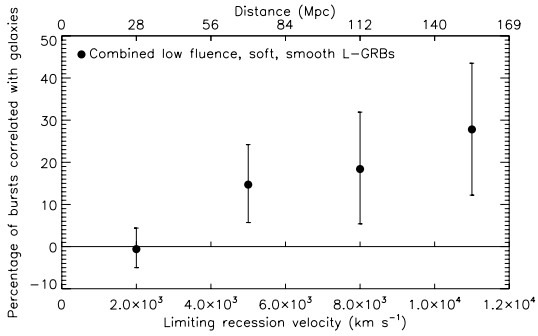

Figure 3. Measured correlation between the combined low-fluence, spectrally soft, single-peaked L-GRBs and galaxies in concentric spheres from the PSCz catalogue.

Table 1. Values of Φ_{100} for PSCz galaxy samples measured including and not including the host of the pseudo-bursts in correlated simulations.

PSCz galaxy shell recession velocity (km s^{-1})	Φ_{100} incl. host (arbitrary units)	Φ_{100} excl. host (arbitrary units) (per cent)
$\leqslant$2000	1875	1684 (90 per cent)
2000–5000	2873	2663 (93 per cent)
5000–8000	2354	2151 (91 per cent)
8000–11000	1810	1616 (89 per cent)

As this table shows, $\geqslant$89 per cent of the correlation signal measured by Φ_{100} is generated from galaxies other than the specific hosts of the pseudo-bursts. It would therefore seem likely that correlation between the real BATSE bursts and galaxy distributions is mainly due to large-scale structure on the sky rather than correlation with individual hosts. Given the size of the BATSE error boxes, this is certainly not surprising, but means that our analysis is unlikely to be sensitive to individual galaxy properties. Indeed, analyses performed weighting Φ by estimated individual galactic mass or star formation rate (estimated using the methods described in Levan et al. 2006) showed no significant change from the unweighted results. However, given the often large error boxes of individual bursts, sensitivity to structure is actually an advantage. Our technique effectively measures the correlation between two 2D signals, and is statistical in its nature – the signal is produced from the sums of contributions of many burst–galaxy candidate pairs and thus enhances any inherently weak individual correlation measurements at the expense of sensitivity to individual pair properties. This also precludes our ability to identify individual burst–galaxy associations. It is also known that the typical hosts of L-GRBs are blue, faint, irregular galaxies (Fruchter et al. 2006) and thus many potential individual hosts may be missing from the galaxy catalogues.

4 DISCUSSION

4.1 Two populations of long bursts?

Our results confirm that nearby L-GRBs as a whole are indeed rare events, with correlation remaining consistent with zero out to $\approx$155 Mpc, but with a 10 per cent upper limit (1σ), equivalent to

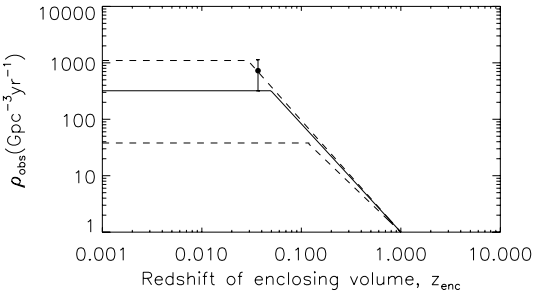

Figure 4. The observed burst rate, ρ_{obs}, within the enclosed volume out to redshift z_{enc}. The filled circle shows the observed burst rate within our investigated total volume. The area enclosed by the dashed lines represents the upper and lower limits of the predicted observed rate for low-luminosity GRBs as a function of enclosing volume (after fig. 5b of Liang et al. 2007).

144 bursts. Restricting the L-GRB sample to those with properties similar to known nearby bursts increased the measured correlation to 28 ± 16 per cent of the subsample (≡50 ± 28 bursts) within the same radius. It is worth emphasizing that this means the 177 burst subsample contains a *lower* limit (1σ) of 22 bursts correlated with local large-scale structure, almost one quarter more than the 1σ *upper* limit (18) expected from the correlation rate of the sample as a whole. The local rate density of under-luminous L-GRBs implied by our result is in agreement with those calculated via detector sensitivity and luminosity function arguments. For example, Soderberg et al. (2006) argue that sub-energetic bursts are 10 times more abundant than typical bright GRBs based on the sensitivities of *BeppoSAX*, *HETE-2* and *Swift* to GRB 980425 and GRB 060218, and similarly Pian et al. (2006) (using BATSE, *HETE-2* and *Swift* sensitivities) found a local rate density at least 100 times greater than that estimated from cosmological bursts alone. In addition, Cobb et al. (2006) estimate an event ratio $\sim 10^2$ between low- and high-luminosity bursts based on assuming the *Swift* population of high-luminosity bursts to be complete to its mean redshift. Furthermore, Liang et al. (2007) suggest that in order to avoid overpredicting the number of intermediate luminosity GRBs observed at low redshifts, the high- and low-luminosity bursts must be characterized by separate luminosity functions. They choose models of the same functional form (smoothed broken power-law), but with the coefficients of each separately constrained to produce GRB rates consistent with those observed. Finally, Guetta & Della Valle (2007) estimate a local GRB rate of 200–1800 Gpc^{-3} yr^{-1} using a luminosity function consistent with the luminosities of local bursts. Fig. 4 shows our results plotted with respect to predicted rates of low-luminosity GRBs from Liang et al. (2007). The results presented here can be seen to provide independent confirmation of these luminosity function based predictions.

4.2 Comparison with SN searches

GRB 980425 was the first GRB to be observationally associated with a supernova (SN) (Galama et al. 1998), and GRB 060218 (e.g. Mirabal et al. 2006; Pian et al. 2006) is the most striking recent example. These nearby SN associated L-GRBs share similar properties (low-fluence, spectrally soft and smooth, single-peaked light curves) as argued by Bloom et al. (1998), and it may therefore seem that a search for temporal and spatial correlation between bursts and supernovae would provide a means of identifying individual GRB hosts, particularly at low redshift. However, the heterogeneity and inherent incompleteness of SN catalogues (due for example to the difficulty of SN detection in dusty environments, biased surveys and magnitude limitations) make it difficult to use them to identify GRB host galaxies. Recent observations also suggest that not all L-GRBs are necessarily accompanied by an observable supernova (Fynbo et al. 2006; Gal-Yam et al. 2006; Della Valle et al. 2006), and of course, not all Type Ib/c SNe produce GRBs (e.g. Soderberg et al. 2006). Nevertheless, several groups have attempted searches for spatial and temporal coincidences of GRBs with SNe [for example Wang & Wheeler (1998),Kippen et al. (1998), Norris, Bonnell & Watanabe (1999) and Pian et al. (2006)]. The results obtained vary depending particularly on any restrictions imposed on the burst or SN properties in the analyses, and generally the statistics remain too poor to draw any firm conclusions from these and other studies. In addition, it has been suggested recently that the host galaxies of Type Ic SNe without GRBs may be systematically different from those with GRBs, particularly in terms of metallicity (Modjaz et al. 2007).

It is therefore apparent that using SNe searches to identify possible nearby GRBs is fraught with difficulty. Soderberg et al. (2006) estimate that only ∼3 per cent of Ib/c SNe give rise to detectable low-luminosity GRBs comparable to GRBs 980425 and 060218. During the lifetime of the BATSE experiment, the Asiago supernova catalogue (Barbon et al. 1999)[2] contains only 33 events classified as Ib, Ibc or Ic within the volume considered here. Further, given that most SN searches, particularly in the 1990s, concentrated on targeting relatively bright galaxies, untypical of GRB hosts, we should expect that few, if any, GRB-SN were discovered by chance in these surveys. Our approach, independent of any assumed correlation other than that GRBs must occur in or near a host galaxy, is therefore justified and enables the placing of limits on the number of observed nearby L-GRBs based on location with respect to potential host galaxy distributions alone.

5 SUMMARY AND CONCLUSIONS

We have analysed the correlations of the entire BATSE catalogue of L-GRBs with measured fluences localized to better than 10° (1437 bursts) with galaxy samples out to ≈155 Mpc from two independent galaxy catalogues. We find that correlation between the L-GRB set as a whole and samples from both galaxy catalogues remains within 1 standard deviation (σ) of zero out to the highest radii considered. However, selecting a subsample of bursts with properties similar to those of the known local L-GRBs significantly increased correlation with large-scale structure on the sky to a level of 28 ± 16 per cent (≡50 ± 28 bursts) within the same radius.

The cumulative correlation rate out to ≈155 Mpc suggests that BATSE most likely observed between two and nine L-GRBs per year similar to, and from within similar distances to, the closest known GRBs to date. This implies an observed local L-GRB rate density within 155 Mpc of 700 ± 360 Gpc^{-3} yr^{-1} (to BATSE detection limits, and assuming the BATSE sky-exposure fraction to be of the order of 0.5). This is in reasonable agreement with 230^{+490}_{-190} Gpc^{-3} yr^{-1} as calculated by Soderberg et al. (2006) via combined analyses of the sensitivities of *BeppoSAX*, *HETE II* and *Swift*. It is also in very good agreement with observed rates of low-luminosity GRBs predicted from luminosity function arguments (Liang et al. 2007; Guetta & Della Valle 2007).

[2] http://web.pd.astro.it/supern/snean.txt

At the time of writing (2007 March), ≈50 *Swift*-detected long-duration GRBs have measured redshifts out of a total of ≈180 detections. The mean redshift of an unbiased sample of 16 *Swift* L-GRBs measured in late 2005 was $z = 2.8$ (Jakobsson et al. 2006), though the highest so far is $z = 6.295$ (Haislip et al. 2006; Kawai et al. 2006) and the lowest is GRB 060218 with $z = 0.0331$. Comparison between data sets from different missions and detectors is difficult [see for example Berger et al. (2005),Band (2006)]. However, if we naively assume the *Swift* GRB catalogue to be similar to the BATSE catalogue, then in a sample of 50 bursts we would expect to find between zero and five within 155 Mpc, as is the case. It may be argued that because we are looking for nearby bursts, these would be more likely to have measured redshifts than the bursts in general, though all three nearest GRBs were significantly under-luminous events. Even so, comparing to the entire *Swift* sample of 180 L-GRBs, our results suggest it contains 9 ± 9 bursts with redshift less than 0.0367. So far, only one has been identified as occurring within our considered volume: GRB 060218. This is certainly consistent with our limits (particularly given the relatively small numbers involved), but we may expect more low-redshift long bursts to be identified in the future, particularly among spectrally soft, under-luminous bursts with little variability.

ACKNOWLEDGMENTS

We thank Pall Jakobsson for useful discussions. RC and RSP acknowledge the support of the University of Hertfordshire. NRT and AJL acknowledge the support of UK PPARC senior and postdoctoral research fellowships respectively.

REFERENCES

Amati L. et al., 2002, A&A, 390, 81
Band D. L., 2006, ApJ, 644, 378
Barbon R., Buondí V., Cappellaro E., Turatto M., 1999, A&AS, 139, 531
Berger E. et al., 2005, ApJ, 634, 501
Bloom J. S., Kulkarni S. R., Harrison F., Prince T., Phinney E. S., Frail D. A., 1998, ApJ, 506, L105
Briggs M. S., Pendleton G. N., Kippen R. M., Brainerd J. J., Hurley K., Connaughton V., Meegan C. A., 1999, ApJS, 122, 503
Cobb B. E., Bailyn C. D., van Dokkum P. G., Natarajan P., 2006, ApJ, 645, L113
Cusumano G., Barthelmy S., Gehrels N., Hunsberger S., Immler S., Marshall F., Palmer D., Sakamoto T., 2006, GCN Circ. 4775, 1
de Vaucouleurs G., de Vaucouleurs A., Corwin H. G., Buta R. J., Paturel G., Fouque P., 1991, Third Reference Catalogue of Bright Galaxies, Vols 1–3, XII. Springer-Verlag, Heidelberg
Della Valle M. et al., 2006, Nat, 444, 1050
Fenimore E. E., Ramirez-Ruiz E., 2000, ApJ, submitted (astro-ph/0004176)
Fruchter A. S. et al., 2006, Nat, 441, 463
Fynbo J. P. U. et al., 2006, Nat, 444, 1047
Gal-Yam A. et al., 2006, Nat, 444, 1053
Galama T. J. et al., 1998, Nat, 395, 670
Gotz D., Mereghetti S., Beck M., Borkowski J., Mowlavi N., 2003, GCN Circ. 2459, 1
Guetta D., Della Valle M., 2007, ApJ, 657, L73
Guidorzi C., Frontera F., Montanari E., Rossi F., Amati L., Gomboc A., Hurley K., Mundell C. G., 2005, MNRAS, 363, 315
Guidorzi C., Frontera F., Montanari E., Rossi F., Amati L., Gomboc A., Mundell C. G., 2006, MNRAS, 371, 843
Haislip J. B. et al., 2006, Nat, 440, 181
Hakkila J., Pendleton G. N., Meegan C. A., Briggs M. S., Kippen R. M., Preece R. D., 2003, in Ricker G., Venderspek R. K., eds, AIP Conf. Proc. Vol. 662, Gamma-Ray Burst and Afterglow Astronomy 2001: A Workshop Celebrating the First Year of the HETE Mission. Am. Inst. Phys., New York, p. 176
Jakobsson P. et al., 2006, A&A, 447, 897
Kaneko Y. et al., 2007, ApJ, 654, 385
Kawai N. et al., 2006, Nat, 440, 184
Kippen R. M. et al., 1998, ApJ, 506, L27
Kouveliotou C., Meegan C. A., Fishman G. J., Bhat N. P., Briggs M. S., Koshut T. M., Paciesas W. S., Pendleton G. N., 1993, ApJ, 413, L101
Levan A. J., Wynn G. A., Chapman R., Davies M. B., King A. R., Priddey R. S., Tanvir N. R., 2006, MNRAS, 368, L1
Li L.-X., Paczyński B., 2006, MNRAS, 366, 219
Liang E., Zhang B., Virgili F., Dai Z. G., 2007, ApJ, 662, 1111
Mirabal N., Halpern J. P., 2006, GCN Circ. 4792, 1
Mirabal N., Halpern J. P., An D., Thorstensen J. R., Terndrup D. M., 2006, ApJ, 643, L99
Modjaz M., Kewley L., Kirshner R. P., Stanek K. Z., Challis P., Garnavich P. M., Greene J. E., Prieto J. L., 2007, AJ, submitted (astro-ph/0701246)
Norris J. P., 2002, ApJ, 579, 386
Norris J. P., Bonnell J. T., Watanabe K., 1999, ApJ, 518, 901
Norris J. P., Cline T. L., Desai U. D., Teegarden B. J., 1984, Nat, 308, 434
Norris J. P., Marani G. F., Bonnell J. T., 2000, ApJ, 534, 248
Norris J. P., Scargle J. D., Bonnell J. T., 2001, in Ritz S., Gehrels N., Shrader C. R., eds, AIP Conf. Proc. Vol. 587, Gamma 2001: Gamma-Ray Astrophysics. Am. Inst Phys., New York, p. 176
Paciesas W. S. et al., 1999, ApJS, 122, 465
Pian E. et al., 2006, Nat, 442, 1011
Polcar J. et al., 2006, A&A, 452, 439
Prochaska J. X. et al., 2004, ApJ, 611, 200
Reichart D. E., Lamb D. Q., Fenimore E. E., Ramirez-Ruiz E., Cline T. L., Hurley K., 2001, ApJ, 552, 57
Reichart D. E., Nysewander M. C., 2005, ApJ, submitted (astro-ph/0508111)
Salmonson J. D., Galama T. J., 2002, ApJ, 569, 682
Saunders W. et al., 2000, MNRAS, 317, 55
Soderberg A. M. et al., 2006, Nat, 442, 1014
Tanvir N. R., Chapman R., Levan A. J., Priddey R. S., 2005, Nat, 438, 991
Wang L., Wheeler J. C., 1998, ApJ, 504, L87
Watson D. et al., 2004, ApJ, 605, L101

This paper has been typeset from a TEX/LATEX file prepared by the author.

Mon. Not. R. Astron. Soc. **000**, 000–000 (0000) Printed 12 September 2008 (MN LATEX style file v2.2)

Short gamma-ray bursts from SGR giant flares and neutron star mergers: two populations are better than one

Robert Chapman[1⋆], Robert S. Priddey[1] and Nial R. Tanvir[2]
[1] *Centre for Astrophysics Research, University of Hertfordshire, College Lane, Hatfield AL10 9AB, UK*
[2] *Department of Physics and Astronomy, University of Leicester, Leicester, LE1 7RH, UK*

12 September 2008

ABSTRACT
There is increasing evidence of a local population of short duration Gamma-ray Bursts (sGRB), but it remains to be seen whether this is a separate population to higher redshift bursts. Here we choose plausible Luminosity Functions (LF) for both neutron star binary mergers and giant flares from Soft Gamma Repeaters (SGR), and combined with theoretical and observed Galactic intrinsic rates we examine whether a single progenitor model can reproduce both the overall BATSE sGRB number counts and a local population, or whether a dual progenitor population is required. Though there are large uncertainties in the intrinsic rates, we find that at least a bimodal LF consisting of lower and higher luminosity populations is required to reproduce both the overall BATSE sGRB number counts and a local burst distribution. Furthermore, the best fit parameters of the lower luminosity population agree well with the known properties of SGR giant flares, and the predicted numbers are sufficient to account for previous estimates of the local sGRB population.

Key words: Gamma-ray Burst, magnetar, SGR

1 INTRODUCTION

Results from the Burst and Transient Source Experiment (BATSE) onboard the *Compton Gamma-Ray Observatory* showed that Gamma-ray Bursts (GRBs) divide observationally into two classes based primarily on their duration (Kouveliotou et al. 1993): long GRBs have durations > 2 seconds, and short GRBs $\leqslant 2$ seconds. Short GRBs (sGRBs) seem to be associated with a variety of host galaxies with no apparent restriction on galactic properties (Prochaska et al. 2006; Berger 2007; Levan et al. 2008), although host identification is not always trivial (Levan et al. 2007). Additionally, a handful of recently detected sGRBs have localisations consistent with origins in nearby galaxies (Ofek et al. 2006, 2007a; Frederiks et al. 2007; Mazets et al. 2007; Levan et al. 2008). Overall, the *Swift* redshift distribution of sGRBs (Berger 2007) peaks closer than that of long GRBs (Jakobsson et al. 2006), though there is evidence that some sGRBs may occur at higher redshifts (Levan et al. 2006a), and that there may be a local population of underluminous long GRBs (e.g. Pian et al. 2006; Soderberg et al. 2006; Liang & Zhang 2006; Liang et al. 2007; Chapman et al. 2007).

The leading progenitor model for sGRBs is the merger of two compact objects, neutron star-neutron star (NS-NS) or neutron star-black hole (Nakar 2007) binaries. The Luminosity Function (LF) of BATSE sGRBs has been investigated previously assuming a single progenitor population (e.g. Schmidt 2001; Ando 2004; Guetta & Piran 2005, 2006; Hopman et al. 2006) in order to determine the intrinsic rate and most likely LF parameters. In a refinement to their previous work, Guetta & Piran (2006) noted that a second population of bursts may be necessary to explain some features of their model fits and the comparison with *Swift* bursts, particularly at lower redshifts. Hopman et al. (2006) considered both primordial and dynamically formed NS binaries, and suggested that the early observed redshift distribution of sGRBs favoured dynamical formation. Further to that work, Salvaterra et al. (2007) suggested that the more recent *Swift* cumulative redshift distribution is better encompassed by including both formation routes with different abundances above and below $z \sim 0.3$. Recently, in an analysis of a large number of models of compact object merger scenarios from population synthesis models, O'Shaughnessy, Belczynski & Kalogera (2008) have shown that the observed sGRB redshift distribution could be reproduced by a reasonable fraction of those models, though this analysis was insensitive to the low end of the redshift distribution on which our work here is focused. Nakar, Gal-Yam & Fox (2006) find the high rate of observed sGRBs within 1 Gpc to imply that a single population of NS binaries responsible for all sGRBs must be dominated by long merger times, inconsistent with

⋆ Email:r.1.chapman@herts.ac.uk

the observed NS binary population. However, they also point out that a non-unimodal luminosity function, such as produced by two separate populations of progenitor, cannot be ruled out for sGRBs.

There are indeed other possible progenitors for sGRBs. At much closer distances still, the initial spike in a giant flare from a Soft Gamma Repeater (SGR) in a relatively nearby galaxy would also appear as a sGRB. For example, the December 27th 2004 event from SGR1806-20 would have been visible by BATSE out to $\approx$ 50 Mpc (Hurley et al. 2005; Palmer et al. 2005; Taylor & Granot 2006; Nakar 2007). Thus it is entirely plausible that some fraction of sGRBs are extragalactic SGR giant flares. Several studies have estimated the likely contributions of SGR flares to BATSE sGRBs. Popov & Stern (2006) estimate a rate of a few percent based on a lack of definite sGRB detections among the shortest BATSE GRBs consistent with locations within the Virgo cluster. Searches for hosts plausibly connected with six well-localised sGRBs (Nakar et al. 2006) suggest a rate of less than 15%, and in a comparison of the spectra of a limited sample of the brightest BATSE sGRBs, Lazzati, Ghirlanda & Ghisellini (2005) conclude only 4%. Palmer et al. (2005), based again on a lack of events from the Virgo cluster, find a rate of less than 5%, though point out that the LF of SGR giant flares may extend to much larger luminosities, such as suggested by Eichler (2002). Ofek (2007) points out that the fraction cannot be less than $\sim$ 1% without being inconsistent with the observed Galactic SGR giant flare rate, and calculate an upper limit of 16% (95% confidence limits) based on a conservative measure of probable IPN sGRB coincidences with bright star forming galaxies within 20 Mpc. This limit is sensitive to their estimate of the completion of the galaxy sample and may be higher still.

Previously, using the full sample of BATSE sGRBs localised to better than 10 degrees, we demonstrated that between 6 and 12 per cent of BATSE sGRBs were correlated on the sky with galaxies within $\approx$ 28 Mpc (Tanvir et al. 2005), and we have now extended this work out to $\approx$ 155 Mpc. Our analysis was based purely on burst/galaxy distribution correlations and unbiased with regards to burst brightness or other assumptions, though our later work showed that this correlation is dependent mostly on large scale structure on the sky rather than individual burst/galaxy pairings (Chapman et al. 2007). The main question we address in this paper is whether a nearby population ($z \leqslant 0.03$) of this magnitude may be produced by a suitable LF describing a single progenitor population, or whether it is necessary to include an intrinsically lower luminosity population as well.

Here we attempt to answer this question by considering first single, and then dual population LFs. The intrinsic rates in the models will be assumed from both the observed Galactic SGR flare rates and the modelled NS-NS merger rates in order to investigate the LF parameters. Obviously there are significant uncertainties in these rates: the Galactic giant flare rate in particular is estimated from only 3 observed events. Regardless of these uncertainties and the exact form of luminosity functions chosen, we find that a single progenitor population described by a unimodal (i.e. with a single peak or knee) LF cannot produce sufficient local events, whereas a dual population reproduces the likely local sGRB distribution as well as the overall number counts[1].

2 METHODS

The number of sGRBs, N, observed above a threshold p in time T and solid angle Ω is given by Equation 1, where $\Phi(L)$ is the sGRB LF, $R_{GRB}(z)$ is the comoving event rate density at redshift z, $dV(z)/dz$ is the comoving volume element at z and z_{max} for a burst of luminosity L is determined by the detector flux threshold and the luminosity distance of the event.

$$N(>p) = \frac{\Omega T}{4\pi} \int_{L_{min}}^{L_{max}} \Phi(L) dl \int_0^{z_{max}} \frac{R_{GRB}(z)}{1+z} \frac{dV(z)}{dz} dz \quad (1)$$

We are of course dealing with detector limited and not bolometric luminosities. Following Schmidt (2001) and Guetta & Piran (2005) we assume a constant median spectral index of -1.1 in the BATSE energy range of 50-300 keV to derive a simplified K correction and conversion to photon flux.

2.1 Intrinsic rates

The sGRB rate per unit volume, $R_{\mathrm{GRB}(z)}$ is given by Equation 2 where N_{GRB} is the number of sGRBs per progenitor, $\rho_{\mathrm{progenitor}}$ is the intrinsic ($z = 0$) progenitor formation rate and $F(z)$ describes the volume evolution of this rate with z.

$$R_{\mathrm{GRB}}(z) = N_{\mathrm{GRB}} \times \rho_{\mathrm{progenitor}} \times F(z)\ \mathrm{Mpc}^{-3} \quad (2)$$

For NS-NS mergers, a burst is produced only once at merger, and we therefore assume $N_{\mathrm{GRB}} = 1$. This is of course an upper limit: any beaming of sGRBs, or a GRB production efficiency per merger of less than 100%, would effectively reduce this number, and reduce the number of bursts observable from the NS-NS merger population. This limit is therefore conservative in the sense that it maximises the possible fraction of bursts produced by mergers in our analysis. The intrinsic NS-NS merger rate is taken as 10^{-5} yr^{-1} per Milky Way equivalent galaxy (Star Formation Rate, SFR $\approx 4\mathrm{M}_{\odot}$ yr^{-1}, e.g. Diehl et al. (2006)) from the population synthesis models of Kalogera et al. (2007). Mergers, of course, occur some time after the formation of the binary itself. Thus the merger rate at redshift z, is dependent not on the SFR at the same z, but on the earlier SFR at higher redshift. $F(z)$ is therefore given by the convolution of the SFR as a function of redshift with a distribution of delay times from binary formation to merger. The population syntheses of Belczynski et al. (2006) suggest a merger delay time (formation plus coalescence) distribution $dP_m/d(\log(t)) \sim constant$ ($\equiv dP_m/dt \propto 1/t$) between 10^7 and 10^{10} years, with a narrow peak at the very lowest times, and we thus assume a delay time probability distribution where $dP_m/d(\log(t))$ is flat between 10^7 and 10^{10} years and zero outside this range, for simplicity and comparison with

[1] Throughout this paper we assume a flat cosmology with $\mathrm{H}_0 = 71\mathrm{km\ s^{-1}\ Mpc^{-1}}$, $\Omega_M = 0.27$ and $\Omega_\Lambda = 0.73$

previous LF analyses. We note, however, that using a delay model including a narrow early 'spike' (with an order of magnitude higher value between 15 and 30 Myr) makes little difference to the derived LF parameters as can be seen from some examples in Tables 1-3.

SFR as a function of z is parameterised according to the SF2 model of Porciani & Madau (2001), normalised to a local SFR of 1.3×10^{-2} $M_{\odot}yr^{-1}Mpc^{-3}$ (Gallego et al. 1995) as given in Equation 3.

$$\mathrm{SFR}(z) = 1.3 \times 10^{-2} \left(\frac{23e^{3.4z}}{e^{3.4z} + 22} \right) \ \mathrm{M_{\odot}\ yr^{-1}\ Mpc^{-3}} \quad (3)$$

An alternative analysis is that the merger rate should be proportional to Stellar Mass Density (SMD), which must be representative of star formation history. We therefore also investigate merger rates which follow a simple single exponential fit to the SMD out to $z \sim 5$ derived from the FORS deep field (Drory et al. 2005) as:

$$\mathrm{SMD}(z) = 10^{8.75} \exp(-\ln(2)z)\ \mathrm{M_{\odot}\ Mpc^{-3}} \quad (4)$$

Over the last 30 years of observations, there have been 3 giant flares from 4 known SGRs in the Milky Way and Magellanic Clouds. The observed local rate of giant flares per Galactic SGR is therefore $\approx 3 \times 10^{-2}$ $\mathrm{yr^{-1}}$, and their short active lifetimes of $\sim 10^4$ years (Duncan & Thompson 1992; Kouveliotou et al. 1998; Kouveliotou 1999) imply $N_{\mathrm{GRB}} \sim 300$ in the SGR case. Magnetars are commonly believed to form in a fraction of core collapse supernovae, and hence their formation should follow the SFR as a function of z. Given the the association of the 4 known SGRs with young stellar populations, this therefore implies a formation rate via core collapse supernovae of 4×10^{-4} $\mathrm{yr^{-1}}$.

However, it is also plausible that magnetars may form via the Accretion Induced Collapse (AIC) of White Dwarf (WD) binaries which contain at least one sufficiently massive and magnetized member (Levan et al. 2006b). In older galaxies with relatively little star formation, this would be the dominant formation route and therefore makes it possible for SGRs to be associated with all types of galaxies, not just those with a relatively high SFR. Following Levan et al. (2006b), the rate of magnetar formation via WD-WD mergers in a Milky Way equivalent galaxy is estimated as 3×10^{-4} $\mathrm{yr^{-1}}$. We therefore assume $F(z)$ for SGRs follows both SFR(z) for magnetar production from supernovae and either the delayed SFR or SMD to allow for production by WD binary mergers.

2.2 Luminosity functions

Luminosity functions for SGR giant flares and NS-NS mergers are not well known. A lognormal LF approximates the shape of the theoretical NS-NS merger luminosity distribution (Rosswog & Ramirez-Ruiz 2003), but other functional forms may be equally valid: for example Guetta & Piran (2005) assumed a broken power law for their LF calculations, and the luminosities of many other astronomical populations are well described by a Schechter function (Schechter 1976).

Given only 3 events, it is not possible to constrain the SGR giant flare LF to any great degree. The 3 observed events have peak luminosities of $\sim 10^{44}$, $\sim 10^{46}$ and $\sim 10^{47}$ erg $\mathrm{s^{-1}}$ (Tanaka et al. 2007) (including a correction for the lower distance estimate of SGR 1806-20 found by Bibby et al. (2008)). The more common short duration bursts from SGRs, with luminosities up to 10^{41} erg $\mathrm{s^{-1}}$ seem to follow a power law distribution in energy, $dN \propto E^{-\gamma} dE$ where $\gamma \sim 1.4 - 1.8$ (Cheng et al. 1996; Göğüş et al. 2000) similar to that found in earthquakes and solar flares. Intermediate bursts with energies and luminosities between the short bursts and giant flares are also seen, and it is possible therefore that this distribution continues to higher energies and includes the giant flares themselves, particularly since Göğüş et al. (2000) found no evidence for a high energy cutoff in their work. However, Cheng et al. (1996) did find evidence of a cutoff around 5×10^{41} erg, and furthermore the intermediate bursts are generally seen following giant flares and may be some form of aftershock rather than representing part of a continuous spectrum of flare activity. Theory suggests that the common bursts are produced by the release of magnetic energy gated by a small scale fracturing of the crust sufficient only to relieve crustal stresses, whereas the giant flares are the result of large scale cracking sufficient to allow external field reconfiguration to a new equilibrium state (Thompson & Duncan 1993, 1995). Assuming the latter is a physically distinct process discontinuous (in terms of energy release) from the short bursts, then it must have some minimum energy release, and a maximum defined by the total destruction of the external field via the Flowers-Ruderman instability (Flowers & Ruderman 1977) where entire hemispheres of the magnetar flip with respect to each other (Eichler 2002). Having only the 3 observed events to go on, a lognormal LF is once again plausible for giant flare luminosities. The possibility of a continuous luminosity distribution between the short, intermediate and giant flares is not ruled out however, and we therefore also consider a single power law LF as well.

To summarise, we consider the possibility that short GRBs may be produced via two different progenitor routes, both NS-NS mergers and SGR giant flares, each population with intrinsically different luminosities. The forms chosen for the luminosity functions examined are as follows:

1. Lognormal distribution

$$\frac{dN}{d\log L} \propto \exp\left(\frac{-(\log L - \log L_0)^2}{2\sigma^2} \right) \quad (5)$$

2. Schechter function

$$\frac{dN}{dL} \propto \left(\frac{L}{L_0} \right)^{-\alpha} \exp\left(-L/L_0\right)\ ,\ L \geqslant L_{min} \quad (6)$$

3. Power Law

$$\frac{dN}{dL} \propto \left(\frac{L}{L_0} \right)^{-\alpha}\ ,\ L_{min} \leqslant L \leqslant L_0 \quad (7)$$

where $L_{min} = 10^{42}$ erg $\mathrm{s^{-1}}$ for normalisation and convergence of the Schechter function. The Power Law distribution is normalised to the observed Galactic rate between $L_{GFmin} = 10^{44}$ erg $\mathrm{s^{-1}}$ and L_0, but the distribution is analysed down to L_{min} to investigate the possible extension of the power law to lower luminosity flares. L_0, and α or σ are the free parameters to be estimated.

2.3 Constraining the models

The C_{max}/C_{min} table from the current BATSE catalogue (Paciesas et al. 1999) provides peak count rate for bursts in units of the threshold count rate. Not all bursts are included and in addition the BATSE threshold was varied historically. Therefore in order to analyse a consistent set of bursts we restricted the table to only those sGRBs recorded when the 64ms timescale threshold was set to 5.5σ above background in at least 2 detectors in the $50-300$ keV range. The all sky equivalent period (including correction for BATSE's sky coverage) this represents is estimated as ~ 1.8 years.

We then examined the differential distributions of predicted overall counts first from various single, and then combined populations of burst progenitor. By varying the parameters of the chosen luminosity functions, we compared the predicted overall counts (dN/dp) to the observed differential distribution from the C_{max}/C_{min} table. For each set of LF parameters, the redshift distribution of sGRBs was calculated, and the nearby distributions compared with the observed correlated distributions from Tanvir et al. (2005). Note that we use an extended version of our previous correlation analysis out to 155 Mpc, and use the correlations measured against galaxies in concentric *shells* (as opposed to *spheres*) of recession velocity (see Chapman et al. 2007) in order to obtain a local differential distribution for the model fitting. χ^2 minimisation was then used to optimise the LF parameters by fitting simultaneously to the overall count rate and the local distributions. We assumed a Poissonian error distribution on the overall count rate, whereas we used the explicit Monte Carlo derived error distribution on the local correlated fraction. Note that the greater number of data points in the number count fits means that the combined χ^2 values are dominated by the goodness of fit to the count rate distribution. To explicitly ask whether any of our chosen single LFs can remain consistent with the BATSE number counts while being forced to produce a local distribution of bursts, we also find the best fits constrained by the correlated fraction alone, and the best fits among distributions forced to produce at least the lower limit of the measured local burst distribution within 112 Mpc (i.e the bottom of the error bar on the third data point in the upper panels of Figures 1 to 4).

In order to check the plausibility and consistency of the best fit models, we further compared the derived redshift distribution to that of sGRBs observed by *Swift*. We caution that this sample is neither uniformly selected nor complete. Previous studies have analysed the early *Swift* distributions (e.g. Guetta & Piran 2006; Hopman et al. 2006; Nakar, Gal-Yam & Fox 2006; Salvaterra et al. 2007; O'Shaughnessy, Belczynski & Kalogera 2008), and it is clearly useful to compare our models to the current best known redshift distribution in order to check that the predictions are not unrealistic. We stress that the *Swift* distribution was not part of the statistical analysis. sGRB redshifts have so far only been found from host galaxy associations, the identification of which is not always unambiguous. Furthermore, even the classification of some bursts as either short or long is controversial since their durations change substantially depending on whether or not emission from the long-soft tails (seen in a number of bursts) is included. Nevertheless, about a dozen probable short-hard bursts have reasonably secure redshifts. Specifically we include the following 10 sGRBs: GRBs 050509B, 050724, 051221a, 060801, 061006, 061201, 061210, 061217 (see Berger (2007) and references therein), 070714B (Graham et al. 2007) and 071227 (D'Avanzo et al. 2007). In order to produce the predicted *Swift* redshift distribution, the *Swift* BAT threshold for sGRBs was assumed to be twice that of BATSE (Band 2006).

NS Merger LF	Parameters ($l_0 \equiv \log L_0$)	Local χ^2/dof	C_{max}/C_{min} χ^2/dof	Overall χ^2/dof
Schechter (*flat*)	$l_0 = 51.75$ $\alpha = 1.25$	11.93	1.01	1.31
Schechter (*spike*)	$l_0 = 51.8$ $\alpha = 1.25$	11.93	1.03	1.33
Schechter (*SMD*)	$l_0 = 50.45$ $\alpha = 0.9$	11.87	1.05	1.34
Lognorm (*SMD*)	$l_0 = 48.9$ $\sigma = 0.75$	11.82	1.09	1.38
Lognorm (*flat*)	$l_0 = 46.4$ $\sigma = 1.5$	11.88	1.18	1.46
Lognorm (*spike*)	$l_0 = 46.6$ $\sigma = 1.45$	11.89	1.19	1.47

Table 1. Results of single population Luminosity Functions, presented in order of decreasing overall goodness of fit (i.e. increasing overall χ^2/dof). The LFs follow merger delay time (formation plus coalescence) distributions either *flat* in log space ($dP_m/d(\log(t)) = constant$), or with a narrow *spike* at early times, or the *SMD* profile of Equation 4. The number of degrees of freedom (dof) for the local, C_{max}/C_{min} and overall distributions are 1, 22 and 26 respectively. l_0 is in units of $\log(\mathrm{erg\ s^{-1}})$, σ in dex and α is dimensionless.

3 RESULTS

Table 1 lists the best fit parameters found from fitting distributions produced by single population NS merger LFs simultaneously to both the overall number counts and the local population as described above. The table is ordered in decreasing overall goodness of fit (i.e. increasing combined χ^2/dof). As mentioned previously, the combined χ^2 is dominated by the fit to the overall BATSE number counts and, as expected, all our chosen single population LFs produce good fits to the C_{max}/C_{min} data leading to acceptable overall fits as measured by the combined χ^2. However, none of the single progenitor population LFs reproduce the local burst population expected from the correlation results (column 3 in Table 1 lists the χ^2/dof results considering the fit to the local distribution only). For example, Figure 1 shows the results from a single Schechter function LF which can be seen to produce effectively no sGRBs within 300 Mpc.

In order to ascertain whether a single merger population can produce the local bursts and remain consistent with the C_{max}/C_{min} data, we then fit single LF populations to the local distribution alone, with no constraints placed on goodness of fit to the overall number counts. As can be seen from Table 2, single Schechter function LFs can produce a local population, but the associated number count distribution is an extremely poor match to the C_{max}/C_{min}

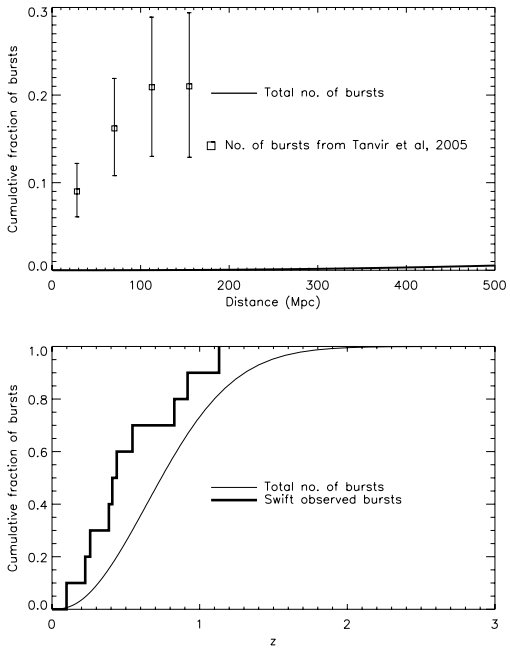

Figure 1. Burst distributions from the best fit merger single population Schechter function LF following a $dP_m/d(\log(t)) = constant$ merger time delay distribution. Top panel shows predicted sGRB distribution within 500 Mpc compared to the local burst fraction measured in Tanvir et al. (2005), bottom panel shows the predicted burst distribution out to $z = 3$ normalised and compared to the *Swift* distribution discussed in the text.

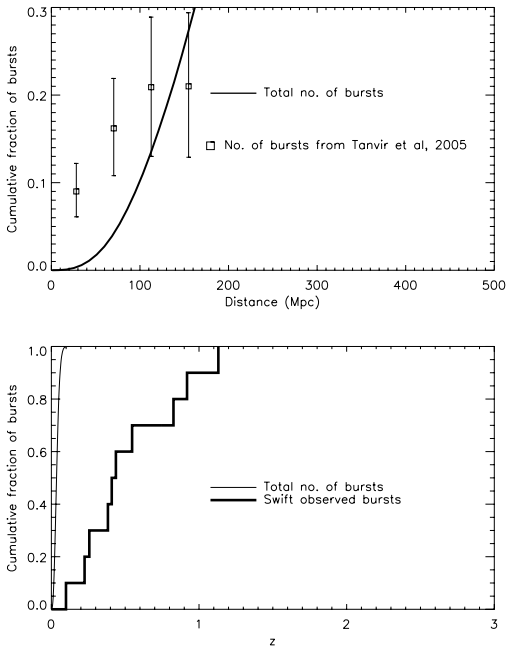

Figure 2. Burst distributions from the best fit of the same merger single Schechter function LF as Figure 1 constrained only to produce at least the lower limit of the local burst population within $\sim$ 112 Mpc (data point 3). Note the unrealistic wider redshift distribution produced by this fit. Panel Details as for Figure 1.

data. With only four data points to constrain the local distribution there is obviously some ambiguity as to its exact shape, and in order to allow some flexibility in this shape and the fraction of local bursts demanded by the fits, we also chose to constrain the single LFs to only have to produce a fixed number of bursts within a certain radius. We chose the lower limit of the correlated bursts within $\sim$ 112 Mpc, i.e. the third data point in the local distribution panels in the Figures. Table 3 shows results from these fits, where it can be seen once again that even with this relaxed local constraint, the single population LFs are still unable to match the number count distribution while producing a local burst population. The inability of either of these local constraints to produce a distribution which fits the number counts is effectively a consequence of the intrinsic sGRB rate calculated in Equation 2 from the assumed merger rates: not enough bursts in total can be produced. In order to produce a large enough fraction of the observed bursts locally, the maximum burst luminosity must be unrealistically low, leading to an extremely unrealistic redshift distribution as demonstrated in Figure 2 and therefore not enough bursts overall. The fit to the C_{max}/C_{min} data can be improved to reasonable χ^2 levels by increasing the intrinsic merger rate by a large factor ($\geqslant 500$), but the overall redshift distribution still remains as unrealistic as in Figure 2.

In contrast, Table 4 shows best fit LF parameters for various combinations of dual NS merger and SGR giant flare luminosity function models, along with their respective minimum χ^2 values. Note that the number of degrees of freedom to consider for the local distribution model is a non-trivial issue: there are only 4 local data points to fit, and we are now using 2 LFs with 2 free parameters each. However, as can be seen from Tables 2 and 3, and the examples of Fig-

NS Merger LF	Parameters ($l_0 \equiv \log L_0$)	Local χ^2/dof	C_{max}/C_{min} χ^2/dof	Overall χ^2/dof
Schechter (*flat*)	$l_0 = 51.1$ $\alpha = 2.2$	0.76	> 100	> 100
Schechter (*spike*)	$l_0 = 51.0$ $\alpha = 2.2$	0.76	> 100	> 100
Schechter (*SMD*)	$l_0 = 53.0$ $\alpha = 2.15$	1.08	> 100	> 100
Lognorm (*spike*)	$l_0 = 43.1$ $\sigma = 1.35$	5.30	> 100	> 100
Lognorm (*flat*)	$l_0 = 43.1$ $\sigma = 1.3$	5.38	> 100	> 100
Lognorm (*SMD*)	$l_0 = 43.0$ $\sigma = 1.4$	6.43	> 100	> 100

Table 2. Results of single population Luminosity Functions constrained to fit the local distribution, presented in order of decreasing goodness of fit. Details as for Table 1.

NS Merger LF	Parameters ($l_0 \equiv \log L_0$)	Local χ^2/dof	C_{max}/C_{min} χ^2/dof	Overall χ^2/dof
Schechter (*flat*)	$l_0 = 48.15$ $\alpha = 0.55$	17.2	> 100	> 100
Schechter (*spike*)	$l_0 = 48.15$ $\alpha = 0.5$	16.8	> 100	> 100
Schechter (*SMD*)	$l_0 = 48.2$ $\alpha = 0.5$	16.5	> 100	> 100
Lognorm (*spike*)	$l_0 = 48.1$ $\sigma = 0.1$	28.4	> 100	> 100
Lognorm (*flat*)	$l_0 = 48.1$ $\sigma = 0.1$	28.3	> 100	> 100
Lognorm (*SMD*)	$l_0 = 48.0$ $\sigma = 0.3$	21.5	> 100	> 100

Table 3. Results of single population Luminosity Functions constrained only to produce at least the lower limit of the local distribution within 112 Mpc (see text). Results presented in the same order as Table 2, with details as for Table 1.

ures 3 and 4, the local bursts are only ever reproduced by the lower luminosity LF, and we can therefore continue to assume the local distribution $dof = 1$. By minimising the combined χ^2 values, all the dual LFs tested reproduced the local distribution well while retaining overall number count fits comparable to those of the single LFs. Furthermore, the best fit LF parameters of the dual models are reasonable, and the overall redshift distribution is much more realistic.

For example, a dual lognormal LF, with merger rates following either a delayed merger model (Figure 3) or the SMD model of Equation 4 (Figure 4), produces a good fit to the expected local population while remaining consistent with the early *Swift* redshift distribution. The upper panels of Figures 3 and 4 show the comparison of these models to the local sGRB distribution determined by our BATSE cross-correlation analysis, and are typical in that all the dual populations reproduce this local population well. Since these data were used to constrain the fit, a good agreement is to be expected, but it is still interesting to note that the merger population contributes only a small fraction to these local bursts. The lower panels show the overall predicted redshift distribution.

As mentioned before, the intrinsic Galactic rates used to normalise the LFs are not well constrained. Hence in Table 4 we also show the results of varying the intrinsic SGR flare rate up and down by an order of magnitude for the dual lognorm (SMD) fit of Figure 4. The production of a local sGRB population is robust against this change, and the overall fit remains good. As may be expected, an increase in the intrinsic flare rate leads to the best fit SGR LF being moved down in luminosity, thus removing a greater fraction of the total flares from observability. Likewise, a lower intrinsic rate generates a higher (and narrower) LF distribution, though in both cases the LF parameters remain entirely plausible.

Figure 5 shows the best fit LFs and associated contours of χ^2 with respect to L_0 for the dual population from Figure 4. Despite the uncertainties in the underlying Galactic rates of the models, the best fit parameters obtained for this and the other dual LFs are plausible given the known properties of SGR giant flares and classic sGRB luminosities.

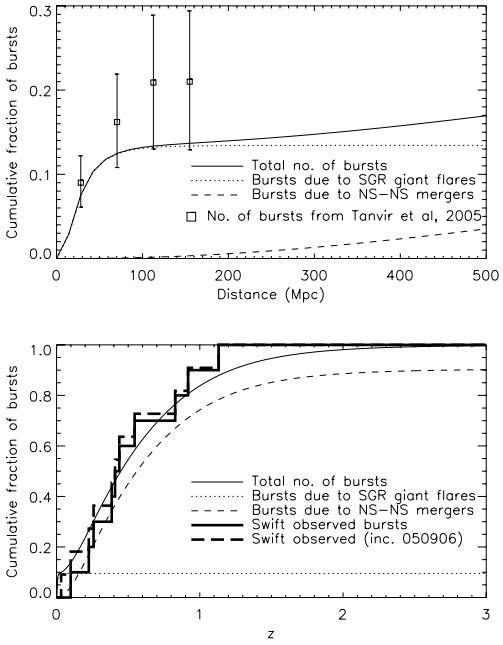

Figure 3. Burst distributions from dual lognormal LF (following $dP_m/d(\log(t)) = constant$ merger time delay distribution) populations. Panel Details as for Figure 1.

We note that the slopes of the SGR flare power law LFs obtained (1.25 - 1.35) are shallower than the slopes found for ordinary SGR burst fluence distributions (1.4 - 1.8) (Cheng et al. 1996; Göğüş et al. 2000).

4 DISCUSSION

The lower panels of Figures 3 and 4 imply that *Swift* should have triggered on about one SGR flare to date (this would rise by a factor of ~ 2 if the redshift completeness for such flares were greater than for sGRBs as a whole, as is likely given that low-redshift host galaxies are easily identified). We note that a possible candidate is GRB 050906, which may have originated in a galaxy at ≈ 130 Mpc (Levan et al. 2008), and the preliminary *Swift* redshift distributions in Figures 3 and 4 are plotted both including and excluding this burst.

There are two recent sGRB events which are candidate extragalactic SGR flares: GRB 051103 whose IPN error box includes the outskirts of M81 at 3.5 Mpc (Golenetskii et al. 2005), and GRB 070201 whose error box similarly overlaps a spiral arm of M31 at only ~ 0.77 Mpc (Perley 2007; Pal'Shin 2007; Mazets et al. 2007). Both have characteristics of SGR giant flares (Frederiks et al. 2007; Mazets et al. 2007; Ofek et al. 2007b), and furthermore the non-detection of gravitational waves by LIGO from GRB 070201 (LIGO Scientific Collaboration 2007) excludes a merger progenitor within M31 with $> 99\%$ confidence. If both these events were due to extragalactic SGRs then this brings to three the number

NS Merger LF	LF Parameters ($l_0 \equiv \log L_0$)	SGR Giant Flare LF	LF Parameters ($l_0 \equiv \log L_0$)	Local $\chi^2/(dof = 1)$	C_{max}/C_{min} $\chi^2/(dof = 20)$	Overall $\chi^2/(dof = 24)$
Schechter (*flat*)	$l_0 = 52.3$ $\alpha = 1.3$	Power law (*flat*)	$l_0 = 46.7$ $\alpha = 1.25$	2.03	1.15	1.04
Schechter (*flat*)	$l_0 = 52.3$ $\alpha = 1.3$	Lognorm (*flat*)	$l_0 = 45.2$ $\sigma = 0.6$	1.45	1.20	1.06
Lognorm (*SMD*)	$l_0 = 48.35$ $\sigma = 1.05$	Lognorm (*SMD*)	$l_0 = 45.3$ $\sigma = 0.55$	1.66	1.31	1.16
Lognorm (*flat*)	$l_0 = 47.2$ $\sigma = 1.2$	Power law (*flat*)	$l_0 = 46.7$ $\alpha = 1.35$	2.06	1.69	1.49
Lognorm (*flat*)	$l_0 = 47.05$ $\sigma = 1.2$	Lognorm (*flat*)	$l_0 = 45.2$ $\sigma = 0.6$	1.55	1.72	1.50
Lognorm (*SMD*)	$l_0 = 48.6$ $\sigma = 0.9$	Lognorm (*SMD*) $(10 \times MW)$	$l_0 = 44.1$ $\sigma = 0.8$	1.57	1.36	1.20
Lognorm (*SMD*)	$l_0 = 48.6$ $\sigma = 0.9$	Lognorm (*SMD*) $(0.1 \times MW)$	$l_0 = 46.3$ $\sigma = 0.2$	3.13	1.28	1.20

Table 4. Results of dual population Luminosity Functions, presented in order of decreasing goodness of fit (i.e. increasing overall χ^2/dof). The LFs follow merger delay time (formation plus coalescence) distributions either *flat* in log space ($dP_m/d(\log(t)) = constant$) or the *SMD* profile of Equation 4. Also shown are two results normalised using order of magnitude different observed Galactic (MW) rates. l_0 is in units of log(erg s^{-1}), σ in dex and α is dimensionless.

of giant flares with peak luminosity $> 10^{47}$erg s^{-1} seen in just a few years.

Levan et al. (2008) estimated that a Galactic SGR giant flare rate of $\sim 0.5 \times 10^{-4}$ yr^{-1} would be sufficient to produce ~ 10 extragalactic flares within a sphere of radius 100 Mpc. Using a power law LF (constrained by a search for positional coincidences between galaxies within 20 Mpc and the IPN error boxes of a sample of 47 sGRBs), Ofek (2007) estimated the rate of extragalactic flares with energy $> 3.7 \times 10^{46}$erg (the energy of the 2004 SGR1806-20 event (Hurley et al. 2005)) to be $\sim 0.5 \times 10^{-4}$ yr^{-1} per SGR, and the 95% confidence lower limit of the Galactic rate to be 2×10^{-4} yr^{-1} per SGR. Our analysis estimates the rate of flares with peak luminosity $> 10^{47}$ erg s^{-1} to be between these two values at $\sim 1 \times 10^{-4}$ yr^{-1} per SGR. We estimate the SFR of galaxies within 5 Mpc listed by Ofek (2007) (with revised distance estimates (Karachentsev et al. 2004)) to be about 22× that of the Milky Way. Adopting our predicted (lognorm following SMD) flare rate, the probability of observing two (one) or more such flares within this volume during the 17 years of IPN3 observation is 1% (14%). This indicates we have been witness to a rather rare coincidence, and is perhaps suggestive that not both GRB 051103 and GRB 070201 are SGR flares.

5 SUMMARY AND CONCLUSIONS

We have examined a selection of plausible Luminosity Functions, singly and in combination, for both neutron star mergers and SGR giant flares as progenitors of short Gamma-ray Bursts. Assuming observed and theoretical Galactic intrinsic rates, merger delay time distributions, Star Formation Rate and Stellar Mass Density parameterisations, we exclude both lognormal and Schechter type LFs for a single NS merger population of progenitor as being unable to produce a nearby sGRB population while remaining consistent with overall BATSE number counts. Indeed, given that even a Schechter function (dominated by low luminosity events) cannot reproduce the likely local population, it is hard to conceive of any unimodal LF which could and still be consistent with the higher redshift distribution. We suggest that at least a bimodal LF, and therefore likely a dual population model, is necessary to account for the local population. Given the uncertainties in the intrinsic rates assumed, we cannot sensibly choose between the LF combinations, but we point out that the best fit LF parameters in all dual populations considered are in reasonable agreement with the known properties of SGR giant flares and classic sGRBs, even when the intrinsic rate of Galactic SGR flares is varied by an order of magnitude in either direction. To put this another way, as is well known a single population Luminosity Function provides a good fit to overall BATSE number counts, but we find that a separate, lower luminosity population of progenitors is both required, and is sufficient, to reproduce a local sGRB population. Furthermore, the properties of this population are in agreement with those observed from Galactic SGR giant flares.

6 ACKNOWLEDGEMENTS

We thank Páll Jakobsson and Andrew Levan for useful discussions. RC and RSP acknowledge the support of the University of Hertfordshire. NRT acknowledges the support of a UK STFC senior research fellowship.

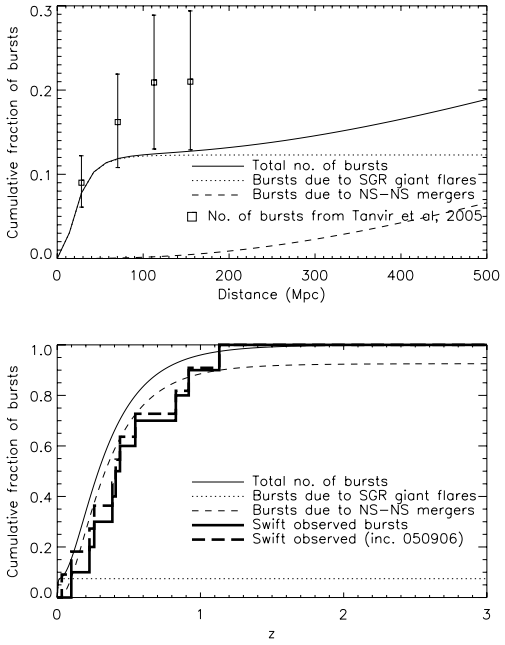

Figure 4. Burst distributions from dual lognormal LF (following SMD) populations. Panel Details as for Figure 1.

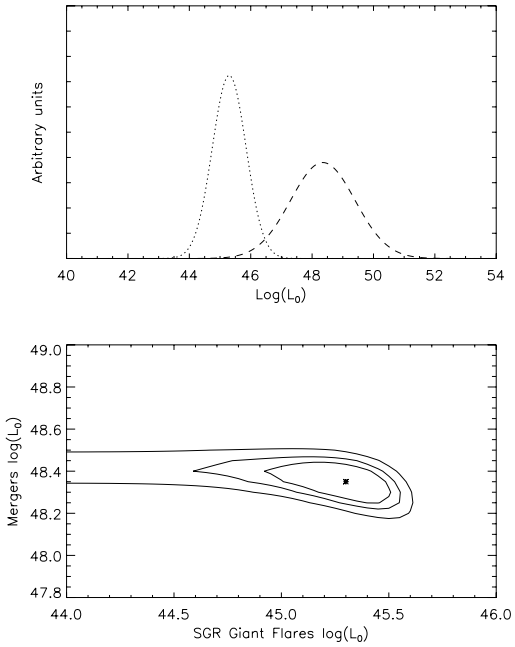

Figure 5. Best fit dual population LFs from Figure 4. The LFs (top panel: dotted line SGR giant flares, dashed line mergers) are lognormal with intrinsic merger rate components following the SMD model of Equation 4. The bottom panel shows contours of χ^2 in $\log(L_0)$ space. Contours shown represent 0.6, 0.9 and 0.99 confidence limits with the minimum χ^2 value plotted as an asterisk.

REFERENCES

Ando S., 2004, Journal of Cosmology and Astro-Particle Physics, 6, 7

Band D. L., 2006, ApJ, 644, 378

Belczynski K., Perna R., Bulik T., Kalogera V., Ivanova N., Lamb D. Q., 2006, ApJ, 648, 1110

Berger E., 2007, ApJ, 670, 1254

Bibby J. L., Crowther P. A., Furness J. P., Clark J. S., 2008, MNRAS, pp L34

Chapman R., Tanvir N. R., Priddey R. S., Levan A. J., 2007, MNRAS, 382, L21

Cheng B., Epstein R. I., Guyer R. A., Young A. C., 1996, Nat, 382, 518

D'Avanzo P., Fiore F., Piranomonte S., Covino S., Tagliaferri G., Chincarini G., Stella L., 2007, GRB Coordinates Network, 7152

Diehl R. et al., 2006, Nat, 439, 45

Drory N., Salvato M., Gabasch A., Bender R., Hopp U., Feulner G., Pannella M., 2005, ApJ, 619, L131

Duncan R. C., Thompson C., 1992, ApJ, 392, L9

Eichler D., 2002, MNRAS, 335, 883

Flowers E., Ruderman M. A., 1977, ApJ, 215, 302

Frederiks D. D., Palshin V. D., Aptekar R. L., Golenetskii S. V., Cline T. L., Mazets E. P., 2007, Astronomy Letters, 33, 19

Gallego J., Zamorano J., Aragon-Salamanca A., Rego M., 1995, ApJ, 455

Golenetskii S., et al., 2005, GRB Circular Network, 4197

Göğüş E., Woods P. M., Kouveliotou C., van Paradijs J., Briggs M. S., Duncan R. C., Thompson C., 2000, ApJ, 532, L121

Graham J. F., Fruchter A. S., Levan A. J., Nysewander M., Tanvir N. R., Dahlen T., Bersier D., Pe'Er A., 2007, GRB Coordinates Network, 6836

Guetta D., Piran T., 2005, A&A, 435, 421

Guetta D., Piran T., 2006, A&A, 453, 823

Hopman C., Guetta D., Waxman E., Portegies Zwart S., 2006, ApJ, 643, L91

Hurley K. et al., 2005, Nat, 434, 1098

Jakobsson P. et al., 2006, A&A, 447, 897

Kalogera V., Belczynski K., Kim C., O'Shaughnessy R., Willems B., 2007, Phys. Rep., 442, 75

Karachentsev I. D., Karachentseva V. E., Huchtmeier W. K., Makarov D. I., 2004, AJ, 127, 2031

Kouveliotou C., 1999, Proceedings of the National Academy of Science, 96, 5351

Kouveliotou C. et al., 1998, Nat, 393, 235

Kouveliotou C., Meegan C. A., Fishman G. J., Bhat N. P., Briggs M. S., Koshut T. M., Paciesas W. S., Pendleton G. N., 1993, ApJ, 413, L101

Lazzati D., Ghirlanda G., Ghisellini G., 2005, MNRAS, 362, L8

Levan A. J. et al., 2007, MNRAS, 378, 1439

Levan A. J. et al., 2006a, ApJ, 648, L9

Levan A. J. et al., 2008, MNRAS, 384, 541

Levan A. J., Wynn G. A., Chapman R., Davies M. B., King

A. R., Priddey R. S., Tanvir N. R., 2006b, MNRAS, 368, L1
Liang E., Zhang B., 2006, ApJ, 638, L67
Liang E., Zhang B., Virgili F., Dai Z. G., 2007, ApJ, 662, 1111
LIGO Scientific Collaboration, Hurley K., 2007, ArXiv e-prints, 0711.1163
Mazets E. P. et al., 2007, ArXiv e-prints, 0712.1502
Nakar E., 2007, Phys. Rep., 442, 166
Nakar E., Gal-Yam A., Fox D. B., 2006, ApJ, 650, 281
Nakar E., Gal-Yam A., Piran T., Fox D. B., 2006, ApJ, 640, 849
Ofek E. O., 2007, ApJ, 659, 339
Ofek E. O. et al., 2007a, ApJ, 662, 1129
Ofek E. O. et al., 2006, ApJ, 652, 507
Ofek E. O. et al., 2007b, ArXiv e-prints, 0712.35850
O'Shaughnessy R., Belczynski K., Kalogera V., 2008, ApJ, 675, 566
Paciesas W. S. et al., 1999, ApJS, 122, 465
Palmer D. M. et al., 2005, Nat, 434, 1107
Pal'Shin V., 2007, GRB Coordinates Network, 6098
Perley D. A., Bloom J. S., 2007, GRB Coordinates Network, 6091
Pian E. et al., 2006, Nat, 442, 1011
Popov S. B., Stern B. E., 2006, MNRAS, 365, 885
Porciani C., Madau P., 2001, ApJ, 548, 522
Prochaska J. X. et al., 2006, ApJ, 642, 989
Rosswog S., Ramirez-Ruiz E., 2003, MNRAS, 343, L36
Salvaterra R., Cerutti A., Chincarini G., Colpi M., Guidorzi C., Romano P., 2007, ArXiv e-prints, 0710.3099
Schechter P., 1976, ApJ, 203, 297
Schmidt M., 2001, ApJ, 559, L79
Soderberg A. M. et al., 2006, Nat, 442, 1014
Tanaka Y. T., Terasawa T., Kawai N., Yoshida A., Yoshikawa I., Saito Y., Takashima T., Mukai T., 2007, ApJ, 665, L55
Tanvir N. R., Chapman R., Levan A. J., Priddey R. S., 2005, Nat, 438, 991
Taylor G. B., Granot J., 2006, Modern Physics Letters A, 21, 2171
Thompson C., Duncan R. C., 1993, ApJ, 408, 194
Thompson C., Duncan R. C., 1995, MNRAS, 275, 255